

Geochemical, Biogeochemical, and
Sedimentological Studies of the
Green River Formation,
Wyoming, Utah, and Colorado

U.S. GEOLOGICAL SURVEY BULLETIN 1973-A-G



AVAILABILITY OF BOOKS AND MAPS OF THE U.S. GEOLOGICAL SURVEY

Instructions on ordering publications of the U.S. Geological Survey, along with the last offerings, are given in the current-year issues of the monthly catalog "New Publications of the U.S. Geological Survey." Prices of available U.S. Geological Survey publications released prior to the current year are listed in the most recent annual "Price and Availability List." Publications that are listed in various U.S. Geological Survey catalogs (see back inside cover) but not listed in the most recent annual "Price and Availability List" are no longer available.

Prices of reports released to the open files are given in the listing "U.S. Geological Survey Open-File Reports," updated monthly, which is for sale in microfiche from the U.S. Geological Survey Books and Open-File Reports Sales, Box 25425, Denver, CO 80225.

Order U.S. Geological Survey publications by mail or over the counter from the offices given below.

BY MAIL

Books

Professional Papers, Bulletins, Water-Supply Papers, Techniques of Water-Resources Investigations, Circulars, publications of general interest (such as leaflets, pamphlets, booklets), single copies of periodicals (Earthquakes & Volcanoes, Preliminary Determination of Epicenters), and some miscellaneous reports, including some of the foregoing series that have gone out of print at the Superintendent of Documents, are obtainable by mail from

U.S. Geological Survey, Books and Open-File Report Sales
Box 25425
Denver, CO 80225

Subscriptions to periodicals (Earthquakes & Volcanoes and Preliminary Determination of Epicenters) can be obtained ONLY from

Superintendent of Documents
U.S. Government Printing Office
Washington, DC 20402

(Check or money order must be payable to Superintendent of Documents.)

Maps

For maps, address mail order to

U.S. Geological Survey, Map Sales
Box 25286
Denver, CO 80225

Residents of Alaska may order maps from

U.S. Geological Survey, Map Sales
101 Twelfth Ave., Box 12
Fairbanks, AK 99701

OVER THE COUNTER

Books

Books of the U.S. Geological Survey are available over the counter at the following U.S. Geological Survey offices, all of which are authorized agents of the Superintendent of Documents.

- ANCHORAGE, Alaska—4230 University Dr., Rm. 101
- ANCHORAGE, Alaska—605 West 4th Ave., Rm G-84
- DENVER, Colorado—Federal Bldg., Rm. 169, 1961 Stout St.
- LAKEWOOD, Colorado—Federal Center, Bldg. 810
- MENLO PARK, California—Bldg. 3, Rm. 3128, 345 Middlefield Rd.
- RESTON, Virginia—National Center, Rm. 1C402, 12201 Sunrise Valley Dr.
- SALT LAKE CITY, Utah—Federal Bldg., Rm. 8105, 125 South State St.
- SAN FRANCISCO, California—Customhouse, Rm. 504, 555 Battery St.
- SPOKANE, Washington—U.S. Courthouse, Rm. 678, West 920 Riverside Ave.
- WASHINGTON, D.C.—U.S. Department of the Interior Bldg., Rm. 2650, 1849 C St., NW.

Maps

Maps may be purchased over the counter at the U.S. Geological Survey offices where books are sold (all addresses in above list) and at the following Geological Survey offices:

- ROLLA, Missouri—1400 Independence Rd.
- FAIRBANKS, Alaska—New Federal Building, 101 Twelfth Ave.

ERRATA

U.S. Geological Survey Bulletin 1973-A-G, Geochemical, biogeochemical, and sedimentological studies of the Green River Formation, Wyoming, Utah, and Colorado.

The final paragraph on page E7 of chapter E should read as follows.

The large solid in the upper left quadrant in figure 44 is iron rich but is not the original bladed goethite. Its massive morphology is common for iron-bearing solids early in most experiments. Three SEM-EDS analyses of this product gave a mean of 75.3 weight percent Fe and 24.6 weight percent S. The mole ratio of Fe:S of 1.75 is much greater than the Fe:S ratio for known crystalline iron sulfides (table 2). Therefore, the exact composition of this substance is unknown, but it is probably a mixture of S₈, poorly crystalline or oxidized iron monosulfide(s), and massive or indistinguishable crystallites of α -FeOOH. Sulfur forms other than S₈ were not distinguished on the basis of SEM-EDS analysis. X-ray diffraction of the 6N HCl-leached solids from this sample detected only goethite and sulfur.

Geochemical, Biogeochemical, and Sedimentological Studies of the Green River Formation, Wyoming, Utah, and Colorado

Edited by MICHELE L. TUTTLE

Chapters A–G are issued as a single volume and are not available separately. Individual chapter titles are listed in volume contents

U.S. GEOLOGICAL SURVEY BULLETIN 1973–A–G

U.S. DEPARTMENT OF THE INTERIOR
MANUEL LUJAN, JR., Secretary



U.S. GEOLOGICAL SURVEY
Dallas L. Peck, Director

Any use of trade, product, or firm names in this publication is for descriptive purposes only and does not imply endorsement by the U.S. Government.

UNITED STATES GOVERNMENT PRINTING OFFICE: 1991

For sale by the
Books and Open-File Reports Section
U.S. Geological Survey
Federal Center
Box 25425
Denver, CO 80225

Library of Congress Cataloging-in-Publication Data

Geochemical, biogeochemical, and sedimentological studies of the Green River formation, Wyoming, Utah, and Colorado / edited by Michele L. Tuttle.

p. cm. — (U.S. Geological Survey bulletin ; 1973-A-G)

Supt. of Docs. no.: I 19.3:1973-A-G

1. Geology, Stratigraphic—Paleogene. 2. Geology—Wyoming.

3. Geology—Utah. 4. Geology—Colorado. 5. Diagenesis. 6. Green River Formation. I. Tuttle, M.L. II. Series.

QE75.B9 no. 1973-A-G

[QE691.5]

557.3 s—dc20

[557.87]

91-10904
CIP

CONTENTS

[Letters designate the chapters]

- (A) Introduction, by Michele L. Tuttle.
- (B) Sulfur geochemistry and isotopy of the Green River Formation, Wyoming, Utah, and Colorado, by Michele L. Tuttle and Martin B. Goldhaber.
- (C) A preliminary study of the carbon and nitrogen isotopic biogeochemistry of lacustrine sedimentary rocks from the Green River Formation, Wyoming, Utah, and Colorado, by James W. Collister and J.M. Hayes.
- (D) Trace elements in pyrites of the Green River Formation oil shales, Wyoming, Utah, and Colorado, by Wendy J. Harrison, D.R. Pevear, and P.C. Lindahl.
- (E) An experimental study of goethite sulfidization—Relationships to the diagenesis of iron and sulfur, by Mark R. Stanton and Martin B. Goldhaber.
- (F) Effects of source, depositional environment, and diagenesis on characteristics of organic matter in oil shale from the Green River Formation, Wyoming, Utah, and Colorado, by Walter E. Dean and Donald E. Anders.
- (G) Petrography of iron sulfide minerals in the Green River Formation of Wyoming, Utah, and Colorado, by Michele L. Tuttle.

Chapter A

Introduction

By MICHELE L. TUTTLE

U.S. GEOLOGICAL SURVEY BULLETIN 1973

GEOCHEMICAL, BIOGEOCHEMICAL, AND SEDIMENTOLOGICAL STUDIES OF THE
GREEN RIVER FORMATION, WYOMING, UTAH, AND COLORADO

CONTENTS

Abstract	A1
Introduction	A1
The Green River Formation: Background	A1
Regional geology	A2
Genetic models	A4
References cited	A5
Appendix—Sample collection, preparation, descriptions, and analyses	A7

FIGURES

1. Map showing Laramide uplifts and basins in parts of Wyoming, Utah, Colorado, and Idaho A3
2. Chart showing stratigraphy of cores used in study A4

TABLE

1. Resources in the Green River Formation A2

Introduction

By Michele L. Tuttle

Abstract

During the Paleogene, the Green River Formation was deposited in two large lakes that occupied the greater Green River basin of Wyoming, Piceance basin of Colorado, and Uinta basin of Utah. New geochemical, biogeochemical, and sedimentological data for samples from these three depositional basins provide a basis for a much needed interdisciplinary approach with which to better understand the deposition and diagenesis of the Green River Formation.

INTRODUCTION

In 1922, Wilmot H. Bradley launched a long and illustrious career committed to describing and understanding all aspects of deposition and diagenesis of the Paleogene (Eocene and locally Paleocene) Green River Formation. He, better than any other geologist, realized that the origin of the Green River rocks must be viewed as an interdisciplinary problem. In 1970, Bradley wrote (p. 985):

A much fuller understanding of the Green River oil shale and its organic chemistry will emerge when the geologists, paleontologists, organic chemists, biologists, paleolimnologists, and biogeochemists, who are now working on it, integrate their findings with those of the others.

Twenty years later, Bradley's recommendation is still valid. Many questions about the origin of the Green River Formation remain, and little progress has been made in testing conflicting hypotheses regarding its formation.

The geochemical and biogeochemical studies described in chapters A–G of this volume represent the broadest interdisciplinary collection of comparable data on the Green River Formation known to the author. They span a wide range of disciplines: inorganic and organic chemistry; stable isotopy of sulfide minerals ($^{34}\text{S}/^{32}\text{S}$) and

organic matter ($^{13}\text{C}/^{12}\text{C}$, $^{15}\text{N}/^{14}\text{N}$, $^{34}\text{S}/^{32}\text{S}$); petrography of sulfide minerals; evaluation of a modern lake as a geochemical analogue for the ancient Green River lakes, Uinta and Gosiute; and an experimental study on iron diagenesis in saline, high pH environments such as the Green River lakes. Additional chapters are planned on detailed major and trace chemistry, stable isotopy of carbonate minerals ($^{13}\text{C}/^{12}\text{C}$, $^{18}\text{O}/^{16}\text{O}$), and sedimentology of core material.

A broad goal of these studies is to provide results that can be integrated into an interdisciplinary understanding of depositional and diagenetic processes, as suggested by Bradley. Because many of the studies used splits from the same sample suite (appendix), results can be directly compared without having to assume similar depositional or diagenetic conditions.

This introductory chapter describes the regional geology of the Green River Formation and summarizes the two most popular genetic models explaining its origin. For the most part, writers of other chapters have drawn their conclusions independent of results from the other studies; no attempt has been made at this time to integrate individual conclusions.

Acknowledgments.— This chapter has greatly benefited from the constructive reviews of Ronald Johnson, George Breit, and Karen Franczyk. Larry Trudell (Laramie Research Institute, Laramie, Wyoming) arranged access to the Blacks Fork core. The work on which this chapter is based was done as part of the U.S. Geological Survey Evolution of Sedimentary Basins Program.

THE GREEN RIVER FORMATION: BACKGROUND

The geology and geochemistry of the Paleogene Green River Formation have received considerable attention since the mid-1920's (for a detailed bibliography on the Green River Formation, see Smith, 1986). Most studies

Table 1. Resources in the Green River Formation

Shale oil.....	1.5×10 ¹³ barrels of oil-equivalent ¹
Sodium carbonate minerals	
NaHCO ₃ (Piceance basin)	2.9×10 ¹⁰ metric tons ²
Na ₃ (CO ₃)(HCO ₃)·2H ₂ O (greater Green River basin).....	7.5×10 ¹⁰ metric tons ³
Oil (Altamont-Bluebell field, Uinta basin)	1.9×10 ¹⁰ barrels ⁴

¹National Petroleum Council (1973).

²Dyni (1974).

³Bradley and Eugster (1969).

⁴Anders and Gerrild (1984).

have focused on aspects of the formation's economic resources (table 1), which include shale oil and sodium carbonate minerals. The formation is also an important source rock for oil-producing fields in Utah. In addition to its economic importance, the formation has interested researchers because it represents the largest and one of the most complex saline-lake deposits in the geologic record (Eugster and Hardie, 1978).

Regional Geology

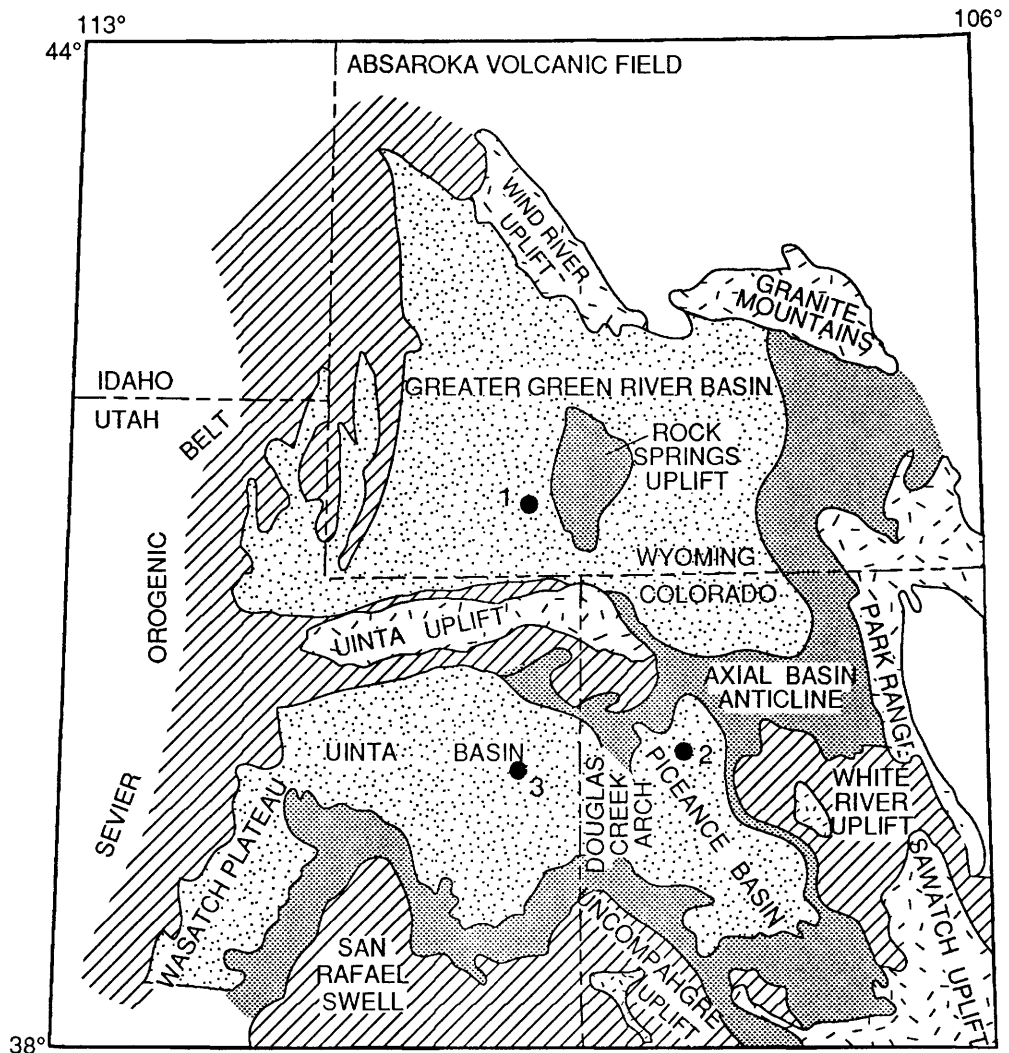
The Green River Formation was deposited in lakes occupying three Laramide fault-bounded basins (fig. 1): the Uinta basin of Utah and the Piceance basin of Colorado were occupied by ancient Lake Uinta, and the greater Green River basin of Wyoming was occupied by ancient Lake Gosiute. These basins existed for 45 m.y. in the latest Cretaceous and early Tertiary. The Green River Formation was deposited during 10–23 m.y. of this time interval (Franczyk and others, in press). During transgressive stages, the lakes covered more than 62,150 km² (the present-day areal extent of the formation) (Bradley, 1929). Because most of these lacustrine rocks are bounded by an erosional edge, the lakes undoubtedly covered a much larger area, particularly in Utah. Figure 2 shows the stratigraphy of Green River rocks in cores from the depocenters of these three depositional basins.

Lacustrine sedimentation (North Horn Formation) began as early as the Late Cretaceous (Maastrichtian) in the southwestern part of the Uinta basin and in the Wasatch Plateau (Fouch and others, 1983). By the late Paleocene, much of the Uinta basin and the Wasatch Plateau was covered by interspersed shallow lakes and wetlands. The Flagstaff Limestone in the Wasatch Plateau and the Flagstaff Member of the Green River Formation in the Uinta basin formed in these environments. These units consist of fossiliferous limestone, nonfossiliferous dolomitic mudstone, sandstone, and bedded and nodular gypsum (Stanley and Collinson, 1979). Similar depositional

environments were present in the Piceance basin at this time (Johnson, 1985). An influx of clastic sediments to both basins occurred in the latest Paleocene through earliest Eocene.

Subsequently, but still during the early Eocene, large, relatively freshwater lakes were established in both the Uinta and Piceance basins (Johnson, 1985); the upper part of the Flagstaff Member (Bradley's Basal Tongue of the Green River Formation) (Johnson, 1985) was deposited in the Uinta basin, and the Cow Ridge Member of the Green River Formation was deposited in the Piceance basin (Johnson, 1985). During this time, the initial phase of lacustrine sedimentation began in the greater Green River basin, with deposition of the freshwater Luman Tongue of the Green River Formation. These and older lake deposits were not penetrated by the cores shown in figure 2 and are not included in the studies presented in these chapters.

During the middle of the early Eocene, the lakes in all three basins expanded. The lakes in the Uinta and Piceance basins coalesced across the Douglas Creek arch to form one large lake. Sandstone, siltstone, shale, and limestone formed in the marginal lacustrine areas (Uinta basin and lake margins in Piceance and greater Green River basins), and illitic-rich oil shale formed in offshore lacustrine areas (center of Piceance and greater Green River basins). During this time, the water of both Lake Uinta and Lake Gosiute was saline enough to kill most of the freshwater mollusc populations that existed during the early freshwater stages, but not saline enough to precipitate saline minerals. The offshore oil shale deposited in the Piceance basin part of Lake Uinta during this time is included in the Garden Gulch Member of the Green River Formation. Marginal lacustrine rocks in the Uinta and Piceance basins are generally included in the Douglas Creek or Anvil Points Members of the Green River Formation. Both offshore and marginal lacustrine rocks deposited in Lake Gosiute comprise the Tipton Shale Member of the Green River Formation. This early Eocene interval (beginning with the middle early Eocene transgression) lasted between 0.5 and 1 m.y. and will be referred to in these chapters as lake stage 1 (fig. 2).



EXPLANATION

-  Present-day limit of Tertiary rocks
 -  Upper Cretaceous outcrop
 -  Present-day outcrop of Lower Cretaceous through Cambrian rocks
 -  Present-day outcrop of Precambrian rocks
- 0 50 100 KILOMETERS

Figure 1. Laramide uplifts and basins in parts of Wyoming, Utah, Colorado, and Idaho. Core holes (solid circles): 1, Blacks Fork no.1 core, greater Green River basin, Wyoming; 2, 01A core, Piceance basin, Colorado; and 3, Coyote Wash core, Uinta basin, Utah. Modified from Johnson (1985).

(Lake stages are used in these chapters to define sections of the Green River Formation that were deposited in similar depositional environments. In some cases, these lake stages correspond to lithostratigraphic members.)

During the latter part of the early Eocene, an increase in the salinity of the lakes coincided with a shift to a drier climate (Sullivan, 1985). As a result, Lake Gosiute shrank significantly (Bradley, 1964, 1973; Eugster and Hardie, 1975). Lake Uinta probably did not decrease significantly in

size, but broad shallow carbonate shelves formed around its margins. The initial phase of oil-shale formation occurred in Lake Uinta in the depocenter of the Uinta basin, and a compositional change in oil shale from illitic rich to dolomitic rich occurred in Lake Uinta in the depocenter of the Piceance basin. Halite (NaCl) and nahcolite (NaHCO_3) are present in oil shale in the Piceance basin but not in the Uinta basin. Marginal lacustrine rocks from this interval are generally included in the Douglas Creek or Anvil Points

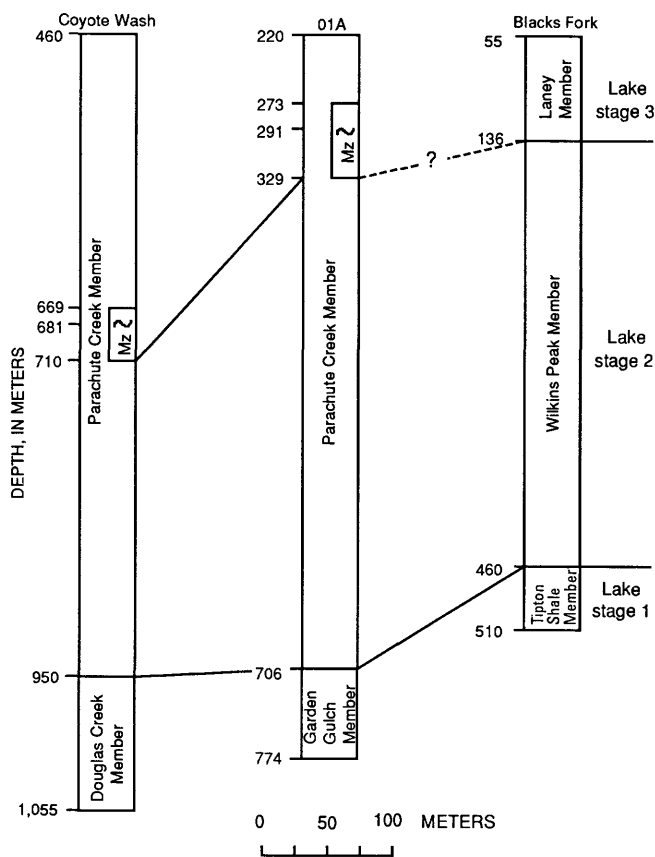


Figure 2. Stratigraphy of cores from depocenters of greater Green River (Blacks Fork), Piceance (01A), and Uinta (Coyote Wash) basins. Mz, Mahogany zone; [—] Mahogany bed. Location of core holes shown in figure 1.

Members and consist of carbonate-rich mudstone, sandstone, and stromatolitic and ostracodal limestone. The Eocene Wilkins Peak Member of the Green River Formation was deposited in the greater Green River basin about this time and consists of greenish-gray dolomitic marlstone and interbedded layers of mudstone, sandstone, oil shale, and volcanic ash. The Wilkins Peak Member is rich in the saline minerals shortite $[\text{Na}_2\text{Ca}_2(\text{CO}_3)_3]$, trona $[\text{Na}_3(\text{CO}_3)(\text{HCO}_3)\cdot 2\text{H}_2\text{O}]$, and halite. This saline deposition lasted 4–5 m.y. and is hereafter referred to as lake stage 2 (fig. 2).

Soon after the beginning of the middle Eocene, the lakes expanded. The Mahogany zone of the Parachute Creek Member in the Piceance and Uinta basins was deposited during this transgression. In the Piceance basin, the zone is made up of carbonate-rich, exceptionally organic carbon rich, laminated oil shale (for a description of sedimentary structures see Bradley, 1929, 1931). This unit contains the richest oil shale in the Green River Formation (shale oil yields average more than 125 L/tonne and some values are as high as 300 L/tonne; Trudell and others, 1970). Saline minerals are not present in this interval although cavities and brecciation formed by dissolution of salt-minerals have

been observed in the lower part of the interval (Bradley, 1931; Trudell and others, 1970; Dyni, 1981). Oil shale in the Uinta basin contains less organic matter (oil yields averaging 80 L/tonne; Cashion, 1967) than that in the Piceance basin and is interlayered with mudstone, siltstone, and sandstone. Johnson (1985) attributed the lower organic contents of the Uinta basin oil shale to dilution by clastic sediments. In the greater Green River basin, the Eocene Laney Member of the Green River Formation overlies the Wilkins Peak Member. The Laney Member was deposited in freshwater or near freshwater conditions; no saline minerals are reported in these rocks. Laterally extensive beds of moderately rich oil shale (averaging 40 L/tonne; Smith and others, 1968) are interbedded with buff to gray limestone, dolomitic limestone, siltstone, mudstone, and volcanoclastic sedimentary rocks. Deposition of the Mahogany zone in the Uinta and Piceance basins is tentatively correlated with deposition of the Laney Member in the greater Green River basin. The stage, hereafter referred to as lake stage 3 (fig. 2), lasted about 0.6 m.y. in the greater Green River basin and a little less than 2 m.y. in the Piceance basin.

Volcanoclastic sedimentation increased in the greater Green River basin toward the end of lake stage 3; the basin was filled, and Lake Gosiute was extinguished about 44 Ma (Mauger, 1977; Surdam and Stanley, 1979). After the end of Lake Gosiute, volcanoclastic wedges that prograded southward in the Piceance basin and intertongue with oil shale eventually filled this basin. Volcanoclastic sedimentation spread into the eastern part of the Uinta basin, but its depocenter was not filled (Johnson, 1985). Most of the part of Lake Uinta in the Uinta basin was filled about 41 Ma (Mauger, 1977); however, in the western part of the basin Lake Uinta persisted into the late Eocene when lacustrine shale, siltstone, sandstone and zones of saline minerals formed.

Genetic Models

Certain features of Lakes Uinta and Gosiute are common to all hypotheses regarding the genesis of the Green River Formation, including the extremely high pH of lake waters, sodium-carbonate-dominated brine chemistry, and high salinity, especially during lake stage 2. In addition, all models assume that the lakes occupied essentially closed basins (no outflow) during most of their history. These basins would have coalesced into one large closed basin when the lakes became connected from time to time (Bradley, 1929).

Actively debated genetic models for the Green River Formation include the playa-lake and stratified-lake models. The playa-lake model was originally proposed by Eugster and Surdam (1973) for the Eocene Tipton Shale and Wilkins Peak Members of the Green River Formation in the greater Green River basin in Wyoming. The depositional

model they proposed (p. 1120) was “***that of a vast alkaline earth playa fringing an alkaline lake...This puts the Green River rocks in direct genetic relationship with the marine tidal flats deposits of the sabkha type***” They stated that the best modern analog is a vastly expanded Deep Springs playa but without high sulfate content. Deep Springs playa, California, is a small playa (5 km²) that has a highly saline shallow lake in its center and precipitation of sodium chloride, sulfate, and carbonate salts around its perimeter.

The stratified-lake model was originally proposed by Bradley (1929, 1931) based on data from the Green River Formation in all three basins. Bradley proposed that minerals, including sodium carbonate minerals, were precipitated from the saline bottom waters of a “deep” stratified lake. He also suggested that during periods when the climate became drier, the waters in Lake Gosiute may have been quite shallow. Sedimentological and geochemical arguments supporting the stratified-lake model in the Piceance basin are presented in Smith (1974), Cole and Picard (1978), Desborough (1978), and Johnson (1981).

REFERENCES CITED

- Anders, D.E., and Gerrild, P.M., 1984, Hydrocarbon generation in lacustrine rocks of Tertiary age, Uinta Basin, Utah—Organic carbon, pyrolysis yield, and light hydrocarbons, *in* Woodward, J., Meissner, F.F., and Clayton, J.L., eds., Hydrocarbon source rocks of the greater Rocky Mountain Region: Denver, Rocky Mountain Association of Geologists, p. 513–529.
- Bradley, W.H., 1929, The varves and climate of the Green River epoch: U.S. Geological Survey Professional Paper 158–E, p. 87–110.
- _____, 1931, Origin and microfossils of the oil shale of the Green River Formation of Colorado and Utah: U.S. Geological Survey Professional Paper 168, 58 p.
- _____, 1964, Geology of the Green River Formation and associated Eocene rocks in southwestern Wyoming and adjacent parts of Colorado and Utah: U.S. Geological Survey Professional Paper 496–A, 86 p.
- _____, 1970, Green River oil shale—Concept of origin extended: Geological Society of America Bulletin, v. 81, p. 985–1000.
- _____, 1973, Oil shale formed in desert environment—Green River Formation, Wyoming: Geological Society of America Bulletin, v. 84, p. 1121–1124.
- Bradley, W.H., and Eugster, H.P., 1969, Geochemistry and paleolimnology of the trona deposits and associated authigenic minerals of the Green River Formation of Wyoming: U.S. Geological Survey Professional Paper 496–B, 71 p.
- Cashion, W.B., 1967, Geology and fuel resources of the Green River Formation, southeastern Uinta basin, Utah and Colorado: U.S. Geological Survey Professional Paper 548, 48 p.
- Cole, R.D., and Picard, M.D., 1978, Comparative mineralogy of nearshore and offshore lacustrine lithofacies, Parachute Creek Member of the Green River Formation, Piceance Creek Basin, Colorado, and eastern Uinta Basin, Utah: Geological Society of America Bulletin, v. 89, p. 1441–1454.
- Curry, H.D., 1964, Oil-content correlations of Green River oil shales, Uinta and Piceance Creek basins: Intermountain Association of Petroleum Geologists, 13th Annual Field Conference, Guidebook, p. 169–171.
- Desborough, G.A., 1978, A biogenic-chemical stratified lake model for the origin of oil shale of the Green River Formation—An alternative to the playa-lake model: Geological Society of America Bulletin, v. 89, p. 961–971.
- Dyni, J.R., 1974, Stratigraphy and nahcolite resources of the saline facies of the Green River Formation in northwest Colorado, *in* Murray, D.K., ed., Rocky Mountain Association of Geologists guide to the energy resources of the Piceance Creek basin, Colorado: Denver, Rocky Mountain Association of Geologists, p. 111–121.
- _____, 1981, Geology of the nahcolite deposits and associated oil shales of the Green River Formation in the Piceance Creek basin, Colorado: Boulder, University of Colorado, Ph.D. thesis, 144 p.
- _____, 1983, Distribution and origin of sulfur in Colorado oil shale, *in* Sixteenth Oil Shale Symposium proceedings: Golden, Colorado School of Mines, p. 144–159.
- Eugster, H.P., and Hardie, L.A., 1975, Sedimentation in an ancient playa-lake complex—The Wilkins Peak Member of the Green River Formation of Wyoming: Geological Society of America Bulletin, v. 86, p. 319–334.
- _____, 1978, Saline lakes, *in* Lerman, A., ed., Lakes—Chemistry, geology, physics: New York, Springer-Verlag, p. 237–294.
- Eugster, H.P., and Surdam, R.C., 1973, Depositional environment of the Green River Formation of Wyoming—A preliminary report: Geological Society of America Bulletin, v. 84, p. 1115–1120.
- Fouch, T.D., Lawton, T.F., Nichols, D.J., Cashion, W.B., and Cobban, W.A., 1983, Patterns and timing of synorogenic sedimentation in upper Cretaceous rocks of central and northeast Utah, *in* Reynolds, N.W., and Dolly, E.D., eds., Mesozoic paleogeography of west-central United States: Denver, Society of Economic Paleontologists and Mineralogists, p. 305–336.
- Franczyk, K.J., Fouch, T.D., Johnson, R.C., and Molenaar, C.M., *in press*, Cretaceous and Tertiary paleogeographic reconstructions for the Uinta-Piceance basin study area: U.S. Geological Survey Bulletin 1787–Q.
- Johnson, R.C., 1981, Stratigraphic evidence for a deep Eocene Lake Uinta, Piceance Creek basin, Colorado: Geology, v. 9, p. 55–62.
- _____, 1985, Early Cenozoic history of the Uinta and Piceance Creek basins, Utah and Colorado, with special reference to the development of Eocene Lake Uinta, *in* Flores, R.M., and Kaplan, S.S., eds., Cenozoic paleogeography of western United States: Denver, Society of Economic Paleontologists and Mineralogists, p. 247–276.
- King, P.B., 1977, The evolution of North America: New Jersey, Princeton University Press, p. 101–132.
- Mauger, R.L., 1977, K-Ar ages of biotites from tuffs in Eocene rocks of the Green River Formation, Piceance Creek basin, Colorado: Geology, v. 3, p. 493–497.

- Miesch, A.T., 1976, Sampling designs for geochemical surveys—Syllabus for a short course: U.S. Geological Survey Open-File Report 76-772, 128 p.
- National Petroleum Council, 1973, U.S. energy outlook—Oil shale availability: Oil Shale Task Group of the Other Energy Resources Subcommittee of the National Petroleum Council's Committee on U.S. Energy Outlook, A.E. Kelley, chairman., 87 p.
- Scott, R.W., Jr., and Pantea, M.P., 1982, Results of USGS oil-shale core drilling in eastern Uinta basin, Utah Coyote Wash-1 drill hole: U.S. Geological Survey Open-File Report 82-966, 58 p.
- Smith, J.W., 1974, Geochemistry of oil shale genesis in Colorado's Piceance Creek basin, *in* Guidebook to the energy resources of the Piceance Creek basin, Colorado: Rocky Mountain Association of Geologists, 25th Annual Field Conference, p. 71-79.
- Smith, J.W., Trudell, L.G., and Stanfield, K.E., 1968, Characteristics of Green River Formation oil shales at Bureau of Mines Wyoming Corehole No. 1: Bureau of Mines Report of Investigations 7172, 92 p.
- Smith, M.C., 1986, Bibliography of the geology of the Green River Formation, Colorado, Utah, and Wyoming, to July 1, 1986: U.S. Geological Survey Open-File Report 86-466, 81 p.
- Snyder, R.P., and Terry, S.S., 1977, Subsurface geology and structure in the vicinity of three drill holes in Piceance Creek basin, Rio Blanco County, Colorado: U.S. Geological Survey Open-File Report 77-271, 78 p.
- Stanley, K.O., and Collinson, J.W., 1979, Depositional history of Paleocene-lower Eocene Flagstaff limestone and coeval rocks, central Utah: American Association of Petroleum Geologists Bulletin, v. 63, p. 311-323.
- Sullivan, Raymond, 1985, Origin of lacustrine rocks of Wilkins Peak Member, Wyoming: American Association of Petroleum Geologists Bulletin, v. 69, p. 913-922.
- Surdam, R.C., and Stanley, K.O., 1979, Lacustrine sedimentation during the culminating phase of Eocene Lake Gosiute, Wyoming (Green River Formation): Geological Society of America Bulletin, v. 90, p. 93-110.
- Trudell, L.G., Beard, T. N., and Smith, J.W., 1970, Green River Formation lithology and oil shale correlations in the Piceance Creek Basin, Colorado: Bureau of Mines Report of Investigations 7357, 11 p.
- Tuttle, M.L., 1988, Geochemical evolution and depositional history of sediment in modern and ancient saline lakes—Evidence from sulfur geochemistry: Golden, Colorado School of Mines, Ph.D. thesis, 312 p.

APPENDIX—SAMPLE COLLECTION, PREPARATION, DESCRIPTIONS, AND ANALYSES

Samples for most of the studies described in the following chapters were collected from core from three wells, one in each of the three depositional basins of ancient Lakes Uinta and Gosiute (fig. 1). This sample distribution allows for comparison of depositional conditions within and among basins. The cores are from the centers of the basins and penetrate the three major depositional units referred to as lake stages 1 through 3. They comprise rocks from within each basin that are little affected by basin-margin processes. The lateral persistence of lithologically and geochemically distinct, laminated beds over many kilometers within each basin, and even between the Uinta and Piceance basins (Curry, 1964; Dyni, 1974, 1983; Johnson, 1985), indicates that samples from the three cores most likely are representative of rocks from each basin depocenter.

Sample Collection

The cores from which most of the samples used in these studies reported in this volume are the Energy Research and Development Administration Blacks Fork core no. 1 (BF), Green River basin, Wyoming; U.S. Bureau of Mines core 01A (01A), Piceance basin, Colorado; and U.S. Geological Survey Coyote Wash no. 1 core (CW), Uinta basin, Utah (locations shown in fig. 1). All of the cores are stored at the U.S. Geological Survey Core Research Center, Lakewood, Colorado. The Blacks Fork core was described by L.G. Trudell of the Laramie Energy Research Center (written commun., 1983), the 01A core by Snyder and Terry (1977), and the Coyote Wash core by Scott and Pantea (1982). Geologic sections of the cores are shown in figure 2. The three cores represent sediment deposited during 14 of the 21 m.y. of the Green River lake system (Tuttle, 1988).

Hierarchical, unbalanced analysis of variance sampling designs (Miesch, 1976) allowed for objective sampling and optimal coverage of the cores given the limitations on the number of samples that could be

analyzed. Samples from the Piceance basin 01A core were collected for the major- and trace-element chemistry study using a design that divided the core into 30.5-m sections; within every other 3.5-m section in the 30.5-m section, two sample intervals were chosen; 20 percent of the ground samples were split for analytical duplication. A total of 190 samples were analyzed in this study. For most of the other studies the cores were divided into sections 18 m long. One sample was collected approximately 15 m from the top of each cored section; a second sample was collected 6 m from the top of about 40 percent of the sections; 10 percent of the samples were split after grinding for analytical duplication. Thirty-five samples were collected from the Blacks Fork core, 41 from the 01A core (a subset of those collected for the major- and trace-element chemistry study), and 39 from the Coyote Wash core. Each sample was about 3 cm long and lithologically homogeneous. Because some Green River depositional rates were very slow (0.04 mm/yr for organic-carbon-rich oil shale to 0.17 mm/yr for organic-carbon-poor marlstone; Bradley, 1929), each sample represents a depositional time span on the order of hundreds of years.

Sample Descriptions, Preparation, and Analyses

The presence of visible sulfide minerals, organic material, tuffaceous material, and laminations and the sample color and grain size were noted in the 01A subset, Coyote Wash, and Blacks Fork samples prior to any further treatment. Descriptions are given in table A1. The samples were described as being calcareous if they reacted vigorously with 10 volume percent HCl and dolomitic if they reacted slowly with HCl. Before grinding, a plug was removed from the sample for thin-section preparation. Samples were then ground with ceramic plates to pass a 115-mesh screen (130- μ m mean diameter) and splits for each study removed.

The whole-rock mineral composition for each sample was determined on a random powder mount using an X-ray diffractometer with nickel-filtered $\text{CuK}\alpha$ radiation. The mineral analyses are qualitative because standards were not run with the samples. X-ray diffraction results are presented in table A1.

Table A1. Macroscopic descriptions and X-ray diffraction mineralogy for 35 samples from the Blacks Fork core no. 1, Wyoming, 41 samples from the 01A core, Colorado, and 39 samples from the Coyote Wash no.1 core, Utah [Abbreviations used in the table are explained below. X-ray mineralogy is listed in order of frequency, not abundance. Core holes: BF, Blacks Fork no. 1; 01, 01A; CW, Coyote Wash]

Abbreviations									
anal	analcime			f	faint	org	organic matter rich		
appt	apatite			f-gr	fine grained	ost	ostracods		
arag	aragonite			fos	fossiliferous	po	pyrrhotite		
b	bladed			grn	green	py	pyrite		
brec	brecciated			gy	gray	qtz	quartz		
brn	brown			hlit	halite	rd	red		
c	continuous laminae			horn	hornblende	sh	shortite		
cal	calcareous			ill	illite	sid	siderite		
calc	calcite			inter	interbedded	sltst	siltstone		
cly	clay (other than illite)			Kfld	potassium feldspar	slty	silty		
cr-gr	coarse grained			l	lens	ss	sandstone		
d	disseminated			lam	laminated	sul	sulfides		
daw	dawsonite			lt	light	tr	trona		
dc	discontinuous laminae			m	medium	tuf	tuffaceous		
dk	dark			mdst	mudstone	v	vuggy		
dol	dolomitic			musc	muscovite	X	trait present		
dolo	dolomite			Nafld	sodium feldspar				
ds	distinct			nahc	nahcolite				
Sample	Depth (meters)	Sample description					Color, grain size	Mineralogy	
		sul	org	cal	dol	tuf			lam
BLACKS FORK CORE NO. 1, GREATER GREEN RIVER BASIN, WYOMING									
Lake stage 3									
BF-1	63	d			X	X	lt gy sltst to f-gr ss	qtz,calc,dolo,Kfld,Nafld,anal,py,ill	
BF-2	70	d	X	X			ds,c dk brn mdst	qtz,calc,dolo,Kfld,anal,py,ill	
BF-3	91	d,l	X	X		X	f,c m brn mdst	qtz,calc,dolo,Kfld,anal,py,ill	
BF-4	98		X		X	X	ds,dc m grn to m brn mdst	qtz,calc,dolo,Kfld,anal,ill,cly	
BF-5	107		X		X		f,c lt brn mdst	qtz,calc,dolo,Kfld	
BF-6	125	d				X	ds,dc lt-m gy sltst	qtz,calc,Kfld,anal,py,cly	
BF-7	135	d,l	X	X			ds,c m-dk gy-brn mdst	qtz,calc,dolo,Nafld,anal,py	
Lake stage 2									
BF-8	144	d,b		X			dk grn mdst to sltst	qtz,dolo,Kfld,sh,po	
BF-9	162	d	X		X		m-dk brn mdst	qtz,dolo,Nafld,sh,py	
BF-10	180	d	X		X		dk brn mdst	qtz,dolo,sh,py	
BF-11	189			X			m grn to gy mdst	qtz,dolo,Kfld,Nafld,sh,ill	
BF-12	199	d		X			m grn to gy mdst	qtz,calc,dolo,Kfld,Nafld,sh,py,po,ill	
BF-13	217	d		X			m grn mdst	qtz,dolo,Nafld,sh,py,ill,cly	
BF-14	235		X	X			m to dk brn mdst	qtz,calc,dolo,Nafld,anal,sh,ill,cly	
BF-15	244		X	X			lt to dk brn mdst	qtz,dolo,Nafld,sh	
BF-16	254	d,l				X	d-c d-dc m grn mdst to m br to grn sltst	qtz,calc,dolo,Kfld,Nafld,anal,ill,cly	
BF-17	272			X			m grn mdst	qtz,calc,dolo,Kfld,Nafld,anal,ill,cly	
BF-18	290			X			dk grn mdst	qtz,calc,dolo,Kfld,Nafld,anal,ill,cly	
BF-19	299		X	X			f-c m brn to grn mdst	qtz,calc,dolo,Nafld,ill	
BF-20	309					X	grn slty mdst	qtz,calc,Nafld,anal,ill,cly	
BF-21	333	d	X		X		d-c m brn to grn mdst	qtz,dolo,Kfld,Nafld,sh,py,ill	

Table A1. Continued

Sample	Depth (meters)	Sample description						Color, grain size	Mineralogy
		sul	org	cal	dol	tuf	lam		
Lake stage 2—Continued									
BF-22	344			X				m grn to gy mdst	qtz,dolo,sh,tr
BF-23	353		X	X			f-c	m grn to brn mdst	qtz,dolo,Nafld,anal,cly
BF-24	363		X	X			d-c	dk brn mdst	qtz,dolo,Nafld,sh,ill
BF-25	381	d		X		X		m grn mdst to m gy slty mdst	qtz,dolo,Kfld,Nafld,sh,tr,py
BF-26	400			X				lt grn mdst	qtz,dolo,Nafld,sh,cly
BF-27	409			X				m grn to gy slty mdst	qtz,dolo,Kfld,Nafld,sh,ill,cly
BF-28	418			X				m grn to gy slty mdst	qtz,dolo,Kfld,Nafld,sh,ill,cly
BF-29	437	d,l		X				m grn mdst	qtz,dolo,Kfld,Nafld,sh,py,ill
BF-30	454	d,b		X		X		lt grn to gy slty mdst	qtz,calc,dolo,Kfld,Nafld,anal,py,po,ill,cly
Lake stage 1									
BF-31	464	d,l	X	X		X	f-dc	lt brn mdst	qtz,calc,dolo,Kfld,Nafld,anal,py,ill
BF-32	473	d,l	X		X	X	d-c	dk brn mdst	qtz,calc,dolo,Kfld,anal,py,ill
BF-33	491	d	X	X			d-c	dk gy to brn mdst	qtz,calc,dolo,Nafld,sid,py,ill,cly
BF-34	500	d,l	X		X	X	d-c	dk brn ost mdst	qtz,calc,dolo,Kfld,anal,py,ill, cly
BF-35	509	d	X	X				dk brn fos mdst	qtz,calc,arag,Nafld,py,cly
01A CORE, PICEANCE BASIN, COLORADO									
Lake stage 3									
01-6	268		X		X		ds,c	dk brn mdst	qtz,calc,arag,dolo,Nafld,anal,cly
01-8	272		X		X		ds,c	lt brn mdst	qtz,dolo,Kfld,daw,cly
01-12	285		X		X		ds,c	m brn mdst	qtz,dolo,Kfld,Nafld,daw,py,cly
01-14	290		X		X	X	ds,c	dk brn mdst	qtz,calc,dolo,Kfld,Nafld,daw,py,cly
01-18	304		X	X			ds,c	dk brn mdst	qtz,calc,dolo,Kfld,Nafld,anal,py,cly
01-24	321	d	X	X			f,dc	m brn mdst, v	qtz,calc,dolo,Kfld,Nafld,anal,ill,cly
01-26	328	d	X	X			f,dc	lt to m brn mdst, v	qtz,calc,dolo,Kfld,Nafld,cly
Lake stage 2									
01-30	340	d	X		X	X	ds,c	m brn mdst	qtz,calc,dolo,Kfld,Nafld,cly
01-36	358		X		X		ds,c	dk brn mdst	qtz,calc,dolo,Kfld,Nafld,ill
01-42	378	d	X		X		ds,c	m brn mdst	qtz,dolo,Kfld,Nfld,anal,ill,cly
01-48	395	d	X		X			brec lt brn mdst	qtz,dolo,Kfld,Nafld,py,cly
01-54	415	d	X		X		f,c	dk brn mdst	qtz,dolo,Kfld,Nafld,anal,py,ill
01-59	429	d,b	X	X				inter m brn mdst and nahc	qtz,dolo,Kfld,Nafld,anal,daw,nahc, py,ill,cly
01-62	437		X	X				inter dk brn mdst	qtz,calc,dolo,Nafld,nahc,hlit
01-65	448	d,l	X	X			ds,cd	lt brn mdst	qtz,dolo,Kfld,Nafld,daw,nahc,py,cly
01-72	468	d	X	X			ds,dc	m brn mdst	qtz,calc,dolo,Kfld,Nafld,daw,nahc,py
01-74	474	l	X	X		X	ds,dc	m brn mdst	qtz,calc,dolo,Kfld,Nafld,daw,nahc,py,cly
01-78	486	d	X		X		ds,dc	dk brn mdst	qtz,dolo,Kfld,Nafld,daw,py,cly
01-84	504		X	X			ds,dc	dk brn mdst, bedded hlit, nahc	qtz,calc,dolo,Nafld,daw,nahc,hlit,cly

Table A1. Continued

Sample	Depth (meters)	Sample description						Color, grain size	Mineralogy
		sul	org	cal	dol	tuf	lam		
Lake stage 2—Continued									
01-86	510	d	X	X				dk brn mdst	qtz,dolo,Kfld,Nafld,daw,nahc,hlit,py,cly
01-89	521	d		X			ds,c	f-gr nahc, lt brn mdst	qtz,dolo,Nafld,daw,nahc,hlit, ill, cly
01-96	541		X		X		ds,c	dk brn mdst	qtz,dolo,Kfld,Nafld,daw,py,cly
01-98	547	l	X		X			dk brn mdst	qtz,dolo,Kfld,Nafld,daw,py,cly
01-102	559	d,l	X		X		ds,dc	dk brn mdst	qtz,dolo,Kfld,daw,py,cly
01-108	578		X	X			ds,dc	lt to m brn mdst	qtz,calc,dolo,Kfld,daw,py
01-110	583	d	X	X				dk brn mdst and cr-gr nahc	qtz,dolo,nahc,ill,cly
01-113	595	l	X		X			dk brn mdst	qtz,dolo,Kfld,Nafld,daw,py,cly
01-120	614		X	X				cr-gr nahc, dk brn mdst	qtz,dolo,Kfld,Nafld,daw,nahc,ill
01-123	625	d	X		X		ds,c	dk brn mdst	qtz,dolo,Kfld,Nafld,daw,py
01-126	632			X				cr-gr nahc	qtz,daw,nahc,ill,cly
01-132	651		X	X			ds,c	inter nahc, m brn mdst	qtz,dolo,Kfld,Nafld,daw,nahc,cly
01-134	657	d	X	X				dk brn mdst	qtz,calc,dolo,Kfld,Nafld,daw, nahc,py,cly
01-138	669		X		X			lt brn mdst	qtz,dolo,Kfld,Nafld,daw,py,cly
01-144	687	d	X	X				m brn mdst and cr-gr nahc	qtz,dolo,Kfld,Nafld,nahc,py,cly
Lake stage 1									
01-150	705		X	X			ds,c	dk brn to gy mdst	qtz,calc,dolo,Nafld,py,ill
01-154	717		X	X			ds,c	dk brn mdst	qtz,dolo,Nafld,py,ill
01-155	728	l	X	X			ds,c	dk brn to gy mdst	qtz,dolo,Nafld,py,ill,
01-162	743		X	X				dk gy to brn mdst	qtz,dolo,Kfld,Nafld,py,ill,cly, aplt
01-165	755	d	X		X		f,c	dk brn mdst	qtz,dolo,Nafld,py,ill,cly
01-168	760		X	X			ds,c	m gy to brn ost mdst	qtz,calc,dolo,py,ill
01-172	773		X		X		f,c	m gy to brn mdst	qtz,dolo,Nafld,py,ill
COYOTE WASH NO. 1 CORE, UINTA BASIN, UTAH									
Lake stage 3									
CW-38	571	d	X		X		ds,c	lt to m brn mdst	qtz,calc,dolo,Nafld,sid
CW-37	587	d	X		X		ds,c	m brn mdst	qtz,calc,dolo,Nafld,ill
CW-36	597		X		X		ds,c	m to dk brn mdst	qtz,calc,dolo,Kfld,Nafld,sid,ill
CW-35	606	d	X	X		X	ds,c	m to dk brn mdst	qtz,calc,dolo,Nafld
CW-34	624	d	X		X		ds,c	dk brn mdst	qtz,calc,dolo,Nafld,daw,sid,py, ill
CW-33	642	d	X		X	X	ds,c	m rd, m brn mdst	qtz,calc,dolo,Kfld,Nafld,daw,py
CW-32	652	d	X		X	X	f,dc	m to dk brn mdst	qtz,calc,dolo,Nafld,daw,py,cly
CW-31	661	d	X	X			f,dc	m to dk brn mdst	qtz,calc,dolo,Kfld,Nafld,daw,py
CW-30	670		X		X		ds,dc	m brn mdst	qtz,calc,dolo,Nafld,daw,sid
CW-29	681	l	X		X	X	ds,dc	dk brn mdst (Mahogany bed)	qtz,calc,dolo,Nafld,daw,py
Lake stage 2									
CW-28	697		X	X				lt brn mdst	qtz,calc,dolo,Kfld,Nafld,anal,ill
CW-27	706	d	X		X		ds,c	m to dk brn mdst	qtz,calc,dolo,Kfld,Nafld,anal,ill
CW-26	716		X		X		ds,c	lt to m brn mdst	qtz,calc,dolo,Nafld
CW-25	726	d	X		X		ds,dc	lt brn mdst	qtz,calc,dolo,Kfld,Nafld,anal, daw,ill
CW-24	734	d	X		X		ds,c	lt to m brn mdst	qtz,calc,dolo,Kfld,Nafld,daw
CW-23	752	d	X		X		ds,c	m brn mdst	qtz,calc,dolo,Kfld,Nafld,anal, sid,py

Table A1. Continued

Sample	Depth (meters)	Sample description					Color, grain size	Mineralogy
		sul	org	cal	dol	tuf		
Lake stage 2—Continued								
CW-22	762		X	X			lt brn mdst	qtz,calc,dolo,Kfld,Nafl,daw
CW-21	771	d,b	X		X		m brn mdst	qtz,calc,dolo,Kfld,Nafl,anal, daw,sid,ill
CW-20	789	d	X		X	ds,c	m brn mdst	qtz,dol,Kfld,Nafl,anal,ill
CW-19	807	d	X		X	f,c	lt gy mdst	qtz,calc,dolo,Kfld,Nafl,daw, muscl,ill
CW-18	815	d,b	X		X	ds,c	lt to m brn mdst	qtz,calc,dolo,Kfld,Nafl,anal,ill
CW-17	825		X	X		ds,c	lt to m brn mdst	qtz,calc,dolo,Kfld,anal,ill,cly
CW-16	843	d	X		X	ds,dc	m to dk brn mdst	qtz,calc,dolo,Kfld,Nafl,anal,py, ill,cly
CW-15	862		X		X	ds,c	lt grn, gy mdst	qtz,calc,dolo,Kfld,Nafl,anal, horn,ill,cly
CW-14	871	d	X		X	ds,c	lt to m brn mdst	qtz,calc,dolo,Kfld,Nafl,anal,ill, cly
CW-13	880	d,l	X		X	f,dc	dk brn mdst	qtz,dolo,Kfld,anal,py,ill
CW-12	898		X		X	ds,dc	lt to m brn ost mdst	qtz,calc,dolo,Kfld,Nafl,anal,ill
CW-11	908		X		X	ds,c	m gr to brn mdst	qtz,calc,dolo,Kfld,Nafl,anal,ill
CW-10	917	d	X	X		ds,dc	m gr to m brn mdst	qtz,calc,dolo,Kfld,Nafl,anal, py,ill,cly
CW-9	926			X			m gr mdst	qtz,calc,dolo,Kfld,Nafl,anal, ill,cly
CW-8	935	d			X		dk grn gy slty mdst	qtz,calc,dolo,Kfld,Nafl,anal, py,ill,cly
Lake stage 1								
CW-7	953				X		m brn to gy mdst	qtz,calc,dolo,Kfld,Nafl,anal,ill, cly
CW-6	971	d		X		ds,c	m to lt gy slty mdst	qtz,calc,dolo,Kfld,Nafl,anal,py, ill,cly
CW-5a	981			X			m gy slty mdst	qtz,calc,dolo,Kfld,Nafl,anal,sid, ill,cly
CW-5	990		X	X		ds,dc	m brn mdst	qtz,calc,dolo,Kfld,Nafl,anal,ill, cly
CW-4	1,008			X			lt gy sltst	qtz,calc,dolo,Kfld,Nafl,anal,ill
CW-3	1,026		X	X		ds,c	m brn mdst	qtz,calc,dolo,arag,Nafl,ill,cly
CW-2	1,035			X		X	m gy brn mdst to sltst	qtz,calc,dolo,Kfld,Nafl,anal,sid, ill,cly
CW-1	1,043	d	X		X	f,dc	dk to m brn mdst	qtz,dolo,Kfld,Nafl,anal,py,cly

Chapter B

Sulfur Geochemistry and Isotopy of the Green River Formation, Wyoming, Utah, and Colorado

By MICHELE L. TUTTLE and MARTIN B. GOLDBER

U.S. GEOLOGICAL SURVEY BULLETIN 1973

GEOCHEMICAL, BIOGEOCHEMICAL, AND SEDIMENTOLOGICAL STUDIES OF THE
GREEN RIVER FORMATION, WYOMING, UTAH, AND COLORADO

CONTENTS

Abstract	B1
Introduction	B1
Sulfur in the Green River Formation	B1
Methods	B3
Sampling methods	B3
Analytical methods	B3
Results	B4
Discussion	B5
Sulfate and its reduction in Lakes Uinta and Gosiute	B5
Sulfidization products	B10
Sulfur geochemistry of Lakes Uinta and Gosiute	B11
Applications to geologic problems	B12
References cited	B13
Appendix 1—Analytical data	B15
Appendix 2—Calculation of gypsum thickness	B20

FIGURES

1. Map showing extent of rocks of Green River Formation and location of cores used in study **B2**
2. Diagram showing method used to collect and analyze forms of sulfur **B4**
3. Depth profiles for total sulfur and $\delta^{34}\text{S}$ values of disulfides in depocenter cores **B5**
4. Rayleigh fractionation plot and frequency histogram for $\delta^{34}\text{S}$ values of disulfides in depocenter cores **B7**
- 5–6. Graphs showing:
 5. Regression lines for sulfur in sulfide minerals versus organic carbon for marine, freshwater, and euxinic sediments and for rocks of Green River Formation **B9**
 6. $\delta^{34}\text{S}$ values of organosulfur versus disulfide sulfur **B10**
- 7–8. Charts summarizing sulfur geochemistry of the Green River Formation during:
 7. Euxinic deposition **B11**
 8. Shallow deposition **B11**
9. Diagram showing mean $\delta^{34}\text{S}$ values in Green River Formation during each lake stage **B12**

TABLES

1. Summary of lake stages represented by samples in this study **B3**
2. Average chemical and isotopic parameters for samples from the three lake stages in the Green River Formation **B6**
3. Dissolved water-column sulfate, sediment sulfur concentrations, and $\delta^{34}\text{S}_{\text{disulfide}}$ values in samples from the Green River Formation and other lacustrine environments **B8**

Sulfur Geochemistry and Isotopy of the Green River Formation, Wyoming, Utah, and Colorado

By Michele L. Tuttle and Martin B. Goldhaber

Abstract

Sulfur geochemistry was used to gain insight into conditions during deposition and diagenesis of the lacustrine Green River Formation (Paleogene). The abundance and isotopic composition of major forms of sulfur (sulfate, monosulfides, disulfides, and organosulfur) in samples from three cores indicate that during the time represented by the sampled core interval (about 8 m.y.) the two ancient Green River lakes (Lakes Uinta and Gosiute) intermittently had similar depositional conditions.

Both lakes received a continuous supply of sulfur, most of which was supplied by inflow. An intermittent source of sulfur was associated with volcanic ash. This volcanic sulfur was depleted in ^{34}S relative to the sulfur reservoir in the lakes, and its isotopic signature is particularly evident in the samples deposited during the low stands of Lake Gosiute (shallow deposition).

The enrichment of ^{34}S in sulfide minerals and organic matter in the Green River Formation supports the concept of reduction of sulfate to hydrogen sulfide (H_2S) in anoxic lake bottom water (monimolimnion) or in anoxic pore water. During periods of stratification, the H_2S :sulfate ratio of the monimolimnion was high. Throughout the saline stage of Lake Uinta, long-term stratification resulted in the progressive enrichment of ^{34}S in the H_2S reservoir. During the same period in Lake Gosiute, progressive enrichment did not occur and $\delta^{34}\text{S}$ values in rocks deposited during this time are highly variable. In both lakes, the high pH of the pore water likely promoted sulfidization of organic matter and kinetically inhibited sulfidization of iron.

These results support the hypotheses that a connection existed between the two Green River lakes coincident with progressive infilling of the basins; that pH affects the sulfidization of organic matter and iron; that sulfidization of organic matter affects the sulfur content of hydrocarbons generated from lacustrine source rocks; and that existing sulfur models and paleosalinity indicators may not be applicable for ancient lacustrine rocks.

INTRODUCTION

Rocks of the Paleogene (Eocene and locally Paleocene) Green River Formation accumulated in two large lakes (fig. 1): Lake Gosiute in the greater Green River basin (southern Wyoming) and Lake Uinta in the Piceance (northwestern Colorado) and Uinta basins (northeastern Utah). Sulfur geochemistry has been used extensively to interpret deposition and diagenesis in marine and freshwater-lacustrine rocks because of the sensitivity of sulfur abundance, residence, and isotopic composition to chemical and biological changes. An investigation of sulfur geochemistry of the Green River Formation therefore should increase our understanding of the overall geochemical and biogeochemical conditions controlling the accumulation and preservation of Green River sediments.

Acknowledgments.—This chapter has benefited greatly from the thorough reviews of Linda Bonnell and Paul Lillis. We wish to thank Robert Rye, U.S. Geological Survey, for access to his isotope laboratory. This work was conducted as part of the U. S. Geological Survey Evolution of Sedimentary Basins Program.

SULFUR IN THE GREEN RIVER FORMATION

Most published sulfur data on the Green River Formation are from rocks in the Uinta and Piceance basins. Reported concentrations of total sulfur range from 0 weight percent in algal carbonate rocks in the Uinta basin, Utah (Boyer and Cole, 1983), to 5 weight percent in organic-carbon-rich shale from the saline zone in the Piceance basin, Colorado (Dyni, 1983). The sulfur is known to be present as sulfate, monosulfide, and disulfide minerals, as well as organosulfur. Primary sulfate minerals have not been identified in the formation (Milton and Eugster, 1959); the

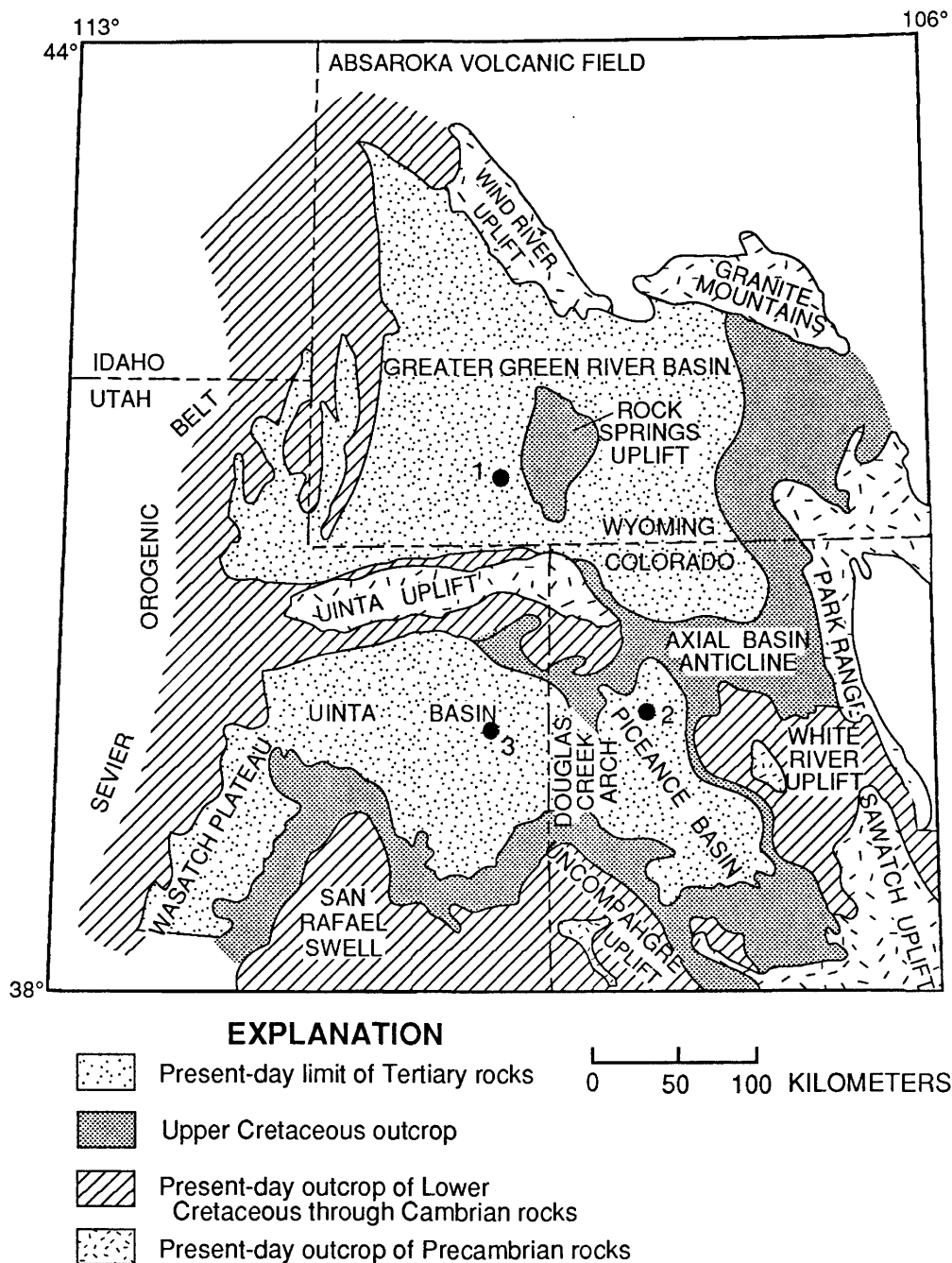


Figure 1. Map showing extent of rocks of Green River Formation (Tertiary rocks) and location of cores used in study. Core holes (solid circles): 1, Blacks Fork core; 2, 01A core; and 3, Coyote Wash core. Modified from Johnson (1985).

abundance of sulfate accounts for less than 4 percent of the total sulfur (Stanfield and others, 1951; Smith and others, 1964). Monosulfide minerals (pyrrhotite and wurtzite) and disulfide minerals (pyrite and marcasite) have been described by Milton and Eugster (1959), Pabst (1970), Cole and others (1978), Cole and Picard (1981), and Melchior and others (1982); monosulfides are reported to be minor

sulfur phases. According to Stanfield and others (1951) and Smith and Young (1983), 50–90 percent of the sulfur in most Green River oil shale is in pyrite and the remaining 10–50 percent is as organosulfur. Sulfur-containing organic compounds in the Green River oil shale include thiophenes, benzothiophenes, and polycyclic thiols (Ingram and others, 1983).

Table 1. Summary of lake stages 1, 2 (2B in the Green River basin), and 3 represented by samples in this study [Samples are from the Blacks Fork core no. 1 (BF), greater Green River basin, Wyoming; 01A core (01A), Piceance basin, Colorado; Coyote Wash no. 1 core (CW), Uinta basin, Utah. Number of samples in parentheses is number of samples for which sulfur forms and their isotopic compositions were analyzed]

Lake stage	Green River basin	Greater Piceance basin	Uinta basin
1	Fresh water	Moderate salinity	Fresh water
	Transgression	Transgression	Transgression
	High productivity	Low productivity	Low productivity
	Organics preserved	Organics preserved	Lake-margin facies
	Open-water facies	Open-water facies	
Number of samples	5 (5)	7 (4)	8 (4)
2	High salinity	High salinity	High salinity
	Regression	Regression	Regression
	Low productivity	High productivity	Moderate productivity
	Organics mineralized	Organics preserved	Organics preserved
	Shallow-water facies	Open-water facies	Open-water facies
Number of samples	23 (23)	27 (11)	21 (15)
3	Fresh water	Moderate-high salinity	Low-moderate salinity
	Transgression	Transgression	Transgression
	High productivity	High productivity	High productivity
	Organics preserved	Organics preserved	Organics preserved
	Open-water facies	Open-water facies	Open-water facies
Number of samples	7 (7)	7 (5)	10 (6)

METHODS

Sampling Methods

The sampling design, cores, and samples used in this study are described in the appendix in Tuttle (this volume). A suite of 115 samples from the three Green River depositional basins was analyzed—35 samples from the Blacks Fork core, greater Green River basin, Wyoming; 41 from the 01A core, Piceance basin, Colorado; and 39 from the Coyote Wash core, Uinta basin, Utah (fig. 1).

The sample suite represents continuous lacustrine deposition during three major evolutionary stages of the lakes during the Eocene. These stages and their associated rock types are discussed in detail in Tuttle (this volume) and summarized in table 1. The first stage (lake stage 1) represents freshwater to brackish-water deposition during early expansion of the lakes. Lake stage 2 was a very saline stage during which the areal extent of Lake Uinta changed little (Johnson, 1985) but that of Lake Gosiute drastically decreased (Bradley, 1973; Eugster and Hardie, 1975). Salinity increases were probably initiated by a regional climatic shift to more arid conditions (Sullivan, 1985). During lake stage 3, the lakes expanded again. Lake Gosiute became a freshwater lake and Lake Uinta became less

saline, probably brackish. During this stage, the richest Green River oil shales were deposited in Lake Uinta.

Analytical Methods

All 115 samples were analyzed for total sulfur, organic and carbonate carbon, and total iron. Seventy-nine of the samples were analyzed for HCl-soluble iron (used to calculate reactive iron concentrations). These last four variables were determined because of the importance of organic carbon on sulfate reduction, carbonate carbon on dilution of iron and sulfur in rocks, and iron species on sulfur processes in sediment. Sulfate, monosulfide sulfur (acid-volatile sulfur), disulfide sulfur, organosulfur, and their isotopic compositions were analyzed in 79 of the samples. The analytical techniques are detailed in Tuttle and others (1986) and Tuttle (1988).

Samples ground to pass a 115-mesh screen (130 μm) were used in all analytical procedures. Concentrations of total sulfur, carbonate carbon, and organic carbon were measured using a commercially available apparatus consisting of an induction furnace coupled to an infrared detection system (sulfur) and thermal conductivity cell (carbon). Total iron concentrations were determined by fusing the sample with lithium metaborate (Ingamells,

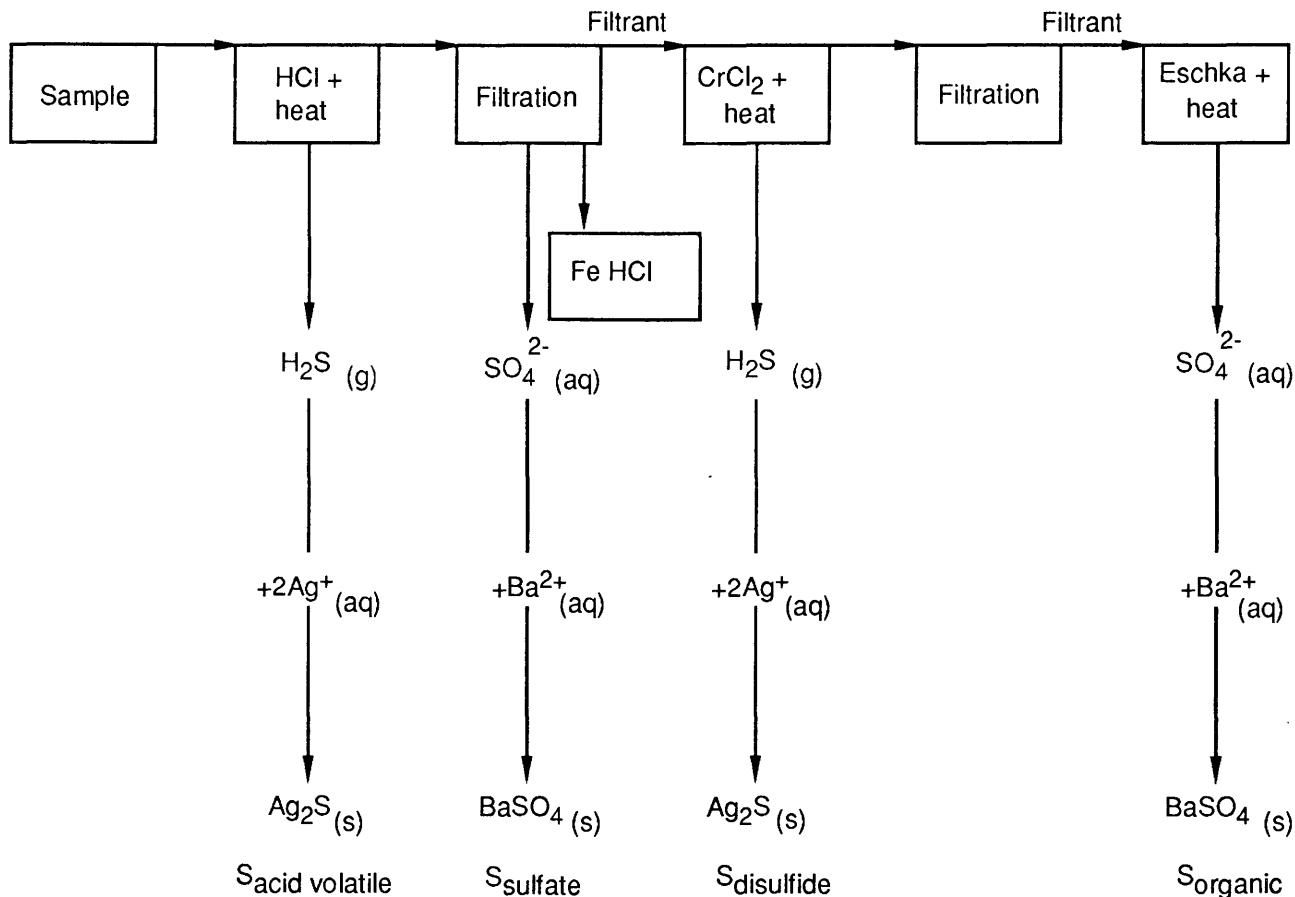


Figure 2. Method used to collect and analyze forms of sulfur. Modified from Tuttle and others (1986).

1970) and dissolving the fusion product in 10 volume percent HCl. Both total iron and HCl-soluble iron (see procedure below) were measured using flame atomic absorption spectrometry. Sulfur species were sequentially collected and gravimetrically analyzed by the separation scheme described in Tuttle and others (1986) and summarized in figure 2. The scheme removes monosulfide sulfur as H_2S gas with hot 6N HCl while solubilizing the sulfate sulfur and reactive iron not bound in disulfides; it reduces and removes disulfide sulfur as H_2S gas with a hot Cr^{2+} -HCl solution; and it collects all residual sulfur (defined as organosulfur) using an Eschka-fusion procedure. Sulfur products from the separation are converted to SO_2 , which is then isotopically analyzed using mass spectrometry. All isotope results are reported relative to the troilite phase of the Cañon Diablo meteorite (CDT standard).

RESULTS

Chemical (dry-weight basis) and sulfur isotopic data are tabulated in appendix 1. Because key geochemical relationships can be obscured by the dilution effect that

authigenic carbonate minerals may have on other element abundances, carbonate-free chemical data are used hereafter. Averages of chemical (carbonate-free basis) and isotopic data for each lake stage in each basin are shown in table 2. In the greater Green River basin core, three samples in lake stage 2 strongly resemble (both geochemically and physically) those in stages 1 and 3. These samples are interpreted to represent fresher water conditions (transgressive stages, lake stage 2A) than those inferred for other stage 2 samples from the core (shallow stages, lake stage 2B).

Depth profiles for total sulfur (weight percent) and $\delta^{34}\text{S}$ (‰, per mil) of disulfides are presented in figure 3. The abundance of sulfur in Piceance basin samples exhibits no apparent trend with time, and values cluster around 1 weight percent. Similarly, the abundance of sulfur in Uinta basin samples shows no time-dependent trends, and values of about 0.5 weight percent are about half those of Piceance basin samples. In contrast, the abundance of sulfur in the greater Green River basin shows a distinct trend with time: abundances are significantly lower in lake stage 2B relative to stages 1 and 3. In the lower part of lake stage 2, one sample from each basin has a very high sulfur content (fig.

3). Although the significance of these anomalies is not known, the samples most likely represent an event that affected the entire Green River lake system.

The predominant sulfur species in most of the Green River samples is iron disulfide (pyrite and less frequently marcasite) (Tuttle, this volume). All disulfide minerals are enriched in ^{34}S relative to the CDT standard (fig. 3, table 2); in many samples, this enrichment is very large. The depth profile of $\delta^{34}\text{S}$ values in Lake Uinta stage 2 disulfides shows that the sediments incorporated progressively more ^{34}S with time. The $\delta^{34}\text{S}$ values for stage 2 of Lake Gosiute are likewise enriched in ^{34}S but show no systematic enrichment with decreasing depth. Instead, ^{34}S -depleted values occur near ash layers. ^{34}S -depleted values are present in the late portion of stage 2 in the greater Green River basin and in the early portion of stage 3 in the Piceance and Uinta basin. The magnitude of this depletion decreases from the greater Green River basin to the Piceance basin and from the Piceance basin to the Uinta basin.

DISCUSSION

The hundreds of meters of lithologically and mineralogically similar lacustrine rocks indicate that in their depositional centers Lakes Uinta and Gosiute were continuous bodies of water through time. Similar stages of geochemical evolution occurred within each lake: a saline stage 2 bracketed by two expansive, fresher water stages 1 and 3. Stage 1 and much of stage 2 are time correlative between the two lakes; however, the time relationship between stage 3 of Lakes Uinta and Gosiute is less certain (R.C. Johnson, written commun., 1989). Sulfur chemical and isotopic data from our study indicate that (1) although the lakes were indeed similar in many aspects, key differences are observed, and (2) the geochemistry of the lakes slowly evolved during the 5.1–8 m.y. intervals of the three lake stages.

Sulfate and Its Reduction in Lakes Uinta and Gosiute

Sulfate-bearing saline minerals are rarely found in Green River rocks, although nonsulfate saline minerals are common at certain stage 2 horizons. The paucity of sulfate-saline minerals has been attributed to low sulfate in lake water in which brine evolution results in a sulfate-poor, sodium-bicarbonate-rich water (Eugster and Hardie, 1975, 1978). This hypothesis, however, is not supported by sulfur abundances in Green River sedimentary rocks; the rocks deposited in basin depocenters contain more sulfur than sediment deposited in sulfate-rich environments such as the oceans and sulfate-rich saline lakes (table 3).

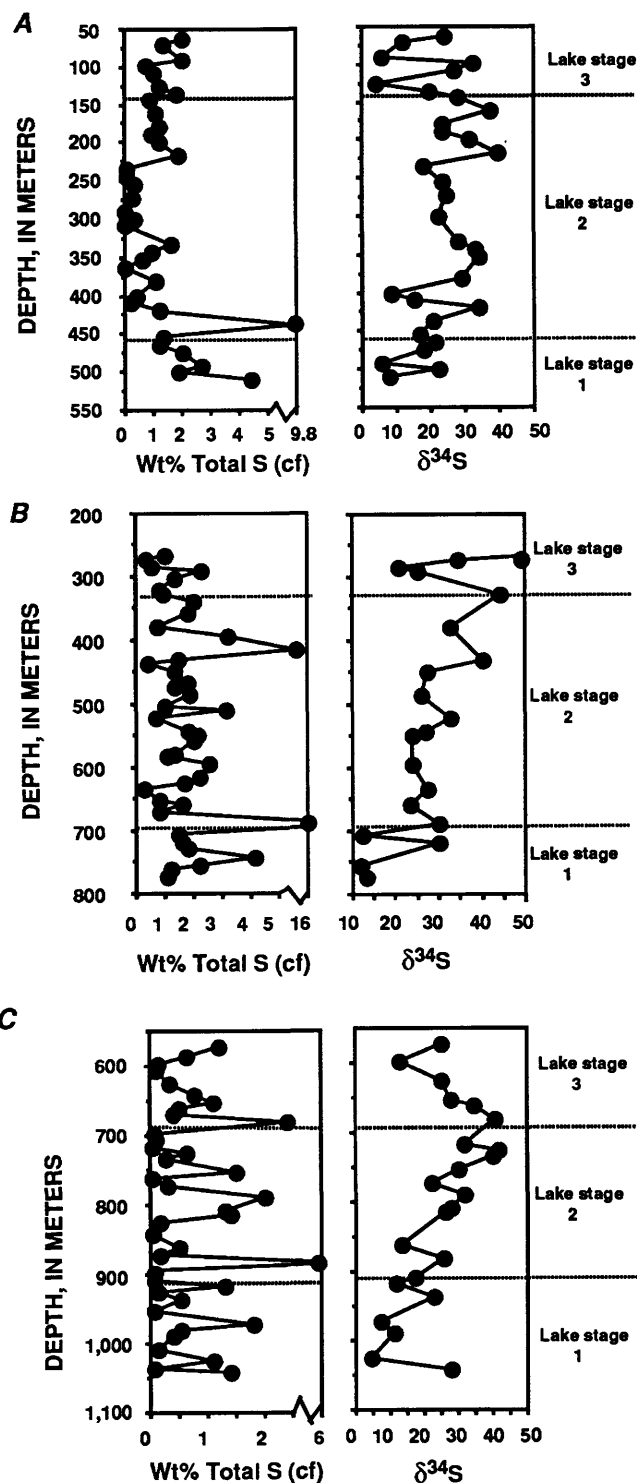


Figure 3. Depth profiles for total sulfur (carbonate-free basis) and $\delta^{34}\text{S}$ values of disulfides in depocenter cores of Green River Formation. A, Greater Green River basin; B, Piceance basin; C, Uinta basin. Lake stages are designated on plots.

Another approach to evaluating lake sulfate concentrations is to estimate the amount of bedded gypsum ($\text{CaSO}_4 \cdot 2\text{H}_2\text{O}$) that could have precipitated during the saline

Table 2. Average chemical and isotopic parameters for samples from the three lake stages in the Green River Formation of the greater Green River basin, Wyoming, Piceance basin, Colorado, and Uinta basin, Utah

[All chemical values (except carbonate carbon) are on a carbonate-free, dry-weight basis. All isotopic data are reported relative to Cañon Diablo troilite standard. x, arithmetic mean; s, standard deviation; n, number of analyses; nd, not determined; leaders (--), too many samples below the limit of determination to calculate mean; leader (-), too few samples to calculate a standard deviation]

	Greater Green River basin					Piceance basin			Uinta basin		
	Stage 1	Stage 2	Stage 3	Stage 2A	Stage 2B	Stage 1	Stage 2	Stage 3	Stage 1	Stage 2	Stage 3
Percent sulfur_{total}											
x	2.4	0.71	1.4	0.96	0.67	1.9	1.7	1.0	0.68	0.78	0.76
s	1.2	0.57	0.51	0.33	0.60	1.0	0.23	0.65	0.67	1.3	0.69
n	5	22	7	3	19	7	25	7	8	21	10
Percent sulfur_{disulfide}											
x	1.8	0.44	0.98	0.39	0.45	1.5	0.86	0.78	0.96	0.77	0.43
s	0.71	0.46	0.52	0.24	0.49	0.95	0.54	0.52	0.60	1.2	0.32
n	5	22	7	3	19	4	11	5	4	15	6
Percent sulfur_{acid-volatile}											
x	--	--	--	0.02	--	--	--	--	--	--	--
s				0							
n				3							
Percent sulfur_{sulfide}											
x	1.9	0.52	0.99	0.41	0.54	1.6	0.89	0.78	0.96	0.90	0.45
s	0.72	0.46	0.51	0.24	0.48	0.94	0.52	0.52	0.60	1.2	0.31
n	5	22	7	3	19	4	11	5	4	15	6
Percent sulfur_{sulfate}											
x	--	--	0.15	0.02	--	--	0.23	0.04	--	--	--
s			0.11	0			0.23	0.03			
n			7	3			11	5			
Percent sulfur_{organic}											
x	0.24	0.05	0.21	0.17	0.04	0.19	0.39	0.25	0.06	0.06	0.17
s	0.09	0.07	0.12	0.14	0.04	0.08	0.50	0.28	0.05	0.05	0.26
n	5	23	7	3	20	4	11	5	4	15	6
Percent iron_{reactive}											
x	2.7	2.2	2.0	0.88	2.3	2.8	2.4	2.5	2.8	3.2	1.9
s	0.41	1.0	0.76	0.32	1.0	1.0	1.1	0.78	1.2	1.1	0.62
n	5	22	7	3	19	4	11	5	4	15	6
Percent iron_{total}											
x	3.2	2.6	2.3	1.9	2.7	3.3	2.8	2.1	3.4	3.7	2.6
s	0.63	1.3	0.84	0.78	1.4	0.88	0.99	0.87	1.0	1.2	0.47
n	5	21	7	3	18	7	25	7	8	15	10
Percent carbon_{organic}											
x	9.4	3.8	7.6	15	2.0	13	15	16	2.2	4.9	14
s	4.1	4.9	4.1	1.0	1.7	8.1	7.5	12	3.2	5.1	11
n	5	22	7	3	20	7	27	7	8	21	10
Percent carbon_{carbonate}											
x	4.8	6.3	4.6	7.3	6.1	3.6	6.2	5.7	3.5	4.8	5.4
s	2.3	2.6	2.7	0.53	2.7	2.3	2.5	1.7	2.1	2.3	1.0
n	5	23	7	3	20	7	27	7	8	21	10

phase (stage 2) of Lakes Uinta and Gosiute. The amount of sulfur contained in our stage 2 samples, on a gypsum equivalence (calculations in appendix 2), indicate that 29 m of pure gypsum could have been deposited at the

depositional center of Lake Uinta in the Piceance basin and 14 m at the center of Lake Gosiute in the greater Green River basin. These calculated thicknesses of sulfate salt are large compared to the aggregate thickness of bedded

Table 2. Average chemical and isotopic parameters for samples from the three lake stages in the Green River Formation of the greater Green River basin, Wyoming, Piceance basin, Colorado, and Uinta basin, Utah— Continued

	Greater Green River basin					Piceance basin			Uinta basin		
	Stage 1	Stage 2	Stage 3	Stage 2A	Stage 2B	Stage 1	Stage 2	Stage 3	Stage 1	Stage 2	Stage 3
DOS_{reactive}											
x	0.60	0.27	0.46	0.33	0.26	0.49	0.39	0.35	0.32	0.25	0.33
s	0.19	0.23	0.24	0.19	0.24	0.20	0.24	0.33	0.21	0.25	0.22
n	5	22	7	3	19	4	11	5	4	15	6
$\delta^{34}\text{S}_{\text{disulfide}}$											
x	14.1	25.6	17.6	31.4	24.5	16.8	28.5	34.7	12.7	26.4	27.6
s	8.7	8.1	10.9	7.3	8.0	8.9	5.0	12.1	10.4	9.2	9.5
n	5	22	7	3	16	4	11	5	4	15	6
$\delta^{34}\text{S}_{\text{sulfate}}$											
x	11.0	23.2	22.5	nd	23.2	nd	27.9	29.4	nd	nd	nd
s	-	9.2	16.6		9.2		3.3	-			
n	2	3	7		3		9	2			
$\delta^{34}\text{S}_{\text{organic}}$											
x	17.9	26.9	18.9	29.9	26.0	17.1	27.9	37.0	15.4	24.6	29.9
s	6.4	7.0	9.7	-	8.0	8.0	4.0	11.2	4.9	9.9	7.3
n	5	8	7	2	6	4	6	4	3	11	4

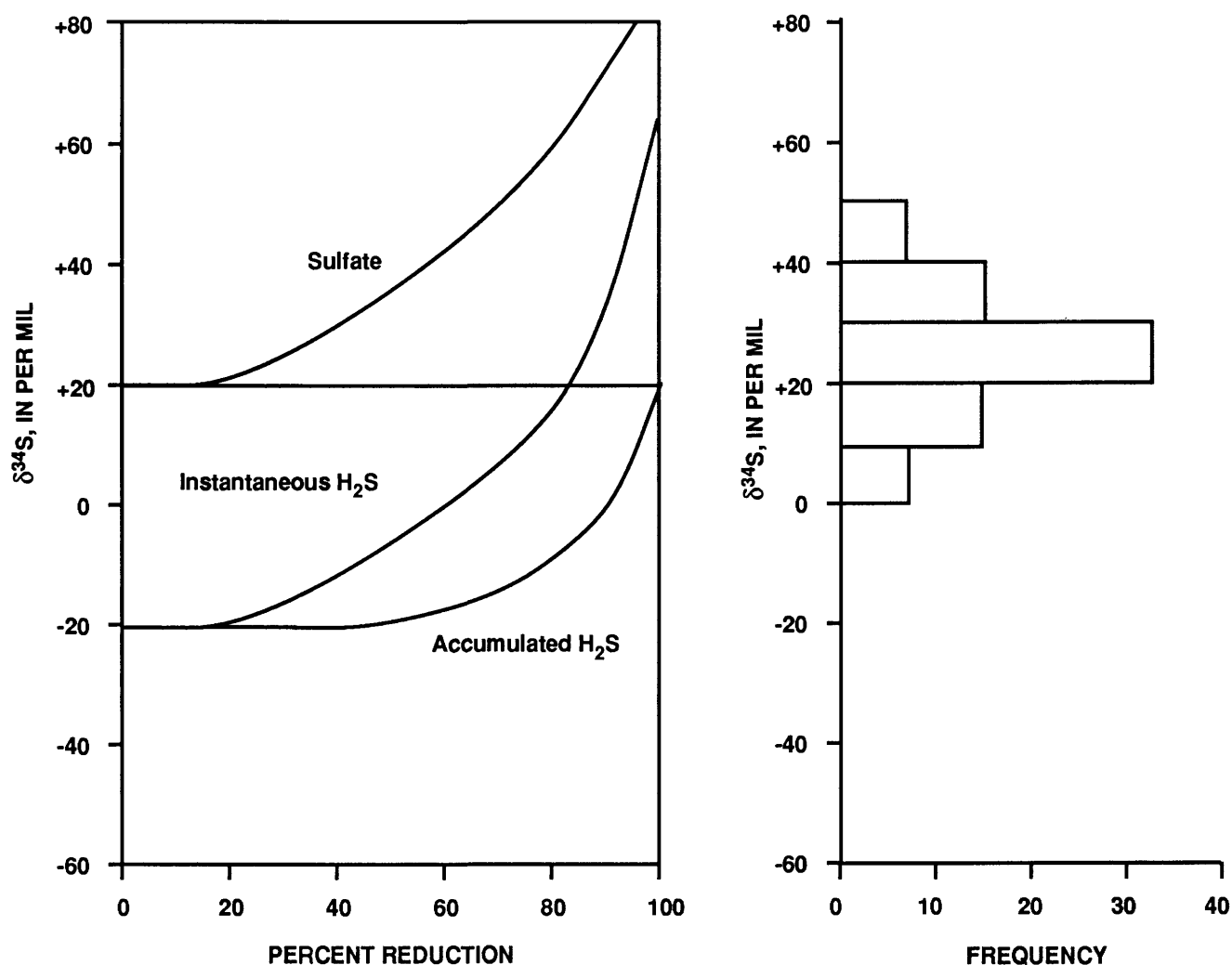


Figure 4. Rayleigh fractionation plot and frequency histogram for $\delta^{34}\text{S}$ values of disulfides in depocenter cores of Green River Formation from greater Green River, Piceance, and Uinta basins. Curves were calculated assuming $\delta^{34}\text{S}$ of inflow was +20‰.

sodium carbonate minerals and halite in the cored interval from the Piceance basin (approximately 33 m); saline minerals in the greater Green River basin core are disseminated, not bedded.

This discrepancy between low sulfate concentrations (absence of sulfate salts in otherwise evaporite-type rocks) in the Green River lakes and high sulfur in the rocks could be reconciled if the sulfate in the two ancient lakes had been extensively reduced by sulfate-reducing bacteria. This process would have lowered water-column/porewater sulfate concentrations below sulfate-mineral saturation, yet allowed a buildup of aqueous sulfide and therefore reduced forms of sulfur in the sediment. Our isotope data (discussed later) clearly support such extensive reduction.

Sulfur isotopes are fractionated during the bacterial reduction of sulfate to sulfide; the accumulated reservoir of sulfide becomes progressively enriched in ^{34}S as a function of the percent sulfate reduced. This isotopic evolution is quantified by the Rayleigh fractionation equations (Nakai and Jensen, 1964) and is plotted in figure 4. If only a small net portion of the sulfate in lake water is reduced, the accumulated sulfide is depleted in ^{34}S relative to sulfate as shown on the left side of the plot in figure 4. This situation is similar to that in marine and some lake environments where H_2S has formed from large, essentially infinite sulfate reservoirs and thus the sulfide is depleted in ^{34}S relative to the initial sulfate. If the sulfate is quantitatively reduced (right side of Rayleigh plot in fig. 4), then the sulfide has the same isotopic composition as the initial sulfate and is enriched in ^{34}S (chosen as +20‰, the most ^{34}S -enriched isotopic composition conceivable for inflow waters). A frequency histogram for $\delta^{34}\text{S}$ values of the disulfide in the Green River Formation is shown in figure 4. The ^{34}S -enriched values in the histogram indicate that, unless there was an input of sulfate extremely enriched in ^{34}S (that is, $\delta^{34}\text{S}$ between +20‰ and +50‰), the sulfur isotopic composition of the disulfide cannot be reconciled by simply invoking complete reduction of porewater sulfate.

Plots of sulfur in sulfide-mineral phases versus organic carbon (organic-C) are commonly used to distinguish between unlimited and limited sulfate reservoirs in marine and freshwater-lake systems (fig. 5A). A linear relation is observed in "normal" marine sediments, where the sulfate reservoir is unlimited and sulfide minerals form diagenetically (Sweeney, 1972). The amount of H_2S that is trapped as sulfide minerals is dependent on the amount of organic carbon in the sediments available for the bacteria during sulfate reduction (extent of reduction is organic-carbon limited). The slope of this line decreases in freshwater sediments because sulfate reduction in the sediment is sulfate limited (Berner and Raiswell, 1984). Under euxinic conditions (H_2S -bearing water column), a linear relation with a positive intercept is observed; the sulfate reservoir is unlimited and sulfide minerals formed in

Table 3. Dissolved water-column sulfate, sediment sulfur concentrations (on a carbonate-free basis), and $\delta^{34}\text{S}$ disulfide values in samples from the Green River Formation and other lacustrine environments [N.A. indicates not available]

	SO_4^{2-} water concentration (mM)	Total S (weight percent)	$\delta^{34}\text{S}$ disulfide (per mil)
Green River Formation			
Piceance basin.....	N.A.	1.6	+27.7
Uinta basin.....	N.A.	.69	+24.6
Greater Green			
River basin	N.A.	1.1	+22.3
Walker Lake ^{1,2}	20	0.94	-14.7
Great Salt Lake^{1,3}			
Stage I (saline).....	180	0.50	-21.4
Stage II (saline)	N.A.	0.44	-19.2
Stage II (fresh).....	N.A.	0.90	-14.5
Soap Lake¹			
Noneuxinic	30	0.08	-29.4
Euxinic	360	0.20	-20.1
Lake Ontario ⁴	0.10	0.13	+18.6
Marine environment ⁵	28	1	-25

¹Tuttle (1988).

²Benson and Spencer (1983).

³Sturm (1980).

⁴Calculated from Nriagu and Coker (1976).

⁵Calculated from data in Goldhaber and Kaplan (1974).

anoxic bottom water are added to those forming in the sediments during diagenesis (Leventhal, 1983). Because most of the mineral-sulfide and organic-carbon data for the Green River Formation (figs. 5B-D) show none of these correlations or trends, models for marine, freshwater, and euxinic sediments shown in figure 5A are limited in their ability to determine the size of the sulfate reservoir or explain controls on sulfate reduction and sulfide-mineral formation in the Green River lake system.

The similar isotopic compositions of organosulfur and coexisting sulfide minerals in the Green River samples suggest that a high proportion of the sulfate reservoir in the Green River lakes was reduced prior to any formation of sulfidization products. Once reduced, sulfur is very reactive and the dissolved sulfide (H_2S) generally reacts readily with available iron to form iron sulfide minerals (Pyzik and Sommer, 1981). If H_2S is in excess relative to reactive iron, organic matter in the sediment can be sulfidized (Nissenbaum and Kaplan, 1972). In marine and freshwater sediments, the sulfidization of organic matter is slow relative to the sulfidization of iron. The H_2S formed at the start of sulfate reduction is depleted in ^{34}S relative to the H_2S formed during later stages of the reduction process (fig.

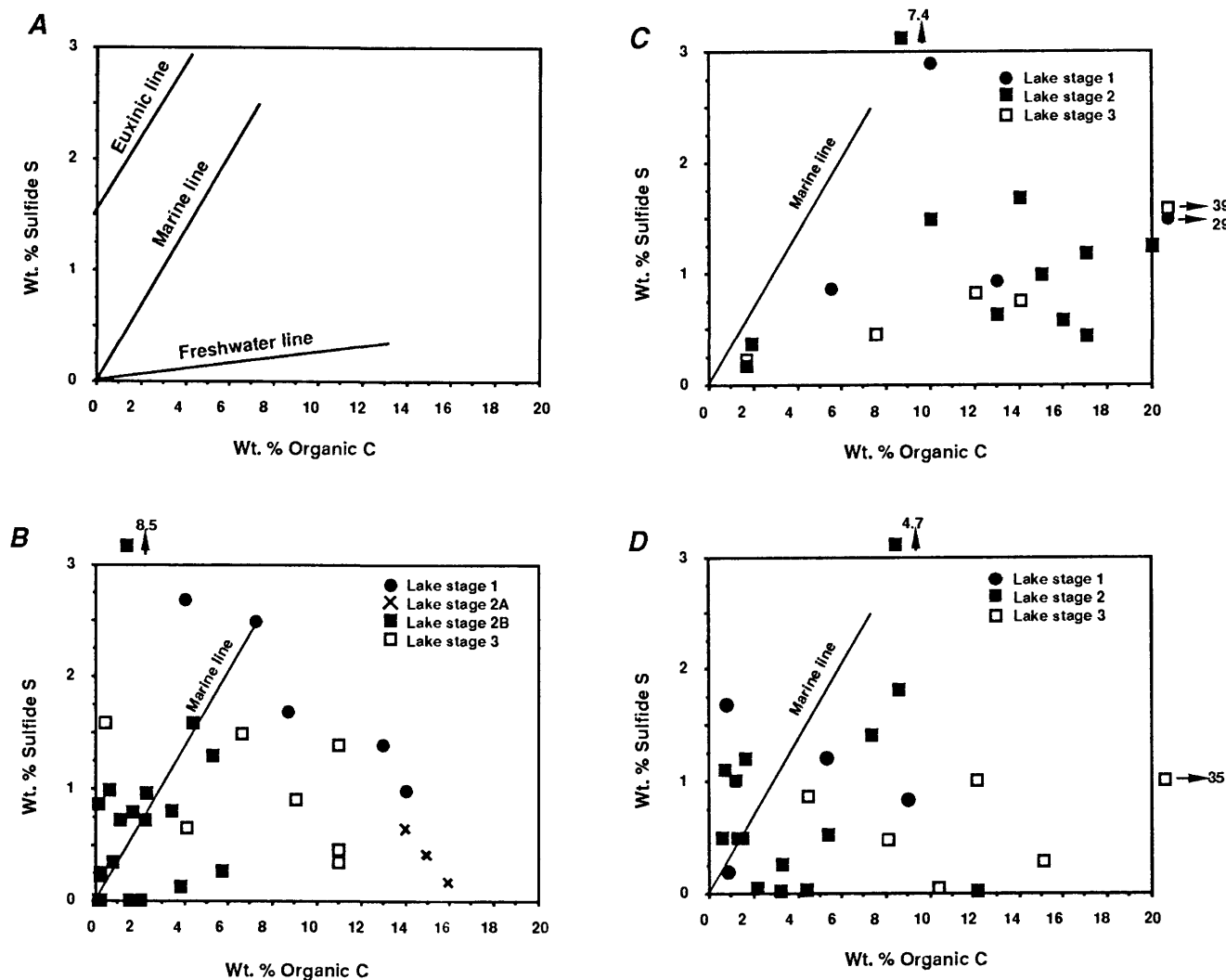


Figure 5. Regression lines for sulfur in sulfide minerals versus organic carbon. *A*, Marine sediments (Sweeney, 1972), freshwater sediments (Bernier and Raiswell, 1984), and sediments deposited in euxinic water columns (Leventhal, 1983). Rocks of Green River Formation from *B*, greater Green River, *C*, Piceance, and *D*, Uinta basins. All data for Green River samples are weight percent calculated on a carbonate-free basis.

4). Therefore, sulfur in sulfide minerals is expected to be depleted in ^{34}S relative to that of the more slowly forming organosulfur, and such is the case in marine sediments (see band of marine data in fig. 6). In contrast, the isotopic compositions of organosulfur in samples from all three Green River cores are quite similar to those of coexisting disulfide sulfur (individual points in fig. 6). Smith and Young (1983) argued that the similar isotopic compositions indicate sulfide-mineral formation from diagenetically released, assimilatory (inherited from living organisms) organosulfur. Organosulfur:organic-carbon ratios (OS/C) for the Green River samples are greater than in living analogs. Thus, the organic matter must actually have been enriched, not depleted, in sulfur.

As argued above, a reservoir of isotopically homogeneous H_2S must have been available during both sulfidization of iron and organic matter. The existence of

such a reservoir is inconsistent with the formation of sulfidization products during progressive reduction of sulfate in the sediment column (as in marine sediments). An isotopically homogeneous H_2S reservoir requires almost complete reduction of the sulfate, such as would occur in either stagnant, anoxic bottom waters of a stratified lake or anoxic pore waters within sediments prior to sulfidization of either iron or organic matter (controls on sulfidization kinetics are discussed in the following section). Almost complete reduction of sulfate in either of these environments would allow for accumulation in the sediments of abundant ^{34}S -enriched sulfide minerals and organosulfur but not sulfate saline minerals.

The presence of H_2S in an anoxic water column (euxinic conditions) would inhibit the aerobic destruction of organic matter and allow for accumulation and preservation of organic matter in the lake sediments. Sediments

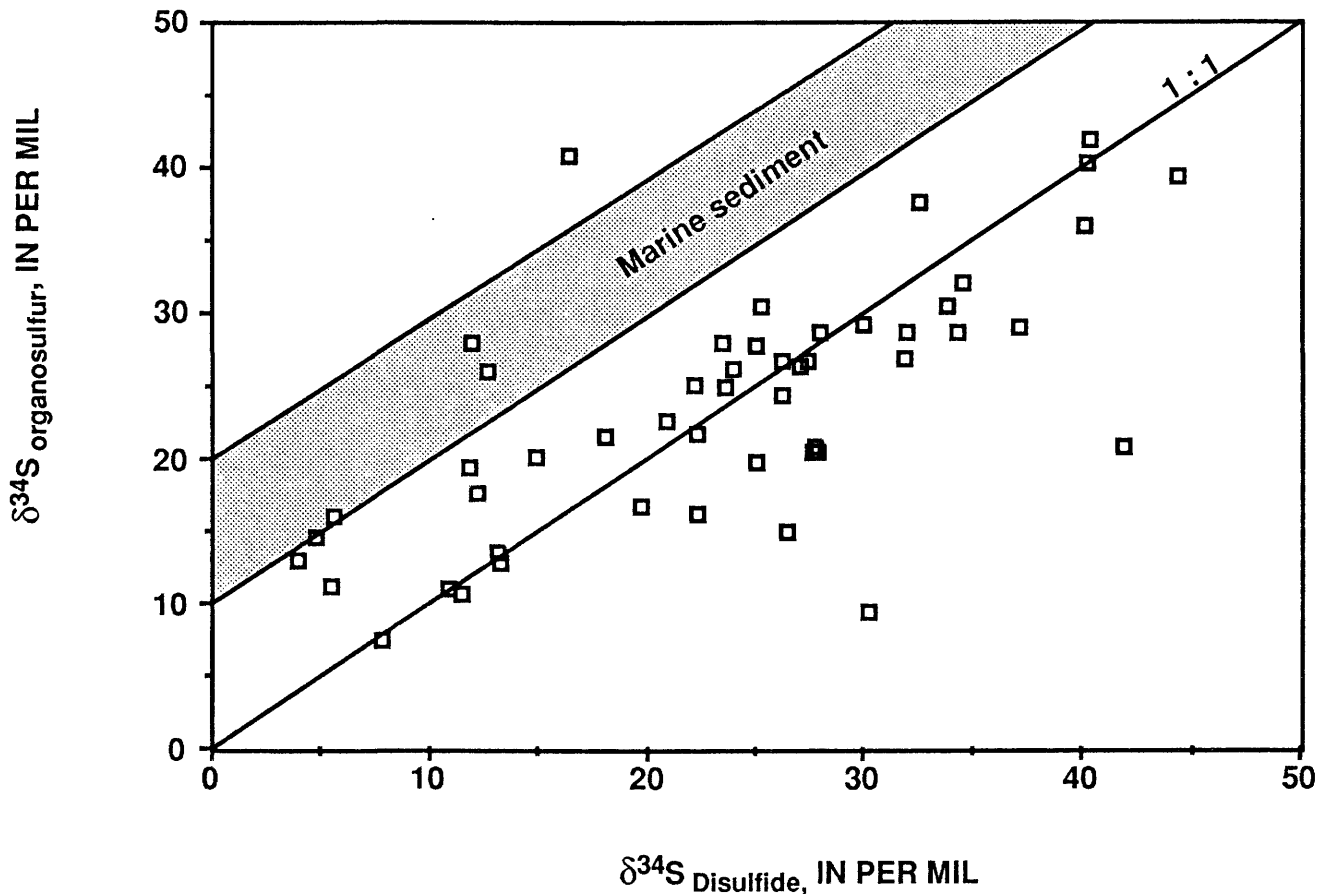


Figure 6. $\delta^{34}\text{S}$ values of organosulfur versus $\delta^{34}\text{S}$ values of disulfide sulfur. Shaded band shows marine data (Orr, 1985); individual points are data for Green River Formation from this study.

deposited in Lake Uinta during all stages and in Lake Gosiute during stages 1, 2A, and 3 contained an amount of well-preserved organic matter sufficient to form oil shale (as much as 39 weight percent organic carbon; fig. 5). These sediments probably were deposited under euxinic conditions. Although some organic-carbon-rich layers are in stage 2 rocks from the greater Green River basin (stage 2A samples), thick sequences of rocks in stage 2B contain relatively little or no organic matter (average 2 weight percent organic carbon; table 2). Low sulfur abundances (average 0.67 weight percent; table 2) are characteristic of these relatively organic-carbon-poor rocks. Organic matter and sulfide minerals were either not produced or not preserved within the depositional center of the greater Green River basin during stage 2B intervals. The few organic-carbon-rich samples of stage 2A suggest that euxinic conditions were intermittent during this otherwise shallow-lake stage. The cause of the decrease in the size of Lake Gosiute and the organic-matter and sulfur abundances in its sediment is unknown. As mentioned earlier, climatic changes may have been a key factor. Another possibility consistent with our data is a change in drainage patterns within the hydrologic basin of Lake Gosiute that would

have resulted in a decrease in water inflow, incoming sulfur, and possibly organic matter production. The absence of stratification and euxinic conditions during this shallowing period resulted in the poor preservation of deposited organic matter and in the formation of very lean oil shale.

The lower amounts of sulfur in Lake Gosiute sediment during this time caused the system to be isotopically sensitive to the influx of ^{34}S -depleted sulfur associated with volcanic ash; Rye and others (1984) showed that volcanic ash has $\delta^{34}\text{S}$ values of from 0‰ to 6‰. This additional supply of sulfur explains the spikes to lower $\delta^{34}\text{S}$ values in stage 2 samples near ash layers in the greater Green River basin.

Sulfidization Products

After the Green River lake sulfate was reduced to H_2S in the water column (euxinic conditions) or sediments (shallow conditions), it would have diffused into and through the sediments along concentration gradients controlled by sulfidization of iron minerals and organic matter. Sulfidization of iron in Green River lake sediments

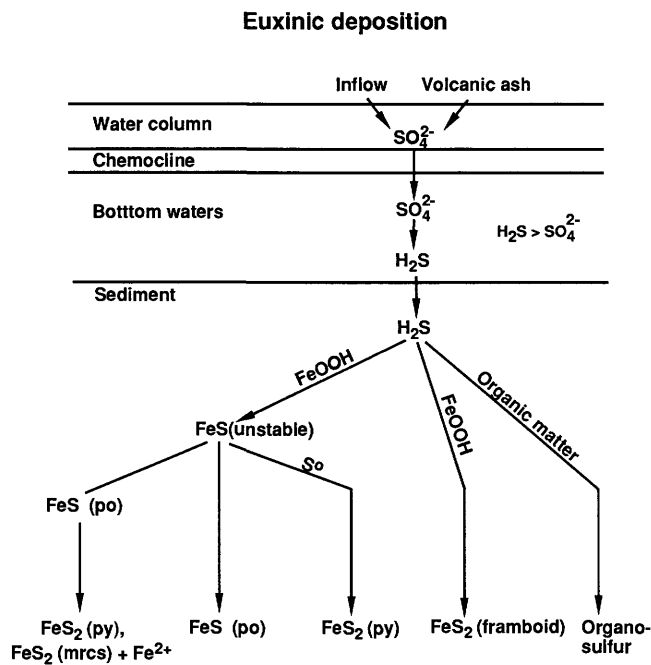


Figure 7. Summary of sulfur geochemistry during euxinic deposition of Green River Formation in Lake Uinta (all stages) and Lake Gosiute (stages 1, 3, and 2A). py, pyrite; mrcs, marcasite; po, pyrrhotite. No depth scale inferred.

was probably initially hindered by high pH, such as observed in the sediments of modern Soap Lake, which has a pH of 9.8 and water chemistry similar to that proposed for the Green River lakes (Tuttle and others, this volume), and in experimental laboratory studies on the sulfidization of goethite (Stanton and Goldhaber, this volume). Eventually, stepwise iron sulfidization occurred in Green River sediments and is recorded in the mineralogy and morphology of the sulfide minerals (Tuttle, this volume).

Pyrite (FeS_2) is the predominant sulfide mineral in the Green River Formation and is present as early diagenetic framboids and later diagenetic anhedral and euhedral grains. Pyrrhotite (FeS) is locally abundant, and its morphology indicates that it formed after compaction. Pyrrhotite is stabilized under very reducing conditions where elemental sulfur is not available to transform precursor FeS phases to FeS_2 (Rickard, 1975). Marcasite (FeS_2 ; mrcs) is commonly associated with pyrrhotite (po) in samples of Green River Formation and probably replaces pyrrhotite according to the equation (De Waal, 1984)



Contemporaneous with formation of the earliest sulfide minerals (precursor FeS and framboidal pyrite), organic matter in the Green River sediments was also sulfidized. As previously mentioned, OS/C ratios indicate enrichment of the organic matter in sulfur, and $\delta^{34}\text{S}$ values

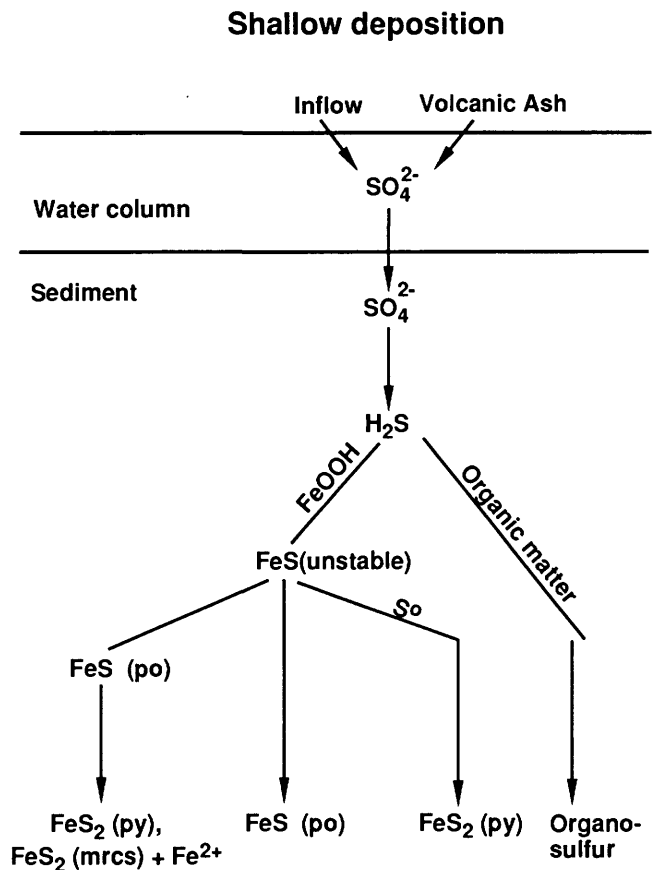


Figure 8. Summary of sulfur geochemistry during shallow deposition of Green River Formation in Lake Gosiute (stage 2B). py, pyrite; mrcs, marcasite; po, pyrrhotite. No depth scale inferred.

of the organosulfur reflect the isotopic composition of the sulfidizing H_2S . Sulfidization of organic matter was likely promoted by the high pH of the pore water. Organic-matter sulfidization increases as pH increases, in part due to the stabilization of polysulfides at higher pH (Aizenshtat and others, 1981; Francois, 1987; LaLonde and others, 1987). Such early sulfidization of organic matter in high-pH environments is well documented in modern Soap Lake sediments (Tuttle, 1988).

SULFUR GEOCHEMISTRY OF LAKES UINTA AND GOSIUTE

Collectively, the results of our study show that the water columns at the depositional centers of Lake Uinta during all stages and Lake Gosiute during stages 1, 2A, and 3 were stratified and probably euxinic. The sulfur geochemistry under these euxinic conditions is summarized in figure 7. Sulfate entered the lake dissolved in inflow waters or adsorbed onto abundant volcanic ash. The H_2S was produced in the water column or pore water by bacterial

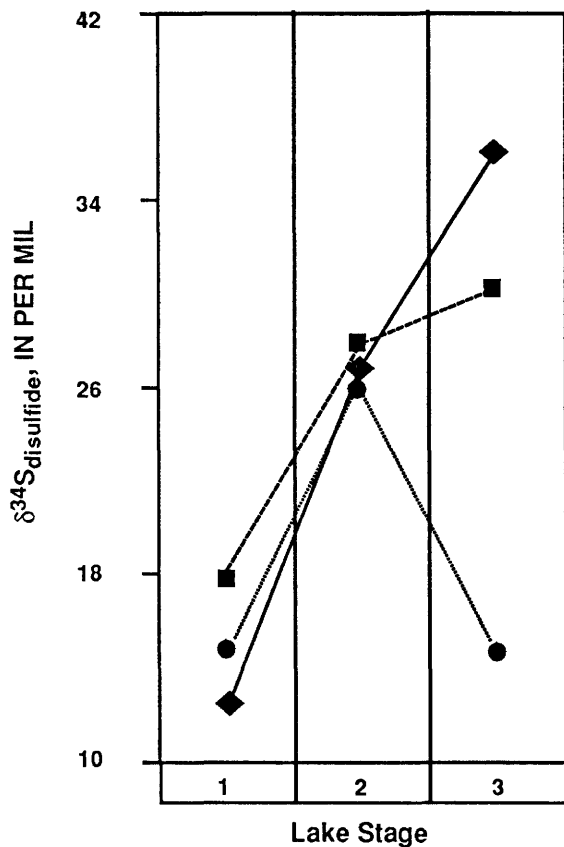


Figure 9. Mean $\delta^{34}\text{S}$ values in Green River Formation from the greater Green River (circles), Piceance (squares), and Uinta (diamonds) basins during each lake stage. Only values from within Mahogany zone were used to calculate stage 3 means for Piceance and Uinta basins.

reduction of sulfate. The H_2S :sulfate ratio in these waters was high, and the accumulation of H_2S in the reducing sediments inhibited aerobic destruction of organic matter. High porewater pH prevented rapid sulfidization of iron and promoted sulfidization of organic matter. The stable sulfur phases preserved in rocks deposited during these stages are pyrite, pyrrhotite, marcasite, and organosulfur.

During stage 2 in Lake Gosiute, shallow conditions prevailed and the water column was only intermittently stratified and euxinic. The sulfur geochemistry of ancient Lake Gosiute during periods of shallow deposition (stage 2B) is summarized in figure 8. Again, sulfate entered the lake dissolved in inflow waters or adsorbed to volcanic ash. Its reduction took place in the sediments. The H_2S slowly reacted with iron and, if present, organic matter. The stable sulfur phases in these rocks are the same as in rocks deposited under euxinic conditions in the lake, although they are generally much less abundant.

APPLICATIONS TO GEOLOGIC PROBLEMS

Data from this study not only aid in understanding the depositional and diagenetic conditions during the formation

of rocks of the Green River Formation but also are useful in developing or testing working hypotheses regarding other aspects of the Green River lake system and ancient lake systems in general.

1. Work done by Bradley (1929) and Surdam and Stanley (1979) suggests that Lakes Uinta and Gosiute may have been hydrologically connected at the onset of basin infilling, but the key geologic evidence has been eroded. Geologic studies of Surdam and Stanley (1980) and Johnson (1985) indicate that infilling of the basins with volcanoclastic rocks occurred from north (greater Green River basin) to south (Piceance basin) and then to the west (Uinta basin). Correlation between the degree of change in lake-stage isotopic values from stage 2 to stage 3 (fig. 9) and the sequence of infilling supports such a connection during lake stage 3. Infilling caused a shift in the chemistry of Lake Gosiute as evidenced from the marked decrease in $\delta^{34}\text{S}$ values. To a lesser degree, this shift in chemistry influenced Lake Uinta in the Piceance basin (by damping the overall evolution of the sulfur isotopes to heavier values) as the water flowed into Lake Uinta in the northeastern corner of the basin. The isotope evolution in Lake Uinta in the Uinta basin was only slightly influenced (essentially no change in the evolution of the isotopes) because the infilling only proceeded to the eastern half of the basin.

2. The hypothesis proposed in this study regarding the effect of pH on sulfidization of organic matter may have broad implications for the origin of sulfur in oils generated from lacustrine source rocks. Sulfur-rich petroleum is generated from ancient, iron-deficient marine source rocks (Vairavamurthy and Mopper, 1987). The shale oil retorted from the Green River rocks has moderate sulfur contents, not because the rocks are iron deficient but because the high pH of the pore water in Lakes Uinta and Gosiute sediments inhibited iron sulfidization and promoted organic-matter sulfidization. The effect of porewater pH during sedimentation on the sulfur content of generated hydrocarbons has not previously been investigated but may be of considerable importance.

3. Our results show that working models developed to study sulfur geochemistry in marine and freshwater systems (Sweeney, 1972; Leventhal, 1983; Berner and Raiswell, 1984) have limited use in interpreting most of the sulfur geochemistry of the Green River Formation. In addition, paleosalinity indicators developed for these two sedimentary environments (such as FeS_2 : FeS ratios; Berner and others, 1979) are not applicable to these rocks. High FeS_2 : FeS ratios are reported to occur in high-salinity depositional environments; the opposite relation is observed in our results, and, in fact, saline stage 2 samples have the lowest ratios.

The failure of these established models and indicators to interpret sulfur geochemistry in these saline lacustrine rocks reinforces the tenet that models developed for one system may not be applicable for others, even when the systems share similar characteristics.

REFERENCES CITED

- Aizenshtat, Z., Stoler, A., Cohen, Y., and Nielsen, H., 1981, The geochemical sulphur enrichment of recent organic matter by polysulfides in the Solar Lake, *in* Bjoroy, M., ed., *Advances in organic geochemistry 1981*: Chichester, England, John Wiley and Sons Limited, p. 279–288.
- Benson, L.V., and Spencer, R.J., 1983, A hydrochemical reconnaissance study of the Walker River basin, California and Nevada: U.S. Geological Survey Open-File Report 83–740, 53 p.
- Berner, R.A., 1970, Sedimentary pyrite formation: *American Journal of Science*, v. 268, p. 1–23.
- 1984, Sedimentary pyrite formation—An update: *Geochimica et Cosmochimica Acta*, v. 48, p. 605–615.
- Berner, R.A., Balwin, T., and Holdren, G.R., 1979, Authigenic iron sulfides as paleosalinity indicators: *Journal of Sedimentary Petrology*, v. 49, p. 1345–1350.
- Berner, R.A., and Raiswell, R., 1984, C/S method for distinguishing freshwater from marine sedimentary rocks: *Geology*, v. 12, p. 365–368.
- Boyer, D.L., and Cole, R.D., 1983, Variations in sulfur mineralization in the Parachute Creek Member of the Green River Formation, Colorado and Utah, *in* Sixteenth Oil Shale Symposium proceedings: Golden, Colorado School of Mines, p. 160–175.
- Bradley, W.H., 1929, The varves and climate of the Green River epoch: U.S. Geological Survey Professional Paper 158-E, p. 87–110.
- 1973, Oil shale formed in desert environment; Green River Formation, Wyoming: *Geological Society of America Bulletin*, v. 84, p. 1121–1124.
- Cole, R.D., Liu, J.H., Smith, G.V., Hinckley, C.C., and Saproschenko, M., 1978, Iron partitioning in oil shale of the Green River Formation, Colorado—A preliminary Mössbauer study: *Fuel*, v. 57, p. 514–520.
- Cole, R.D., and Picard, M.D., 1981, Sulfur-isotope variations in marginal-lacustrine rocks of the Green River Formation, Colorado and Utah: *Society of Economic Paleontologists and Mineralogists Special Publication* 31, p. 261–275.
- De Waal, S.A., 1984, Experimental simulation of the supergene reaction pyrrhotite to marcasite + Fe²⁺ + electrons: *Transactions of the Geological Society of South Africa*, v. 87, p. 273–279.
- Dyni, J.R., 1983, Distribution and origin of sulfur in Colorado oil shale, *in* Sixteenth Oil Shale Symposium proceedings: Golden, Colorado School of Mines, p. 144–159.
- Eugster H.P., and Hardie, L.A., 1975, Sedimentation in an ancient playa-lake complex—The Wilkins Peak Member of the Green River Formation of Wyoming: *Geological Society of America Bulletin*, v. 86, p. 319–334.
- 1978, Saline lakes, *in* Lerman, Abraham, ed., *Lakes—Chemistry, geology, physics*: New York, Springer-Verlag, p. 237–294.
- Francois, R., 1987, A study of sulphur enrichment in the humic fraction of marine sediments during early diagenesis: *Geochimica et Cosmochimica Acta*, v. 51, p. 17–27.
- Goldhaber, M.B., and Kaplan, I.R., 1974, The sulfur cycle, *in* Goldberg, E.D., ed., *The sea*, v. 5: New York, John Wiley and Sons, p. 569–655.
- Ingamells, C.O., 1970, Lithium metaborate flux in silicate analysis: *Analytica Chimica Acta*, v. 52, p. 323–334.
- Ingram, L.L., Ellis, J., Crisp, P.T., and Cook, A.C., 1983, Comparative study of oil shales and shale oils from the Mahogany zone, Green River Formation (U.S.A.) and Kerosene Creek seam, Rundle Formation (Australia): *Chemical Geology*, v. 38, p. 185–212.
- Johnson, R.C., 1985, Early Cenozoic history of the Uinta and Piceance Creek Basins, Utah and Colorado, with special reference to the development of Eocene Lake Uinta, *in* Flores, R.M., and Kaplan, S.S., eds., *Cenozoic paleogeography of the west-central United States*: Denver, Society of Economic Paleontologists and Mineralogists, p. 247–276.
- LaLonde, R.T., Ferrara, L.M., and Hayes, M.P., 1987, Low-temperature, polysulfide reactions of conjugated enecarbonyls—A reaction model for the geologic origin of S-heterocycles: *Organic Geochemistry*, v. 11, p. 563–571.
- Leventhal, J.S., 1983, An interpretation of carbon and sulfur relationships in Black Sea sediments as indicators of environments of deposition: *Geochimica et Cosmochimica Acta*, v. 47, p. 133–137.
- Melchior, D.C., Wildeman, T.R., and Williamson, D.L., 1982, Mössbauer investigation of the transformations of the iron minerals in oil shale during retorting: *Fuel*, v. 61, p. 516–522.
- Milton, C., and Eugster, H.P., 1959, Mineral assemblages of the Green River Formation, *in* Abelson, P.H., ed., *Researches in geochemistry*: New York, John Wiley, p. 118–150.
- Nakai, N., and Jensen, M.L., 1964, The kinetic isotope effect in the bacterial reduction and oxidation of sulfur: *Geochimica et Cosmochimica Acta*, v. 28, p. 1893–1912.
- Nissenbaum, A., and Kaplan, I.R., 1972, Chemical and isotopic evidence for the *in-situ* origin of marine humic substances: *Limnology and Oceanography*, v. 17, p. 570–582.
- Nriagu, J.O., and Coker, R.D., 1976, Emission of sulfur from Lake Ontario sediments: *Limnology and Oceanography*, v. 21, p. 485–489.
- Orr, W.L., 1985, Kerogen/asphaltene/sulfur relationships in sulfur-rich Monterey oils: *Advances in Organic Geochemistry*, v. 10, p. 499–516.
- Pabst, A., 1970, Pyrite of unusual habit simulating twinning from the Green River Formation of Wyoming: *The American Mineralogist*, v. 56, p. 133–145.
- Pyzik, A.J., and Sommer, S.E., 1981, Sedimentary iron monosulfides—Kinetics and mechanism of formation: *Geochimica et Cosmochimica Acta*, v. 45, p. 687–698.
- Rickard, D.T., 1975, Kinetics and mechanism of pyrite formation at low temperature: *American Journal of Science*, v. 275, p. 636–652.
- Rye, R.O., Luhr, J.F., and Wasserman, M.D., 1984, Sulfur and oxygen isotopic systematics of the 1982 eruptions of El Chichon volcano, Chiapas, Mexico: *Journal of Volcanology and Geothermal Research*, v. 23, p. 109–123.
- Smith, J.W., and Young, N.B., 1983, Stratigraphic variation of sulfur isotopes in Colorado Corehole Number 1, *in* Sixteenth Oil Shale Symposium proceedings: Golden, Colorado School of Mines, p. 176–188.

- Smith, J.W., Young, N.B., and Lawlor, D.L., 1964, Direct determination of sulfur forms in Green River oil shale: *Analytical Chemistry*, v. 36, p. 618–622.
- Stanfield, K.E., Frost, I.C., McAuley, W.S., and Smith, H.N., 1951, Properties of Colorado oil shale: U.S. Bureau of Mines Report of Investigations 4825, 27 p.
- Sturm, P. A., 1980, The Great Salt Lake brine system, *in* Gwynn, J.W., ed., *Great Salt Lake—A scientific historical, and economic overview*: Utah Department of Natural Resources Bulletin 116, p. 147–162.
- Sullivan, R., 1985, Origin of lacustrine rocks of Wilkins Peak Member, Wyoming: *American Association of Petroleum Geologists Bulletin*, v. 69, p. 913–922.
- Surdam, R.C., and Stanley, K.O., 1979, Lacustrine sedimentation during the culminating phase of Eocene Lake Gosiute, Wyoming (Green River Formation): *Geological Society of America Bulletin*, v. 90, p. 93–110.
- 1980, Effects of changes in drainage-basin boundaries on sedimentation in Eocene lakes Gosiute and Uinta of Wyoming, Utah, and Colorado: *Geology*, v. 8, p. 135–139.
- Sweeney, R.E., 1972, Pyritization during diagenesis of marine sediments: Los Angeles, University of California, Ph.D. thesis, 184 p.
- Tuttle, M.L., 1988, Geochemical evolution and depositional history of sediment in modern and ancient saline lakes—Evidence from sulfur geochemistry: Golden, Colorado School of Mines, Ph.D. thesis, 312 p.
- Tuttle, M.L., Goldhaber, M.B., and Williamson, D.L., 1986, An analytical scheme for determining forms of sulphur in oil shales and associated rocks: *Talanta*, v. 33, p. 953–961.
- Vairavamurthy, A., and Mopper, K., 1987, Geochemical formation of organosulphur compounds (thiols) by addition of H₂S to sedimentary organic matter: *Nature*, v. 329, p. 623–625.

APPENDIX 1—ANALYTICAL DATA

The analytical data for 35 samples from the Blacks Fork core, greater Green River basin, Wyoming; 41 samples from the 01A core, Piceance basin, Colorado; and 39 samples from the Coyote Wash core, Uinta basin, Utah, are tabulated in table A1. Chemical data are reported on a dry-weight percent basis; isotopic values are reported as $\delta^{34}\text{S}$ relative to the troilite phase in the Cañon Diablo meteorite (CDT standard). The limit of determination on the sulfur species data is 0.01; < signifies that concentrations are below that level.

Reactive iron (Fe_r) and the degree of sulfidization (DOS_r), both calculated parameters, are also given in table A1. Fe_r is operationally defined as iron that is initially available for sulfidization by H_2S (Berner, 1984). It includes the measured HCl-soluble iron and iron residing in disulfide minerals and is calculated as

$$\text{Fe}_r = \text{Fe}_{\text{HCl}} + \text{Fe}_{\text{di}}$$

where Fe_{HCl} is HCl-extractable iron (iron in carbonate, oxide, acid-volatile sulfide, and possibly clay- mineral phases), Fe_{di} is iron in disulfide minerals, and Fe_{av} is the iron in acid-volatile sulfide minerals. Fe_{di} and Fe_{av} are

calculated from the sulfur data, assuming stoichiometric FeS and FeS_2 . DOS_r is a measure of the fraction of the reactive iron sulfidized and is calculated as

$$\text{DOS}_r = [\text{Fe}_{\text{di}} + \text{Fe}_{\text{av}}] / \text{Fe}_r$$

DOS_r is similar to Berner's (1970) degree of pyritization (DOP). The former, however, also includes acid-volatile sulfides.

Abbreviations used in this appendix are as follows.

Meters	Depth interval (in meters)
Di-S	Disulfide sulfur
SO4-S	Sulfate sulfur
R-Fe	Reactive iron
Org-C	Organic carbon
DOSr	Degree of sulfidization
T-S	Sulfur
Av-S	Acid-volatile sulfur
Org-S	Organosulfur
T-Fe	Total iron
CO3-C	Carbonate carbon
del	$\delta^{34}\text{S}$

Table A1. Analytical data

[BF, Blacks Fork core, greater Green River basin, Wyoming; unlettered numbers, 01A core, Piceance basin, Colorado; cw, Coyote Wash core, Uinta basin, Utah. Boxhead abbreviations explained in appendix 1, preceding]

Sample	Meters	T-S%	DI-S%	Av-S%	SO4-S%	Org-S%	R-Fe%	T-Fe%	Org-C%	CO3-C%	DOSr	del-Di	del-Av	del-SO4	del-Orig
BLACKS FORK CORE															
Lake stage 3															
BF-1	63	1.8	1.4	0.02	0.15	0.02	2.9	3.0	0.39	2.1	0.44	23.8		52.1	
BF-2	70	1.2	0.65	<	0.05	0.26	0.94	1.1	6.5	5.6	0.62	11.8		22.2	19.4
BF-3	91	1.5	1.1	<	0.12	0.15	2.0	2.4	4.9	5.1	0.49	5.4		13.0	11.3
BF-4	98	0.56	0.36	<	0.03	0.20	1.9	2.2	8.3	4.4	0.18	32.5			37.7
BF-5	107	0.79	0.27	0.01	0.16	0.26	1.2	1.5	8.8	7.2	0.17	26.4		25.5	15.0
BF-6	125	1.2	0.65	0.01	0.34	0.14	1.2	1.4	4.1	0.24	0.49	3.9		2.9	13.0
BF-7	135	1.1	0.87	<	0.04	0.12	0.93	1.2	7.0	7.7	0.84	19.7		19.0	16.7
Lake stage 2															
BF-8	144	0.61	0.17	0.34	0.01	0.03	1.3	1.4	1.5	6.2	0.57	27.7	27.4		20.9
BF-9	162	0.68	0.38	<	<	0.18	0.67	0.87	8.2	7.9	0.55	37.2			29.1
BF-10	180	0.75	0.09	<	<	0.02	0.43	0.89	9.7	6.9	0.25	23.2			
BF-11	189	0.60	0.51	<	<	0.04	0.90	1.1	2.2	7.2	0.52	23.5			28.1
BF-12	199	0.75	0.61	0.01	<	0.03	1.3	1.2	1.5	7.3	0.41	31.0			
BF-13	217	1.2	1.0	<	<	0.06	1.5	1.5	2.8	7.2	0.60	39.3			
BF-14	235	0.02	0.01	<	<	0.02	0.56	0.71	0.99	9.9	0.02	17.8			
BF-15	244	0.02	0.01	<	<	0.01	0.39	0.53	0.70	11	0.04				
BF-16	254	0.32	0.18	0.07	0.01	0.01	3.2	3.7	0.19	1.2	0.09	23.4	25.7		
BF-17	272	0.18	0.17	<	0.01	0.01	1.7	1.9	0.15	5.4	0.09	24.3			
BF-18	290	0.02	0.01	<	<	<	1.7	1.7	0.14	5.7	0.01				
BF-19	299	0.25	0.19	<	<	0.04	0.87	1.1	4.1	7.7	0.17	22.2			25.2
BF-20	308	0.02	0.01	<	<	0.01	3.2	3.8	0.14	1.1	0.01				
BF-21	333	0.97	0.83	<	<	0.04	1.7	2.0	3.3	7.6	0.43	27.6			20.6
BF-22	344	0.51	0.39	<	<	0.01	0.77	1.0	0.58	9.1	0.47	32.7			
BF-23	353	0.32	0.22	0.01	<	0.10	1.2	1.5	8.3	7.1	0.20	33.8			30.6
BF-24	363	0.02	0.01	<	0.02	0.01	1.4	1.5	1.2	8.1	0.01				
BF-25	381	0.97	0.77	<	0.08	0.01	2.5	2.8	0.12	2.3	0.27	28.7		33.8	
BF-26	400	0.26	0.21	<	0.02	<	1.2	1.4	0.49	7.6	0.07	8.1			
BF-27	409	0.13	0.10	<	<	0.03	1.5	2.0	2.9	4.7	0.06	14.8			20.1
BF-28	418	0.86	0.56	<	0.08	0.12	2.5	2.3	1.2	6.0	0.20	33.8			
BF-29	437	8.5	7.4	0.01	0.06	<	8.4	9.0	1.2	2.7	0.77	20.7			18.7

Table A1. Analytical data—Continued

Sample	Meters	T-S%	DI-S%	Av-S%	SO ₄ -S% Org-S%	R-Fe%	T-Fe%	Org-C%	CO ₃ -C%	DOSr	del-Di	del-Av	del-SO ₄	del-Org
Lake stage 2—Continued														
01A CORE														
BF-30	454	0.97	0.01	0.80	0.02	0.02	3.9	4.4	0.47	4.5	0.35	16.4	17.6	40.9
Lake stage 1														
BF-31	464	1.1	0.87	0.02	<	0.16	2.7	2.6	12	2.3	0.30	20.9		22.7
BF-32	473	1.7	1.4	<	0.01	0.13	2.2	2.9	7.3	3.2	0.57	18.0		21.6
BF-33	491	2.2	1.9	<	0.06	0.30	2.3	2.9	5.8	3.9	0.75	5.5	11.9	16.1
BF-34	500	1.5	1.1	<	0.01	0.23	1.3	1.8	11	7.0	0.61	22.3		21.8
BF-35	509	2.8	1.7	<	0.07	0.15	1.9	2.3	2.5	7.4	0.77	7.8	10.0	7.5
Lake stage 3														
6	268	0.71	0.54	0.01	0.04	0.12	1.6	1.7	9.6	6.0	0.30	49.1	32.7	51.9
8	272	0.25	0.18	0.01	0.03	0.03	2.7	2.8	1.3	4.3	0.06	34.3	26.1	28.7
12	285	0.38	0.33	0.01	0.01	0.03	2.4	2.5	5.4	5.6	0.13	20.8		
14	290	2.0	1.4	0.01	0.08	0.64	1.4	1.8	34	2.6	0.89	25.0		27.9
18	304	0.83						1.5	13	7.2				
24	321	0.55						1.2	10	6.4				
26	328	0.59	0.52	0.01	<	0.08	1.3	1.5	7.5	7.5	0.35	44.3		39.4
Lake stage 2														
30	340	1.5						2.9	14	5.3				
36	358	1.3						1.8	23	5.3				
42	378	0.61	0.32	0.20	0.03	0.06	3.1	3.0	10	3.8	0.20	32.5	20.0	
48	395	2.5						2.3	7.0	4.5				
54	415	5.0						4.1	5.6	2.2				
59	429	1.1	0.85	0.01	0.04	0.22	1.6	1.7	12	5.4	0.47	40.1	33.8	36.0
62	437	0.24						0.85	18	7.4				
65	448	0.9	0.69	0.01	0.13	0.07	1.5	1.8	10	6.3	0.41	27.4	27.3	26.7
72	468	1.3						2.3	13	5.3				
74	474	0.93						2.1	11	5.2				
78	486	1.4	1.3	0.01	0.08	0.01	2.4	2.4	11	4.9	0.49	26.2	26.5	26.8
84	504	0.78						1.0	7.4	4.7				
86	510	2.4						3.4	14	4.7				
89	521	0.42	0.24	0.01	0.07	0.10	0.9	0.96	1.2	7.4	0.23	32.7	31.0	26.4
96	541	1.2	0.97	0.01	0.06	0.12	2.4	2.4	6.8	6.7	0.37	27.0	26.7	26.4
98	547	1.6	0.42	0.03	0.45	0.28	1.8	2.3	12	4.5	0.23	23.6	22.9	23.7

Table A1. Analytical data—Continued

Sample Meters	T-S%	Di-S%	Av-S%	SO4-S%	Org-S%	R-Fe%	T-Fe%	Org-C%	CO3-C%	DOSr	del-Di	del-Av	del-SO4	del-Org
Lake stage 2—Continued														
102	559	1.4				1.9	15	5.8						
108	578	0.94				1.4	17	5.2						
110	583	0.38				0.41	0.94	13						
113	595	1.8	0.93	0.08	0.42	2.3	2.5	14	5.6	0.41	23.9	26.4	26.3	
120	614	1.2				1.2	11	8.9						
123	625	1.4				3.5	8.9	3.8						
126	632	0.08	0.06	0.01	0.01	0.1	0.10	0.55	14	0.79	27.4			
132	651	0.47				1.0	8.5	8.6						
134	657	1.2	0.32	0.02	0.39	1.7	2.0	13	4.9	0.19	23.4	24.6		
138	669	0.52				1.3	17	7.3						
144	687	11	4.7	0.59	4.6	1.3	8.8	9.3	6.2	0.59	29.8	31.1		
Lake stage 1														
150	705	1.1	1.1	0.01	0.06	0.18	1.5	1.5	22	0.68	12.1	28.3	17.7	
154	717	1.5	0.85	0.02	0.01	0.15	1.9	2.4	12	0.42	30.2		9.4	
155	728	1.7				3.4	12	1.3						
162	743	3.7				4.2	14	1.8						
165	755	1.9	2.5	0.01	0.01	0.23	3.5	3.4	8.6	0.62	11.9		28.1	
168	760	0.83				2.0	3.2	6.2						
172	773	0.73	0.59	0.01	<	0.71	2.1	2.3	3.7	0.25	13.1		13.5	
COYOTE WASH CORE														
Lake stage 3														
cw-38	571	0.95	0.66	<	<	0.03	2.4	2.6	3.4	0.24	25.0		19.9	
cw-37	587	0.46				2.3	3.5	5.2						
cw-36	597	0.08	0.01	<	<	0.05	1.6	1.8	6.6	0.01	12.6		26.0	
cw-35	606	0.07				1.5	6.2	6.3						
cw-34	624	0.25	0.16	0.05	<	0.08	1.6	1.8	11	0.14	25.2	28.5	30.5	
cw-33	642	0.63				1.5	7.2	3.8						
cw-32	652	0.79	0.70	<	<	0.08	1.5	1.7	8.2	0.40	27.9		28.7	
cw-31	661	0.36	0.30	0.03	<	0.08	0.90	2.0	5.6	0.34	34.6	41.7	32.2	
cw-30	670	0.30				1.6	26	4.7						
cw-29	681	1.8	0.76	<	0.23	0.69	2.3	2.0	27	0.28	40.3	40.5	41.9	
Lake stage 2														
cw-28	697	0.04	<	<	<	0.04	1.6	1.6	2.5	8.4	0.00		40.4	

Table A1. Analytical data—Continued

Sample	Meters	T-S%	Di-S%	Av-S%	SO4-S%	Org-S%	R-Fe%	T-Fe%	Org-C%	CO3-C%	DOSr	del-Di	del-Av	del-SO4	del-Org
Lake stage 2—Continued															
cw-27	706	0.10					0.99	4.9	2.9						
cw-26	716	0.02	0.01	<	<	0.03	3.5	2.4	4.4		0.00	31.8			26.9
cw-25	725	0.50	0.39	<	0.06	0.03	1.8	2.4	0.90		0.19	41.9		40.8	20.9
cw-24	734	0.17	0.31	<	<	0.04	1.4	1.3	3.2	8.0	0.20	40.2			40.4
cw-23	752	1.0	0.93	<	<	0.08	2.0	2.1	4.9	6.4	0.42	30.0			29.2
cw-22	762	0.02					1.0	2.4	8.6						
cw-21	771	0.25	0.17	0.05	<	0.04	2.8	3.7	2.8	2.7	0.09	22.3			16.2
cw-20	789	1.8	0.64	1.0	<	0.10	3.6	4.1	7.6	2.2	0.63	31.9	32.1		28.7
cw-19	807	0.89	0.72	<	0.04	0.02	1.4	1.6	0.70	6.2	0.43	27.9		22.7	24.5
cw-18	815	1.1	0.29	0.67	0.02	0.03	3.0	3.3	1.2	4.3	0.47	26.2	26.8		19.4
cw-17	825	0.13	0.01	<	<	0.09	1.0	1.3	8.6	5.3	0.01				
cw-16	843	0.03					2.0	19	3.1						
cw-15	862	0.40	0.38	<	<	0.02	3.6	3.9	1.1	4.3	0.09	13.2			12.8
cw-14	871	0.12					1.8	4.8	6.9						
cw-13	880	4.0	3.3	<	<	0.12	3.4	3.7	5.8	6.0	0.83	25.6			
cw-12	898	0.04					2.6	1.3	7.5						
cw-11	907	0.04	0.03	<	<	0.02	1.7	2.3	1.8	3.6	0.02	17.2			
cw-10	917	1.0	0.84	<	<	0.01	3.1	3.7	0.60	4.1	0.25	11.4			10.7
cw-9	926	0.13					3.4	0.50	1.3						
cw-8	935	0.52	0.46	<	<	0.02	3.3	4.0	0.40	1.2	0.12	23.0			
Lake stage 1															
cw-7	953	0.06					2.7	0.90	2.6						
cw-6	971	1.5	1.3	<	<	0.01	2.9	3.7	0.60	3.4	0.40	7.3			
cw-5a	981	0.47					3.8	0.50	1.9						
cw-5	990	0.37	0.16	<	0.07	0.02	2.2	3.0	0.60	2.1	0.07	10.9		38.2	11.0
cw-4	1008	0.11					2.1	0.30	2.1						
cw-3	1026	0.80	0.59	<	0.02	0.08	0.90	1.2	6.2	6.1	0.56	4.7			14.6
cw-2	1035	0.04					2.9	0.30	2.4						
cw-1	1043	0.86	0.78	<	<	0.05	2.6	2.9	3.3	7.5	0.25	27.8			20.6

APPENDIX 2—CALCULATION OF GYPSUM THICKNESS

The equivalent bedded gypsum thickness in the stage 2 (saline) interval of the 01A and Blacks Fork cores was calculated as follows. The average amount of sulfur (table

2) was converted to moles of sulfur per gram rock. A density of 2.3 for Green River oil shale (Smith, 1969) was used to convert the amount of grams to a volume. The moles equivalent gypsum and the density of gypsum were used to convert the volume into a thickness (meters) of bedded gypsum equivalence.

Chapter C

A Preliminary Study of the Carbon and Nitrogen Isotopic Biogeochemistry of Lacustrine Sedimentary Rocks from the Green River Formation, Wyoming, Utah, and Colorado

By JAMES W. COLLISTER and J.M. HAYES

U.S. GEOLOGICAL SURVEY BULLETIN 1973

GEOCHEMICAL, BIOGEOCHEMICAL, AND SEDIMENTOLOGICAL STUDIES OF THE GREEN RIVER FORMATION, WYOMING, UTAH, AND COLORADO

CONTENTS

Abstract	C1
Introduction	C1
Methods	C2
Class fractionation of total extract	C2
Inorganic nitrogen analysis	C3
Combustion procedure and cryogenic distillation	C3
Results	C3
Discussion	C5
Depositional models for the Green River Formation	C6
Isotopically enriched organic nitrogen	C8
Models of nitrogen cycling in the Green River lakes	C9
Saline (playa-lake) stages	C10
Fresh (meromictic lake) stages	C11
Comparison of Piceance, Uinta, and greater Green River basins	C12
Isotopically depleted total organic carbon	C12
Sources of isotopically depleted organic carbon	C13
Anaerobic photosynthetic bacteria	C13
Methanogens and methylotrophs	C13
Summary	C14
References cited	C14

FIGURES

- 1–3. Depth profiles of total organic carbon content and $\delta^{13}\text{C}$ and $\delta^{15}\text{N}$ compositions of kerogen in Green River Formation for:
 1. 01A core, Piceance basin, Colorado C6
 2. Blacks Fork core, greater Green River basin, Wyoming C7
 3. Coyote Wash no. 1 core, Uinta basin, Utah C7
- 4–6. Diagrams showing:
 4. Distribution of ^{15}N in freshwater environments C9
 5. Proposed nitrogen cycle for saline stages of Green River lakes C10
 6. Microbial nitrogen cycle for meromictic lakes C11

TABLES

1. Observed fractionation factors for the major pathways in the nitrogen cycle C2
- 2–4. Data bases for the:
 2. 01A core, Piceance basin, Colorado C4
 3. Blacks Fork core no. 1, greater Green River basin, Wyoming C5
 4. Coyote Wash no. 1 core, Uinta basin, Utah C5
5. Isotopic composition of organic and inorganic nitrogen of evaporites of the Green River Formation from the 01A core, Piceance basin, Colorado C8

A Preliminary Study of the Carbon and Nitrogen Isotopic Biogeochemistry of Lacustrine Sedimentary Rocks from the Green River Formation, Wyoming, Utah, and Colorado

By James W. Collister and J.M. Hayes¹

Abstract

The Paleogene Green River Formation in the tri-State region of Wyoming, Utah, and Colorado contains the world's largest known reserve of oil shale. The unusually high organic content of these lacustrine rocks is a striking example of the productivity and preservation potential of hydrocarbons deposited in modern saline lacustrine environments. In order to reconstruct the biogeochemistry of this lacustrine setting, carbon and nitrogen isotopic compositions of Green River organic material were studied. The results of this study indicate that a complex nitrogen cycle existed in this lake system. Isotopic compositions of organic nitrogen in the Green River sedimentary rocks are highly enriched and significantly variable (+10.8 to +20.7‰). Because isotopic fractionation accompanying nitrogen fixation is negligible, organisms utilizing this pathway to meet their nitrogen requirements should reflect the isotopic composition of atmospheric N₂ (0‰). The existence of ¹⁵N-enriched organic matter in these rocks requires a complex nitrogen cycle in the lake system and indicates that nitrogen was not a limiting nutrient for primary growth. Cyanobacterial assimilation of ammonia and nitrate enriched in ¹⁵N from the microbial processes of denitrification and nitrification probably accounts for the isotopic enrichment.

The carbon isotopic composition of Green River kerogens is from -41.4 to -28.8‰. Geoporphyrins can serve as isotopic biomarkers for primary photosynthate and can therefore provide an estimated range of ¹³C compositions of primary producers in the Green River lakes. Nickel geopor-

phyrins from two samples have $\delta^{13}\text{C}$ values of -23.6 and -28.6‰. A large isotopic depletion (-17‰) in at least one kerogen relative to the associated geoporphyrins indicates large contributions of isotopically depleted organic material to the sediments. Possible sources of isotopically depleted carbon include photosynthetic sulfur bacteria at the chemocline of a stratified lake and methane cycling by methylotrophs.

INTRODUCTION

Organic matter comprises an unusually large volume fraction (1–40 percent; Robinson, 1976) of the total rock in the lacustrine Paleogene (Eocene, locally Paleocene) Green River Formation of Wyoming, Utah, and Colorado. Modern hypersaline environments are some of the most productive on earth (Warren, 1986), and the accumulation of organic carbon in the Green River Formation suggests that the saline Green River lake system supported a highly productive community and provided an environment that favored preservation of organic material. Production of biomass requires phosphorus, sulfur, and nitrogen, as well as the carbon, hydrogen, and oxygen that are plentiful in lacustrine environments. Although concentrations of phosphorus commonly are biolimiting, particularly in unpolluted lacustrine environments, the presence of large quantities of organic material in the Green River rocks indicates that fluvial inputs of phosphate must have been substantial. (We can speculate that the remarkable organic richness of the Green River sediments is due to fertilization of the lake system by erosion of the Permian Phosphoria Formation.) Given adequate supplies of phosphorus, lacustrine communities can obtain nitrogen by fixation of N₂. In order

¹Biogeochemical Laboratories, Departments of Chemistry and of Geology, Geology Building, Indiana University, Bloomington, Indiana, 47405-5101.

Table 1. Observed fractionation factors for the major pathways in the nitrogen cycle

Isotope effect	Observed fractionation factors	
	$\alpha(\text{react}/\text{prod})$	Reference
Kinetic isotope effects		
Nitrogen fixation		
Atmospheric $\text{N}_2 \rightarrow \text{Fixed nitrogen}$	1.000	Hoering and Ford (1960).
	1.004	Delwiche and Stein (1970).
	0.996-1.009	Wada and others (1975).
	1.0022	Takigiku (1987).
	1.0024	Macko and others (1987).
Nitrification: $\text{NH}_4^+ \rightarrow \text{NO}_2^-$	1.02	Miyake and Wada (1971).
Denitrification: $\text{NO}_3^- \rightarrow \text{N}_2$	1.02	Delwiche and Stein (1970), Miyake and Wada (1971), Wellman and others (1968).
	1.04	Cline and Kaplan (1975).
Inorganic nitrogen assimilation		
Nitrate assimilation: $\text{NO}_3^+ \rightarrow \text{Cell-N}$	1.011-1.013	Macko and others (1987).
	1.013-1.023	Wada and Hattori (1978).
Ammonium assimilation: $\text{NH}_4^+ \rightarrow \text{Cell-N}$	1.013	Macko and others (1987).
	0.993-1.010	Wada and others (1975).
Decomposition: Sediment organic-N $\rightarrow \text{NH}_4^+$	1.001	Miyake and Wada (1975).
Equilibrium isotope effects		
Ammonia volatilization: $\text{NH}_4^+(\text{aq}) \rightarrow \text{NH}_3(\text{gas}), 25^\circ\text{C}$	1.034	Kirschenbaum and others (1947).
Solution of nitrogen gas: $\text{N}_2(\text{solution}) \rightarrow \text{N}_2(\text{gas}), 0^\circ\text{C}$	1.00085	Klots and Benson (1963).

to study the production of organic material in the Green River lake system, we chose to focus on the nutrition of the producer community and, in particular, on the cycling of nitrogen within these lakes. Nitrogen isotopic analyses provide a new view of this phenomenon.

Unlike phosphorus, nitrogen has an active redox cycle and passes through many mobile forms. The biogeochemical nitrogen cycle is comprised of processes in which nitrogen is present in a combination of oxidation states (-3 to +5). A restricted group of microorganisms mediates most of the reactions in this cycle. Organic material is decomposed to produce ammonia and CO_2 in a process termed mineralization. Ammonia produced by mineralization has several possible fates. In anaerobic environments, ammonium is directly assimilated by plants and bacteria. In aerobic environments, ammonium is oxidized to nitrate by nitrifying bacteria. Evaporation of surface waters and concomitant volatilization of ammonia removes ammonia from the lacustrine system. Nitrate is either assimilated directly by plants, or, in anaerobic environments, is reduced to N_2 by the process of denitrification, in which denitrifying bacteria utilize NO_3^- as a terminal electron acceptor. The loss of N_2 from sediments to the atmosphere by denitrification is balanced by nitrogen-fixing bacteria that convert N_2 to organic nitrogen (herein

referred to as organic-N). The observed isotopic fractionation factors for the major pathways in the nitrogen cycle are summarized in table 1.

METHODS

For isotopic analysis of total organic carbon, 5–10 mg of powdered, decalcified sample was combusted in a sealed quartz combustion tube at 850°C (Knoll and others, 1986). The percentage of total organic carbon in the sample was determined from the yield of CO_2 . Kerogen was isolated using the method described by Wedeking and others (1983), and carbon, hydrogen, and nitrogen elemental contents were obtained by use of a Carlo Erba model 1106 elemental analyzer. Total extractable organic matter was obtained by Soxhlet extraction with 50/50 (v/v) dichloromethane-methanol for about 72 hours. Excess solvent was removed by rotary evaporation at $20\text{--}30^\circ\text{C}$.

Class Fractionation of Total Extract

Subfractions of the total extracts enriched in geophyryns were prepared following the method outlined by Takigiku (1987). A modification of this method was

employed to isolate large quantities of geoporphyrins from gilsonite. A 2.5 cm by 40 cm column was packed with activated silica gel. About 200 mg of gilsonite (a pyrobitumen from the Uinta basin present as dike and fracture fillings; Hunt and others, 1954) was taken up in a minimal amount of hexane and transferred to the top of the column. The saturate fraction was eluted using 250 mL of n-hexane, followed by 250 mL of a 2 percent solution of dichloromethane in petroleum ether to elute saturated hydrocarbons and some aromatic compounds. The fraction enriched in geoporphyrins was then eluted using 250 mL of a 70/50/5 (v/v/v) mixture of hexane, toluene, and ethyl acetate. This subfraction was further purified by thin-layer chromatography (TLC) as outlined by Takigiku (1987). Purities of the porphyrin subfractions were checked using ultraviolet-visible spectrophotometry. Identification of nickel geoporphyrins was based on analysis of visible spectra. Final purification of the porphyrin fractions was carried out using high-pressure liquid chromatography (HPLC) (Altech 605RPD C18 reverse-phase column, 4.6 mm by 250 mm, 5- μ m particle size, eluted isocratically using 80/20 v/v acetonitrile/methanol at 1 mL/min).

Inorganic Nitrogen Analysis

Three varieties of evaporites from the Green River Formation were examined: bedded nahcolite, nodular nahcolite, and bedded halite. Weighed samples of powdered evaporite mineral were dissolved in deionized water and filtered through a 0.2–2 μ m cellulose filter to remove particulate material. The filtrate was analyzed using ion exchange chromatography to detect the presence of nitrate and nitrite.

Separation of the organic fractions from the evaporite mineral phase was carried out using a separatory funnel extraction. Several grams of powdered evaporite mineral was placed in a 500-mL separatory funnel together with 100 mL of dichloromethane and 250 mL of deionized water. Upon dissolution of the mineral phase, the water layer was recovered and filtered. The remaining material was then washed twice with approximately 200 mL of deionized water. The water layer from each washing was filtered and added to the original aqueous phase. Purified saline minerals were recovered by evaporation of the water. Total extractable organic material was recovered by draining and filtering the dichloromethane layer through a 2- μ m Teflon filter. Excess solvent was removed by rotary evaporation at 20–30 °C. The remaining insoluble material was transferred to a Nalgene bottle and centrifuged for 30 minutes. Kerogen was isolated from insoluble material using the procedure of Wedeking and others (1983).

Combustion Procedure and Cryogenic Distillation

Throughout this study, a modified Dumas combustion (Macko, 1981) was utilized for preparation of samples of N₂ from kerogens and extracts. An organic sample of approximately 15–25 mg was placed in a Vycor combustion tube (9 mm outside diameter by 150 mm long). Approximately 2 g of CuO wire and 1 g copper shavings were placed in the tube together with a 0.5-cm square of silver foil. The combustion tubes were evacuated, sealed, and placed in a muffle furnace. Combustion of the samples was carried out at 850 °C for at least 12 hours, followed by at least 2 hours at 550 °C to allow for complete reduction of nitrogen oxides.

After combustion, an O-ring compression fitting was used to adopt tubes to the cracker described by Baker (1987). Operation of the cracker released gaseous contents of each tube to a vacuum system. Nitrogen gas was collected on 2–3 pellets (5 mm by 3 mm diameter) of 5-angstrom molecular sieve (–196 °C, 10 minutes; Kobayakawa and others, 1962) placed in a Pyrex collection tube (6 mm by 120 mm). Prior to collection of N₂, the sieves were degassed on line by heating at 200 °C for approximately 15 minutes. Because of the large amounts of CO₂ and H₂O produced during combustion of large samples required for nitrogen analysis, the end of the combustion tube was immersed in liquid nitrogen for several minutes prior to admitting the sample into the vacuum line. Samples of CO₂ were subsequently cryogenically distilled and collected for mass spectrometric analysis.

Samples of N₂ were released from the molecular sieve by heating at 90 °C for 2 minutes. The sample was then introduced into the mass spectrometer, and the molecular sieves were kept at 90 °C to ensure that none of the nitrogen remained on the sieves.

All isotopic analyses were carried out on a Finnigan Delta-E mass spectrometer. Overall analytical uncertainties are $\pm 0.2\%$ for $\delta^{13}\text{C}$ and $\pm 0.6\%$ for $\delta^{15}\text{N}$ (95 percent confidence limits).

RESULTS

Results of the geochemical analyses are shown in tables 2–4 (sample descriptions are given in Tuttle, this volume). Two distinct features are readily apparent: (1) the organic matter is extremely enriched in ¹⁵N compared to other reported values, and (2) the same material is depleted in ¹³C compared to most modern lacustrine organic material. Organic material from lake sediments shows a broad range of isotopic compositions (–8 to –38‰), but organic matter from most lacustrine sediments has $\delta^{13}\text{C}$ values in the range of –18 to –28‰ (Stuiver, 1964, 1975; Deines, 1980). Figures 1–3 show total organic carbon

Table 2. Data base for 01A core, Piceance basin, Colorado

[Location of core hole shown in Tuttle (this volume, fig. 1). TOC is total organic carbon; KER is kerogen; DOL is dolomite. Leaders (--) indicate not determined]

Sample	Depth (meters)	Weight percent				C:N ratio	H:C ratio	$\delta^{13}\text{C}$ DOL ¹
		TOC	$\delta^{13}\text{C}$ TOC	$\delta^{13}\text{C}$ KER	$\delta^{15}\text{N}$ KER			
01-6	268	9.60	-29.9	-31.2	20.7	33	1.67	9.1
01-8	272	1.30	-28.7	-41.4	15.6	91	1.02	6.0
01-12	285	5.40		-32.0	19.1	45	1.57	8.6
01-14	290	34.00	-30.9	-31.4	18.4	45	1.71	6.3
01-24	321	10.00	-29.8	-30.4	19.4	38	1.56	7.5
01-26	328	7.50	-31.4	-32.1	17.0	31	1.43	6.0
01-36	358	23.00	-29.2	-29.4	14.7	48	1.61	10.4
01-59	429	12.00	-33.5	-33.7	15.2	37	1.66	-5.7
01-62	437	18.00	-31.4	-32.3	15.8	29	1.61	1.5
01-65	448	10.00	--	-33.0	16.3	28	1.54	3.3
01-72	468	13.00	-30.6	-31.1	16.4	36	1.56	5.7
01-78	486	11.00	--	-31.6	16.5	26	1.60	7.2
01-84	504	7.40	-30.9	-31.4	16.6	42	1.60	4.1
NaCl	512	--	--	-36.5	11.5	--	--	--
01-89	521	1.20	-30.1	-31.5	17.3	31	1.60	2.9
01-96	541	6.80	-31.7	-32.5	16.1	31	1.49	4.5
01-98	547	12.00	--	-29.9	17.8	34	1.62	6.8
01-102	559	15.00	-31.1	-31.7	17.6	34	1.70	6.4
01-113	595	14.00	-31.0	-31.5	16.4	45	1.68	7.2
01-126	632	0.55	--	-34.9	10.8	26	1.04	6.5
NaHCO ₃	646	--	--	-33.6	12.9	36	1.50	--
01-132	651	8.50	-32.3	-32.7	13.7	43	1.66	6.1
01-134	657	13.00	-32.0	-31.0	16.8	38	1.64	7.8
b NaHCO ₃	680	--	--	-35.5	12.0	--	--	--
01-144	687	6.20	--	-31.8	18.0	36	1.94	4.5
01-150	705	22.00	-32.9	-33.4	13.4	38	1.56	7.6
01-154	717	12.00	-30.0	-30.5	14.3	53	1.44	3.1
01-165	755	12.00	-30.9	-31.3	16.0	43	1.65	5.7
01-172	773	14.00	-29.9	-30.3	14.5	32	1.55	11.4

¹From M.L. Tuttle (U.S. Geological Survey, written commun., 1987).

(TOC, in percent) content and carbon and nitrogen isotopic compositions of samples of kerogen from the three cores plotted versus depth.

Kerogen isolates from the Green River Formation show a broad range of nitrogen isotopic compositions; $\delta^{15}\text{N}$ values are from +10.8 to +20.7‰. The $\delta^{15}\text{N}$ values for the associated total extracts are depleted in ^{15}N by 0.7–4.8‰ relative to the kerogens. Nitrogen isotopic compositions of organic material, total inorganic nitrogen (inorganic-N), and nitrate from Green River Formation evaporites are compared in table 5. $\delta^{15}\text{N}$ values for total inorganic-N in these samples are from +8.0 to +9.5‰. These values are depleted in ^{15}N relative to kerogen and total extractable organic matter isolated from the same samples (table 5).

Another striking observation is the depletion of ^{13}C in the organic matter in the Green River Formation; $\delta^{13}\text{C}$ values for kerogens are from -41.4 to -28.8‰. Total

extracts are enriched in ^{13}C relative to associated kerogens by 1–4‰ (tables 2–4), and dolomite in the core samples is enriched in ^{13}C . $\delta^{13}\text{C}$ values for dolomite in the Blacks Fork and 01-A cores are shown in tables 2 and 3 (core locations shown in Tuttle, this volume, fig. 1). These values, from -5.7 to +11.4‰ versus PDB, are enriched in ^{13}C as compared to many lacustrine carbonate rocks. Stuiver (1970) measured $\delta^{13}\text{C}$ values for carbonate minerals from four lakes in North America of from -7.5 to +4‰. Other studies of lacustrine carbonate minerals indicate $\delta^{13}\text{C}$ values from -7.7 to +6.3‰ (Broecker and Olson, 1959; Oana and Deevey, 1960; Stuiver, 1975; Lee and others, 1987). The most ^{13}C enriched value was for tufa along the lakeshore of Pyramid Lake (Broecker and Olson, 1959). Stuiver (1964) measured $\delta^{13}\text{C}$ values for carbonate minerals from Searles Lake (a saline lake in California) of from +1 to +4.6‰ and one value of +10.1‰.

Table 3. Data base for Blacks Fork core no. 1, Green River basin, Wyoming

[Location of core hole shown in Tuttle (this volume, fig. 1). TOC is total organic carbon; KER is kerogen; DOL is dolomite. Leaders (–) indicate not determined]

Sample	Depth (meters)	Weight percent				C:N ratio	H:C ratio	$\delta^{13}\text{C}$ DOL ¹
		TOC	$\delta^{13}\text{C}$ TOC	$\delta^{13}\text{C}$ KER	$\delta^{15}\text{N}$ KER			
BF-4	98	8.30	-32.4	-32.9	14.9	–	–	10.1
BF-6	125	4.10	-30.4	-31.1	10.1	50	1.88	-1.5
BF-7	134	7.00	-29.8	-30.0	12.1	30	1.68	5.7
BF-8	144	1.50	-29.3	-30.8	16.7	–	–	4.0
BF-13	217	2.80	-31.1	–	18.0	–	–	2.5
BF-19	299	4.10	-31.2	-32.2	17.7	–	–	2.1
BF-22	344	0.58	-25.7	-32.3	11.4	–	–	4.3
BF-23	353	8.30	-32.1	-32.8	18.3	–	–	3.1
BF-31	464	12.00	-33.9	-34.5	18.9	–	–	4.0
BF-34	500	11.00	-31.8	-32.2	13.3	–	–	9.1

¹From M.L. Tuttle (U.S. Geological Survey, written commun., 1987)

Table 4. Data base for Coyote Wash no. 1 core, Uinta basin, Utah

[Location of core hole shown in Tuttle (this volume, fig. 1). TOC is total organic carbon; KER is kerogen; DOL is dolomite. Leaders (–) indicate not determined]

Sample	Depth (meters)	Weight percent				C:N ratio	H:C ratio
		TOC	$\delta^{13}\text{C}$ TOC	$\delta^{13}\text{C}$ KER	$\delta^{15}\text{N}$ KER		
CW-38	571	3.40	-29.6	-29.5	18.6	26	1.47
CW-31	661	5.60	-29.8	-29.5	18.2	31	1.48
CW-29	681	27.00	-28.5	-28.8	17.9	34	1.72
CW-28	697	2.50	–	-32.4	20.5	–	–
CW-26	716	2.40	-30.8	-32.1	16.2	32	1.62
CW-20	789	7.60	-28.3	-28.8	16.9	34	1.74
CW-18	815	1.20	-30.3	-31.1	10.4	24	1.83
CW-13	880	5.80	-30.8	-31.0	16.6	29	1.71
CW-11	908	1.80	-30.8	-31.8	15.0	36	1.77
CW-1	1,043	3.30	-30.5	-31.4	14.3	33	1.98

Nickel geoporphyryns were isolated from the extracts of two samples from the 01A core (Colorado). Geoporphyryns from samples 01–8 and 01–36 have $\delta^{13}\text{C}$ values of -23.6‰ , and -28.6‰ , respectively. Nickel geoporphyryns isolated from gilsonite from the Uinta basin have a $\delta^{13}\text{C}$ value of -28.5‰ .

DISCUSSION

The variability of the nitrogen isotopic compositions of the organic matter in this sequence of rocks must carry information regarding (1) the nutrition of the organisms in these lakes and (2) the cycling of nitrogenous compounds in this ecosystem; however, more significant than the variability is the enrichment in ^{15}N (see Letolle, 1980). Such extreme enrichment in ^{15}N for total organic-N is known from only a few ancient and modern sediments (fig. 4). In a study of nitrogen isotopes in the Scheldt estuary, Mariotti and others (1984) measured $\delta^{15}\text{N}$ values for NH_4^+ and

suspended organic matter in the water column. These authors observed extreme ^{15}N enrichments, as well as dramatic seasonal variability, in the $\delta^{15}\text{N}$ values for both fractions. $\delta^{15}\text{N}$ values of NH_4^+ were from +10 to greater than $+30\text{‰}$, and those for suspended organic matter were from +2 to $+18\text{‰}$. Mariotti and others (1984) speculated that algae were assimilating a pool of ^{15}N -enriched ammonium produced by nitrification. Cifuentes and others (1988) measured $\delta^{15}\text{N}$ values of particulate organic matter (POM) in the Delaware estuary and found large seasonal effects on the nitrogen isotopic composition of this material. In the winter, $\delta^{15}\text{N}$ values for POM were between $+5.5$ and $+12.2\text{‰}$, and a maximum $\delta^{15}\text{N}$ value of $+18.7\text{‰}$ was observed in April. These authors suggested that algae were assimilating a pool of ammonium enriched in ^{15}N ($>30\text{‰}$) generated by fractionations accompanying previous assimilation. Kerogen isolated from the Eocene Messel shale (West Germany) was chosen for comparison of a stratified lake that existed during the same epoch as the

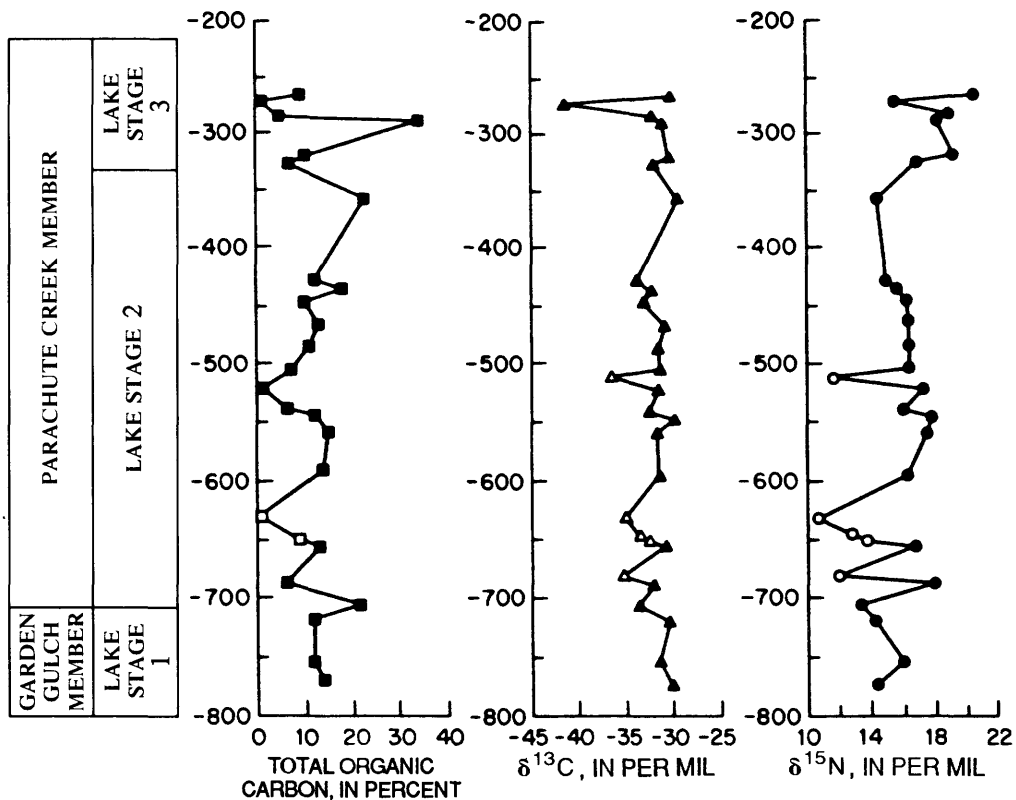


Figure 1. Depth (in meters) profiles of total organic carbon content and $\delta^{13}\text{C}$ and $\delta^{15}\text{N}$ compositions of kerogen in Green River Formation for 01A core, Piceance basin, Colorado. Open symbols represent samples whose mineralogy indicates extreme evaporitic conditions. Location of core shown in Tuttle (this volume, fig. 1).

Green River lakes. This material has a $\delta^{15}\text{N}$ value of +6.8‰ (Collister, 1989).

If, as is likely, isotopic compositions of inorganic-N sources were roughly constant, the observation of wide variations in the abundance of ^{15}N must indicate either significant variations in the biological cycling of nitrogen. Further, the presence of ^{15}N -enriched organic matter indicates that nitrogen inputs either were, on average, highly enriched in ^{15}N or were extensively reworked and fractionated. As shown by the fractionation factors summarized in table 1, processes capable of causing significant isotopic shifts involve assimilation, oxidation, reduction, and volatilization of nitrogen. Of course, these processes occur to one degree or another in almost all environments, yet they do not cause ^{15}N -enrichments approaching those recorded by Green River rocks. Processes occurring in the Green River lake system must have been unusual in that they allowed the escape of considerable quantities of ^{15}N -depleted material. Moreover, the escape of ^{15}N -depleted material occurred while large quantities of organic-N were being sequestered in accumulating sediments. The significant isotopic fractionation is, therefore, a signal that nitrogen was not the limiting nutrient in the Green River lake system. Because the 01A core is the

most densely sampled of the three cores analyzed, most of our interpretation of the biogeochemistry of the Green River Formation is based on the geochemical data for this core.

Depositional Models for the Green River Formation

Two models of deposition have been proposed for the lacustrine origin of the Green River Formation. The first, involving a meromictic or permanently stratified lake, has been discussed in detail by Bradley (1948, 1964), Bradley and Eugster (1969), Smith (1974), and Desborough (1978). The second, involving a playa-lake complex, was introduced by Eugster and Surdam (1973) and has been elaborated in more recent articles (Eugster and Hardie, 1975; Lundell and Surdam, 1975; Surdam and Stanley, 1979).

In the meromictic-lake model, the lakes are thought to have been deeper than 30 m (100 ft) and have chemically and thermally stratified water columns (Sullivan, 1980). At their margins, the lakes gradually shallowed to shoals and other shallow-water environments (Sullivan, 1980). Shallow-water sedimentary rocks include calcareous and

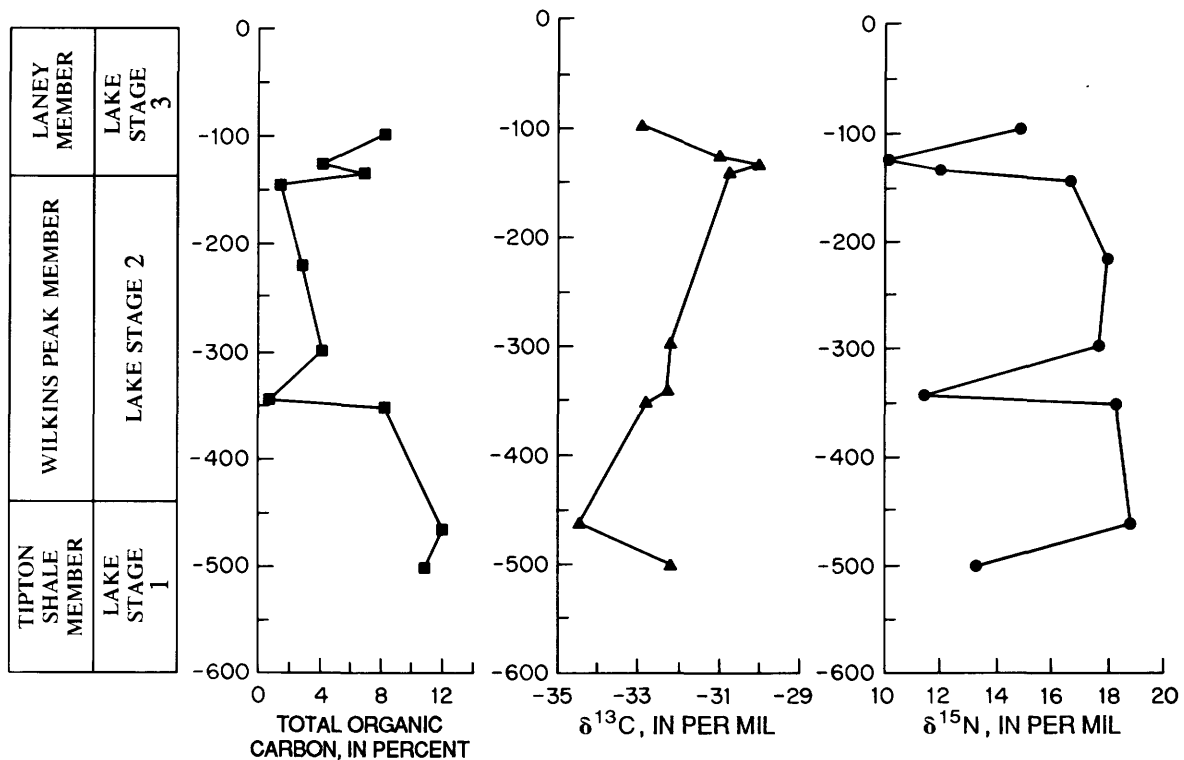


Figure 2. Depth (in meters) profiles of total organic carbon content and $\delta^{13}\text{C}$ and $\delta^{15}\text{N}$ compositions of kerogen in Green River Formation for Blacks Fork core, greater Green River basin, Wyoming. Location of core shown in Tuttle (this volume, fig. 1).

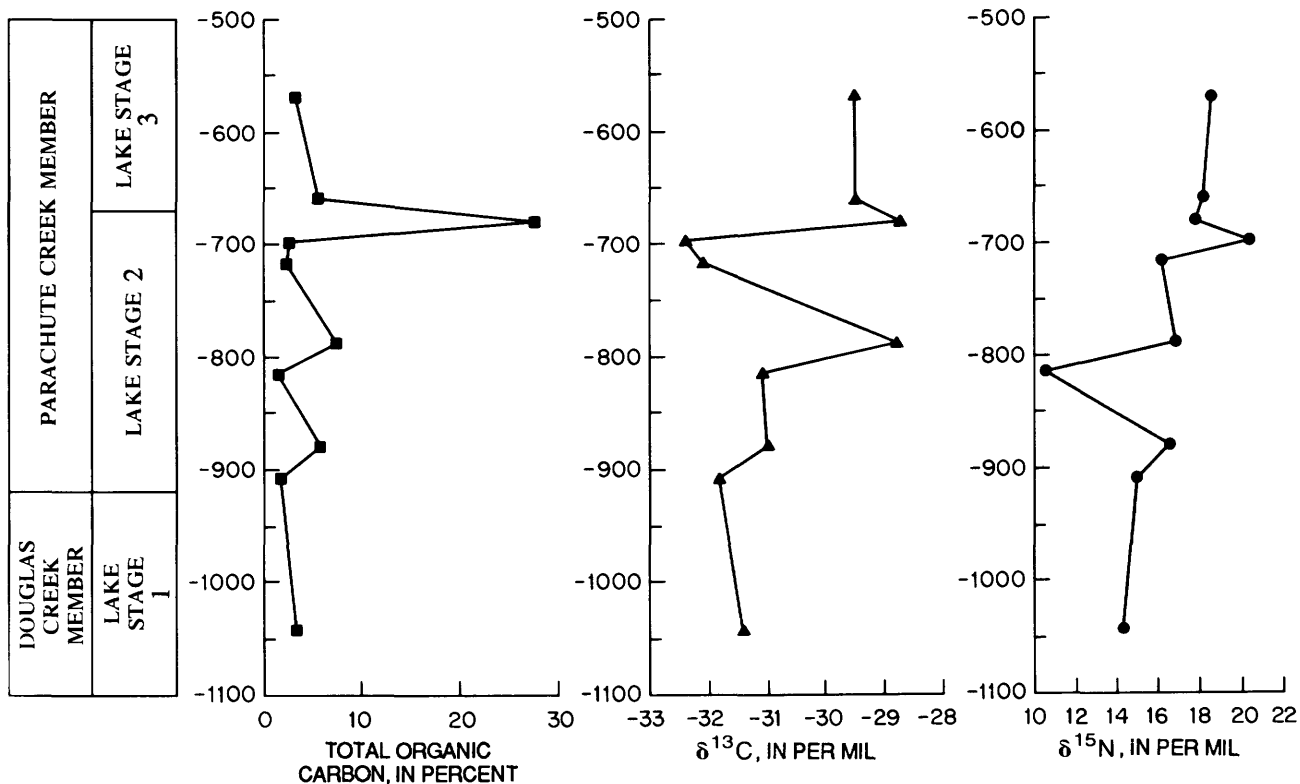


Figure 3. Depth (in meters) profiles of total organic carbon content and $\delta^{13}\text{C}$ and $\delta^{15}\text{N}$ compositions of kerogen in Green River Formation for Coyote Wash no.1 core, Uinta basin, Utah. Location of core shown in Tuttle (this volume, fig. 1).

Table 5. Isotopic composition of organic and inorganic nitrogen of evaporites of the Green River Formation from the 01A core, Piceance basin, Colorado

[Location of core shown in Tuttle (this volume, fig. 1). Leaders (--) indicate not determined. $\delta^{15}\text{N}$ in per mil]

Sample	Depth (meters)	NO_3^- detected	$\delta^{15}\text{N}$ (kerogen)	$\delta^{15}\text{N}$ (NO_3^-)
Bedded halite.....	512	+	11.5	9.5
Nodular nahcolite.....	648	+	10.8	8.0
Bedded nahcolite	680	--	12.0	--

dolomitic mudstone, fine clastic sandstone, marlstone, and limestone of the carbonate facies, and deeper water rocks include laminated carbonate (oil shale) rocks (Sullivan, 1980). Organic material preserved in the oil shale facies was derived from abundant plant and animal life in the upper euphotic zones (Sullivan, 1980). The lack of bioturbation in the Green River Formation indicates that monimolimnetic waters in the Green River lakes were a hostile environment for metazoan grazers, probably because they were anoxic (Sullivan, 1980). As a result, the bottom waters of these lakes had a high preservation potential for organic matter that originated in the surface waters and accumulated on the lake bottoms (Sullivan, 1980). Bradley (1929) interpreted the varves of the oil shale facies as representing a yearly cycle in these lakes. The organic-rich accumulation on the bottom of the centers of the basins was modified in the summer months by a large influx of carbonate due to increased photosynthetic activity of blue-green algae in the warmer surface waters. This process is thought to account for the characteristic varves of the Green River Formation, which consist of organic-rich laminae alternating with carbonate laminae (Sullivan, 1980).

Although the meromictic-lake model accounts for many aspects of the Green River Formation, Sullivan (1980) listed several observations that the model does not adequately explain: (1) the absence of a modern analogue; (2) sedimentary structures indicative of shallow water; (3) the presence of Magadi-type chert similar to that found in alkaline lakes of East Africa; (4) the close association of oil shale and trona, which suggests related depositional environments for these rocks; and (5) the predominance of dolomite as compared to calcite in these rocks, which is consistent with the playa-lake model.

The playa-lake model was proposed by Eugster and Surdam (1973) to explain inconsistencies of the deep stratified model. This model is based mostly on observations made at the margins of the basins. In this model, broad alluvial fans flanked the mountains surrounding the lakes and graded into broad playa flats (Sullivan, 1980). Shallow perennial lakes maintained by ground water and springs were located in the basin centers. The playa flats were areas of high evaporation, and

evaporation in the capillary zone above the water table on the playa produced a crust of alkaline salts (Sullivan, 1980) and resulted in deposition of dolomitic and calcareous mudstone of the carbonate facies (Eugster and Surdam, 1973).

In the playa-lake model, only evaporites and laminated carbonate rocks (oil shale) are of truly lacustrine origin. Evaporite minerals were formed in the lakes because of the high evaporation rates, and the oil shales probably formed in the shallow lakes under less arid conditions (Sullivan, 1980). Such an environment would support abundant microscopic aquatic plants due to the high nutrient concentration of the waters, and the accumulation of this algal ooze would lead to the formation of oil shale (Sullivan, 1980).

Boyer (1982) suggested that these two models of deposition are not necessarily mutually exclusive but may be complementary. He proposed that periods of meromixis in the Green River lakes may have resulted directly from prior episodes of brine generation in playa-lake environments.

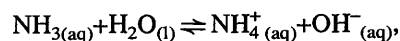
Isotopically Enriched Organic Nitrogen

If the primary producers, mainly cyanobacteria (Bradley, 1931, 1970; Robinson, 1979), in the Green River lakes had met their nitrogen requirements solely by means of nitrogen fixation, then the nitrogen isotopic composition of the organic matter should be similar to that of atmospheric nitrogen (0‰). Alternatively, the isotopic composition of cyanobacteria assimilating combined inorganic-N would closely reflect the isotopic composition of the inorganic-N source (Mariotti and others, 1984).

Mineralogical evidence strongly suggests that the depositional environment of the Green River lakes was highly evaporitic and alkaline and had a pH of from 8 to 9.5 (Smith and Robb, 1973). In such an environment, ammonia volatilization is likely to be an important physical process. The fractionation factor associated with this process is the largest for any in the nitrogen cycle [$\alpha(\text{NH}_4^+/\text{NH}_3)=1.034$]. This fractionation, which enriches the residual ammonium in ^{15}N , can be described as an open-system fractionation. The concentrations of NH_3 and NH_4^+ in solution are pH dependent and are described by the Henderson-Hasselbalch equation,

$$\text{pH}=\text{pK}_a+\log \frac{[\text{base}]}{[\text{acid}]}$$

The K_a for ammonium is 5.6×10^{-10} , and pK_a is 9.25. For the equilibrium of ammonia in an aqueous solution,



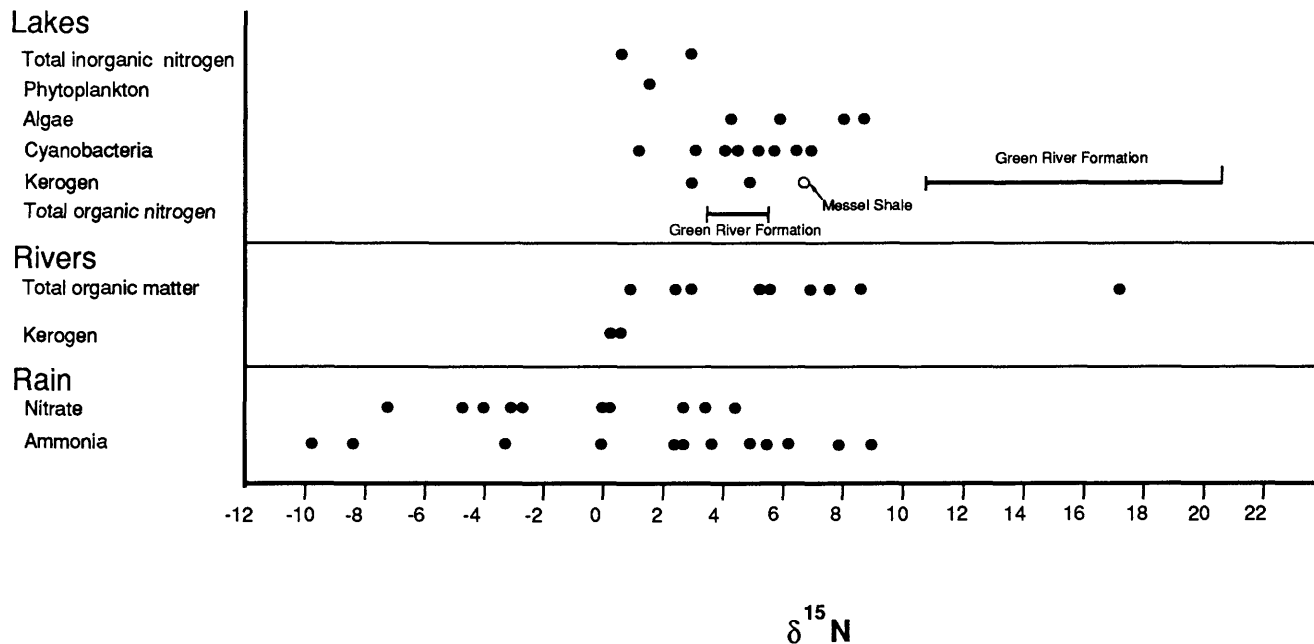
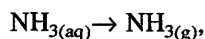


Figure 4. Distribution of ^{15}N in freshwater environments. Data from Hoering (1957), Pang and Nriagu (1976, 1977), Peters and others (1978), Sweeney and others (1978), Wada and others (1975), Estep and Vigg (1985), and Collister (1989, Messel shale).

the concentrations of ammonia and ammonium at differing pH can be calculated by

$$\text{pH} = 9.25 + \log \frac{[\text{NH}_3]}{[\text{NH}_4^+]}$$

The rate of ammonia volatilization,



depends on the concentration of NH_3 in solution, which is controlled by pH. As pH increases, a larger fraction of the total ammonia is in the un-ionized form and volatilization proceeds more rapidly. At pH 8, 5 percent of the total ammonium is in the form of NH_3 ; at pH 9.5, the upper limit suggested by Smith and Robb (1973), 65 percent of the total ammonium is in the form of NH_3 . Accordingly, in such a system losses of NH_3 will be extensive. Because NH_3 is always depleted in ^{15}N by 34‰ relative to NH_4^+ , residual NH_4^+ will be increasingly enriched in ^{15}N . Thus, changes in the pH of the Green River lakes would have significantly affected rates of volatilization of NH_3 and, therefore, the isotopic composition of the ammonium available for assimilation.

Assimilation of isotopically heavy residual ammonium would yield algal material enriched in ^{15}N . But if such assimilation was the only important step in the fractionation of nitrogen isotopes of the Green River lake system, algae growing during the most saline and alkaline stages ought to be the most enriched in ^{15}N . In fact, isotopic data from the 01A core (table 2) show the opposite

relationship. Samples of kerogens isolated from shale representing “fresh water” conditions are the most enriched in ^{15}N ; those from the most evaporitic horizons are depleted in ^{15}N . Thus, although ammonia volatilization probably was pronounced and must have produced an isotopically heavy pool of aqueous ammonium during saline stages, other biologically imposed fractionations of the nitrogen isotopes must also have occurred and played an important role.

Models of Nitrogen Cycling in the Green River Lakes

We would expect the biogeochemical nitrogen cycle in a playa lake to be different from that in a stratified lake. Thus, models explaining the isotopic composition of organic matter in the Green River Formation are based upon these end members. Five samples (shown separately in fig. 1) possessing mineralogy indicative of extreme evaporitic conditions were chosen to represent the playa-lake end member: three evaporites (bedded halite, bedded nahcolite, and nodular nahcolite) and samples 01-126 and 01-132 (for mineralogic compositions see Tuttle, this volume). We chose the Mahogany zone of the Parachute Creek Member of the Green River Formation (lake stage 3) in the Piceance basin as being representative of the meromictic-lake end member. The following discussion presents models of nitrogen cycling for these two environments based upon nitrogen isotopic compositions of preserved organic material. It must be kept in mind, however, that these two

sets of samples were chosen to represent end members of depositional conditions and that many horizons in the Green River Formation may represent transitional stages between these two environments.

Saline (playa-lake) Stages

A proposed nitrogen cycle for the shallow, saline stages (well-mixed water column) of the Green River lakes is shown in figure 5. During these stages, reduced freshwater influx decreased nutrient supply and limited primary production. Rates of ammonification would be expected to decrease because of the decrease in detrital organic material being supplied to the sediments. Levels of salinity under these conditions were apparently almost 22 percent (Bradley and Eugster, 1969); nitrification is inhibited at salinities above 15 percent (Rubenchik, 1929; Post and Stube, 1988). During the most saline stages, therefore, fluvial input would be the principal source of NO_3^- . Any nitrate entering the lakes in streams probably was quickly assimilated by the algal population before it could diffuse into the anoxic zone of the sediments. At the

resulting low levels of nitrate, denitrification would also be severely limited.

According to Stanier and others (1986), heterocystous cyanobacteria, when grown in the presence of nonlimiting concentrations of combined inorganic-N (NH_4^+ or NO_3^-), do not produce heterocysts (the specialized cells containing nitrogenase, the enzyme responsible for nitrogen fixation). Further, in the presence of combined inorganic-N, nitrogenase synthesis is inhibited in nonheterocystous cyanobacteria (Stanier and others, 1986). Under similar nonlimiting conditions, both phytoplankton and bacteria preferentially assimilate ammonium in the presence of both ammonium and nitrate (Mariotti and others, 1984). If the concentration of ammonium becomes small (as would be the case in the alkaline stages due to loss through volatilization), a larger fraction of the nitrogen used by the biota will be derived from nitrate or N_2 (by nitrogen fixation). Control of the nitrogen isotopic composition of the organic material would pass from ammonium to nitrate (from fluvial input and reduced levels of nitrification) and N_2 (from nitrogen fixation). The nitrogen isotopic composition of organic material in the Green River rocks indicates that nitrogen fixation was not the major source of nitrogen. Nitrate from

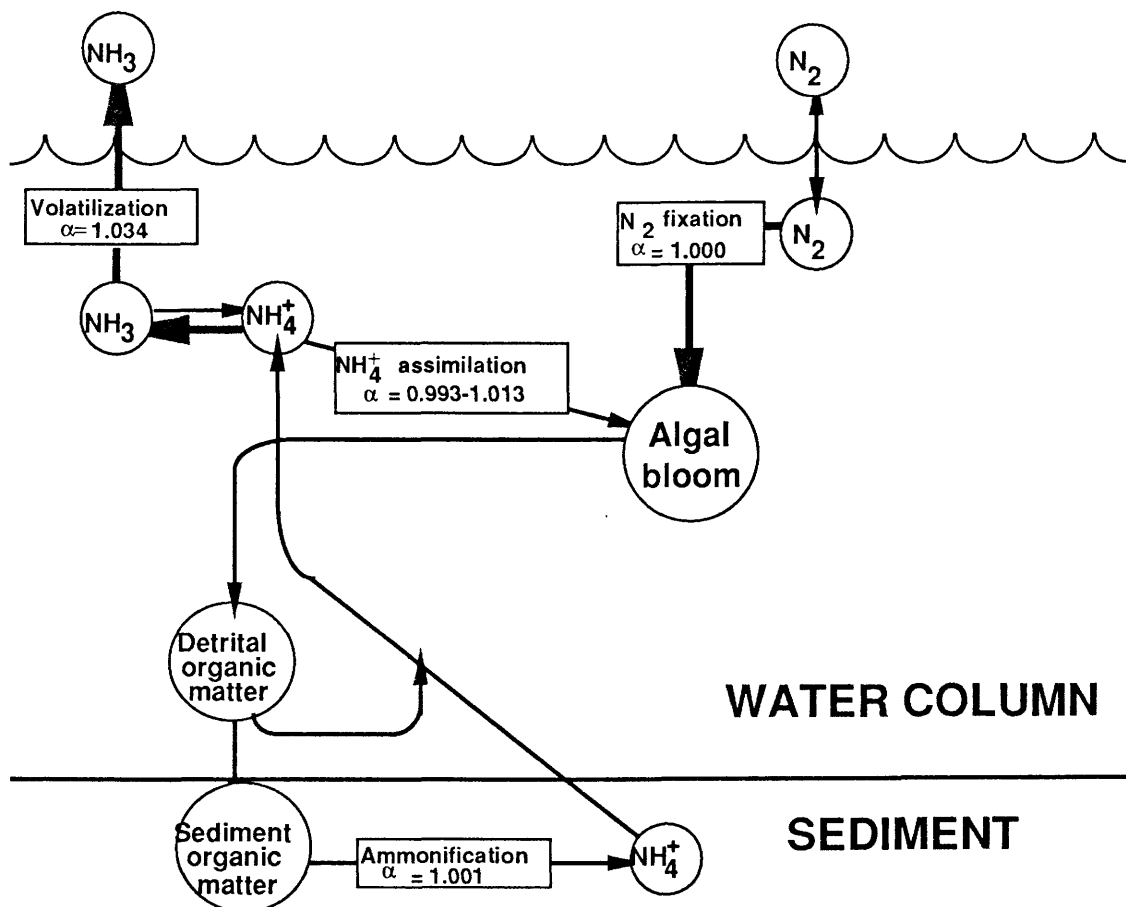


Figure 5. Proposed nitrogen cycle for saline stages of Green River lakes.

evaporites has an isotopic composition of +8 to +10‰ (table 5). Use of this inorganic-N source would produce algal material having nitrogen isotopic compositions in the range of +6 to +10‰ (Mariotti and others, 1984), and, even if rates of evaporation were high, the $\delta^{15}\text{N}$ of organic-N would decline. Isotopic compositions of nitrogen in kerogens from the most evaporitic facies are from +10 to about +12‰. These materials are marginally enriched in ^{15}N relative to organic-N derived entirely from nitrate at +8 to +10‰, but this enrichment can be attributed to assimilation of a mixed inorganic-N source comprised of a small pool of ammonium (enriched in ^{15}N) and a much larger pool of nitrate and dissolved N_2 (depleted in ^{15}N). Even if concentrations of nitrate were so low as to be nutritionally insignificant, assimilation of a mixture of isotopically heavy ammonium and atmospheric N_2 could account for the relative depletion of ^{15}N in organic matter from the saline facies of the Green River Formation.

Fresh (meromictic lake) Stages

During fresher stages, flooding of the lake basins from increased precipitation produced a stratified meromictic lake having a saline monimolimnion (Desborough, 1978; Sullivan, 1980; Boyer, 1982). A proposed nitrogen cycle for such a lake is shown in figure 6. Increased nutrient supply (from increased precipitation delivering higher loads of dissolved nutrients) would support increased primary

productivity. A larger input of detrital organic matter to the sediments would support greater rates of ammonification, and greater amounts of ammonium would be released into the overlying water column. "Fresh-water" conditions in the mixolimnion (the salinity was still approximately that of seawater; Bradley and Eugster, 1969) would be compatible with the salinity tolerance of nitrifying bacteria, and ammonium from the monimolimnion would support high rates of nitrification. Nitrate produced during nitrification would become available to denitrifiers upon diffusion into the monimolimnion. The increased supply of detrital organic material and the generation of nitrate by nitrification would support a large population of denitrifying bacteria. A similar coupling of nitrification and denitrification rates has been shown to occur in modern estuarine sediments (Jenkins and Kemp, 1984) and in modern lake sediments (Knowles, 1979).

Several potential sources of isotopically enriched inorganic-N species are indicated in figure 6. The ammonium remaining after volatilization and nitrification would be enriched in ^{15}N . In fresh stages, loss of ammonia to the atmosphere would be decreased, and consequently a larger pool of ammonium would be available for assimilation. Assimilation of ^{15}N -enriched ammonium would, in turn, produce isotopically enriched algal cellular nitrogen. Another source of isotopically enriched inorganic-N during the fresher stages of these lakes is the residual pool of nitrate from denitrification, assimilation of which would

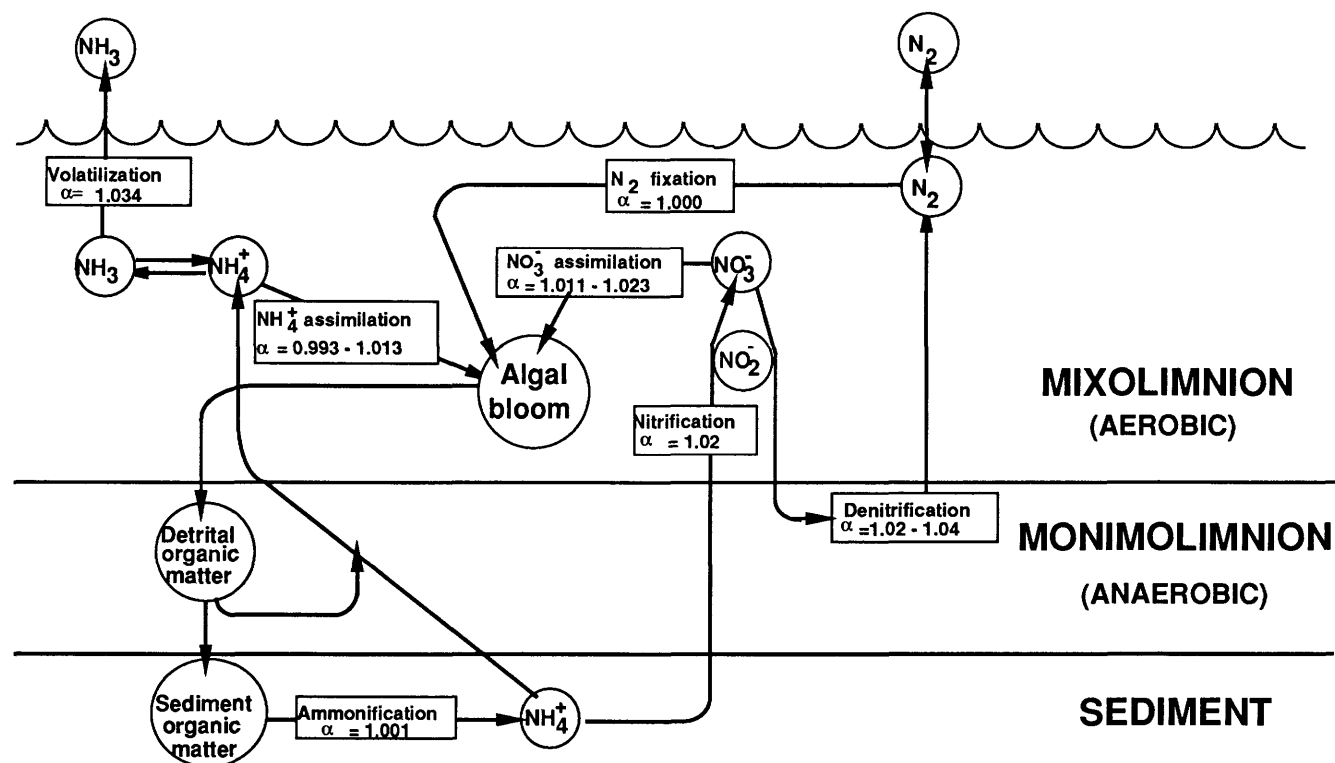


Figure 6. Microbial nitrogen cycle for meromictic lakes.

also cause enrichment of total cell nitrogen. Finally, because of the elevated levels of combined inorganic-N species expected during these lake stages, nitrogen fixation would be expected to be less important to primary producers.

Therefore, extreme ^{15}N enrichments during the meromictic stages of these lakes probably was due to assimilation of ^{15}N -enriched ammonium and nitrate. The ^{15}N -enriched nitrate was produced by the process of denitrification, and the ^{15}N -enriched ammonium was produced by the processes of volatilization and nitrification (fig. 6).

Comparison of Piceance, Uinta, and Green River Basins

Although our discussion up to this point has focused primarily on the 01A core (Piceance basin), some generalizations can be made regarding the other basins. Organic material from all three cores shows both extreme ^{15}N enrichments and a broad range of $\delta^{15}\text{N}$ values. Kerogens from both the 01A and the Coyote Wash (Lake Uinta) cores show an overall ^{15}N -enrichment through time, although large deviations from this trend exist for individual samples. In contrast, kerogens from the Blacks Fork (Lake Gosiute) core show the most enriched values in rocks from the saline lake stage 2, and kerogens from a few samples from lake stages 1 and 3 suggest depletion of ^{15}N in those stages. The overall pattern of ^{15}N enrichment suggests that nitrogen was not generally a limiting nutrient in either lake; however, differences in the nitrogen isotopic signal through time indicate that details of the nitrogen cycles in these lakes were different.

Lake Gosiute (Wyoming) was considerably shallower than Lake Uinta and during lake stage 2 was significantly reduced in surface area (Tuttle, this volume). Sample BF-22 (Lake Gosiute), which contains the saline minerals shortite and trona (Tuttle, this volume, appendix), is the most saline sample analyzed from the Blacks Fork core and may indicate a playa-lake environment. Kerogen isolated from this sample has a $\delta^{15}\text{N}$ value of +11.4‰, consistent with our model of nitrogen cycling in playa-lake environments. The remainder of the samples from lake stage 2, however, are more enriched in ^{15}N (+16.7 to +18.3‰, table 3) and perhaps the community was utilizing one or more sources of ^{15}N -enriched inorganic-N. In both lakes, volatilization produced residual ammonium enriched in ^{15}N . The extent to which this enrichment also occurred in organic-N would depend upon the importance of NH_4^+ as a nitrogen source. We can, therefore, speculate that during lake stage 2 NH_4^+ supplied a larger fraction of total nitrogen requirements in Lake Gosiute than in Lake Uinta.

Isotopically Depleted Total Organic Carbon

Isotopic variations in dissolved inorganic carbon (DIC) can be pronounced in lakes, and one consequence is

that phytoplankton can have very negative $\delta^{13}\text{C}$ values (–35 to –45‰; Oana and Deevey, 1960; Deevey and others, 1963; Deevey and Stuiver, 1964; Rau, 1978, 1980). Organic material in the Green River Formation has a wide range of $\delta^{13}\text{C}$ compositions. Interestingly, the range of isotopic compositions for the kerogens (–29.4 to –41.4‰) is much broader than that for total organic carbon (–28.7 to –33.5‰).

Kerogens and total organic carbon, commonly analyzed in sedimentary isotopic studies, derive not only from primary producers but also from many other organisms including photosynthetic bacteria, a wide variety of heterotrophs, chemolithotrophs, methanogens, and methylotrophs. Consequently, the isotopic composition of the total organic material reflects not only that of the primary photosynthate but also isotope effects associated with a variety of secondary processes. In an attempt to resolve primary and secondary processes, sedimentary geoporphyryns were analyzed to more accurately determine the isotopic composition of the primary producers in these lakes.

Geoporphyryns are derived from the heteroaromatic tetrapyrrole nucleus of chlorophyll and can be considered to be “isotopic biomarkers” for primary producers. The tetrapyrrole nucleus is enriched in ^{13}C relative to total biomass by about 0.5‰ (Hayes and others, 1987; Takigiku, 1987); thus the isotopic composition of photosynthate of ancient primary producers can be estimated by the equation

$$\delta_p \approx \delta_{\text{por}} - 0.5,$$

where δ_p is the isotopic composition of the primary photosynthate and δ_{por} is the isotopic composition of the related porphyryns. Because of their low abundances in Green River Formation extracts, geoporphyryns from only three samples were analyzed. Consequently, isotopic variations in porphyryns from the Green River Formation may be considerably greater than that observed. The heaviest porphyryn (sample 01-8) has a $\delta^{13}\text{C}$ value of –23.6‰, whereas that of the lightest (sample 01-36) is –28.6‰. Nickel geoporphyryns isolated from gilsonite (Uinta basin) have a $\delta^{13}\text{C}$ value of –28.5‰. Corresponding values for total primary organic material are –24.1 and –29.1, respectively. Assuming the fractionations between aqueous CO_2 and total cell carbon observed in oceanic plankton (18–19‰; Deuser and others, 1986) and in neutral carbonate springs (19‰; Estep, 1984) are similar to those of algae in the Green River lakes, the isotopic composition of the CO_2 dissolved in the photic zone of the Green River lakes must have varied at least between –4.6 and –9.6‰.

Because structures of the nickel geoporphyryns in the Green River Formation are not known, their precise origins are uncertain. Assuming the predominant organism to be blue-green algae (Bradley, 1970), it is reasonable to suggest that the majority of the porphyryns derive from algal chlorophylls (Bradley, 1963). However, significant amounts

of porphyrins may have been produced by photosynthetic bacteria. Because DIC in the anaerobic part of the photic zone of meromictic lakes is commonly depleted in ^{13}C (Oana and Deevey, 1960; Deevey and others, 1963), photosynthetic bacteria fixing this CO_2 should synthesize ^{13}C -depleted tetrapyrroles.

An alternate explanation for the isotopic range of the nickel geoporphyryns is that they reflect different sources of organic material having distinctive isotopic compositions. The geoporphyryns from algal material would be expected to be isotopically enriched relative to those from photosynthetic bacteria. Isotopic variations of porphyrin fractions from the Green River Formation may reflect changes in the abundance of algal versus bacterial primary production in response to changing lake conditions.

Sources of Isotopically Depleted Organic Carbon

Anaerobic Photosynthetic Bacteria

One source of isotopically depleted carbon material in meromictic lakes is photosynthetic sulfur bacteria (Fry, 1986). In such lakes, the isotopic composition of the DIC is increasingly depleted with depth (Deevey and others, 1963; Takahashi and others, 1968). In the aerobic photic zone of Green Lake, Fayetteville, New York, the isotopic composition of the dissolved bicarbonate is between -6 and -12‰ (Deevey and others, 1963; Takahashi and others, 1968); however, at depths where photosynthetic sulfur bacteria occur (17–20 m; Fry, 1986), the isotopic composition of the DIC is between -17 and -21‰ (Deevey and others, 1963; Torgersen and others, 1981). Thus, the photosynthetic sulfur bacteria (*Chromatium* and *Chlorobium*), which occur below the aerobic photoheterotrophs, fix ^{13}C -depleted CO_2 and consequently their cell material can be extremely depleted in ^{13}C ($\delta^{13}\text{C}$, -40‰ ; Fry, 1986).

Sample 01–36, in which the ^{13}C -depleted primary material is found, is from the saline facies of the Parachute Creek Member in the Piceance basin. This member reflects a lake stage in which evaporation rates greater than inflow resulted in increased salinity and decreased surface area of the lake (Tuttle, 1988). Sample 01–8, however, in which the isotopically heaviest primary organic material was observed, is from the Mahogany zone and represents a period in which inflow rates increased and the lake expanded and freshened. In the Piceance basin, with the exception of sample 01–8, the most ^{13}C -depleted kerogens are from the Parachute Creek Member below the Mahogany zone (table 1). Within this part of the member, the mineralogy of the samples containing the most depleted kerogens include the saline minerals dawsonite, nahcolite, and halite (table 2).

The ^{13}C -depletion of kerogens from the saline facies of the Parachute Creek Member in the Piceance basin may

reflect nutrient-limited primary production in the aerobic zone. Algal contribution to the overall organic matter would be greatly reduced, and the contribution from photosynthetic bacteria would become more important. These factors would both serve to produce ^{13}C -depleted total organic material in the sediments representing these saline lake stages.

Methanogens and Methylotrophs

Enrichment of ^{13}C in dolomite from the Green River Formation relative to that estimated for dissolved CO_2 in the photic zone of these lakes indicates that aqueous CO_2 in the sediment pore waters was not in isotopic equilibrium with dissolved CO_2 in the overlying water column. This disequilibrium is particularly striking if the CO_2 in the monimolimnia of these lakes had isotopic compositions similar to those of dissolved CO_2 in the monimolimnia of modern-day meromictic lakes (-21 to -27‰ ; Oana and Deevey, 1960; Takahashi and others, 1968), and it requires a mechanism for enrichment of ^{13}C in dissolved inorganic carbon in sedimentary pore waters.

The presence of ^{13}C -enriched dolomites in anoxic pore waters from marine and lacustrine systems has been attributed to activities of methanogenic bacteria in the sediment (Irwin and others, 1977). Extreme ^{13}C enrichment in nahcolite from the Green River Formation of the Piceance basin ($\delta^{13}\text{C}$ values from $+10$ to $+20\text{‰}$) was suggested by Reitsemá (1980) to indicate that bacterial fermentation by methanogenic bacteria was the source of this ^{13}C -enriched CO_2 . Reitsemá pointed out that nahcolite precipitation depends on the presence of an excess of CO_2 and that amounts of CO_2 below the concentration in equilibrium with the atmosphere lead to the formation of trona. Reitsemá concluded that methanogenesis produced locally high concentrations of ^{13}C -enriched CO_2 that led to precipitation of ^{13}C -enriched nahcolite. The presence of dolomite having $\delta^{13}\text{C}$ values as high as $+11\text{‰}$ also indicates that methanogenesis was an important process in these lakes.

Kerogen from one sample (01–8) is depleted in ^{13}C relative to the associated geoporphyryn by more than 17‰ . Takigiku (1987) suggested that the isotopic difference between geoporphyryn precursors and related lipids in fresh biomass is approximately -4‰ . Therefore, in newly deposited primary organic material, the lipid fraction should be depleted relative to the porphyrins by 4‰ . The 17‰ depletion of kerogen in sample 01–8 relative to the geoporphyryn in this sample suggests that the isotopic composition of this kerogen (and probably other kerogen in the cores) reflects a secondary input of ^{13}C -depleted organic matter. Assimilation of ^{13}C -depleted methane from methanogenesis by micro-aerophilic methylotrophs living at the aerobic-anaerobic boundary has been suggested to explain similar isotopic "mismatches" observed in the Messel shale (Hayes and others, 1987; Takigiku, 1987). Incorporation of this

isotopically light methane would in turn result in ^{13}C -depleted biomass. The same process in the Green River lakes may account for the observed depletion of ^{13}C in kerogen relative to geoporphyryns.

SUMMARY

The Paleogene Green River Formation was deposited in a highly productive system of alkaline, saline lakes in which algae and cyanobacteria were probably the main primary producers. The accumulation of organic material in this formation indicates that conditions favored preservation of organic material. Very large quantities of nutrients must have been supplied to the lake basins, and fluvial inputs of phosphorus from erosion of the Phosphoria Formation probably were substantial. Extreme enrichments in ^{15}N in preserved organic matter from the Green River Formation suggest that nitrogen was not limiting in this lake system.

The broad variability of $\delta^{15}\text{N}$ values for organic material in the Green River Formation provides information regarding (1) the nutrition of the organisms in these lakes and (2) the cycling of nitrogenous compounds in this ecosystem. Although volatilization of ammonia in this alkaline environment probably produced ^{15}N -enriched ammonium in the surface waters of these lakes, other biological fractionations must have been superimposed on this effect to produce the observed trends in nitrogen isotopic composition of the organic matter. Kerogens from the fresher stages of this lake system are the most enriched in ^{15}N and those from the most saline and evaporitic stages are relatively depleted. Evaporation of NH_3 ought to have been maximized during the latter stages. It is, therefore, surprising that evaporitic stages do not display the highest levels of ^{15}N enrichment. To explain this paradox, it is suggested that isotope effects associated with nitrification and denitrification must also have played an important role in the control of overall nitrogen isotopic compositions. The isotope effect associated with nitrification would tend to increase ^{15}N in ammonium and that effect associated with denitrification would increase ^{15}N in nitrate. Taken together, these processes would enhance ^{15}N enrichment associated with volatilization of ammonia. During saline stages, high salinity limited nitrification. This in turn limited the process of denitrification because these two microbial processes are coupled through NO_3^- . This simpler nitrogen cycle resulted in less reworking of the organic material during the saline stages. Consequently, ^{15}N was less strongly enriched during the saline stages in spite of higher levels of evaporation.

The carbon isotopic composition of kerogens from the Green River Formation is from -41.4 to -28.8% , whereas that of nickel geoporphyryns from two samples is -23.6 and -28.6% . Geoporphyryns can be regarded as isotopic biomarkers for primary producers and therefore may provide an estimated range of ^{13}C compositions of primary producers in the Green River lakes. In at least one

sample, a large isotopic depletion (17%) in a kerogen relative to the associated geoporphyryn indicates significant contributions of ^{13}C -depleted organic material into the sediments. Possible sources of isotopically depleted carbon include photosynthetic bacteria at the chemocline of a stratified lake and capture of isotopically light methanogenic-methane by methylootrophs.

REFERENCES CITED

- Baker, K.L., 1987, An investigation of ^2H and ^{13}C abundances in a sequence of related oils of increasing maturity: Bloomington, Indiana University, M.S. thesis, 106 p.
- Boyer, B.W., 1982, Green River laminites—Does the playa-lake model really invalidate the stratified lake model?: *Geology*, v. 10, p. 321–324.
- Bradley, W.H., 1929, The varves and climate of the Green River epoch: U.S. Geological Survey Professional Paper 158, p. 87–110.
- , 1931, Origin and microfossils of the oil shale of the Green River Formation of Colorado and Utah: U.S. Geological Survey Professional Paper 168, 58 p.
- , 1948, Limnology and the Eocene lakes of the Rocky Mountain region: *Geological Society of America Bulletin*, v. 59, p. 635–648.
- , 1963, Paleolimnology, in Frey, D.G., ed., *Limnology in North America*: Madison, University of Wisconsin Press, p. 621–652.
- , 1964, Geology of the Green River Formation and associated Eocene rocks in southwestern Wyoming and adjacent parts of Colorado and Utah: U.S. Geological Survey Professional Paper 496–A, 86 p.
- , 1970, Green River oil shale—Concept of origin extended: *Geological Society of America Bulletin*, v. 81, p. 985–1000.
- Bradley, W.H., and Eugster, H.P., 1969, Geochemistry and paleolimnology of the trona deposits and associated authigenic minerals of the Green River Formation, Wyoming: U.S. Geological Survey Professional Paper 496–B, 71 p.
- Broecker, W.S., and Olson, E.A., 1959, Lamont radiocarbon measurements IV: *American Journal of Science Radio-carbon Supplement*, v. 1, p. 111–132.
- Cifuentes, L.A., Sharp, J.H., and Fogel, M.L., 1988, Stable carbon and nitrogen isotope biogeochemistry in the Delaware estuary: *Limnology and Oceanography*, v. 33, p. 1102–1115.
- Cline, J.D., and Kaplan, I.R., 1975, Isotopic fractionation of dissolved nitrate during denitrification in the eastern tropical North Pacific Ocean: *Marine Chemistry*, v. 3, p. 271–299.
- Collister, J.W., 1989, The carbon and nitrogen biogeochemistry of the organic rich lacustrine sediments of the Green River Formation: Bloomington, Indiana University, M.S. thesis, 93 p.
- Deevey, E.S., Nakai, N., and Stuiver, M., 1963, Fractionation of sulfur and carbon isotopes in a meromictic lake: *Science*, v. 139, p. 407–408.
- Deevey, E.S., and Stuiver, M., 1964, Distribution of natural isotopes of carbon in Linsley Pond and other New England lakes: *Limnology and Oceanography*, v. 9, p. 1–11.

- Deines, P., 1980, The isotopic composition of reduced carbon, *in* Fritz, P., and Fontes, J.C., eds., *Handbook of environmental geochemistry: The Terrestrial Environment*, v. 1, p. 329–406.
- Delwiche, C.C., and Steyn, P.L., 1970, Nitrogen isotope fractionation in soils and microbial reactions: *Environmental Science and Technology*, v. 4, p. 929–935.
- Desborough, G.A., 1978, A biogenic-chemical stratified lake model for the origin of oil shale of the Green River Formation—An alternative to the playa-lake model: *Geological Society of America Bulletin*, v. 89, p. 961–971.
- Deuser, W.G., Degens, E.T., and Gulliard, R.R.L., 1968, Carbon isotope relationships between plankton and sea water: *Geochimica et Cosmochimica Acta*, v. 32, p. 657–660.
- Estep, M.L.F., 1984, Carbon and hydrogen isotopic compositions of algae and bacteria from hydrothermal environments, Yellowstone National Park: *Geochimica et Cosmochimica Acta*, v. 48, p. 591–599.
- Estep, M.L.F., and Vigg, S., 1985, Stable carbon and nitrogen isotope tracers of trophic dynamics in natural populations and fisheries of the Lahontan Lake system, Nevada: *Canadian Journal of Fisheries and Aquatic Science*, v. 42, p. 1712–1719.
- Eugster, H.P., and Hardie, L.A., 1975, Sedimentation in an ancient playa-lake complex—The Wilkins Peak Member of the Green River Formation of Wyoming: *Geological Society of America Bulletin*, v. 86, p. 319–334.
- Eugster, H.P., and Surdam, R.C., 1973, Depositional environments of the Green River Formation of Wyoming—A preliminary report: *Geological Society of America Bulletin*, v. 84, p. 1115–1120.
- Fry, B., 1986, Sources of carbon and sulfur nutrition for consumers in three meromictic lakes of New York State: *Limnology and Oceanography*, v. 31, 79–88.
- Hayes, J.M., Takigiku, R., Ocampo, R., Callot, H.J., and Albrecht, P., 1987, Isotopic compositions and probable origins of organic molecules in the Eocene Messel shale: *Nature*, v. 329, p. 48–51.
- Hoering, T.C., 1957, The isotopic composition of the ammonia and the nitrate ion in rain: *Geochimica et Cosmochimica Acta*, v. 12, p. 97–102.
- Hoering, T.C., and Ford, H.T., 1960, The isotope effect in the fixation of nitrogen by *Azotobacter*: *Journal of the American Chemical Society*, v. 82, p. 376–378.
- Hoering, T.C., and Moore, H.E., 1958, The isotopic composition of the nitrogen in natural gas and associated crude oil: *Geochimica et Cosmochimica Acta*, v. 13, p. 225–232.
- Hunt, J.M., Stewart, F., and Dickey, P.A., 1954, Origin of hydrocarbons of Uinta Basin, Utah: *American Association of Petroleum Geologists Bulletin*, v. 38, p. 1671–1698.
- Irwin, H., Curtis, C., and Coleman, M., 1977, Isotopic evidence for source diagenetic carbonates formed during burial of organic-rich sediments: *Nature*, v. 269, p. 209–213.
- Jenkins, M.C., and Kemp, W.M., 1984, The coupling of nitrification and denitrification in two estuarine sediments: *Limnology and Oceanography*, v. 29, p. 609–619.
- Kirschenbaum, I., Smith, J.S., Crowell, T., Graff, J., and McKee, R., 1947, Separation of the nitrogen isotopes by exchange reaction between ammonia and solutions ammonium nitrate: *The Journal of Chemical Physics*, v. 15, p. 440–446.
- Klots, C.E. and Benson, B.B., 1963, Isotope effect in solution of oxygen and nitrogen in distilled water: *The Journal of Chemical Physics*, v. 38, p. 890–892.
- Knoll, A.H., Hayes, J.M., Kaufman, A.J., Swett, K., and Lambert, I.B., 1986, Secular variations in carbon isotope ratios from Upper Proterozoic successions Svalbard and East Greenland: *Nature*, v. 321, p. 832–838.
- Knowles, R., 1979, Denitrification, acetylene reduction and methane metabolism in lake sediment exposed to acetylene: *Applied and Environmental Microbiology*, v. 38, p. 480–493.
- Kobayakawa, M., Hayashi, S., and Titani, T., 1962, Formation of nitric oxide at the separation of nitrogen gas for mass spectrometric analysis: *Mass Spectrometry*, v. 3, p. 34–36.
- Lee, C., McKenzie, J.A., and Sturm, M., 1987, Carbon isotope fractionation and changes in the flux and composition of particulate matter resulting from biological activity during a sediment trap experiment in Lake Greifen, Switzerland: *Limnology and Oceanography*, v. 32, p. 83–96.
- Letolle, R., 1980, Nitrogen-15 in the natural environment, *in* Fritz, P., and Fontes, J.C., eds., *Handbook of environmental geochemistry: The Terrestrial Environment*, v. 1, p. 407–433.
- Lundell, L.L., and Surdam, R.C., 1975, Playa-lake deposition—Green River Formation, Piceance Creek Basin, Colorado: *Geology*, v. 3, p. 493–497.
- Macko, S.A., 1981, Stable nitrogen isotope ratios as tracers of organic geochemical processes: Austin, University of Texas, Ph.D. thesis, 181 p.
- Macko, S.A., Fogel, M.L., Hare, P.E., and Hoering, T.C., 1987, Isotopic fractionation of nitrogen and carbon in the synthesis of amino acids by microorganisms: *Chemical Geology (Isotope Geosciences Section)*, v. 65, p. 79–92.
- Mariotti, A., Lancelot, C., and Billen, G., 1984, Natural isotopic composition of nitrogen as a tracer of origin for suspended organic matter in Scheldt estuary: *Geochimica et Cosmochimica Acta*, v. 48, p. 549–555.
- Miyake, Y., and Wada, E., 1971, The isotope effect on the nitrogen in biochemical, oxidation-reduction reactions: *Records of Oceanographic Works in Japan*, v. 11, p. 1–6.
- Oana, S., and Deevey, E.S., 1960, Carbon 13 in lake waters, and its possible bearing on paleolimnology: *American Journal of Science*, v. 256-A, p. 253–272.
- Pang, P.C., and Nriagu, J.O., 1976, Distribution and isotope composition of nitrogen in Bay of Quinte (Lake Ontario) sediments: *Chemical Geology*, v. 18, p. 93–105.
- _____, 1977, Isotopic variations of the nitrogen in Lake Superior: *Geochimica et Cosmochimica Acta*, v. 41, p. 811–814.
- Peters, K.E., Sweeney, R.E., and Kaplan, I.R., 1978, Correlation of carbon and nitrogen stable isotope ratios in sedimentary organic matter: *Limnology and Oceanography*, v. 23, p. 598–604.
- Post, F.H., and Stube, J.C., 1988, A microcosm study of nitrogen utilization in the Great Salt Lake, Utah: *Hydrobiologia*, v. 158, p. 89–100.
- Rau, G., 1978, Carbon-13 depletion in a subalpine lake—Carbon flow implication: *Science*, v. 201, p. 901–902.
- _____, 1980, Carbon-13/carbon-12 variation in subalpine lake aquatic insects—Food source implications: *Canadian Journal of Fisheries and Aquatic Science*, v. 37, p. 742–746.

- Reitsema, R.H., 1980, Dolomite and nahcolite formation in organic rich sediments—Isotopically heavy carbonates: *Geochimica et Cosmochimica Acta*, v. 44, p. 2045–2049.
- Robinson, W.E., 1976, Origin and characteristics of Green River oil shale, in Yen, T.F., and Chilingarian, G.V., eds., *Oil shale—Developments in petroleum science*, v. 5: New York, Elsevier, p. 61–79.
- _____ 1979, The origin, deposition, and alteration of the organic material in Green River oil shale: *Organic Geochemistry*, v. 1, p. 205–218.
- Rubenchik, L., 1929, Nitrification at high salt concentrations: *Chemical Abstracts*, v. 23, p. 3947.
- Smith, J.W., 1974, Geochemistry of oil-shale genesis in Colorado's Piceance Creek Basin, in *Guidebook to the energy resources of the Piceance Creek Basin, Colorado*: Rocky Mountain Association of Geology Field Conference, 25th, p. 71–79.
- Smith, J.W., and Robb, W.A., 1973, Aragonite and the genesis of carbonates in Mahogany zone oil shales of Colorado's Green River Formation: Bureau of Mines Report of Investigations 7727, 21 p.
- Stanier, R.Y., Ingraham, J.L., Wheelis, M.L., and Painter, P.R., 1986, *The microbial world* (5th ed.): New Jersey, Prentice-Hall, 689 pp.
- Stuiver, M., 1964, Carbon isotopic distribution and correlated chronology of Searles Lake sediments: *American Journal of Science*, v. 262, p. 377–392.
- _____ 1970, Oxygen and carbon isotope ratios of fresh-water carbonates as climatic indicators: *Journal of Geophysical Research*, v. 75, p. 5247–5257.
- _____ 1975, Climate versus changes in ^{13}C content of the organic component of lake sediments during the late Quaternary: *Quaternary Research*, v. 5, p. 251–262.
- Sullivan, R., 1980, A stratigraphic evaluation of the Eocene rocks of southwestern Wyoming: Geological Survey of Wyoming Report of Investigations 20, 50 p.
- Surdam, R.C., and Stanley, K.O., 1979, Lacustrine sedimentation during the culminating phase of Eocene Lake Gosiute, Wyoming (Green River Formation): *Geological Society of America Bulletin*, v. 90, p. 93–110.
- Sweeney, R.E., Liu, K.K., and Kaplan, I.R., 1978, Oceanic nitrogen isotopes and their uses in determining the source of sedimentary nitrogen, in Robinson, R.W., ed., *Stable isotopes in the earth sciences*: New Zealand Department of Scientific and Industrial Resource, p. 9–26.
- Takahashi, T., Broecker, W., Li, Y.H., and Thurber, D., 1968, Chemical and isotopic balance for a meromictic lake: *Limnology and Oceanography*, v. 13, p. 272–292.
- Takigiku, R., 1987, Isotopic and molecular indicators of origins of organic compounds in sediments: Bloomington, Indiana University, Ph.D. thesis, 219 p.
- Torgersen, T., Hammond, D.E., Clarke, W.B., and Peng, T.H., 1981, Fayetteville, Green Lake, New York ^3H - ^3He water mass ages and secondary chemical structure: *Limnology and Oceanography*, v. 26, p. 110–122.
- Tuttle, M.L., 1988, Geochemical evolution and depositional history of sediment in modern and ancient saline lakes—Evidence from sulfur geochemistry: Golden, Colorado School of Mines, Ph.D. thesis, 312 p.
- Wada, E., and Hattori, A., 1978, Nitrogen isotope effects in the assimilation of inorganic nitrogenous compounds by marine diatoms: *Geomicrobiology Journal*, v. 1, p. 85–10.
- Wada, E., Kadonaga, T., and Matuso, S., 1975, ^{15}N abundance in nitrogen of naturally occurring substances and global assessment of denitrification from isotopic viewpoint: *Geochemical Journal*, v. 9, p. 139–148.
- Warren, J.K., 1986, Shallow-water evaporitic environments and their source rock potential: *Journal of Sedimentary Petrology*, v. 56, p. 442–454.
- Wedeking, K.W., Hayes, J.M., and Matzigkeit, U., 1983, Procedure of organic geochemical analysis, in Schopf, J.W., ed., *Earth's earliest biosphere—Its origin and evolution*: Princeton, Princeton University Press, p. 428–441.
- Wellman, R.P., Cook, F.D., and Krouse, H.R., 1968, Nitrogen-15 microbial alteration of abundance: *Science*, v. 161, p. 269–270.

Chapter D

Trace Elements in Pyrites of the Green River Formation Oil Shales, Wyoming, Utah, and Colorado

By WENDY J. HARRISON, D.R. PEVEAR, and P.C. LINDAHL

U.S. GEOLOGICAL SURVEY BULLETIN 1973

GEOCHEMICAL, BIOGEOCHEMICAL, AND SEDIMENTOLOGICAL STUDIES OF THE
GREEN RIVER FORMATION, WYOMING, UTAH, AND COLORADO

CONTENTS

Abstract	D1
Introduction	D1
Sample descriptions	D3
Pyrite separation	D5
Trace-element analytical methods	D12
Results and discussion	D12
Electron microprobe analyses	D14
Geochemical interpretation	D15
Conclusions	D17
References cited	D17
Appendix 1—Petrographic description of shale samples in West Willow no. 3 core	D19
Appendix 2—Analytical methods	D19

FIGURES

1. Map showing location of West Willow no. 3 core hole, Colorado D2
2. Chart showing location of pyrite-rich samples in West Willow no. 3 core D3
3. Graph showing mineralogy of samples of Green River Formation from West Willow no. 3 core D4
4. Drawings showing classification of common macroscopic and microscopic iron-sulfide morphotypes in Green River Formation D5
5. Photomicrographs of morphotypes of pyrite in Green River Formation D6
6. Scanning electron micrographs of pyrites in Green River Formation D8
- 7-9. Element correlation diagrams for :
 7. Copper and cobalt in pyrites extracted from Green River oil shale D13
 8. Cobalt, molybdenum, nickel, and copper in whole-rock samples of Green River oil shale D14
 9. Copper in pyrite extracts and in whole-rock samples of Green River oil shale D14
10. Elemental X-ray intensity images of pyrite-rich oil shale D15
11. Graph showing fields of stability of solids as a function of pH and Eh in system Mn-S-CO₂-H₂O D16

TABLES

1. Semiquantitative X-ray diffraction mineralogy of shale D3
2. X-ray mineralogy of pyrite extracts D3
3. Pyrite morphotypes observed in petrographic section D8
4. Trace-element contents of pyrites D12
5. Measured, calculated, and published trace-element, H₂O, and ash contents of whole-rock samples D13

Trace Elements in Pyrites of the Green River Formation Oil Shales, Wyoming, Utah, and Colorado

By Wendy J. Harrison,¹ D.R. Pevear,² and P.C. Lindahl³

Abstract

Pyrites extracted from oil shale of the Paleogene Green River Formation (West Willow prospect, Colorado) were analyzed for As, Cd, Co, Cu, Mn, Mo, Ni, Pb, Se, and Zn by atomic absorption spectrophotometry. The purpose of this study was to confirm a mode of occurrence for these elements for use in chemical equilibrium modeling of leachates from oil shale.

Concentrations in the pyrite separates (>99 percent pure) are (in parts per million) As, 120–1,700; Cd, 0.16–9.1; Co, 38–220; Cu, 243–1,130; Mn, 12–1,900; Mo, 25–185; Ni, 69–223; Pb, 110–710; Se, <20; and Zn, 17–1,280. Electron microprobe analysis was used, where possible, to confirm that the trace metals were substituted into the pyrite structure and are not present as discrete metal sulfide phases in the pyrite extracts. Results of electron microprobe analysis also show that pyrites forming at different times during diagenesis have different trace-element suites.

The trace elements studied may be subdivided into two groups. Cadmium, cobalt, manganese, and zinc show a change in mode of occurrence from sulfide hosted in shale from depths below 610 m to carbonate hosted in samples from above 610 m. The remaining elements (As, Cu, Mo, Ni, Pb) show no stratigraphic variations. Mass-balance calculations show that substitution into pyrite is the principal mode of occurrence for As, Cu, Ni, and Pb in all samples and for Cd, Co, Mn, and Zn in the deeper samples. Molybdenum has another as yet undetermined mode of occurrence in addition to pyrite, and the possibility that cadmium and zinc may also

be present in wurtzite (ZnS) cannot be precluded because this phase was probably lost during pyrite separation.

INTRODUCTION

The possibility that trace elements associated with oil shale can cause significant problems in processing and environmental pollution is widely recognized (Margheim, 1975; Stollenwerk and Runnels, 1977; Fox, 1979; McWhorter, 1980; Klieve and others, 1981; Jackson and Jackson, 1982; Peterson and Wagner, 1982). Numerous studies of trace-element abundances in oil shale from the Paleogene (Eocene, locally Paleocene) Green River Formation of Colorado have been made (for example, Cooke, 1973; Meddaugh and Salotti, 1983), but few studies have addressed the more significant and difficult task of determining modes of occurrences for trace elements in the shales. Notable contributions to this problem are those of Desborough and others (1976) and Saether and others (1981).

Mode of occurrence is an essential item of information in assessing the processing and environmental behavior of trace elements. The knowledge that a given trace element is associated with a sulfide mineral, for example, makes possible prediction of the behavior of that element both in processing (such as volatilization or catalytic poisoning) and during subsequent storage and (or) disposal of the shale.

The geochemical association of the group of elements known as heavy metals (Pb, Zn, Ni, Co, Cu, Cd, Mo, As, Se) and sulfide minerals (pyrite, FeS₂; pyrrhotite Fe_{1-x}S) is well known (Fleischer, 1955; Hawley and Nichol, 1961; Springer and others, 1964; Roberts, 1981). Several of these elements can cause health problems, and their emission levels are regulated by the Environmental Protection Agency. Arsenic is known to be a catalytic poison during

¹Department of Geology and Geological Engineering, Colorado School of Mines, Golden, Colorado 80401.

²Exxon Production Research Company, P.O. Box 2189, Houston, Texas 77001.

³Argonne National Laboratory, 9700 South Cass Avenue, Argonne, Illinois 60439-4815.

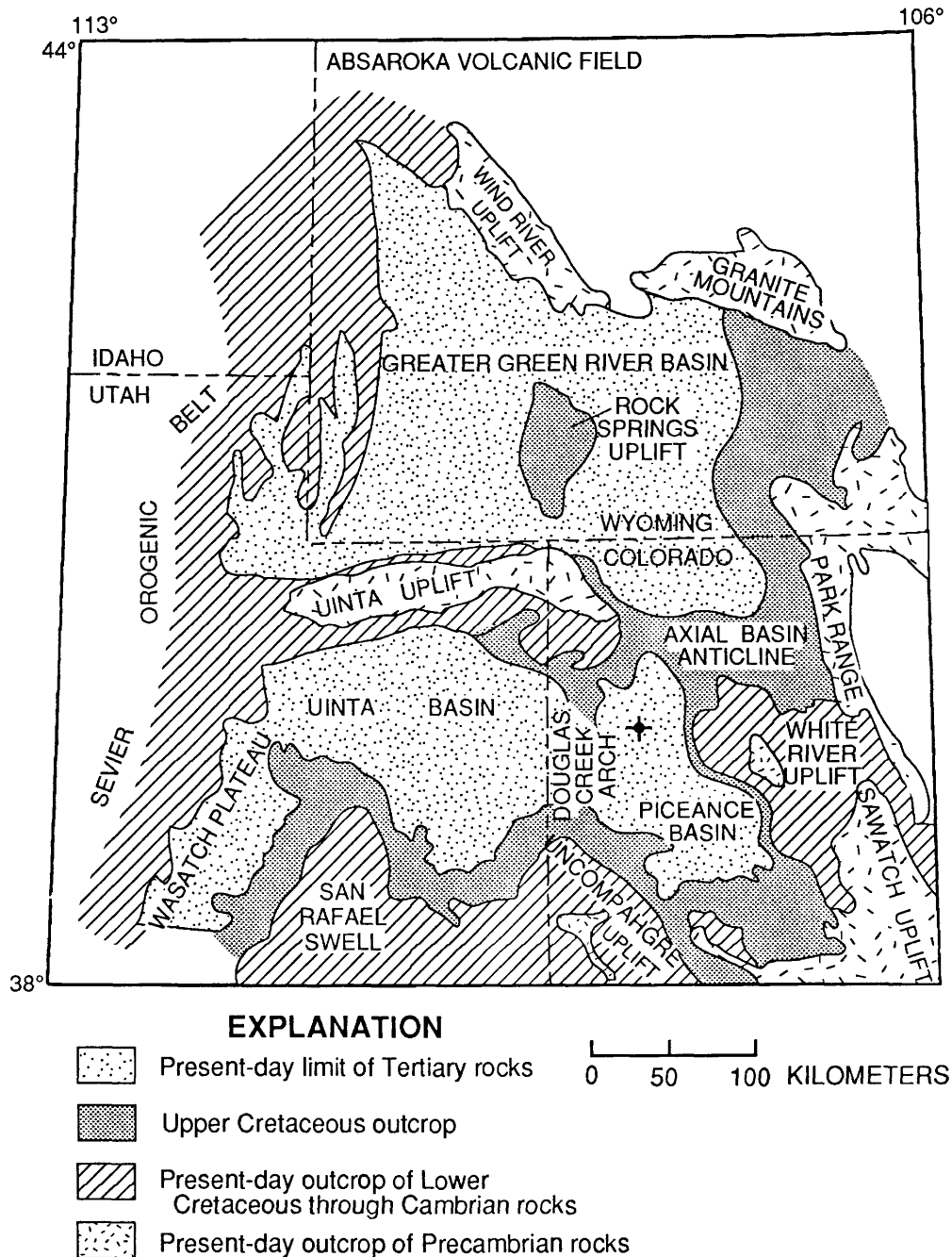


Figure 1. Location of West Willow no. 3 core hole (sec. 7, T. 3 S., R. 97 W., Rio Blanco County, Colorado). Core is from Exxon Coal Resources West Willow Lease Block.

shale retorting (M. Siskin, Exxon Research and Engineering Company, written commun., March 1981).

The purpose of our study was to determine the concentrations of As, Cd, Co, Cu, Mn, Mo, Ni, Pb, Se, and Zn in pyrite extracted from Green River oil shale. Pyrite is the principal sulfide mineral in the shale (Milton, 1977), and, because its stability temperature is exceeded in many shale processing schemes, the potential for heavy-metal release is enhanced. The oxidation of pyrite when exposed

to groundwater provides a further opportunity for trace-metal contamination. Knowledge of trace-metal contents in pyrite is thus needed before quantitative prediction of the contamination potential of oil shale can be made by chemical equilibrium modeling (Harrison, 1990).

Acknowledgments.—Discussions with H.J. Gluskoter (U.S. Geological Survey), G.J. Grabowski, Jr. (Exxon Production Research Company), and K.O. Stanley (Exxon Company, International) were helpful in constructing this

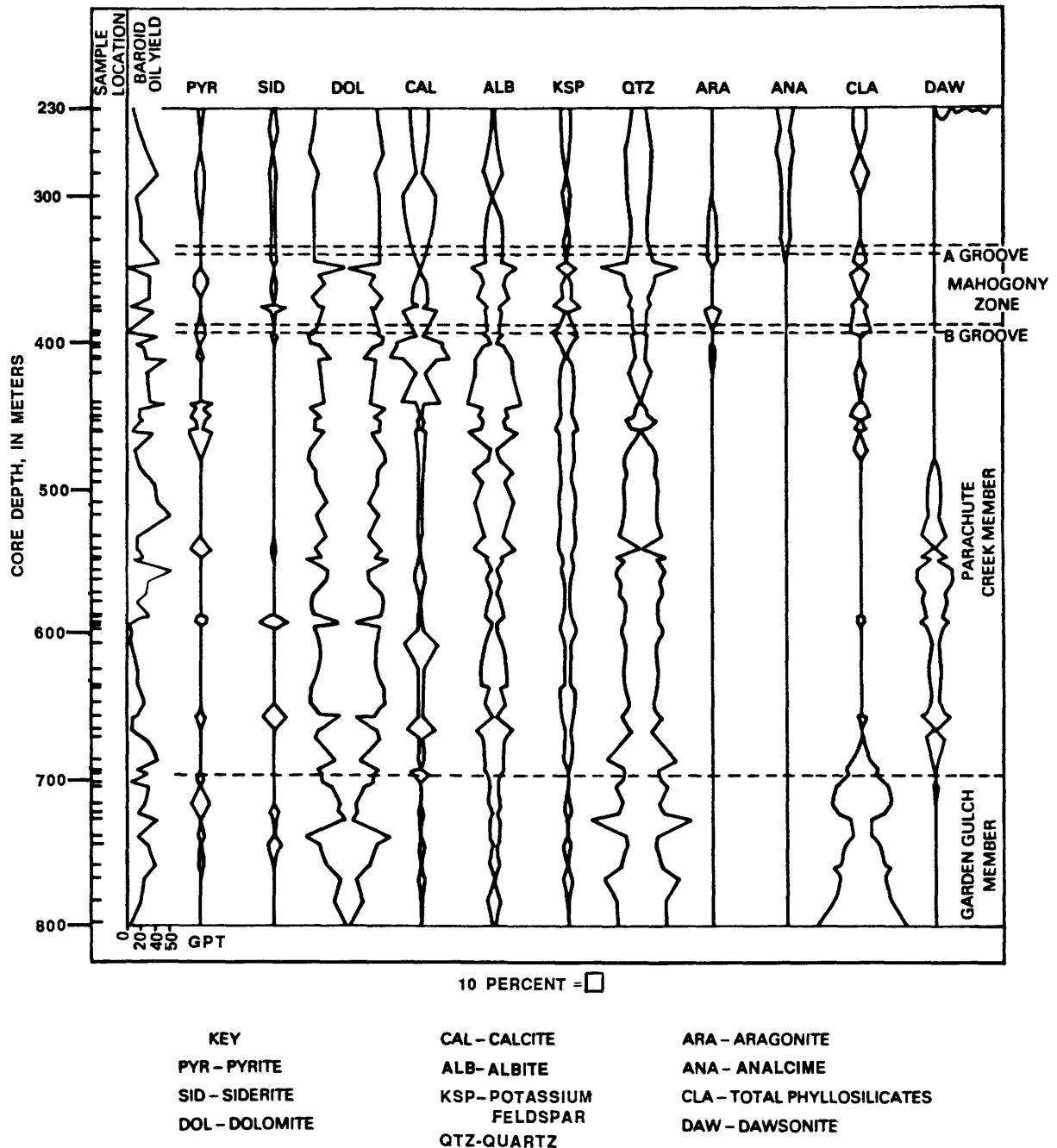


Figure 3. Mineralogy of samples of Green River Formation from West Willow no. 3 core. Baroid oil yield in gallons per ton.

descriptions are presented in appendix 1. Percentages of the minerals dawsonite, aragonite, quartz, potassium feldspar, albite, calcite, dolomite, siderite, pyrite, and total phyllosilicates are shown in table 1 and are probably accurate to ± 20 percent at best, perhaps ± 50 percent for some minerals such as pyrite.

Our data are a subset of a larger data set of mineral abundances for the whole core. The larger data set also shows a change in mineralogy at a depth of about 607 m, below which dawsonite, quartz, and siderite are significant rock-forming phases (fig. 3). Calcite, clay, and aragonite are more abundant in higher parts of the formation.

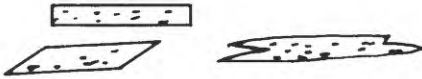
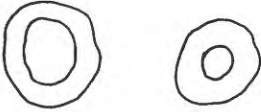
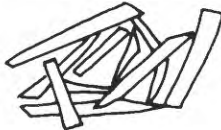
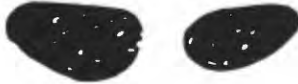
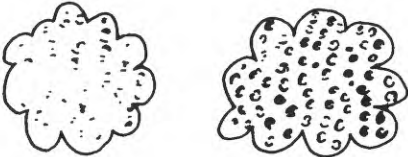
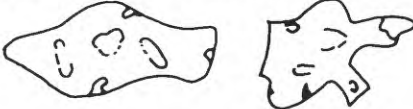
COMMON IRON-SULFIDE MORPHOTYPES IN THE GREEN RIVER FORMATION	
MACROSCOPIC (1 mm-10 m)	MICROSCOPIC (less than 1 mm)
<p>PODS AND LENSES</p> 	<p>BLADES (spicular)</p> 
<p>CONCRETIONS</p> 	<p>COMPOUND BLADE CLUSTERS AND BANDS</p> 
<p>BOUDINAGES</p> 	<p>SPECKS (less than 4 microns)</p> 
<p>STRINGERS</p> 	<p>GRANULAR BLEBS</p> 
<p>MEGAFRAMBOIDS</p> 	<p>IRREGULAR MASSIVE BLEBS</p> 
	<p>CUBES (few encountered)</p> 

Figure 4. Classification of common macroscopic and microscopic iron-sulfide morphotypes in Green River Formation. Modified from Boyer and Cole (1983).

PYRITE SEPARATION

Pyrite was removed, together with some other sulfide phases, from powdered shale samples by a series of acid dissolutions and density separations described in appendix 2. Pyrite extracts were examined by scanning electron microscopy (SEM) and XRD to assess purity. Results of

XRD analysis of the pyrite extracts are shown in table 2; all samples contain pyrite and small amounts of marcasite (see Milton, 1977). In addition, pyrrhotite was identified in one sample, and two samples had several very low intensity peaks that could not be assigned to any mineral. Pyrrhotite is soluble during the acid decomposition treatment and may have been removed from many of our samples.

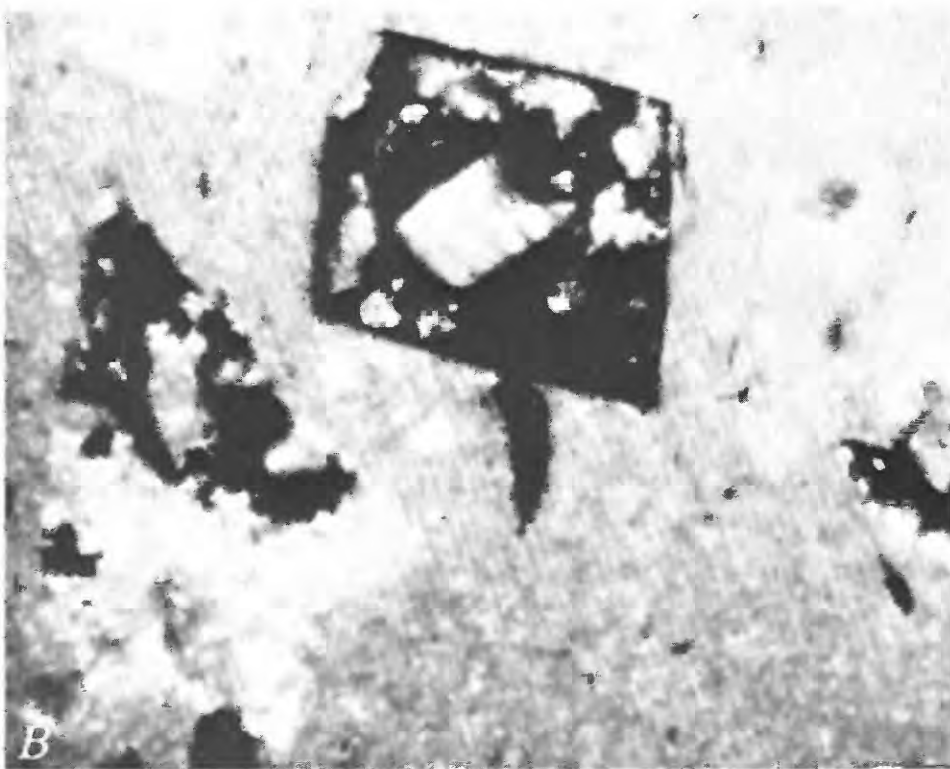
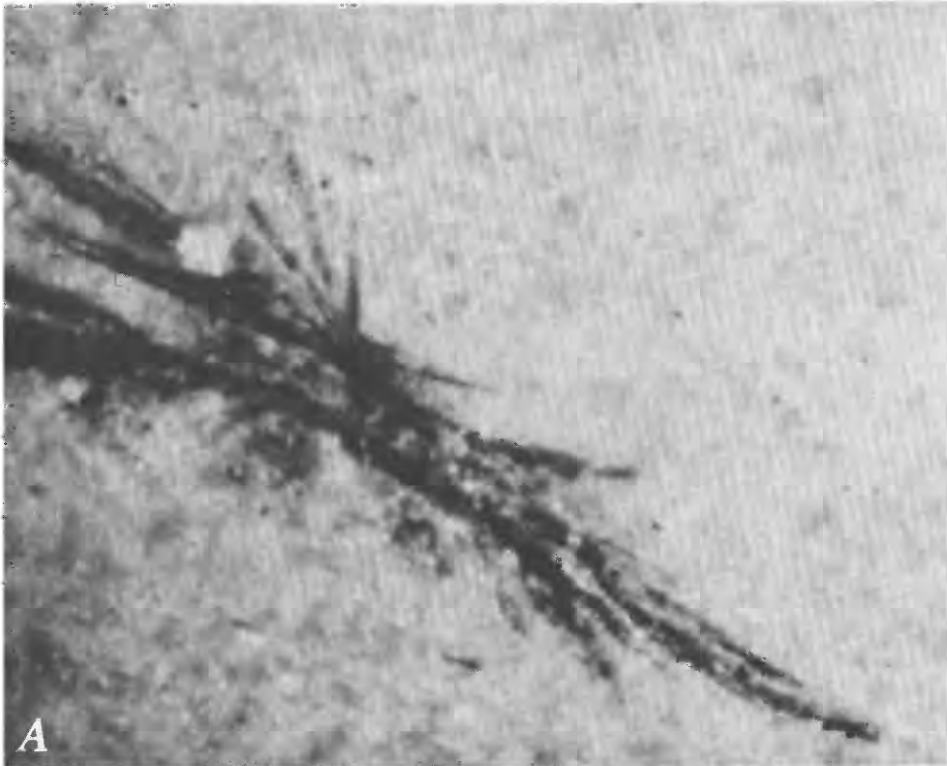


Figure 5 (above and facing page). Morphotypes of pyrites in Green River Formation. *A*, Bladed morphology; pyrite replacing salt minerals or pyrrhotite, 1 cm=46 μ m. *B*, Pyrite replacement of dolomite rhomb, 1 cm=46 μ m. *C*, Diagenetic pyrite blebs, 1 cm=28 μ m. *D*, Finely disseminated, syndepositional pyrite, 1 cm=103 μ m.

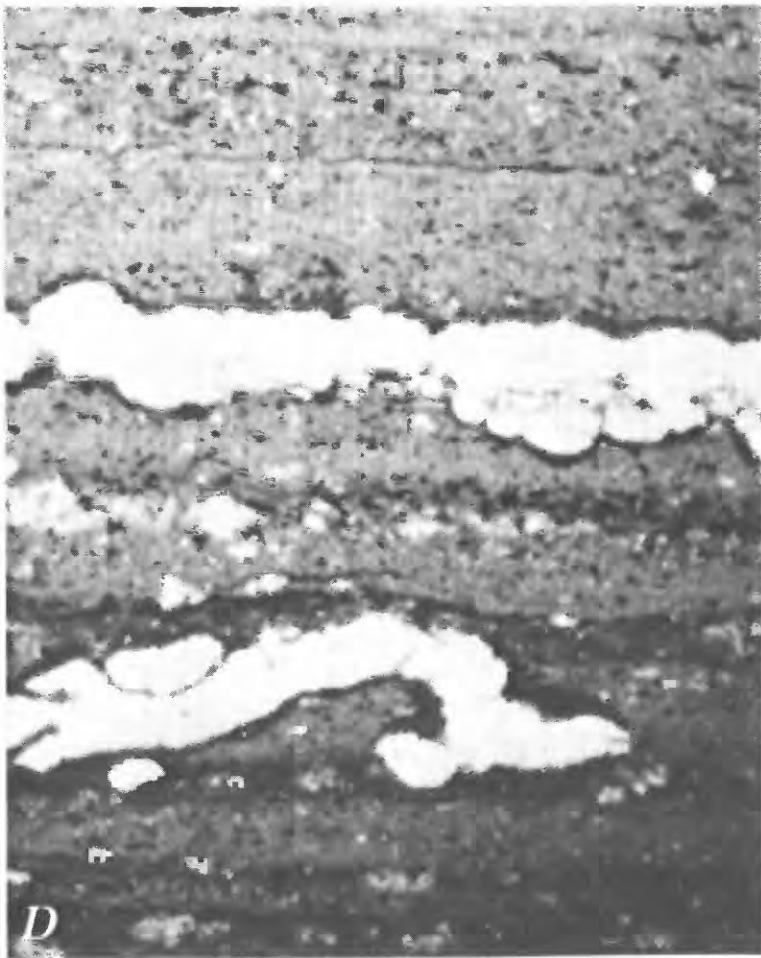
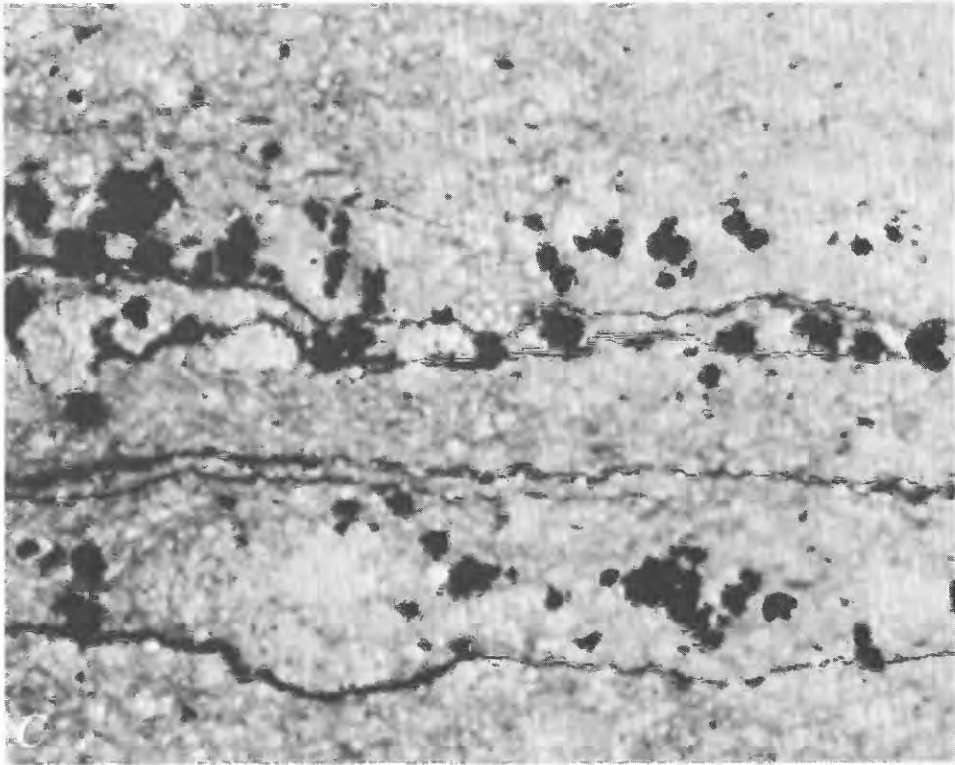


Table 3. Pyrite morphotypes observed in petrographic section
 [Location of core hole West Willow no. 3 shown in figure 1. Location of samples shown in figure 2]

Sample	Disseminated	Irregular blebs	Cubes	Blades	Fracture filling
377.3			yes		
397.3		yes			
415.7			yes		
470.1		yes		yes	
557.7		yes	yes		yes
608.6	yes	yes			
612.5	yes				
682.1	yes				
682.4					

A very few fragments of organic matter and undissolved minerals (tentatively identified as rutile TiO_2 and feldspar KAlSi_3O_8) were found, and the samples are estimated to be more than 99 percent pure. Wurtzite (ZnS), reported to be widespread (Milton, 1977), was not observed in SEM or XRD investigations, but it is soluble in most dilute acids and, if present, may have been dissolved during pyrite extraction.

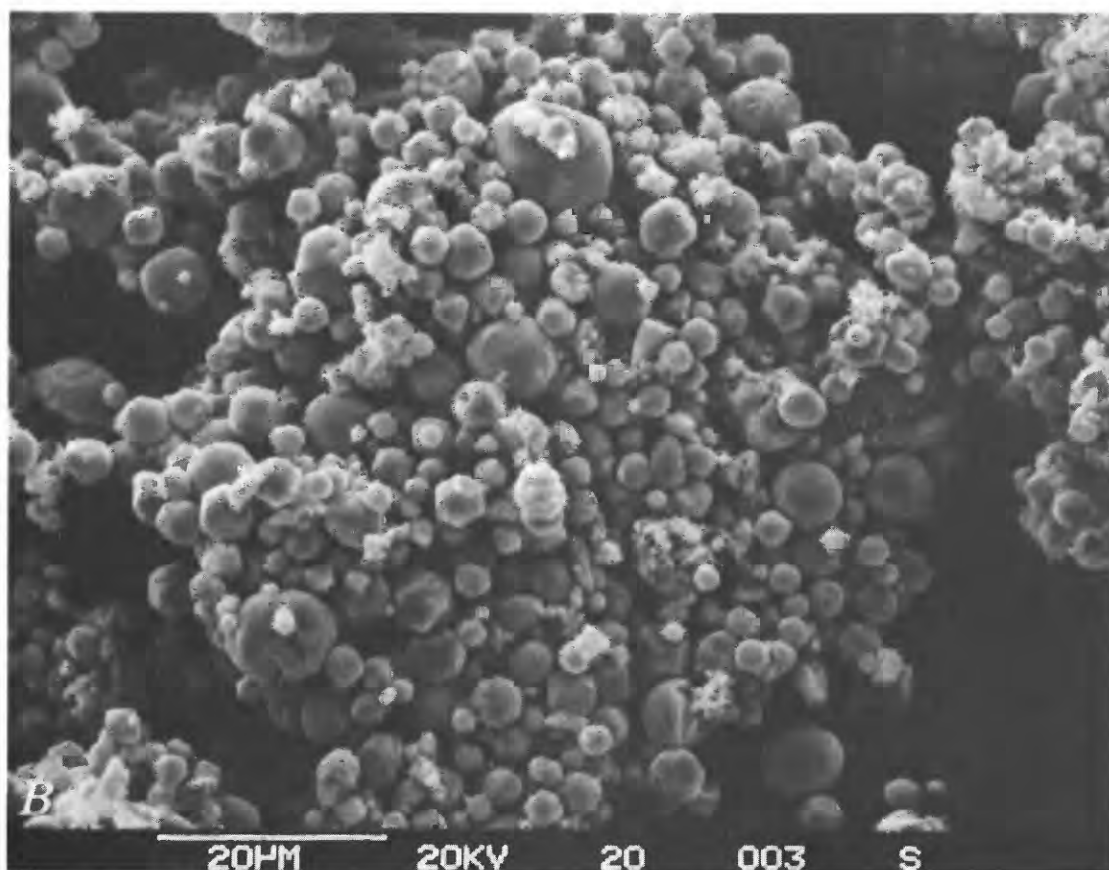
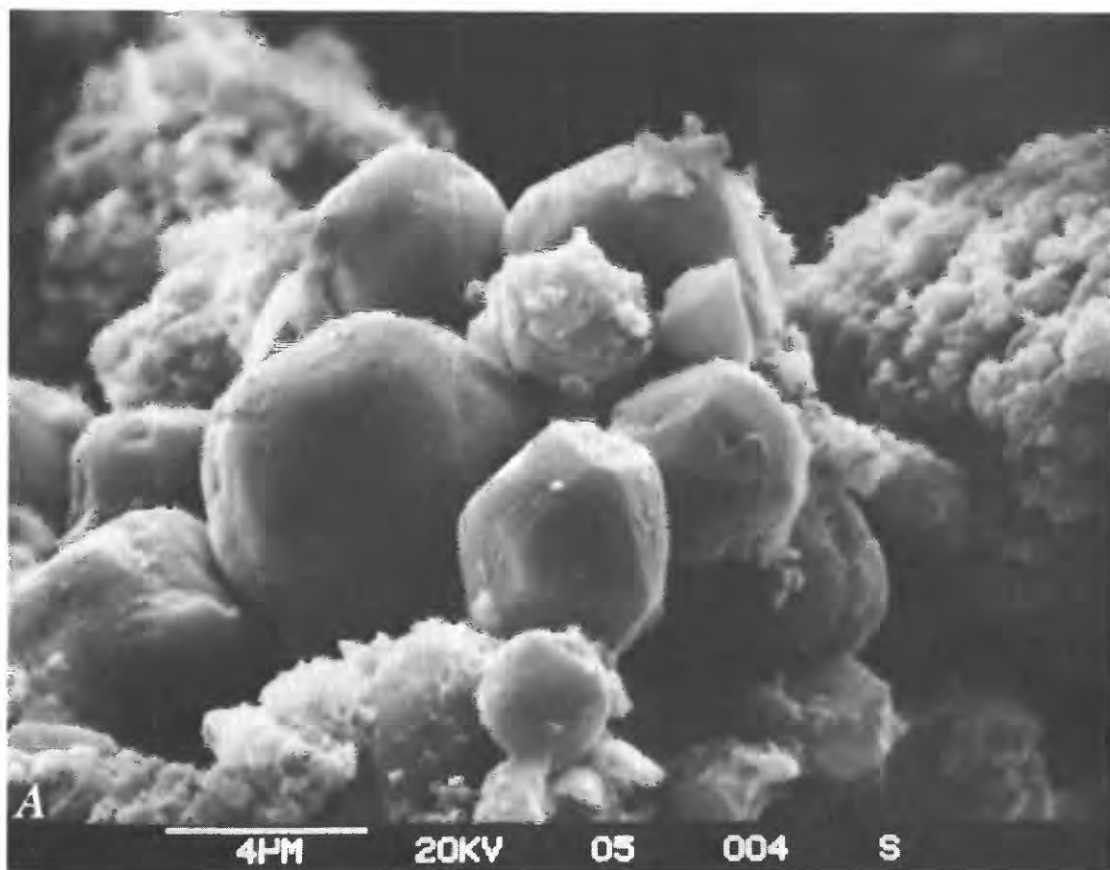
A number of morphotypes of pyrite have been identified from the Green River Formation (Pabst, 1971; Boyer and Cole, 1983). Figure 4 shows the classification scheme devised by Boyer and Cole (1983). In our samples we observed abundant blades (a replacement texture after some saline minerals and (or) pyrrhotite blades), specks (finely disseminated pyrite), bands, and blebs (irregular pyrite masses). Examples are shown in figure 5. A distinct stratigraphic distribution of these morphotypes was noted in the West Willow no. 3 core (table 3). Disseminated pyrite can be distinguished from tiny pyrite cubes, which are scattered throughout samples and concentrated into lenses and blebs, by lack of crystal morphology (either not present or too fine grained to see).

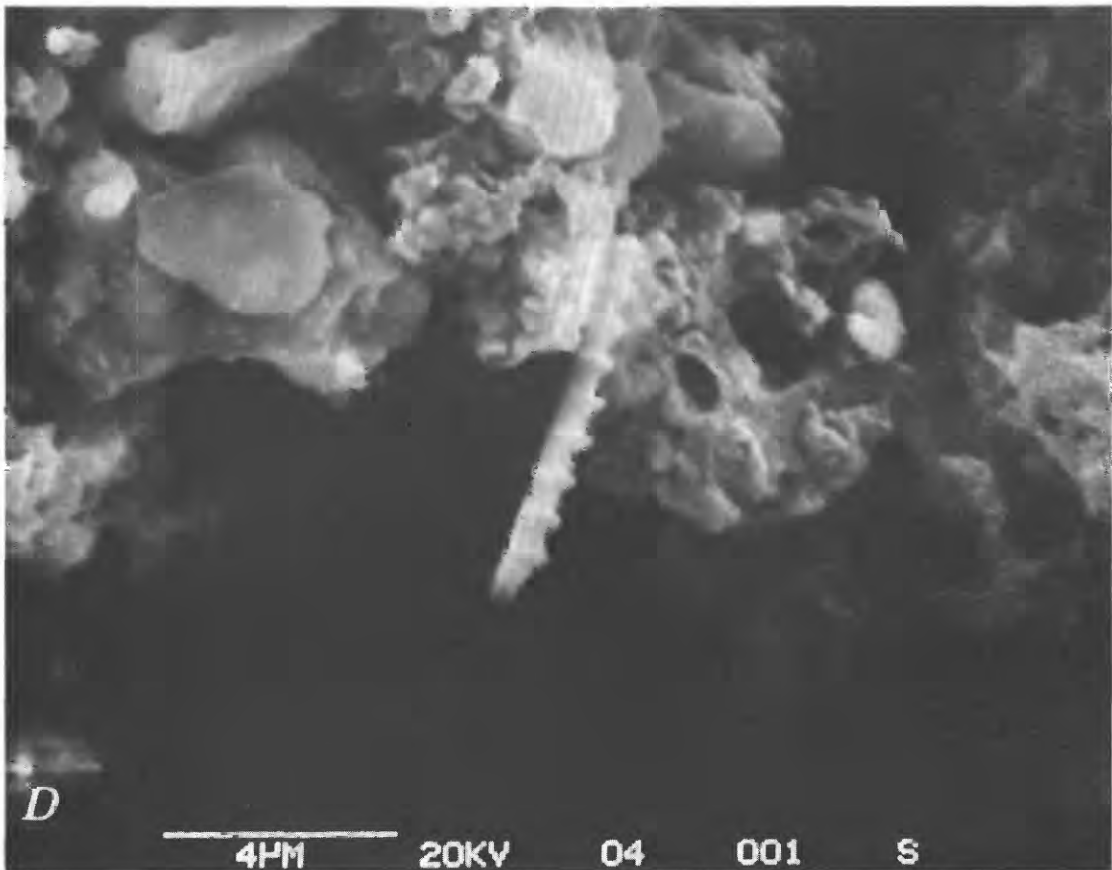
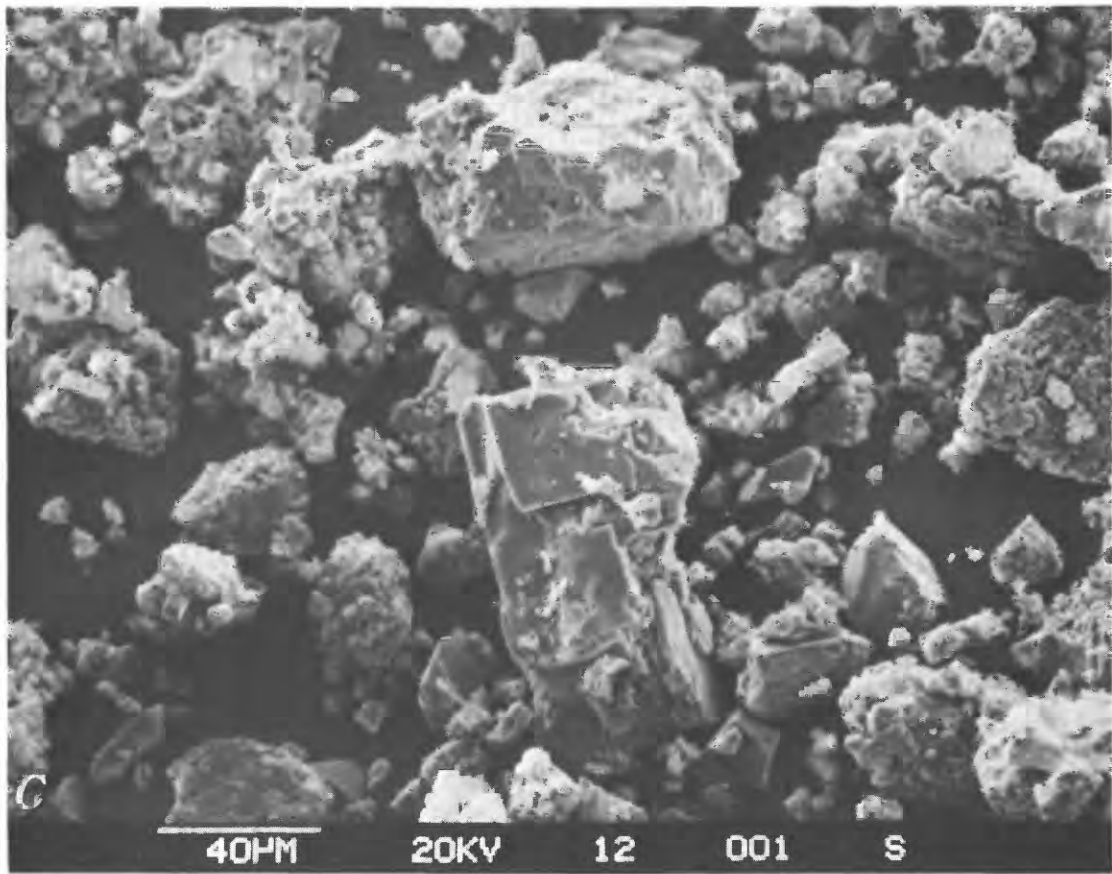
An SEM investigation of the pyrite extracts yielded information about pyrite morphology on a different scale: (1) spongy pyrite masses, (2) small euhedral crystals, (3) spheres, (4) fragments of large crystals and pseudomorphs, (5) replacement of organic material, and (6) pyrrhotite hexagonal plates (fig. 6). (Our identification of pyrrhotite is based on the hexagonal crystal morphology and XRD data. Sweeney and Kaplan (1973) also identified the hexagonal plate morphology as characteristic for pyrrhotite.) The textural features of extracted pyrite observed using SEM are difficult to relate to those observed at lower magnification in petrographic thin sections. It is of interest that the fine textures illustrated in figures 6C and D have been preserved despite the physical and chemical dissolution procedures used to extract the sulfide minerals. We do not believe that the spheres represent abraded crystals, rather they are a morphology typical of a pyrite precursor, greigite (Fe_3S_4), now preserved as pyrite (Sweeney and Kaplan, 1973).

Spheres and crystals have a comparable range of sizes; abrasion likely would have reduced the range observed in the sphere population relative to that of the crystal population. The spheres could represent disaggregated framboids; however, the general absence of framboidal pyrite in this particular core and the absence of any partially disaggregated fragments argue against this hypothesis. (Framboidal pyrite was not observed in petrographic thin sections of these rocks; however, it commonly is associated with organic matter, and any small quantities of framboidal pyrite present might have been lost during the separation procedure.) Blades (fig. 5A) observed in thin section comprise many tiny pyrite crystals as do some of the blebs and larger irregular masses.

We suggest that the spheres and tiny euhedral pyrite crystals formed at the time of deposition of the organic-rich sediments, either as pyrite or an iron-sulfide precursor (Lord and Church, 1983). All other pyrite morphologic types formed later, during and after diagenesis, and all show replacement features of various kinds. Our conclusion is in agreement with Dyni's (1983) identification of three stages of sulfide mineralization in the Green River Formation: (1) early diagenetic phase (our finely disseminated pyrite), (2) late diagenetic phase (blades and the replacement of other minerals formed during sediment dewatering), and (3) postlithification phase (pyrite precipitated in fractures and cracks).

Figure 6 (following pages). Scanning electron micrographs of pyrites in Green River Formation. A, Small euhedral crystals, spheres, and spongy pyrite masses. B, Small pyrite spheres. C, Pyrite replacement of crystal fragments and spongy pyrite masses. D, Shell fragment replaced by pyrite. E, Hexagonal pyrrhotite plates. F, Energy-dispersive X-ray intensities from sample shown in C.





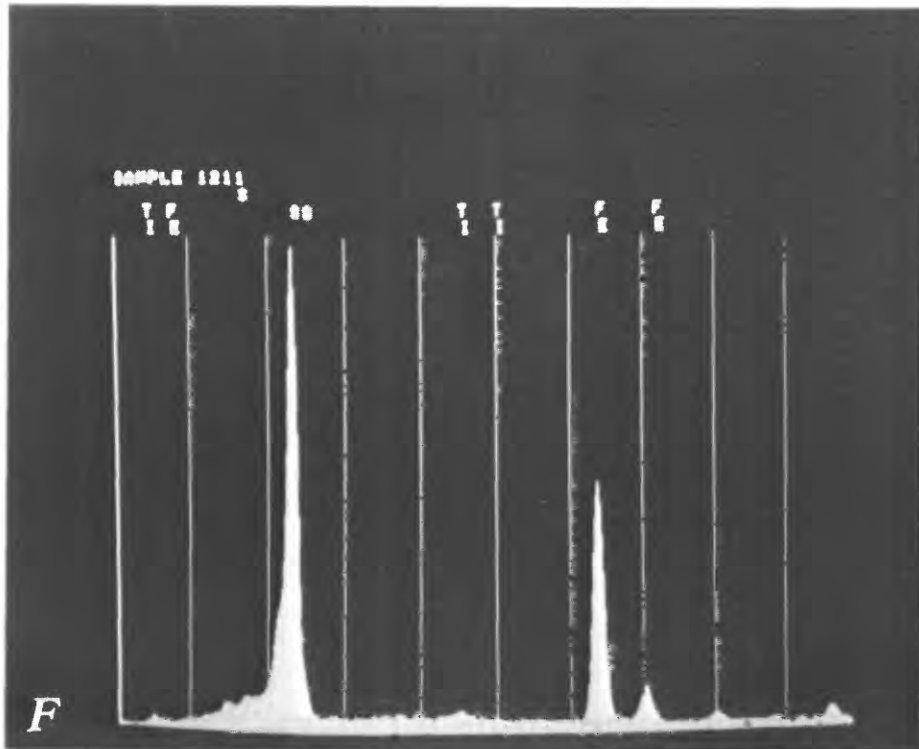
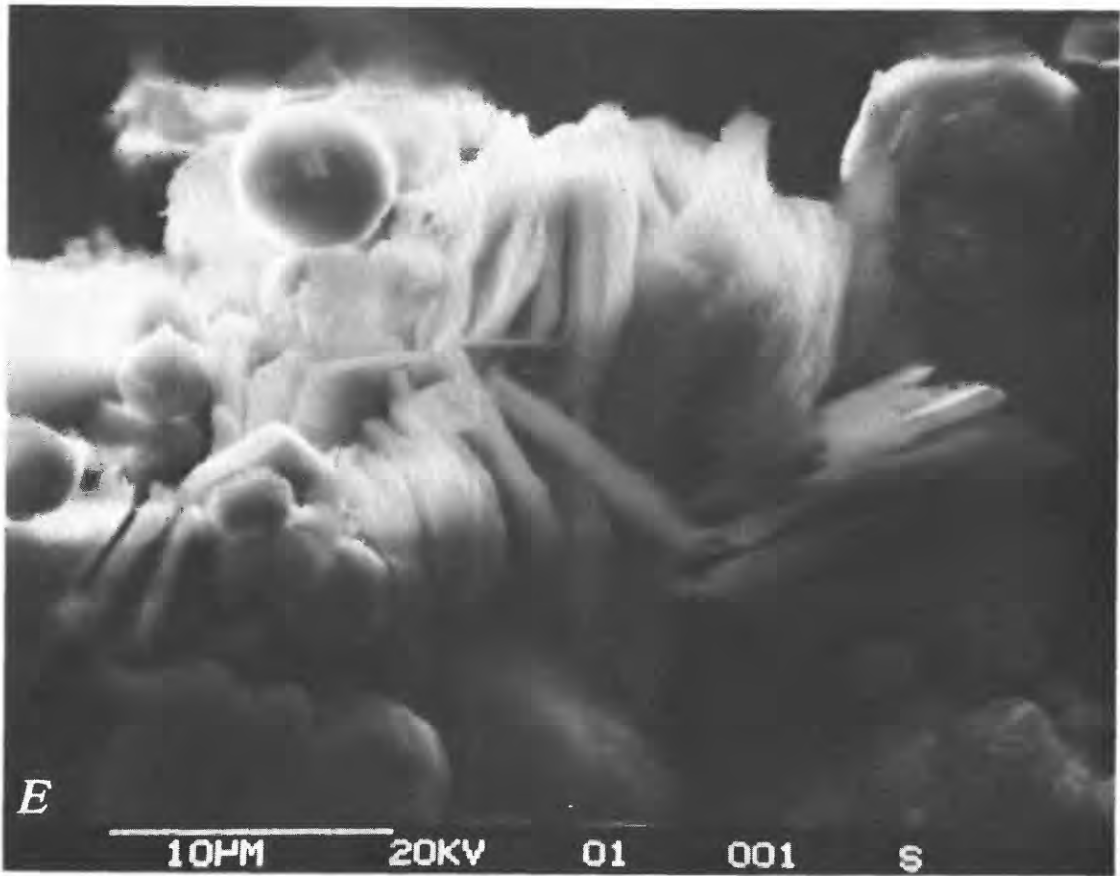


Table 4. Trace-element contents of pyrites

[Location of core hole West Willow no. 3 shown in figure 1; location of samples shown in figure 2. Concentrations in parts per million; oil yield in gallons per tonne]

Sample	Zone	Baroid oil yield	As	Cd	Co	Cu	Mn	Mo	Ni	Pb	Zn
377.3	Mahogany	9.57	220	0.26	99	882	41	41	223	710	72
397.3	L6	5.41	360	0.16	93	552	25	25	155	230	76
415.7	R6	26.37	130	0.34	75	516	17	185	96	200	39
470.1	L5	7.55	120	0.18	113	243	14	124	103	240	22
557.7	R4	12.34	1,770	0.52	50	328	34	47	219	110	46
608.6	R4	23.0	200	0.20	38	292	12	179	110	230	17
612.5	L3	8.42	220	1.4	150	878	1,420	151	127	150	158
682.1	R3	13.74	340	9.1	161	771	1,900	111	69	110	1,280
682.4	R3	4.16	200	2.9	220	1,130	1,800	181	158	270	441

TRACE-ELEMENT ANALYTICAL METHODS

Pyrite mineral separates obtained from the samples of oil shale were dissolved in nitric acid, and solutions were analyzed using atomic absorption (AA) spectrophotometry. Conventional flame AA was used to determine Fe and the trace elements Co, Cu, Mn, Ni, Pb, and Zn. Flameless AA using a heated graphite atomizer (HGA) was employed to determine the trace elements As, Cd, Mo, and Se because concentrations of these elements are below the flame AA detection limits. Unfortunately, the selenium content proved to be below that of the flameless AA detection limit due to interference caused by the high iron content in the samples. Further details of instrumental parameters are given in appendix 2.

RESULTS AND DISCUSSION

Trace-metal concentrations in pyrites extracted from the oil shale are given in table 4. Only selenium is present in amounts below the detection limit of the primary analytical techniques (<10–20 ppm). Two groups of trace elements can be identified: (1) those for which there is no systematic stratigraphic variation (Cu, Pb, Ni, As, Mo) and (2) those for which a distinct increase in concentration is observed below 608.6 m depth (Mn, Zn, Cd, Co). The magnitude of the increase, from a factor of 100 for manganese, 10 for zinc and cadmium, to 5 for cobalt, argues against analytical or sample preparation error. Also of note is that a considerable amount of the increase is in a short vertical stratigraphic interval; for example, compare data for samples 682.1 and 682.4 (table 4) (all sample numbers represent depth, in meters), separated by only a third of a meter. There is no correlation between element content in pyrite and whole-rock oil yield in these samples and no correlation between individual elements other than that

between zinc and cadmium, which is very common, and copper and cobalt (fig. 7).

Trace-element concentrations in whole-rock samples were determined for mass-balance considerations. These data are shown in table 5 and analytical details are described in appendix 2. Although the number of samples is limited, correlations between molybdenum and cobalt (fig. 8A), nickel and cobalt (fig. 8B), cobalt and copper (fig. 8C), and nickel and copper (fig. 8D) most likely are significant. Comparison of pyrite extract contents with whole-rock contents show only one significant correlation, that for the element copper (fig. 9). The lack of correlation between whole-rock and pyrite trace-element contents indicates complexities in the modes of occurrences for these elements.

Our pyrite extraction technique is not quantitative because very fine grained pyrite remains with the kerogen during the sink/float separations. Nevertheless, mass-balance calculations were attempted with the intent of estimating the percentage of each trace element that is sulfide associated. In these calculations (table 5), whole-rock trace-element contents were determined by assuming that all of each trace element is in the pyrite; the percentage of pyrite in the rock was determined from XRD analysis. The theoretical whole-rock contents were then compared (table 5) with the analytical data and a compilation of literature data from Cook (1973), Desborough and others (1976), Giaugue and others (1981), and Meddaugh and Salotti (1983).

Although detailed comparison of the calculated and analytically determined whole-rock content was not possible because of the errors inherent in the XRD determination of pyrite abundance, a high percentage of the Cu, Pb, Co, Ni, and As in our samples most likely is sulfide associated, held in some way in the pyrite structure. Below 608.6 m in the West Willow no. 3 core, Mn, Zn, and Cd are also, predominantly sulfide associated; above this level,

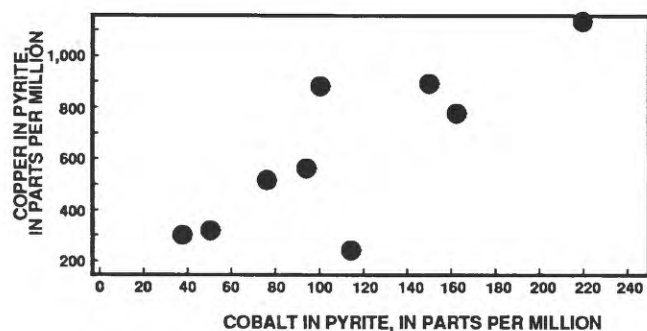


Figure 7. Correlation between copper and cobalt in pyrites extracted from Green River oil shale.

some other phase, probably carbonate, is the principal host of these three elements. Part of the molybdenum is also sulfide associated, but our calculated values are generally lower than those reported in the literature (table 5) and molybdenum may have a second mode of occurrence (see also Giauque and others, 1981).

Our working hypothesis is that all the heavy metals are substituted directly into the pyrite structure; however, a very small amount of a sulfide mineral such as ZnS, MnS, or PbS in the pyrite extract could easily account for the measured trace-element contents. X-ray diffraction data show that the pyrite extracts are composed primarily of pyrite and some marcasite (a polymorph of FeS₂) and pyrrhotite (Fe_{1-x}S), but the XRD technique is not sensitive to small quantities of minerals. No separate sulfide phases

Table 5. Measured, calculated, and published trace-element, H₂O, and ash contents of whole-rock samples

[Location of core hole West Willow no. 3 shown in figure 1; location of samples shown in figure 2. Trace-element contents except Se in parts per million; Se, H₂O, and ash contents in weight percent; nd, not determined; blank indicates no data available]

Whole-rock analyses												
Sample	As	Cd	Co	Cu	Mn	Mo	Ni	Pb	Se	Zn	H ₂ O	Ash
377.3	8.2	<0.10	9.2	78	330	16	31	24	<0.00	95	0.28	76
397.3	16	<0.10	6.9	41	325	3.1	25	12	<0.00	88	0.37	75
415.7	9.0	<0.10	5.4	30	160	18	18	4.1	<0.00	48	0.30	58
470.1	9.4	<0.10	7.2	49	250	14	31	14	<0.00	99	0.61	81
557.7	52	<0.10	6.2	42	295	17	33	9.6	<0.00	120	0.52	77
608.6	99	<0.10	6.8	41	240	7.5	36	7.7	<0.00	89	0.47	71
612.5	23	<0.10	19	100	175	73	100	17	<0.00	125	0.23	75
682.1	15	<0.10	9.1	43	170	42	29	8.3	<0.00	73	0.35	79
682.4	26	<0.10	15	98	150	93	41	4.8	<0.00	115	0.26	76
Calculated trace-element contents												
Sample	Percent pyrite		As	Cd	Co	Cu	Mn	Mo	Ni	Pb	Zn	
	X-ray	Assumed										
377.3	0	5	44	0.05	20	175	8	8	45	140	14	
397.3	4	5	72	0.03	19	110	3	5	31	46	15	
415.7	4	5	26	0.07	15	100	3	37	19	40	8	
470.1	14	15	8	0.01	8	16	41	8	7	16	1.5	
557.7	15	15	120	0.03	3	22	2.3	3	15	7	3	
608.6	6	10	20	0.02	4	29	1.2	18	11	23	2	
612.5	10	10	22	0.14	15	88	140	15	13	15	16	
682.1	2	5	68	2.0	32	155	380	22	14	22	255	
682.4	7	10	20	0.3	22	115	180	18	16	27	44	
Published values												
Reference	Percent assumed		As	Cd	Co	Cu	Mn	Mo	Ni	Pb	Zn	
	pyrite											
Desborough and others (1976)	Low		25	<1	5	33	181	7	20	19	49	
	High		75	1.2	20	114	296	40	40	58	112	
Cook (1973)			7.2	nd	39	15	34	nd	11	10	13	
Meddaugh and Salotti (1983)	Average		10.8					47.5				
	High		71					83				
Giauque and others (1981)	Low		5	nd	4	11	190	4	11	5	38	
	High		133	nd	14	63	460	53	31	41	153	

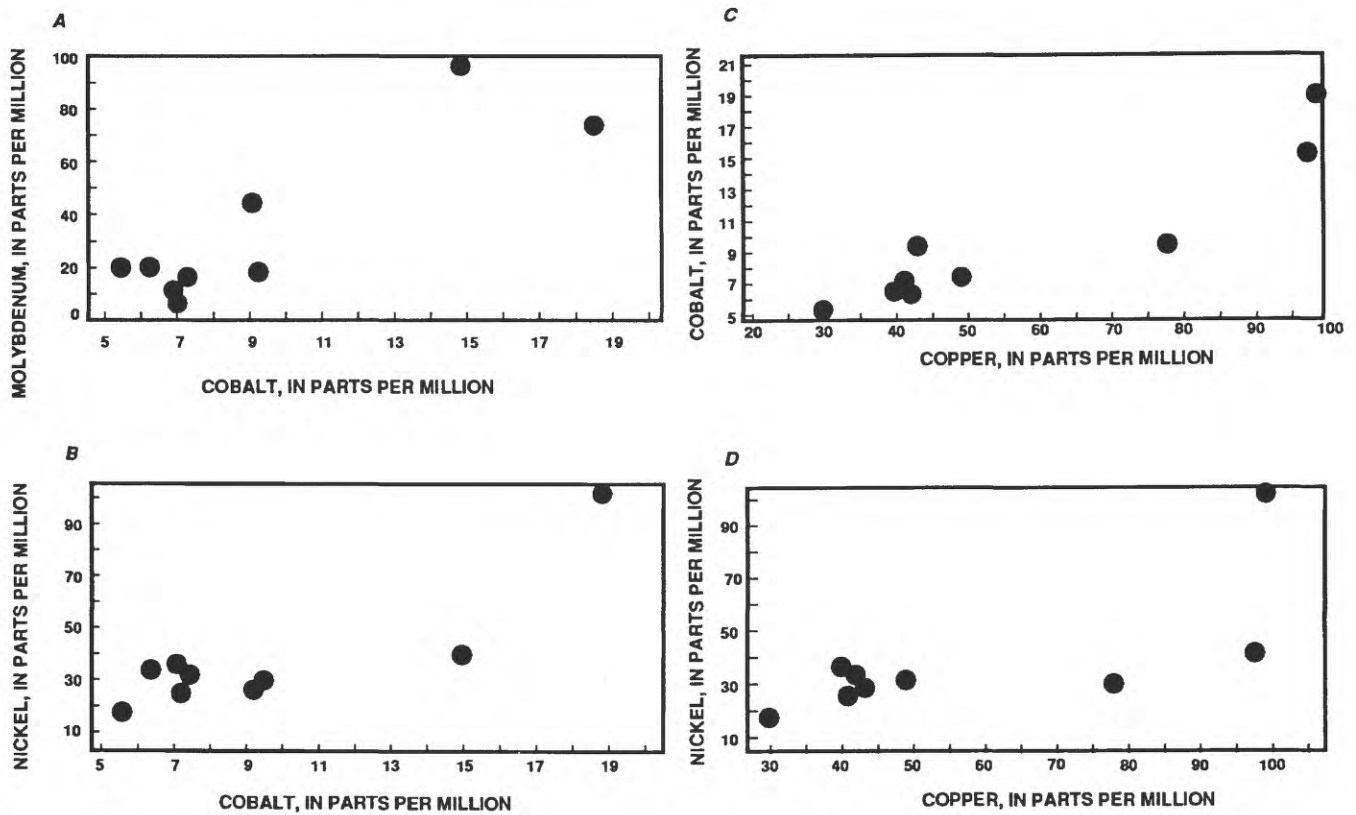


Figure 8. Correlation between cobalt, molybdenum, nickel, and copper in whole-rock samples of Green River oil shale.

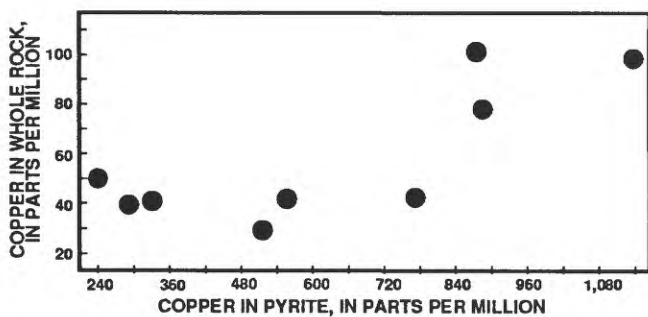


Figure 9. Correlation between copper in pyrite extracts and in whole-rock samples of Green River oil shale indicates that pyrite may be primary mode of occurrence for this element.

were found when the samples were examined by SEM. The most conclusive evidence of mode of occurrence comes from a preliminary study of pyrite using the electron microprobe.

Electron Microprobe Analyses

To obtain more conclusive evidence for our hypothesis that trace metals are substituted into pyrite and

are not present as trace amounts of metal-sulfide phases, we analyzed some of the pyrites for a suite of trace elements. Preliminary data indicate that some of the elements are substituted in the pyrite structure.

We analyzed for Mn, Zn, As, Cu, and Pb in samples 453.1, 612.5, and 682.1 and in two samples not from the interval originally studied, 344.8 and 810. Operating conditions for the Cameca electron microprobe were an accelerating voltage of 30 kV and a beam current of 100 nanoamps. Counting times were 30 seconds for all elements except arsenic, for which 10-second counting times were employed because significant volatilization was observed. Detection limits are about 100 ppm for As, Mn, and Zn, 200 ppm for Cu, and 500 ppm for Pb. Pyrites having known contents of the elements analyzed were used as standards. Lead and copper concentrations commonly were not sufficiently above the detection limits for quantitative data to be obtained, and no concentrations can be quoted for these two elements until we obtain more appropriate standards. The presence or absence of lead and copper, however, can be reliably noted. Elemental X-ray maps of a polished pyrite-rich section of oil shale from 810 m depth in the core are shown in figure 10. Although the resolution is poor for the arsenic distribution (concentration about 650 ppm), its association with pyrite, in a rather uniform pattern, is clear.

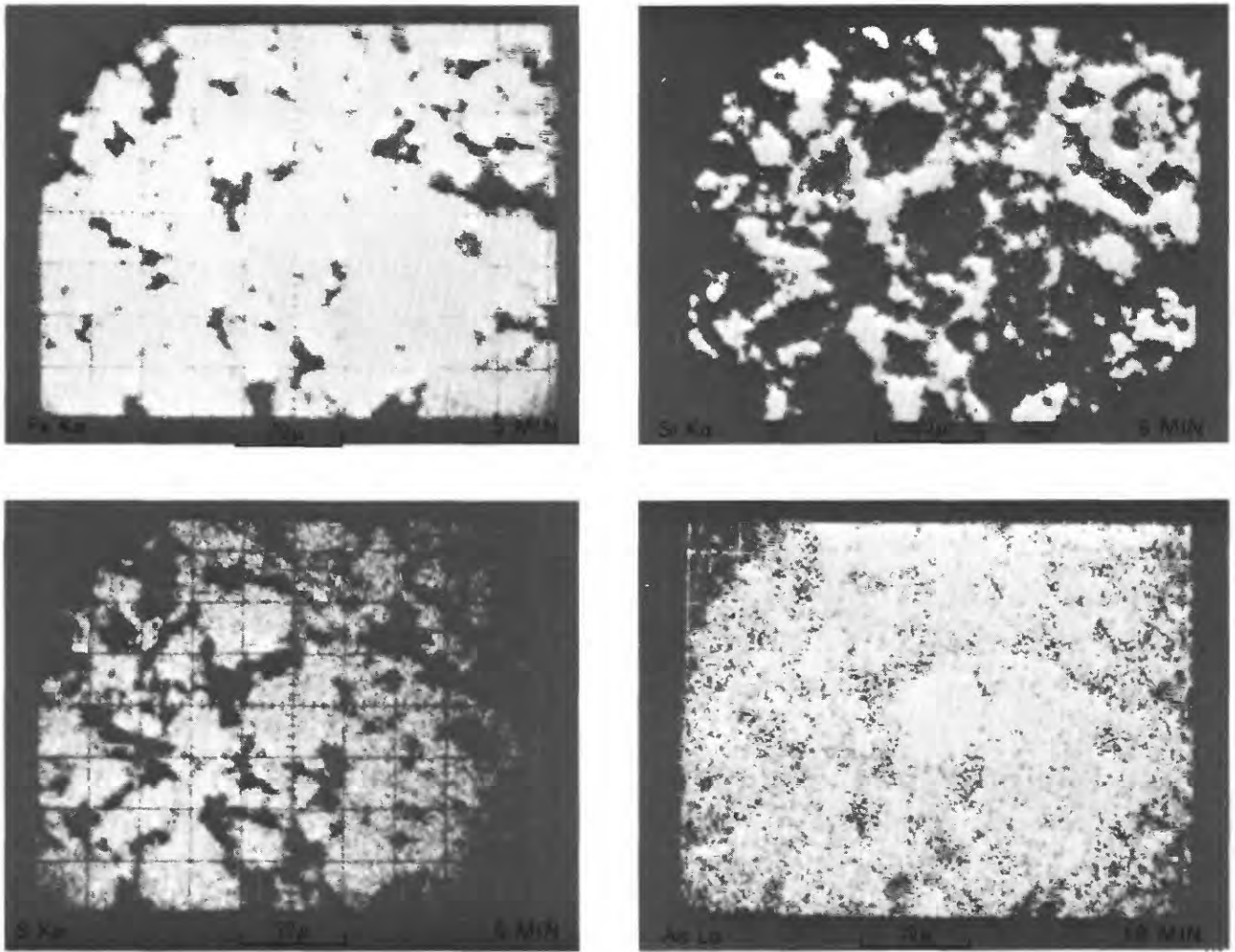


Figure 10. Elemental X-ray intensity images (maps) of polished pyrite-rich oil shale (sample WW-810; sample location shown in fig. 2). Antipathetical relationship between Fe K_{α} distribution, exposed for 5 min, and Si K_{α} distribution, exposed for 5 min, illustrates distribution of pyrite and silicate material in section. Correlation of S K_{α} and As L_{α} distribution with Fe K_{α} distribution shows the quite homogeneous arsenic substitution in pyrite.

Different morphologic forms of pyrite contain distinctive suites of trace elements. Fine-grained, euhedral, disseminated pyrite, typically only in samples below 608.6 m in the West Willow core (see appendix 1), contains large amounts of manganese, from 2,000 to 3,500 ppm, zinc of as much as about 160 ppm, and detectable copper and lead. Arsenic was very rarely detected. Larger pyrite grains in replacement or diagenetic textures, such as fracture filling or replacement of pre-existing crystals, contain no manganese (or rarely 100–200 ppm), but many contain arsenic, copper, and lead. Arsenic contents are from 200 to 1,000 ppm. We could not distinguish different trace-element suites among these later formed pyrites.

We tentatively conclude that there are stratigraphic and morphologic controls on trace-element contents in the pyrites, both of which we can account for in the geochemical model described below.

GEOCHEMICAL INTERPRETATION

Our assignment of the metals As, Co, Cu, Mo, Ni, and Pb to a sulfide mode of occurrence, Mn, Zn, and Cd to both carbonate and sulfide, and Mo to another, yet undetermined (in this study) mode of occurrence agree with published data on the Green River Formation (Desborough and others, 1976; Saether and others, 1980, quoted in Giaugue and others, 1981; Giaugue and others, 1981). The incorporation of manganese in pyrite is surprising. More than 50 percent of the 900 pyrite analyses reported by Fleischer (1955) show less than 10 ppm Mn, although contents as high as 10,000 ppm are recorded. Pyrrhotite, on the other hand, readily accepts manganese and zinc into its lattice (Wedephol, 1969). The geochemical coherence of manganese and cobalt is well documented (Burns, 1976), and the elements Mn,

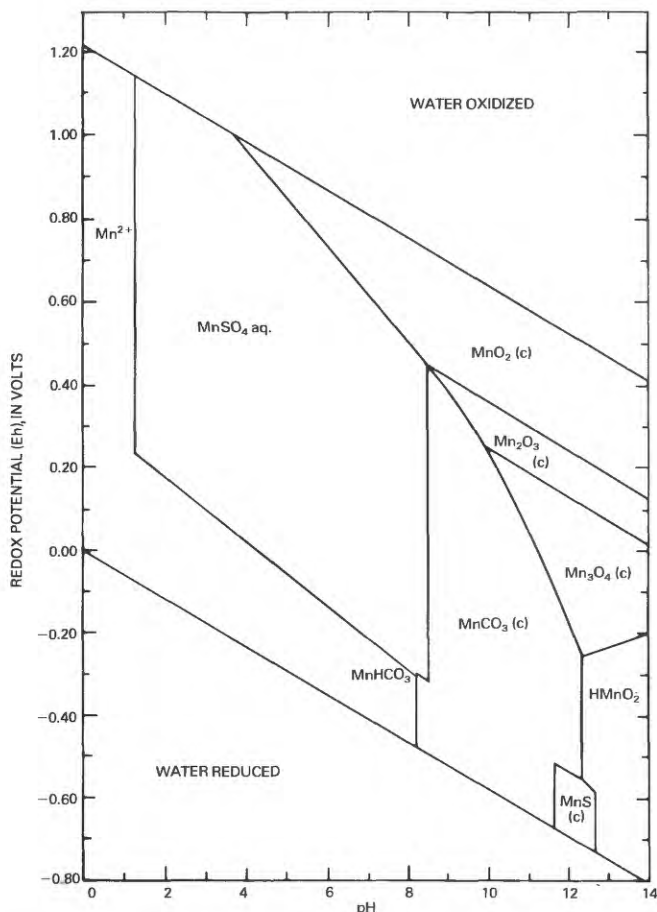


Figure 11. Fields of stability of solids as a function of pH and Eh at 25 °C and 1 atm in system Mn-S-CO₂-H₂O. Total CO₂ species activity is 2,000 mg/L as HCO₃⁻, total sulfur species activity is 2,000 mg/L as SO₄²⁻ (Hem, 1972).

The incorporation of manganese in pyrite may have implications for the water chemistry at the time of sediment accumulation. Manganese sulfide (MnS-alabandite) forms only under very restricted conditions. In order to precipitate MnS, the aqueous sulfide to carbonate activity ratio must be $\geq 10^{-5}$ (compare ratios of 10^{-15} for precipitation of PbS, ZnS, FeS₂, and CuS; Boden, 1957). The presence of abundant carbonate minerals in the Green River Formation implies that the carbonate activity ratio was high; thus, the formation of MnS would require exceptionally high sulfide activities. Because we cannot estimate the activity of either aqueous sulfide or carbonate with any accuracy, it is not easy to improve on the Eh-pH diagram shown in figure 11, reproduced from Hem (1972). The stability field of MnS moves to lower values of pH and higher values of Eh as sulfur activity increases (Garrels and Christ, 1965).

Two alternative hypotheses can be put forward for the change, or apparent change, in mode of occurrence of Mn, Co, Cd, and Zn with depth in the core. First, a reduction in aqueous sulfide activity, pH, or alkalinity would favor the stability of these four elements in carbonate phases relative to sulfide phases. Alternatively, small pyrite grains may have been removed by leaching from higher parts of the section—that is, they were not preserved—and the change in mode of occurrence is only apparent. In support of the former is the change in major mineralogy of the deeper samples, notably the presence of the mineral dawsonite [NaAl(CO₃)(OH)₂], the formation of which presumably requires high alumina solubilities that are present under alkaline conditions. In support of the latter is the presence of the well-documented “leached zone” (406–720 m depth, fig. 3). It is difficult, however, to envisage the selective removal of tiny pyrite crystals (<1–5 μm) from such a low-porosity formation, and presumably any leaching of the pyrite must have occurred during sediment dewatering and compaction. We believe that a change in lake-water and possibly porewater chemistry is the best interpretation for our data: small pyrite crystals formed in much smaller quantities in samples above 607 m, and Mn, Co, Cd, and Zn have a different mode of occurrence in this part of the formation.

An important generalization can be made from our analysis of trace-element data: the Green River Formation is not a homogeneous, uniform mineral assemblage. Rather, changes in trace-element mode of occurrence indicate that chemically significant variations exist on a large scale within the formation. Furthermore, the observation that, depending on its paragenesis, one mineral (pyrite) may have various trace-element contents is indicative of a grain-to-grain-scale heterogeneity that reflects a complex diagenetic history for the oil shale. The homogeneity noted by many workers is in part related to averaging whole-rock analyses over significant intervals, a process that masks information that can be obtained by more detailed study.

Zn, Co, and Cd are all enriched in the pyrites from the lower part of the core.

Sweeney and Kaplan (1973) showed experimentally that one mechanism for the formation of pyrite from aqueous solution involves addition of sulfur to the precursor mackinawite (FeS_{0.9}) to produce greigite (Fe₃S₄) or pyrrhotite (Fe_{1-x}S). Further addition of sulfur results in pyrite formation. The morphologic types typical of greigite (spherules 1–5 μm) and of pyrrhotite (hexagonal plates), which we also observed in the West Willow no. 3 core, were observed by Sweeney and Kaplan (1973) to be retained by the pyrite except when it formed at high temperature (>170 °C) when the spherules formed euhedral crystals. We propose that Mn, Zn, Cd, and Co were incorporated into the greigite and pyrrhotite precursors and retained during subsequent pyrite formation.

Pyrite that formed later, during diagenesis, has a different trace-element chemistry. This pyrite, precipitated directly from pore water, contains As, Pb, and Cu that may have been remobilized from organic material and clays.

CONCLUSIONS

Pyrites extracted from oil shales of the Green River Formation were analyzed by atomic absorption spectrophotometry for the elements As, Cd, Co, Cu, Mn, Mo, Ni, Pb, and Zn. Two distinct types of pyrite were identified on the basis of electron microprobe analysis. Manganese-rich, finely disseminated pyrite formed during sediment deposition (stage 1 of Dyni's (1983) classification), and manganese-free pyrite containing As, Pb, and Cu and showing a variety of replacement textures formed during and after diagenesis (stages 2 and 3 of Dyni's (1983) classification).

A stratigraphic variation in the mode of occurrence of Mn, Zn, and Cd was observed. Below about 610 m in the West Willow no. 3 core, these three elements are sulfide hosted. Above this depth, carbonate minerals are probably the host mineral for the trace elements. This change is related to evolution of the alkalinity and salinity of the sedimentary environment that favored the stability of manganese, zinc, and cadmium carbonate minerals relative to sulfide minerals.

REFERENCES CITED

- Boden, P.B., Jr., 1957, Some limitations of the possible composition of the ore forming fluids: *Economic Geology*, p. 333-353.
- Boyer, D.L., and Cole, R.D., 1983. Variations in sulfur mineralization in the Parachute Creek Member of Green River Formation, Colorado and Utah, in *Sixteenth Oil Shale Symposium proceedings*: Golden, Colorado School of Mines, p. 160-175.
- Burns, R.G., 1976, The uptake of cobalt into ferromanganese nodules, soils and synthetic manganese (IV) oxides: *Geochimica et Cosmochimica Acta*, v. 40, p. 95-102.
- Chao, T.T., and Sanzolone, R.F., 1977, Chemical dissolution of sulfide minerals: *U.S. Geological Survey Journal of Research*, p. 409-412.
- Cole, R.D., 1975, *Sedimentology and sulfur isotope geochemistry of Green River Formation (Eocene), Uinta Basin, Utah, Piceance Creek Basin, Colorado*: Salt Lake City, University of Utah, Ph.D. thesis, 276 p.
- Cook, E.W., 1973, Elemental abundances in Green River oil shale: *Chemical Geology*, v. 11, p. 321-324.
- Czamanske, G.K., and Ingamells, C.O., 1970, Selective chemical dissolution of sulfide minerals—A method of mineral separation: *American Mineralogist*, v. 55, p. 2131-2134.
- Desborough, G.A., Pitman, J.K., and Huffman, C., Jr., 1976, Concentration and mineralogical residence of elements in rich oil shales of the Green River Formation, Piceance Creek Basin, Colorado, and the Uinta Basin, Utah—A preliminary report: *Chemical Geology*, v. 17, p. 13-26.
- Dolezal, J., Povondra, P., and Sulcek, Z., 1968, Decomposition techniques in inorganic analysis: London, Iliffe, p. 224.
- Dyni, J.R., 1983, Distribution and origin of sulfur in Colorado oil shale, in *Sixteenth Oil Shale Symposium proceedings*: Golden, Colorado School of Mines, p. 144-159.
- Fleischer, M., 1955, Minor elements in some sulfide minerals: *Economic Geology 50th Anniversary Volume*, p. 970-1024.
- Fox, J.P., 1979, Water quality effects of leachates from an in-situ oil shale industry: Lawrence Berkeley Laboratory, Report LBL-9987, Berkeley, California.
- Garrels, R.M., and Christ, C. L., 1965, *Solutions, minerals, and equilibria*: San Francisco, Freeman, Cooper & Company, 450 p.
- Giauque, R.D., Fox, J.D., and Smith, J.W., 1981, Characterization of two core holes from the Naval Oil Shale Reserve Number 1: U.S. Department Energy Report PB81-167736, 176 p.
- Harrison, W.J., 1990, Modelling fluid-rock interactions in sedimentary basins, in Cross, T.A., ed., *Quantitative dynamic stratigraphy*: New Jersey, Prentice-Hall, p. 195-231.
- Hawley J.E., and Nichol, I., 1961, Trace elements in pyrite, pyrrhotite and chalcopyrite of different ores: *Economic Geology*, v. 56, pp. 467-487.
- Hem, J.D., 1972, Graphical methods for representing form and stability of aqueous metal ions: *Chemical Geology*, v. 9, p. 119-132.
- Hubert, A.E., and Lakin, H.B., 1973, Atomic absorption determination of thallium and indium in geological materials, in *Geochemical Exploration 1972: International Geochemistry Symposium, 4th, London, 1972, Proceedings*, p. 383-387.
- Jackson, L.P., and Jackson, K.F., 1982, The co-disposal of retorted shale and process waters—Effect on shale leachate composition, in *Fifteenth Oil Shale Symposium proceedings*: Golden, Colorado School of Mines, p. 505-515.
- Klieve, J.R., Rawlings, G.D., and Hoeflein, J.R., 1981, Assessment of oil shale retort waste water treatment and control technology: Monsanto Research Corporation, National Technical Information Service, PB 81-187288.
- Lindahl, P.C., 1981, Modification to the graded neutral density filter used in the deuterium arc background corrector: *Atomic Spectroscopy*, v. 2, p. 134.
- Lord, C.J., and Church, T.M., 1983, The geochemistry of salt marshes—Sedimentary ion diffusion, sulfate reduction, and pyritization: *Geochimica et Cosmochimica Acta*, v. 47, p. 1381-1393.
- Lynch, J.J., 1971, The determination of copper, nickel, and cobalt in rocks by atomic absorption spectrometry using cold leach, in Boyle, R.W., and McGerrigle, J.I., eds., *Geochemical exploration: Canadian Institute of Mining and Metallurgy Special Volume*, v. 11, p. 313-314.
- Margheim, G.A., 1975, *Water pollution from spent oil shale: Fort Collins, Colorado State University*, Ph.D. thesis.
- McWhorter, D.B., 1980, Reconnaissance study of leachate quality from raw mined oil shale-laboratory columns: Monsanto Research Corporation, National Technical Information Service, PB 81-129017.
- Meddaugh, W.S., and Salotti, C.A., 1983, Mineralogy and geochemistry of Green River Formation oil shales, C-A tract, Colorado, in *Sixteenth Oil Shale Symposium proceedings*: Golden, Colorado School of Mines, p. 113-123.
- Milton, C., 1977, Mineralogy of the Green River Formation: *Mineralogical Record*, October 1977, p. 368-379.

- Pabst, A., 1971, Pyrite of unusual habit simulating twinning from the Green River Formation of Wyoming: *American Mineralogist*, v. 56, 133–145.
- Peterson, E.J., and Wagner, P., 1982, Some chemical and mineralogical considerations important for understanding leachate chemistry, in *Fifteenth Oil Shale Symposium proceedings*: Golden, Colorado School of Mines, p. 516–528.
- Rickard, D.T., 1975, Kinetics and mechanism of pyrite formation at low temperatures: *American Journal of Science*, v. 275, p. 636–652.
- Roberts, F.I., 1982, Trace element chemistry of pyrite—A useful guide to the occurrence of sulfide base metal mineralization: *Journal Geochemistry Exploration*, v. 17, p. 49–62.
- Rubeska, I., 1968, The determination of trace elements in sulfide minerals by atomic absorption spectrophotometry with absorption tubes: *Analytica Chimica Acta*, v. 40, p. 187–194.
- Saether, O.M., Runnells, D.D., Rinstiner, R.A., and Smythe, W.R., 1981, Fluorine—Its mineralogical residence in the oil shale of the Mahogany Zone of the Green River Formation, Piceance Creek Basin, Colorado, USA: *Chemical Geology*, v. 31, p. 169–184.
- Shapiro, L., 1975, Rapid analysis of silicate, carbonate and phosphate rocks (revised ed.): U.S. Geological Survey Bulletin 1401, p. 43–46.
- Smirnova, N.P., Nesterenko, G.V., and Almukamedov, A.E., 1968, The mode of occurrence of nickel and cobalt in mafic rocks: *Geochemistry International*, v. 5, p. 363–372.
- Springer, G., Schachner-Korn, D., and Long, J.V.P., 1964, Metastable solid solution reactions in the system FeS_2 - CoS_2 - NiS_2 : *Economic Geology*, v. 59, p. 475–491.
- Stanton, R.E., 1966, Rapid methods of trace analysis for geochemical applications: London, Edward Arnold, p. 96.
- Stollenwerk, K.C., and Runnells, D.O., 1977, Leachability of arsenic, selenium, molybdenum, boron and fluorine from retorted oil shale. Pacific Chemistry Engineer Congress, 2nd, Denver, 1977, Proceedings, p. 1023–1030.
- 1981, Composition of leachate from surface retorted and unretorted Colorado oil shale: *Environment Science Technology*, v. 15, p. 1340–1346.
- Sweeney, R.E., and Kaplan, I.R., 1973, Pyrite framboid formation—Laboratory synthesis and marine sediments. *Economic Geology*, v. 68, p. 618–634.
- Teseneer, R.L., and Brown, H.S., 1979, Trace element content of pyrite in the North Carolina slate belt—Implications for exploration: Abstracts, Society Mineral Engineering of American Institute of Mining Engineers, preprint 79–49, p. 7.
- Wedephol, K.H., 1969, Handbook of geochemistry 11–3: New York, Springer-Verlag, p. 25–D–16, 25–D–17.

APPENDIX 1—PETROGRAPHIC DESCRIPTION OF SHALE SAMPLES IN WEST WILLIOW NO. 3 CORE

[Sample number indicates depth in core in meters. Core location shown in figure 1]

WW 377.3 Fine-grained (10–15 μm) dolomite; pronounced organic-rich/organic-poor layering; organic material golden and amorphous; scattered larger clasts of organic-poor dolomite; abundant disseminated euhedral crystals of pyrite.

WW 367.8 Very fine grained (<5 μm) dolomite. Scattered detrital quartz (<50 μm) and untwinned feldspar grains; brown biotite and a colorless micaceous mineral; fragments of coaly material and pale-golden amorphous organic material. Pyrite blebs, made up of small euhedral crystals clumped together, are distributed irregularly through sample.

WW 415.7 Tuffaceous fragments (quartz and albitic feldspar) in fine-grained (<5 μm) dolomite. Abundant grains of quartz and feldspar (≤ 50 μm); golden amorphous organic material concentrated in some layers; thin brown “stringers”; small disseminated euhedral pyrite crystals; abundant larger pyrite (as large as 100 μm) associated with tuffaceous fragments.

WW 470.1 Fine-grained (<5 μm) dolomite containing detrital quartz and feldspar grains (≤ 50 μm) and very little organic material. Pale-yellow coloration caused by cryptocrystalline phosphate (apatite). Bladed salt crystals pseudomorphed by dolomite, calcite, and pyrite; pyrite in irregular blebs.

WW 554.8 Fine-grained dawsonite-bearing oil shale; dawsonite partly replaced by calcite and dolomite, but numerous leached areas remain. Micaceous minerals abundant golden amorphous organic material distributed in distinct layers; pyrite as small blebs and scattered crystals and as fracture filling.

WW 557.7 No thin section available.

WW 608.6 Fine-grained (<5 μm) dolomitic oil shale containing abundant partly leached dawsonite crystals (≤ 100 μm). Quartz, feldspar, and a micaceous mineral; uniform yellow amorphous organic material and rare stringers and brown blobs; small scattered crystals of pyrite (<10 μm), no larger blebs or clumps of crystals.

WW 612.5 Fine-grained dolomitic oil shale containing abundant large (≤ 50 μm) dawsonite crystals and quartz grains. Golden amorphous organic material prominently layered; abundant finely disseminated pyrite grains and rare larger blebs.

WW 682.1 Fine-grained dolomitic oil shale (<5 μm) containing large feldspar grains (≤ 50 μm). Small dawsonite crystals concentrated in layers several millimeters thick; distinct layering of golden amorphous material; pyrite finely disseminated throughout, locally higher concentrations in more organic-rich layers; disseminated pyrite crystals (<10 μm diameter).

WW 682.4 No thin section available.

APPENDIX 2—ANALYTICAL METHODS

Separation of Pyrite Samples from Shale

Pyrite was extracted from powdered samples by a series of acid dissolutions and density separations. To dissolve the carbonate fraction, a 30–50-g sample was heated in HCl until no reaction occurred on the addition of more acid (3–4 hrs). The residue was separated from the HCl by centrifugation. Next, the silicate minerals were dissolved by treating the residue with HF, and the sample was left overnight in HF. It was water washed and dried at 50 °C. The hardened residue (kerogen) was removed by two successive sink/float separations in 75 percent bromoform and a third in 100 percent bromoform. The sink fraction, primarily pyrite, was washed in acetone and then water and finally fired at 50 °C. A few tenths of a gram of sulfides was generally obtained. Because a significant amount of pyrite encapsulated in kerogen was lost in the float fraction, the resulting pyrite separates do not represent the total pyrite content of the sample.

Preparation of Pyrite Samples for Analysis

Several chemical reagents have been used for dissolution of sulfide minerals, including aqua regia (Stanton, 1966), nitric and tartaric acids (Rubeska, 1968), hydrogen peroxide–ascorbic acid (Smirnova and others, 1968; Lynch, 1971), water-bromine (Czamanske and Ingamells, 1970), a solution of bromine in carbon tetrachloride and nitric acid (Hubert and Lakin, 1973), and potassium chlorate–hydrochloric acid (Dolezal and others, 1968). Recently, Chao and Sanzolone (1977) evaluated the effectiveness of these chemical treatments. They reported that dissolution of pyrite using either 4*N* nitric acid or potassium chlorate–hydrochloric acid followed by 4*N* nitric acid was very effective (86–100 percent dissolution by sulfur determination).

Because the pure pyrite-mineral separates are extremely precious, one sample dissolution procedure had to suffice for the 11 elements to be determined. The nitric acid dissolution procedure was selected because it provides a relatively uncomplicated sample solution matrix that can be used in both flame and flameless AA analysis.

The pyrite mineral separates, about 0.1 g, two additional pyrite samples (a South Dakota pyrite and RICO pyrite (Ward Scientific)), and an ASK Reference Material (sulfide ore, ASK-3) were prepared for spectrochemical analysis by treatment with 10 mL of 4*N* nitric acid in a 50-mL Teflon beaker. This mixture was heated to boiling for 15 min on a hot plate. After cooling to ambient, the sample was diluted to volume, 50 mL, in linear polyethylene volumetric flasks. The sample solution was stored in a linear polyethylene bottle.

Table A1. Atomic absorption spectrophotometry instrument parameters for pyrite analyses

Element	Wavelength (nm)	Slit (nm)	Source	Atomizer ¹	Background correction
Arsenic	193.7	0.7	EDL/11W	HGA	Yes
Cadmium	228.8	0.7	HCL/8ma	HGA	Yes
Cobalt	240.7	0.2	HCL/30ma	Flame/Air-C ₂ H ₂	Yes
Copper	324.8	0.7	HCL/15ma	Flame/Air-C ₂ H ₂	No
Iron	248.8	0.2	HCL/30ma	Flame/Air-C ₂ H ₂	No
Manganese	279.5	0.2	HCL/25ma	Flame/Air-C ₂ H ₂	No
Molybdenum	313.3	0.7	HCL/29ma	HGA	Yes
Nickel	231.1	0.2	HCL/25ma	Flame/Air-C ₂ H ₂	Yes
Lead	283.3	0.7	EDL/10W	Flame/Air-C ₂ H ₂	Yes
Selenium	196.0	0.7	EDL/10W	HGA	Yes
Zinc	213.9	0.7	HCL/15ma	Flame/Air-C ₂ H ₂	Yes

¹For HGA parameters see table A2.

Table A2. Atomic absorption spectrophotometry HGA parameters for pyrite analyses

Element	Temperature (°C)			Sample volume (μL)	Gas ¹ flow (mL/min)	Graphite tube
	Dry	Char	Atomize			
Arsenic	100	1,000	2,700	15	40	Standard
Cadmium	100	250	2,100	10	40	Standard
Molybdenum	100	1,000	2,800	20	40	Pyro
Selenium	100	800	2,700	50	40	Standard

¹Argon.

Analytical Methods for Pyrite Analyses

Atomic absorption spectrophotometry (AA) is a commonly used instrumental method for the quantitative determination of inorganic elements in geological samples. In addition, the capabilities of AA such as high sensitivity, low detection limits, and flame and flameless capacity make it an ideal instrumental technique for trace-element determinations. Rubeska (1968) used AA to determine selected trace elements in various sulfide samples including pyrites. Teseneer and Brown (1979) used AA to determine Co, Au, Hg, and Ni in pyrites from the North Carolina Slate belt.

Flame AA measurements were performed using a Perkin-Elmer Model 5000 atomic absorption spectrophotometer equipped with a data station printer. Flameless AA measurements were performed using a Perkin-Elmer Model 703 atomic absorption spectrophotometer equipped with a Model 400 HGA with AS-40 autosampler, PRS-10 printer, 056 recorder, and D₂ arc background corrector. The D₂ arc background corrector was modified as described by Lindahl (1981). Instrument parameters for the AA analyses of these pyrite samples are given in table A1. Supplemental information for those elements determined by flameless AA (HGA) is given in table A2. No matrix modification was needed.

Results for the determinations of iron and the trace elements in the ASK Reference Material sulfide ore, ASK-3, are reported in table A3 along with results for duplicate samples of a South Dakota cluster pyrite and RICO pyrite. Instrument precision for both flame and flameless measurements was better than 2 percent relative, and method precision for duplicate samples, including sampling, sample homogeneity, sample preparation, and instrumental imprecisions, is from better than 1 percent relative to 18 percent. Typically, the agreement between duplicate sample analyses for these trace elements is 5–13 percent. The method precision for each element, based on duplicate analyses of the three samples, is Fe (0–2 percent), As (3–5 percent), Cd (0–13 percent), Co (0–6 percent), Cu (0–12 percent), Mn (0–18 percent), Mo (5 percent), Ni (0–11 percent), Pb (5 percent), and Zn (0–7 percent). The accuracy of the data was determined by comparing our results with the recommended results for the ASK Reference Material ASK-3. The bias and accuracy, expressed at percent relative error, for the elements determined is Fe (–10 percent), As (+5 percent), Cd (–3 percent), Co (–2 percent), Cu (–16 percent), Mn (–7 percent), Mo (–3 percent), Ni (–32 percent), Pb (–22 percent), and Zn (–8 percent). Values for bias and accuracy could not be determined for selenium. Values determined

for most of the trace elements in ASK-3 including As, Cd, Co, Mn, and Mo are in excellent agreement with accepted values (± 10 percent); Cu and Ni are notable exceptions. Fe, Pb, and Zn, major components in ASK-3, all show negative bias; accuracies for Fe and Zn are about 10 percent and for Pb 22 percent. The overall good agreement between our data for ASK-3 and accepted values indicates that dissolution of samples with dilute HNO₃ is a satisfactory procedure for the preparation of pyrite samples for the determination of trace elements by flame and flameless AA.

Rock Sample Analysis

All trace elements determined in pyrite separates were also determined in associated whole-rock samples for mass-balance calculations (table 5). Each rock sample was fused with a 2:1 mixture of lithium tetraborate (Li₂B₄O₇):lithium metaborate (LiBO₂) by the method of Shapiro (1975). In this procedure, 0.2000 g of sample is mixed with 1.2 g of flux mixture. The resulting mixture is fused in a new graphite crucible in a muffle furnace at 1,000 °C for 1 hour. The melt is cooled, and the fusion bead is dislodged from the crucible and transferred to hot (near boiling) 10 percent nitric acid and dissolved by stirring. The cooled solution is diluted to 250 mL and then analyzed by either inductively coupled plasma emission spectroscopy (ICP) or atomic absorption spectrophotometry (AA).

Co, Cu, Mn, Mo, Ni, and Zn were determined by ICP. Operating parameters are given in tables A4 and A5. As, Cd, and Pb (instrument parameters in tables A6–A8) were determined by heated graphite atomizer–AA, and Se (instrument parameters in table A9) was determined (although undetected) by hydride generation–AA.

Table A3. Results for determinations of iron and trace elements in duplicate samples of ASK Reference Material (sulfide ore, ASK-3), pyrite standard (RICO), and South Dakota cluster pyrite (SD)
[EPR, concentration measured in this study; Lit., published concentration. Analytical reference materials are described in text. All values except Fe (weight percent) are in parts per million. Blank in column indicates no data available]

Sample	Fe		As		Cd		Co		Cu		Mn		Mo		Ni		Pb		Se		Zn	
	EPR	Lit	EPR	Lit	EPR	Lit	EPR	Lit	EPR	Lit	EPR	Lit	EPR	Lit	EPR	Lit	EPR	Lit	EPR	Lit	EPR	Lit
ASK-3	32.2	35.6	650	630	290	310	84	86	1,250	1,400	242	260	40	40	25	37	1.63	2.1	ND ¹	ND	8.58	9.20
ASK-3	32.1	35.6	670	630	290	310	84	86	1,110	1,400	241	260	38	40	25	37	ND ²	2.1	ND	ND	8.45	9.20
RICO	42.3	46.6 ³	<10		0.16		10		14	125	18		ND		17		76		ND	ND	14	
RICO	42.3	46.6	<10		0.14		10		14	111	15		ND		19		80		ND	ND	15	
SD	35.3		3,140		6.3		16		961		64		ND		14		5,440		ND	ND	961	
SD	35.8		3,310		6.3		15		948		61		ND		14		ND		ND	ND	948	

¹Not detected <20 ppm.

²Not determined.

³Theoretical percent Fe based on FeS₂.

Table A4. Inductively coupled plasma emission spectrometer operating parameters

Instrument	Jarrell-Ash Model 1155V vacuum spectrometer
Nebulizer	MAK (Herritt-Gordon Mines Ltd., Ft. Saskatchewan, Alberta, Canada T8L 2P2)
Sample uptake rate.....	1.9 mL/min
Argon flow rates	
Sample	52 L/min
Coolant	14.5 L/min
Plasma	0.2 L/min
Forward power.....	1.05 kW
Reflected power.....	<5 W
Plasma viewing height.....	16 mm above top of load coil
Exposure time.....	10 sec

Table A5. Wavelengths, detection limits, and maximum concentrations of linear ranges for inductively coupled plasma emission spectrometry analyses

Element	Wavelength (Å)	Limit (mg/L)	Concentration (mg/L)
Cobalt	2286.156	0.05	1,000
Copper	3247.540	.05	500
Manganese	2576.104	.005	500
Molybdenum	2020.300	.01	100
Nickel	2316.037	.05	100
Zinc	2138.560	.01	500

Table A6. Atomic absorption spectrophotometric analysis operating parameters for determination of arsenic

Spectrophotometer	Perkin-Elmer Model 4000 (PRS-10 printer, 056 recorder, and D2 arc background corrector)
Autosampler	Perkin-Elmer AS-40
Atomization source.....	Perkin-Elmer heated graphite atomizer with Model 400 programmer
Wavelength.....	193.7 nm
Detection limit.....	1 µg/L
Light source.....	EDL, 8 W, background corrected
Graphite tube	Standard
Sample aliquot.....	20 µL
Purge gas	Argon

	Programmer keyboard entries			
Step number	1	2	3	4
Temp (°C)	125	1,100	2,700	100
Ramp (s)	13	25	1	5
Hold (s)	30	30	5	0
Read				
Record			X	X
Gas flow (mL/min)	*	*	50	*

*Purge gas flow rate controlled by internal pressure regulator.

Table A7. Atomic absorption spectrophotometric analysis operating parameters for determination of cadmium

Spectrophotometer	Perkin-Elmer Model 4000 (PRS-10 printer, 056 recorder, and D2 arc background corrector)		
Autosampler	Perkin -Elmer Model AS 40		
Atomization source	Perkin-Elmer heated graphite atomizer with Model 400 programmer		
Wavelength.....	228.8 nm		
Detection limit	0.1 µg/L		
Light source.....	HCL, 8 ma, background corrected		
Graphite tube	Standard		
Sample aliquot.....	20 µL		
Purge gas	Argon		

Programmer keyboard entries

Step number	1	2	3	4
Temp (°C)	125	350	1,900	2,500
Ramp (s)	13	10	1	1
Hold (s)	30	60	5	5
Read			x	
Record			x	
Gas flow (mL/min)	*	*	50	*

*Purge gas flow rate controlled by internal pressure regulator.

Table A8. Atomic absorption spectrophotometric analysis operating parameters for determination of lead

Spectrophotometer	Perkin-Elmer Model 4000 (PRS-10 printer, 056 recorder, and D2 arc background corrector)		
Autosampler	Perkin-Elmer Model AS-40		
Atomization source	Perkin-Elmer heated graphite atomizer with Model 400 Programmer		
Wavelength.....	283.3		
Detection limit.....	1 µg/L		
Light source.....	EDL, 10 W, background corrected		
Graphite tube	Standard		
Sample aliquot.....	20 µL		
Purge gas	Argon		

Programmer keyboard entries

Step number	1	2	3	4
Temp (°C)	125	500	2,700	100
Ramp (s)	13	10	1	5
Hold (s)	30	60	5	0
Read			x	
Record			x	
Gas flow (mL/min)	*	*	50	*

*Purge gas flow rate controlled by internal pressure regulator.

Table A9. Atomic absorption spectrophotometric analysis operating parameters for determination of selenium

Spectrophotometer	Perkin-Elmer Model 5000 (PRS-10 printer, 056 recorder, and D2 arc background corrector)		
Hydride generator	Perkin-Elmer Model MHS-10		
Recorder	Perkin-Elmer Model MHS-10		
Wavelength.....	196.0 nm		
Detection limit.....	1 µg/L		
Light source.....	EDL, 6 W, not background corrected		
Sample aliquot.....	10 µL		
Flame.....	Air/acetylene (lean)		
Reductant.....	3 percent NaBH ₄ in 1 percent NaOH		

Chapter E

An Experimental Study of Goethite Sulfidization—Relationships to the Diagenesis of Iron and Sulfur

By MARK R. STANTON and MARTIN B. GOLDHABER

U.S. GEOLOGICAL SURVEY BULLETIN 1973

GEOCHEMICAL, BIOGEOCHEMICAL, AND SEDIMENTOLOGICAL STUDIES OF THE GREEN RIVER FORMATION, WYOMING, UTAH, AND COLORADO

CONTENTS

Abstract	E1
Introduction	E1
Methods	E2
Results and discussion	E5
Low pH (≤ 7.0) results	E5
Goethite	E5
X-ray diffraction	E5
Saturation state	E6
Pyrite formation rates	E6
Pyrite morphology and texture	E6
Development of pyrite morphology	E7
Spheres produced at low H_2S concentrations	E10
Sphere diameters	E10
High pH results	E11
Relationships to iron and sulfur diagenesis	E12
Rates of pyrite formation	E14
Pyrite texture	E14
Other reaction products	E15
Absence of other sulfide reaction products	E15
Conclusions	E18
Summary	E18
References cited	E19

FIGURES

1. Diagram showing analytical method for determination of iron and sulfur products from reaction of goethite and H_2S E3
- 2–3. Graphs showing:
 2. Time versus concentration for iron and sulfur species E5
 3. FeS saturation curve E6
- 4–5. Scanning electron microscope photomicrographs illustrating:
 4. Solids formed at low pH E7
 5. Pyrites formed at low $H_2S_{(g)}$ concentration E12
6. Histogram of modal sphere diameters E13
7. Graph showing modal sphere diameter versus reaction time at two ionic strengths E13
8. Scanning electron microscope photomicrographs illustrating decrease in pyrite sphere size with increasing ionic strength E15
9. Graph showing modal sphere diameter versus ionic strength E18

TABLES

1. Initial reaction conditions, rates of pyrite formation, reaction products, and pyrite morphology E3
2. $Fe^{2+}:S^{2-}$ mole ratios for early formed samples showing composition of FeS solids E4
3. Modal sphere diameter and size range for pyrite spheres formed in experiments 7 and 12 E14

An Experimental Study of Goethite Sulfidization— Relationships to the Diagenesis of Iron and Sulfur

By Mark R. Stanton and Martin B. Goldhaber

Abstract

The geochemical characteristics of iron sulfide minerals have been used to examine iron and sulfur diagenesis of the Eocene Green River Formation. To better understand the origin of iron sulfide minerals, we experimentally studied formation of these minerals under conditions that may have existed during deposition of the Green River Formation. Our study determined the types of products generated during goethite sulfidization and the rates of pyrite formation when goethite was converted to pyrite.

Goethite (α -FeOOH) was reacted with aqueous hydrogen sulfide (H_2S) over a range of pH, ionic strength, and total iron and total sulfide concentrations. Pyrite (FeS_2), elemental sulfur (S^0), and iron monosulfide (FeS) were the dominant solid products formed at pH less than or equal to 7.0. Rough-textured spheres are the dominant morphology of pyrite; framboids and euhedral crystals of pyrite were not produced. At pH greater than 7.0, elemental sulfur and FeS formed, but pyrite was not detected; unreacted goethite remained as a solid phase. Other sulfide minerals present in some Green River sedimentary rocks, such as pyrrhotite and marcasite, were not detected.

Authigenic pyrite formed rapidly under conditions of low pH (<5.0). At neutral pH, the rate of pyrite formation was slow compared to that of acidic pH. Pyrite was not detected in experiments at pH values greater than 9.0. Formation of pyrite in alkaline solution requires either extended time of reaction or reaction pathways that operate only in complex natural settings. The formation of euhedral and framboidal pyrite in unconsolidated sediments likely requires processes or conditions that were not observed in our experiments.

INTRODUCTION

Authigenic iron sulfide minerals are present in virtually all subaqueous sediments in which organic matter and sulfate are present (Goldhaber and Kaplan, 1974). They

form at low temperature (<50 °C) and pressure (1 atm), mainly through the action of aqueous hydrogen sulfide ($H_2S_{(aq)}$) produced by bacterial sulfate reduction. This $H_2S_{(aq)}$ reacts with iron-bearing minerals to produce iron "monosulfides" such as mackinawite ($FeS_{0.9}$) or greigite (Fe_3S_4) (Berner, 1970). These iron monosulfide minerals (FeS) are converted to pyrite (FeS_2) by reaction with zerovalent sulfur (S^0): $FeS + S^0 \rightarrow FeS_2$. Pyrite may also directly precipitate from a ferrous polysulfide solution without the formation of an intermediate FeS precursor (Howarth, 1978); however, direct precipitation may be inhibited below 100 °C (Schoonen and Barnes, 1988). The kinetics and mechanisms of pyrite formation have been experimentally studied by many researchers; for example, Berner (1964a, 1969, 1970), Rickard (1969a, b), Roberts and others (1969), Hallberg (1972), Pyzik and Sommer (1981), Murowchick and Barnes (1987), and Schoonen and Barnes (1988). Nevertheless, the mechanistic details of FeS_2 formation are not clearly understood, and the origin of iron sulfide minerals probably varies from one geochemical environment to another. The "reactivity" of various iron sources toward sulfide has, until recently, received little attention (Berner, 1964a; Canfield and Berner, 1987; Canfield, 1989). The transitional role of iron monosulfides during their conversion to iron disulfides is also poorly understood (Berner, 1972; Sweeney and Kaplan, 1973; Rickard, 1975). In particular, insufficient experimental information is available concerning the overall sequence of reactions during iron sulfidization.

An aspect of our ongoing experimental studies of pyrite formation, applicable to the Eocene Green River Formation, is to identify the nature of iron sulfidization in environments such as alkaline saline lakes. Sediments in these lakes contain sulfate, $H_2S_{(aq)}$, and iron, yet only minor amounts of authigenic FeS and FeS_2 are produced (Tuttle, 1988). The paucity of sulfide minerals may reflect a lack of

reactive iron sources (Canfield, 1989) or kinetic hindrance due to high pH (Berner, 1964a, 1969). Because the factors governing the formation of iron sulfide minerals in environments of this type are not well documented, a companion purpose of this study was to examine goethite sulfidization and iron sulfide formation at high pH (7–10).

Textural and morphological variations of pyrite may be indicative of distinct pathways of pyrite formation in unconsolidated sediments, but the geochemical controls on these differences are not well known (Raiswell, 1982). The two most commonly observed pyrite textures in sediments are well-developed single euhedral crystals (mainly cubes) and framboids or polyframboids (Sweeney and Kaplan, 1973; Kribek, 1975; Raiswell, 1982). Framboids are aggregates of euhedral crystallites and are from 1 to more than 100 μm in diameter (Kribek, 1975); aggregates of several framboids result in the “polyframboidal” texture described by Love and Amstutz (1966). Euhedral pyrite may result from direct precipitation of pyrite or conversion of an FeS precursor phase. Framboidal pyrite textures, on the other hand, are believed to be produced only from the conversion of an FeS precursor (Raiswell, 1982). This report examines pathways and products qualitatively; a detailed chemical and kinetic treatment of all experimental parameters is in progress.

Acknowledgments.—This work was part of the U.S. Geological Survey Evolution of Sedimentary Basins Program. We extend our appreciation to N. Fishman, J. Fitzpatrick, and G. Breit for critical review of this manuscript.

METHODS

Synthetic $\alpha\text{-FeOOH}$ was prepared by the method of Atkinson and others (1968), which employs the alkaline hydrolysis of $\text{Fe}(\text{NO}_3)_3 \cdot \text{H}_2\text{O}$ in KOH to form the iron oxyhydroxide precipitate. After aging at 90–100 $^\circ\text{C}$ for 10 hours, the precipitate was rinsed with distilled water until dissolved nitrate was less than 1 ppm, and then it was stored under N_2 until needed. Flame atomic absorption spectrophotometry analysis (AA) for dissolved iron from a 0.05- μm filtration of this rinsed suspension was below the detection limit of 3.5 $\mu\text{M/L}$ Fe. X-ray powder diffraction (XRD) of the iron oxyhydroxide detected only $\alpha\text{-FeOOH}$. Scanning electron microscope (SEM) observations of the $\alpha\text{-FeOOH}$ solids revealed that the solids are acicular blades approximately 1 μm long and 0.2 μm wide.

Two types of experiments were performed during this study. The first type consisted of “free-drift” inorganic reactions in which the pH was allowed to change as the experiment proceeded. In the free-drift reactions, the initial pH ($\text{pH}_{(\text{init})}$) was less than 5.0 (table 1). The pH change did not exceed ± 1.3 and generally remained within ± 0.8 units of the initial pH. The second type of experiment consisted of inorganic reactions that were maintained at constant pH

(± 0.2) by means of a pH-stat. In this second group, the pH ranged from 5.6 to 10.0 (table 1).

The experimental conditions are representative of natural environments such as estuaries or saline lakes that have ionic strengths between 0.01 M (freshwater) and 0.7 M (seawater) (Garrels and Christ, 1965). The ionic strength (I) was 0.1 M in all but five experiments; in those, ionic strengths were from 0.3 to 2.0 M (table 1). The amount of total added iron (1.3×10^{-3} – 5.7×10^{-3} M/L) was two to three orders of magnitude greater than total particulate iron in oxidizing waters (Kester and others, 1975) or dissolved iron in porewater of reducing sediments (Morse and others, 1987). Values for total dissolved sulfide in sedimentary environments vary but are generally less than 5.0×10^{-3} M/L (Pyzik, 1976). Calculated total dissolved sulfide used in these experiments, the sum of $\text{H}_2\text{S}_{(\text{aq})}$, $\text{HS}^-_{(\text{aq})}$, and S^{2-} , was from 8.3×10^{-5} to 8.3×10^{-3} M/L.

All reagents and solutions were prepared from reagent-grade chemicals and CO_2 -free, O_2 -free distilled water. Experiments were carried out in a gas-tight, 1.5-L glass reaction vessel. After deoxygenation of the reaction water with ultra high purity N_2 , KCl was added to adjust the ionic strength. N_2 was then flowed through for an additional 8–16 hours. A mixture of H_2S and N_2 gas was then bubbled through the mixture for the duration of the experiment. The pressure and composition of the H_2S - N_2 gas mixture were precisely maintained through the use of a mass flow controller system (MKS Instruments). The goethite suspension was rapidly stirred and deoxygenated with N_2 for a minimum of 24 hours, then added to the reaction vessel after stabilization of the H_2S flow and solution pH. The addition of goethite to the solution was taken as the starting point for the reaction (time=0). For the constant-pH experiments, pH was maintained at a set value by the addition of HCl or KOH (depending upon the initial experimental conditions) using a pH-stat. Stirring rates were kept high in all experiments to minimize surface-controlled reactions.

Analyses for the various forms of iron and sulfur were performed as shown in figure 1 and described next. This series of chemical extractions and gravimetric techniques was based on the fact that iron monosulfides are soluble in 6N HCl, whereas pyrite is insoluble in this acid (Berner, 1964a). The pH of each sample was measured using a double junction reference/AgCl glass electrode pair. Generally, one sample per day was taken from the bulk mixture over a 1–2 week period. Samples were withdrawn into a N_2 -purged 50-mL syringe that formed a gas-tight seal with the sampling port. The gas flow and stirring were not interrupted for the sampling process. Sample treatment was carried out in a glove box that was continuously purged with nitrogen.

The concentration of AVS, acid-volatile sulfides (FeS), was determined by filtering a raw sample through a 0.05- μm membrane filter and washing excess sulfide from

Table 1. Initial reaction conditions, rates of pyrite formation, reaction products, and pyrite morphology

Expt. no. ¹	pH(init)	H ₂ S(g) (vol. percent)	Ionic strength (M)	Fe(tot) (mM)	Rate FeS ₂ formation (M/min) ²	Initial solids ³	Final solids ³	FeS ₂ morphology ⁴	Sphere sizes ⁵
5(F)	4.62	10	0.1	4.75	1.8×10 ⁻⁷	M,S	P,S	Sph	nd
6(F)	4.11	10	0.1	4.75	5.0×10 ⁻⁷	M,S	P,S	Sph	4.7
7(F)	4.62	10	0.1	4.75	6.0×10 ⁻⁷	M,S	P,S	Sph	4.4
8(F)	4.75	10	0.1	2.55	1.2×10 ⁻⁸	M,S	P,S	Sph	3.2
9(F)	4.91	10	0.1	1.32	2.2×10 ⁻⁷	M,S	P,S	Sph	nd
10(F)	4.45	10	0.3	2.55	6.6×10 ⁻⁸	M,S	P,S	Sph	1.9
11(F)	4.99	10	0.7	2.55	6.0×10 ⁻⁸	M,S	P,S	Sph	0.7
12(F)	4.69	10	2.0	2.55	1.0×10 ⁻⁸	M,S	P,S	Sph	0.5
13(F)	4.42	10	0.3	2.55	6.1×10 ⁻⁸	M,S	P,S	Sph	2.1
15(S)	6.01	0.1	0.1	2.55	4.4×10 ⁻⁸	M,G	P,G,M	Sph	1.5
16(S)	7.10	0.1	0.1	2.55	dnf	M,G,S	G,M	na	na
18(S)	9.50	10	0.3	4.33	dnf	M,G,GR	S,G,GR,M	na	na
19(S)	7.00	1.0	0.1	3.27	2.6×10 ⁻⁹	M,G,S	P,S,M	Sph	nd
28(F)	4.92	1.0	0.1	3.27	2.3×10 ⁻⁸	M,G,S	P,M	Sph	1.4
29(F)	4.61	0.1	0.1	3.27	3.2×10 ⁻⁸	M,G,S	P,S,M	Sph	1.3
30(F)	4.59	0.1	0.1	1.70	1.3×10 ⁻⁸	M,G,S	P,S,G,M	Sph	1.8
31(S)	5.69	0.1	0.1	5.70	dnf	M,G,S	G,S,M	na	na
32(S)	9.00	10	0.1	1.70	dnf	M,G,S,GR	S,M	na	na
33(S)	10.0	1.0	0.1	1.70	dnf	M,G,S,GR	S,GR,M	na	na

¹Free-drift (pH unconstrained);S, constant pH (±0.2 units).

²Overall rate of amount formed from when pyrite was first detected to end of experiment. Rate values are subject to experimental error of ±20 percent. dnf, did not form.

³M, mackinawite or FeS(am); S, elemental sulfur; G, goethite; P, pyrite; GR, green rust. Initial products are those present in first sample; final products are those present in last sample. No quantities are given because amount and type of product depend on time of sampling of reaction mixture, which differed for each experiment. Generally, initial products were present within first 24 hours.

⁴Sph, spherical; na, not applicable.

⁵Sphere size given is modal diameter (um) of final sample. na, not applicable; nd, not determined.

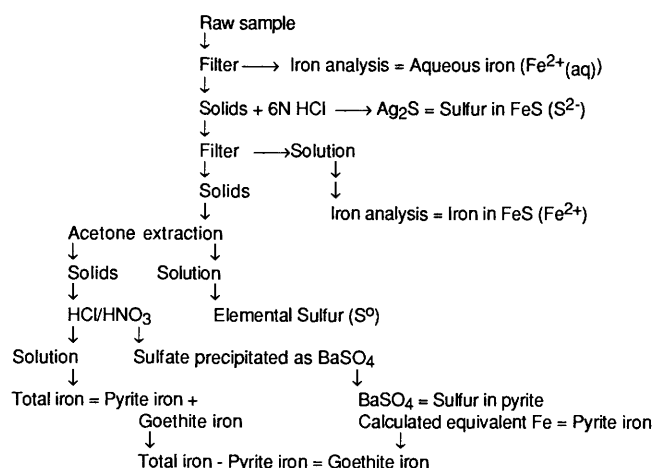


Figure 1. Analytical method for determination of iron and sulfur products from reaction of goethite and H₂S.

the solids using deoxygenated distilled water (fig. 1). Next, H₂S(g) evolved from a 25 °C, 6N HCl leach of the solids was precipitated as Ag₂S. This Ag₂S was filtered, dried, and weighed to obtain the total sulfide present in the iron monosulfide. The iron content of this 6N HCl filtrate was determined using AA and represents iron in the monosulfide. The concentration of aqueous iron in the original filtrate, Fe²⁺_(aq), also was determined using AA and is iron released into solution during the Fe(III) reduction–goethite dissolution steps (Pyzik and Sommer, 1981). The accuracy of the AA method for all iron analyses is ±10 percent. The crystalline goethite was only slowly soluble in 6N HCl and was not dissolved in the short time necessary for this sample treatment step (<10 minutes). (Fe²⁺,Fe³⁺)-oxyhydroxides formed at high pH were also removed in this step.

Total elemental (zerovalent) sulfur (S⁰) was determined by cyanolysis in acetone (Bartlett and Skoog, 1954). An aliquot of the dried, 6N HCl-treated solids was

refluxed in acetone to extract the solid S⁰. The solution was separated by filtration, then NaCN and FeCl₃ were added to form the (Fe³⁺SCN)²⁺ complex. The concentration of (Fe³⁺SCN)²⁺ was determined spectrophotometrically at 465 nm. Based on iron sulfide mineral mixtures (FeS+FeS₂) spiked with known amounts of elemental sulfur, this method was effective in extracting 95 percent of the solid S⁰ from the products. Sulfur was not extracted from the iron sulfide phases.

The sulfur extracted in this step represents total zerovalent sulfur of unspecified chain length or structure. This sulfur formed by the redox reaction of Fe(III) and sulfide (2Fe³⁺+H₂S_(aq) (or HS⁻_(aq))→S⁰+2Fe²⁺+2H⁺). Sulfur species such as S₈, the stable form of elemental sulfur at room temperature, may subsequently form from this zerovalent sulfur. Solid dipyramidal crystals of sulfur seen in microscopic examination are S₈ and contain all zerovalent sulfur atoms. The distribution of S⁰-bearing species in the reactant solution was not determined.

The amounts of pyrite and goethite were estimated by oxidation in aqua regia of the solids that remained after extraction of S⁰. Previous extractions had removed all but pyrite and goethite. FeS and (Fe²⁺,Fe³⁺)-oxyhydroxides present in high pH samples were removed in the 6N HCl step.

Aqua regia oxidized the sulfide sulfur in pyrite to sulfate (SO₄²⁻), which was then precipitated as BaSO₄. The BaSO₄ solids were separated by filtration, dried, and weighed. Iron originally in pyrite was calculated as the difference between sulfur in barite and iron in the filtrate. Residual iron is attributed to goethite (fig. 1).

X-ray diffraction was used after each chemical treatment for qualitative mineral identification and to determine the effectiveness of each successive extraction. A Philips XRG-3000 diffractometer equipped with a graphite focusing monochromator using Ni-filtered Cu K_α radiation at 30 kV and 20 mA was used for all diffraction work. Samples were scanned at 2°/2θ per minute from 10° to 70° 2θ. Samples not leached with 6N HCl (generally duplicate raw samples) were scanned after mixing the filtered sample with high-vacuum lubricant in an attempt to inhibit oxidation; unfortunately, this technique did not always prevent oxidation of FeS or produce useful X-ray results. X-ray diffraction was able to detect mineral species at concentrations of 5 volume percent or greater.

Spatial and textural relationships of the solid products, based on SEM observations, were used to infer some possible pathways for the transformation of goethite to pyrite. Polished and unpolished mounts of the sample were prepared from runs in which pyrite was detected by XRD. Unpolished gold-coated mounts were used to view the solids to determine morphology, size, and texture. Carbon-coated polished grain mounts were used to obtain a two-dimensional surface for iron and sulfur analysis Goldstein and others, 1981). Because FeS and

(Fe²⁺,Fe³⁺)_x(OH)_x solids are highly susceptible to oxidation in air, few of these solids were examined. Diameters of the product FeS₂ spheres, measured to 0.1 μm, were determined visually from SEM photomicrographs. SEM energy-dispersive spectroscopy (EDS) analyses of the polished spheres are within ±5 weight percent of the iron and sulfur values obtained from a pyrite standard. Polished mounts were also examined under reflected light to look for mineralogical features not detected by SEM.

Due to poor diffraction characteristics of the amorphous, early formed FeS, Fe²⁺:S²⁻ mole ratios obtained from AA and Ag₂S gravimetry in the AVS analysis were used to characterize the mineralogy of the early FeS fraction. The Fe:S ratios for crystalline iron sulfide minerals are given in table 2.

The saturation state of the solution and distributions of aqueous and mineral species were modeled using the computer program PHREEQE (Parkhurst and others, 1980). This equilibrium model uses Debye-Huckel activity coefficients to calculate activities for aqueous iron and sulfur species for all ionic strengths. The log of the ratio of the ion activity product (IAP) to the solubility product (K_{sp}) is used to determine the saturation state of the solution with

Table 2. Fe²⁺:S²⁻ mole ratios for early formed samples (<24 hours) showing composition of FeS solids [Fe²⁺ is from 6N HCl leach filtrate. S²⁻ is sulfide precipitated as Ag₂S from 6N HCl leach. nd, not determined. Fe:S compositions of crystalline iron sulfide minerals are shown below. FeS composition based on these ratios is primarily that of mackinawite (Fe:S=1.1)]

Experiment no.	Time (hours)	Fe ²⁺ :S ²⁻ ratio
5	2	1.10
6	1	1.11
7	2	1.09
8	22	1.00
9	21	1.34
10	5	1.15
11	2	1.24
12	2	1.15
15	3	0.95
29	2	0.96
30	2	0.89
Mean value is 1.09 (s ± 0.12)		
Mineral name	Formula	Fe:S mole ratio
Mackinawite ¹	FeS _{1-x}	1.1
Pyrite	FeS ₂	0.5
Marcasite	FeS ₂	0.5
Greigite	Fe ₃ S ₄	0.75
Pyrrhotite ²	Fe _{1-x} S	0.9

¹Weight percentages and Fe:S ratios based on FeS_{0.9}.

²Weight percentages and Fe:S ratios based on Fe_{0.9}S.

respect to mineral phases in the system. Negative values of this ratio ($\log(IAP/K_{sp})$) indicate solution undersaturation and probable mineral dissolution; positive values point to solution saturation and thus mineral precipitation. Values of zero indicate equilibrium or metastability of the solution and solid phases.

RESULTS AND DISCUSSION

Low pH (≤ 7.0) Results

Experimental conditions and results are summarized in table 1. Because pyrite was not detected at high pH (>7.0), most of the discussion on pyrite formation focuses on the experiments from pH 4 to 7. Unless specified, low pH refers to pH values less than or equal to 7.0, whereas high pH values are those greater than 7.0. This separation was chosen because pyrite was not detected at pH values greater than 7.0. Similarly, low H_2S refers to experiments run at 1.0 or 0.1 $H_2S_{(g)}$ volume percent, whereas high H_2S refers only to those experiments run at 10 percent $H_2S_{(g)}$. The high pH results are discussed by comparing the reaction products to the pyrite-yielding sequence of low pH.

All the low pH experiments displayed the same reaction sequence. First, rapid reduction of Fe^{3+} and complete dissolution of α -FeOOH occurred within 2–8 hours at $pH_{(init)}$ of 4.11–4.99 to form FeS, S^0 , and $Fe^{2+}_{(aq)}$. Dissolution was followed by a period of slow reaction of FeS, S^0 , and $Fe^{2+}_{(aq)}$ to form FeS_2 . Finally, pyrite formed rapidly once undersaturation with respect to FeS was attained. The rate of this overall process varied with conditions but was most rapid at pH of 4–5 and 10 percent $H_2S_{(g)}$ (table 1). Figure 2 illustrates the reaction sequence and changes in the concentrations of iron and sulfur species with time.

α -FeOOH dissolved rapidly (0–2 hours) at pH of less than 5.0 and 10 percent $H_2S_{(g)}$. The resulting solution was calculated to be saturated with mackinawite, amorphous FeS, greigite, marcasite, and pyrite. The major iron species after goethite dissolved was Fe(II) in the aqueous and FeS phases. More than 90 percent of the iron added as goethite was incorporated into the aqueous and FeS phases under these conditions. The initial, rapid redox reaction of goethite and H_2S is consistent with the results of Pyzik and Sommer (1981), who reported that Fe(III) was reduced by bisulfide ($HS^-_{(aq)}$) prior to goethite dissolution and release of Fe(II). The reduced iron subsequently reacted with $H_2S_{(aq)}$ or $HS^-_{(aq)}$ to form FeS.

Goethite

α -FeOOH was detected as a residual component of the solids under almost all experimental conditions. In

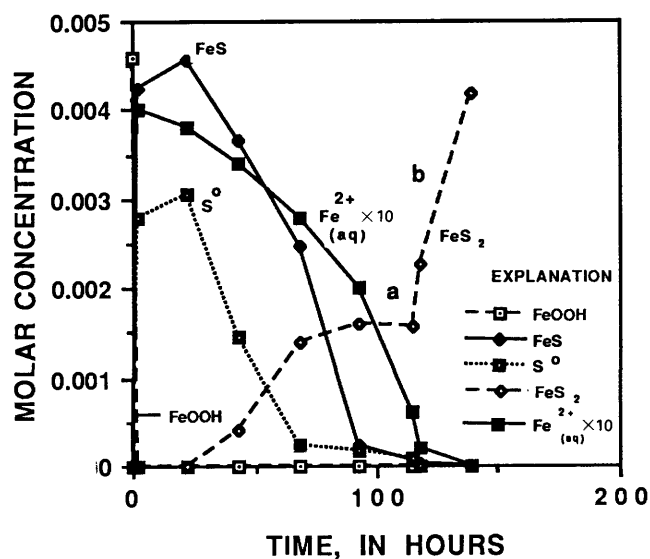


Figure 2. Time versus concentration for iron and sulfur species, experiment 7. Results are typical of a reaction sequence at low pH (<7.0). Goethite is rapidly consumed by reaction with H_2S , and FeS, S^0 , and $Fe^{2+}_{(aq)}$ are formed. The part of pyrite curve labeled "a" represents slow formation of pyrite while solution is saturated with FeS. The part labeled "b" represents rapid formation of pyrite once solution becomes undersaturated with FeS.

solids from the earliest stages of low pH reactions, α -FeOOH was detected visually after treatment with 6N HCl. In low H_2S runs, it was detected by XRD in unleached samples or was visible as an unreacted solid (table 1). And, in most high pH reactions, goethite was a major, unreacted constituent. X-ray diffraction studies suggest that this goethite is not a poorly crystalline oxidation or alteration product of reaction or sample treatment but rather the material added at the start of the experiment. Thus, α -FeOOH was consumed rapidly at low pH but remained as a major phase for the duration of the run at high pH.

X-Ray Diffraction

In the first 8 hours of low pH experiments, XRD patterns of unleached samples were characteristic of an amorphous substance (wide, poorly defined peaks). As the reactions progressed beyond approximately the 8-hour point, mackinawite peaks became evident. Detection of FeS in unleached samples by XRD at pH greater than 9.0 was difficult because of the presence of ferrous-ferric oxyhydroxides. Goethite was present in some early samples from low pH experiments (0–8 hours) and in all high pH samples. Elemental sulfur was detected as a product of every experiment in amounts that varied depending on the conditions and extent of reaction. Similarly, pyrite was first detected at different elapsed times depending on conditions, but once detected it became more abundant and more

crystalline (relative to the earlier samples). Diffraction patterns from some early samples contain pyrite peaks having greater half-widths (generally an indicator of poor crystallinity) than pyrite peaks from samples near the end of a run.

Mole ratios of $\text{Fe}^{2+}:\text{S}^{2-}$ are not given for the experiments run at pH 9.0 or higher (experiments 18, 32, and 33) because the FeS and iron oxyhydroxides ("green rust") that formed were both dissolved by 6N HCl. Thus, the filtrate contained total iron from two solids that could not be assigned to individual minerals. Additionally, FeS formed so slowly in these experiments that it was not useful to sample the reaction mixture until after 24 hours.

$\text{Fe}^{2+}:\text{S}^{2-}$ mole ratios from the earliest stages of the low pH experiments gave ratios of AVS iron to sulfide of between 0.8 and 1.3 (table 2). The mean of these ratios is 1.09 (± 0.12). The ratio of Fe:S in mackinawite ($\text{FeS}_{0.9}$) is 1.1; in pyrite and marcasite (FeS_2), it is 0.5. If only greigite were present, this ratio should have been 0.75 (3Fe:4S). Based on the $\text{Fe}^{2+}:\text{S}^{2-}$ ratios obtained by analysis and XRD data, mackinawite and (or) amorphous FeS are the dominant sulfide phase(s) produced early in these experiments. Ratios of Fe:S of less than 1.1 might represent several possible mixtures of mackinawite, pyrite, and greigite (Hallberg, 1972), but the existence and proportions of such mineral groupings could not be resolved using the available data. High Fe:S mole ratios (>1.1) may be due to variations in the stoichiometry of the FeS or $\text{FeS}_{(\text{am})}$; amorphous FeS may contain as little as 0.87 S per 1.0 Fe (Morse and others, 1987), an Fe:S ratio of 1.15. Adsorption of sulfide or iron also may have altered the Fe:S ratios (Rickard, 1969a; Pyzik, 1976).

Saturation State

Figure 3 depicts the change over time in the saturation state of the solution with respect to FeS for experiment 7. The sample at 68 hours is the last solution that is oversaturated with FeS; after this time, the rate of FeS_2 formation increases. Samples at 93 and 115 hours indicate a transitional period of FeS metastability, and beyond 115 hours the solutions are undersaturated with respect to FeS. Because the concentration of $\text{H}_2\text{S}_{(\text{aq})}$ and other parameters were constant, FeS undersaturation resulted from the decrease in iron concentration by its incorporation into pyrite. The solution remained saturated with pyrite, the only other iron mineral detected. In figure 2, the first slope increase of the pyrite formation line ("a") represents the continuous slow rate of production of FeS_2 during the time when FeS and S^0 are dominant in the system. The part of the line labeled "b" indicates the rapid formation of pyrite following the undersaturation of FeS.

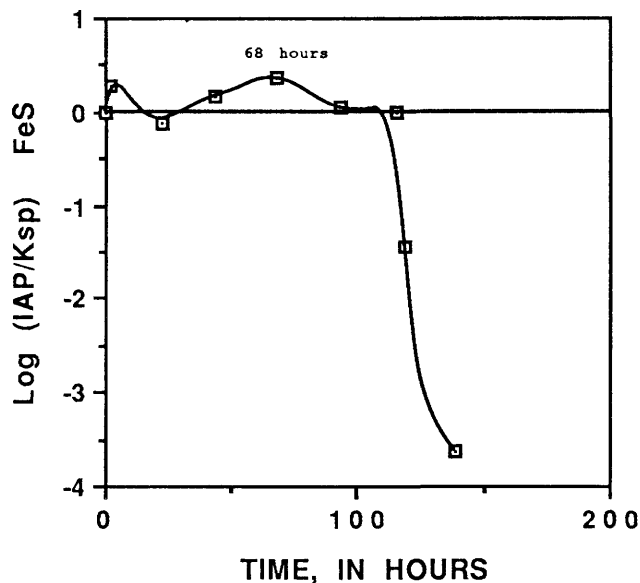


Figure 3. FeS saturation curve, experiment 7. Values greater than zero indicate FeS oversaturation; values less than zero indicate FeS undersaturation. A change toward FeS undersaturation begins at approximately 68 hours. Note rapid FeS dissolution coincident with rapid FeS_2 formation shown in figure 2.

Pyrite Formation Rates

In experiments run at or below pH 7.0, the overall rate of pyrite formation—that is, the slope of FeS_2 versus time—varies from 6.0×10^{-7} M/min at $\text{pH}_{(\text{init})}$ of 4.11 to 2.6×10^{-9} M/min at $\text{pH}_{(\text{init})}$ of 7.0 (table 1). Pyrite formed most rapidly in experiments 5, 6, and 7, which had 10 percent $\text{H}_2\text{S}_{(\text{g})}$ at low initial pH. The slowest rates of pyrite formation were in experiments run at $\text{pH}_{(\text{init})}$ of almost 7.0, or at $\text{H}_2\text{S}_{(\text{g})}$ of 1.0 or 0.1 volume percent. The rate of pyrite formation is undetectable at pH values greater than 7.0. The slower rates or lack of pyrite formation (for example, experiment 19) at high pH are probably a result of retardation of the goethite dissolution/FeS formation process that proceeded rapidly at low pH values. The overall reaction represented as $\text{FeS} + \text{S}^0 \rightarrow \text{FeS}_2$ does occur at alkaline pH but is very slow at low temperatures (Berner, 1969; Rickard, 1975).

Pyrite Morphology and Texture

Pyrite produced in these experiments is mainly spherical, from less than 1 to slightly more than 5 microns in diameter. According to semiquantitative SEM-EDS analysis, pyrite spheres consist only of iron and sulfur in the proportions of one mole of iron to two moles of sulfur. Departures from this ratio were observed in nonspherical solids, in samples that were incompletely reacted (as in the

earliest stages of an experiment), or in samples that were not 6N HCl and acetone leached. Solids possessing this 1Fe:2S ratio produce XRD patterns characteristic of pyrite.

Development of Pyrite Morphology

Contrasting experimental conditions and extent of reaction resulted in systematic differences in pyrite morphology. Figure 4 is a sequence of SEM photomicrographs from experiment 7 depicting the formation and change of pyrite morphology and texture. This sequence is typical of all low pH experiments. Euhedral pyrite (that is, well-developed crystal faces) was not seen as a product under any conditions.

Except for the sample shown in figure 4A, the solids were leached with 6N HCl and acetone before they were

examined. Based on SEM-EDS analysis, chemical extraction, and XRD, the solids shown in figures 4B-E are pyrite. The dipyrramids in figure 4A (2 hours) are crystalline elemental sulfur; the smallest sulfur crystal is approximately 2 μm in diameter and the largest is almost 22 μm (measured along the minor axis of the dipyramid).

The large solid in the upper left quadrant in figure 4A is iron rich but is not the original bladed goethite. Its massive morphology is common for iron-bearing solids early in most experiments. Three SEM-EDS analyses of this product gave a mean of 75.3 weight percent Fe and 24.6 weight percent S. The mole ratio of Fe:S of 1.75 is much greater than the Fe:S ratio for known crystalline iron sulfides (table 2). Therefore, the exact composition of this substance is unknown, but it is probably a mixture of S_8 , poorly crystalline or oxidized iron monosulfide(s), and

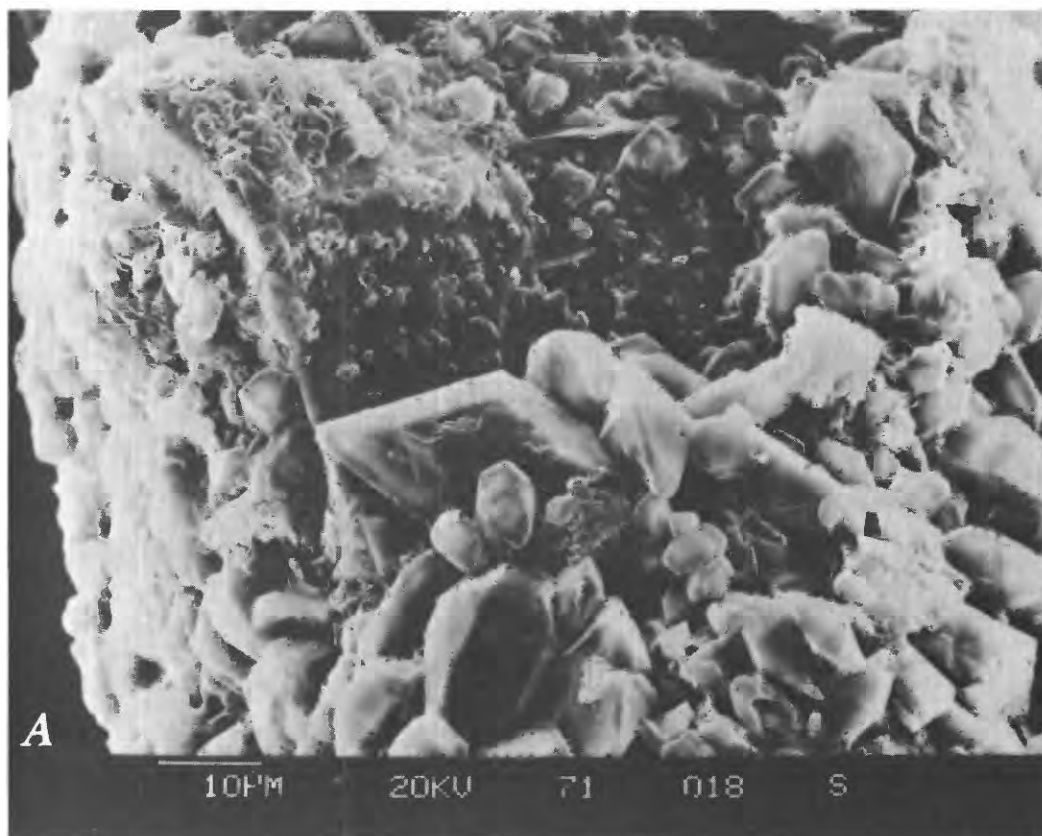
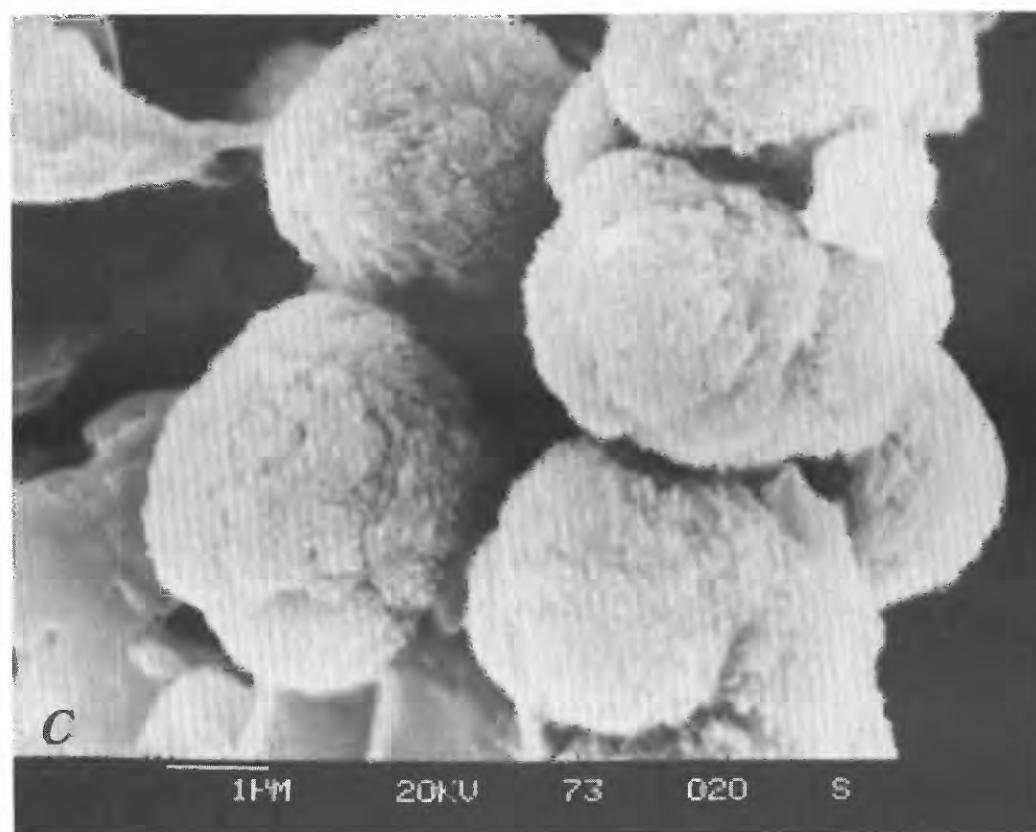
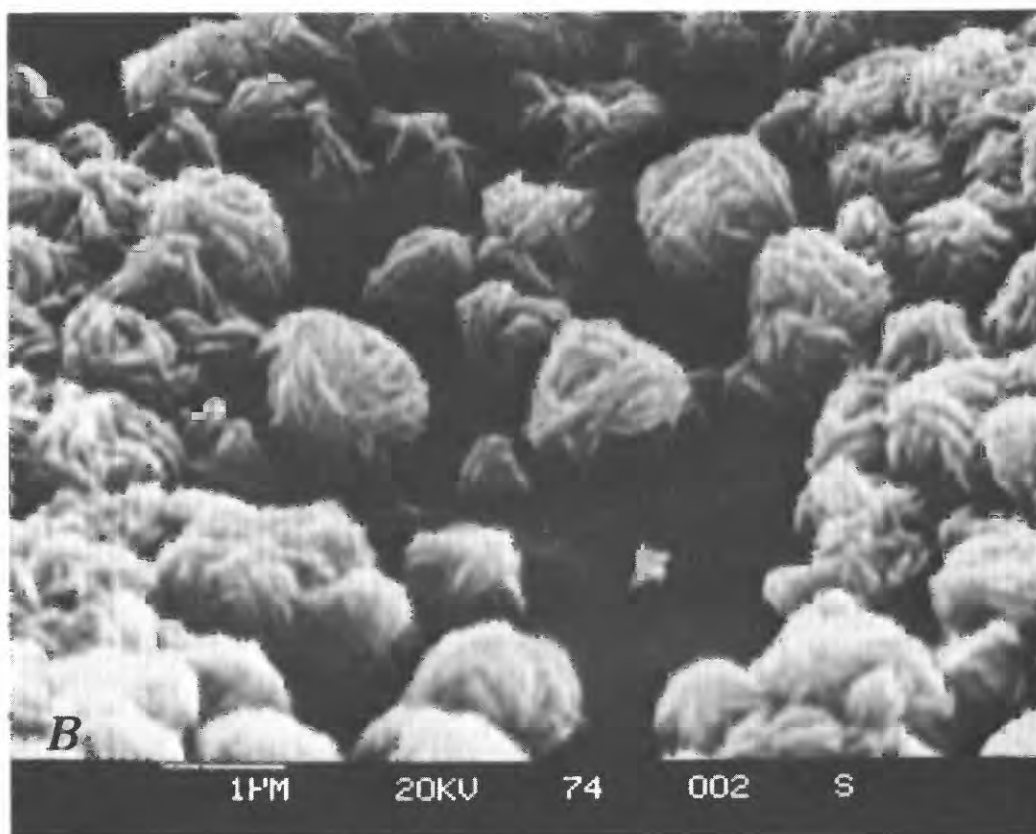
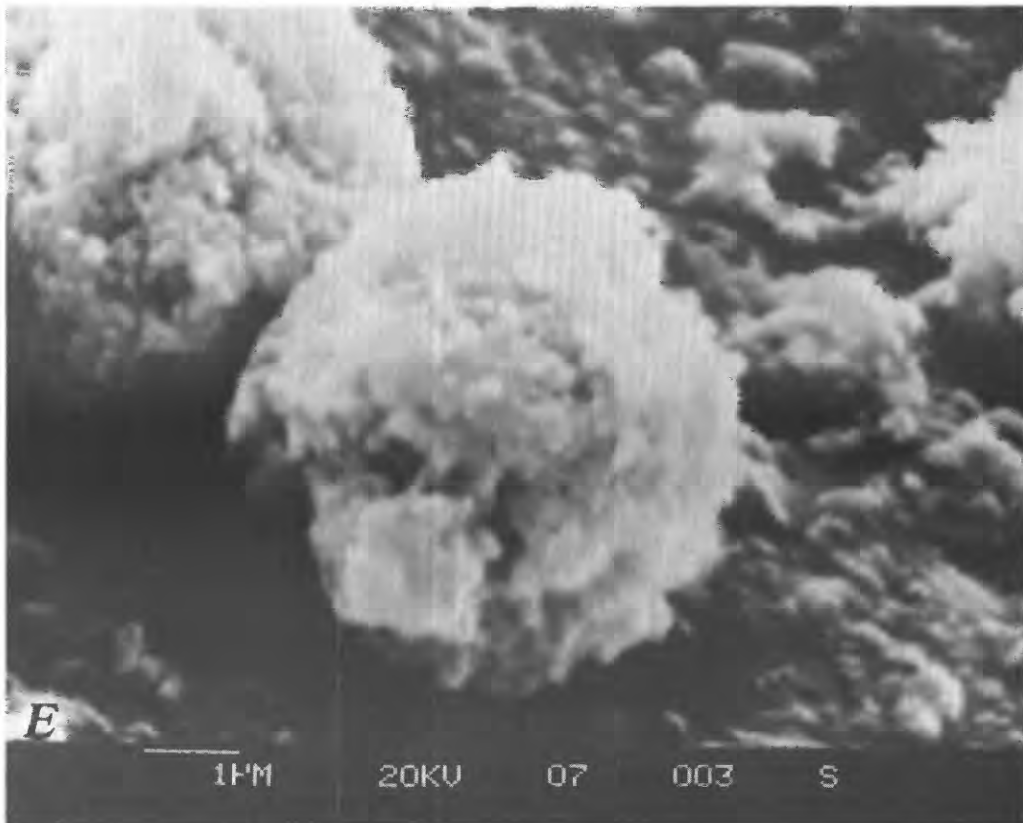
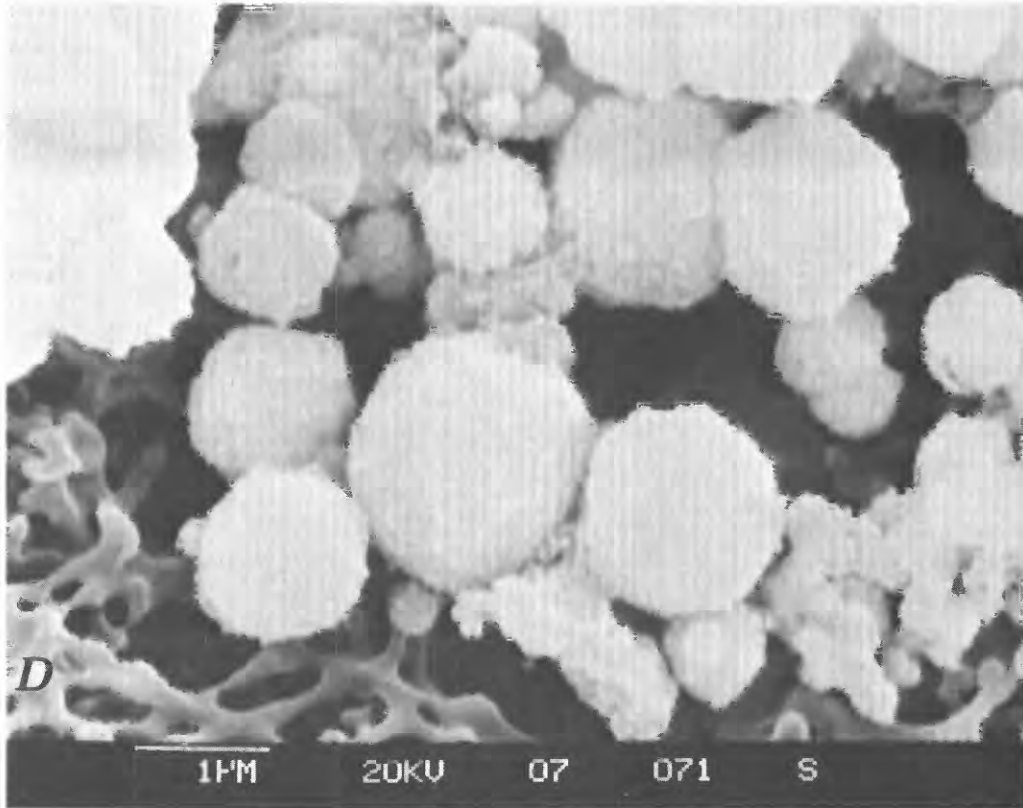


Figure 4 (above and following pages). Scanning electron microscope photomicrographs of solids formed in experiment 7. Sequence illustrates development of pyrite texture and morphology with increasing time of reaction at low pH (4–5). *A*, Elemental sulfur dipyrramids and massive “intermediate” iron-rich sulfur-bearing phase formed during goethite dissolution/FeS formation. Bar, 10 μm ; time, 2 hours. *B*, Spherical pyrite morphology typical of FeS_2 formed early in reaction. Bar, 1 μm ; time, 22 hours. *C*, Pyrite microspheres showing platy surface texture of spheres. This spherical shape with rough-surfaced texture was the dominant form of pyrite. Bar, 1 μm ; time, 43 hours. *D*, Range of pyrite sphere sizes approximately halfway through the experiment. Bar, 1 μm ; time, 68 hours. *E*, Large pyrite spheres at the end of experiment 7. The rough surface and spherical shape are typical of spheres formed in experiments run at low pH values and high H_2S (10 percent) concentration. Bar, 1 μm ; time, 139 hours.





Sulfur forms other than S_8 were not distinguished on the basis of SEM-EDS analysis. X-ray diffraction of the 6N massive or indistinguishable crystallites of α -FeOOH. HCl-leached solids from this sample detected only goethite and sulfur.

Pyrite agglomerates that have incipient spherical morphology had formed by 22 hours (fig. 4B). At this point, pyrite was a minor component ($<1 \times 10^{-5}$ M Fe as pyrite) of the total iron in the solids. The sphere size is about 1 μm , smaller than the majority of the sulfur dipyrramids shown in figure 4A. These spheres did not form directly from either the elemental sulfur dipyrramids or the large, iron-rich "intermediate phase" shown in figure 4A, and a dissolution-/precipitation mechanism must have been operating at this time if the solids shown in figure 4A were being consumed.

X-ray diffraction and ultraviolet-visible spectrophotometry of each sample obtained during experiment 7 show that elemental sulfur was present while pyrite was being formed (fig. 2). Later samples were leached with acetone prior to SEM examination, so sulfur dipyrramids were removed. Although solid sulfur was not seen in subsequent micrographs in this series, other methods demonstrate that acetone-extractable elemental sulfur was present.

Uniform pyrite spheres formed after 43 hours (fig. 4C). These spheres are atypically large for this sample but exhibit in detail the platy rough surface texture characteristic of most spheres that formed by 48 hours. These rough-surfaced spheres are the major type of pyrite in all experiments in which pyrite formed. This spherical texture may have been inherited by continued growth on the smaller, spherical grains shown in figure 4B.

Figure 4D shows the surface texture of the spheres after 68 hours. The spheres became rougher and more nodular as the experiment progressed. Figure 4E shows the texture typical of the pyrite by 139 hours. This series of photomicrographs shows that the spherical morphology of pyrite developed early in the reaction. Although an increasingly rough surface texture developed over time, the spherical shape persisted throughout the experiment. Additionally, the diameters of the spheres increased (discussed later).

Spheres Produced at Low H_2S Concentrations

The concentration of $H_2S_{(aq)}$ may affect sphere size and texture. Pyrite spheres formed in experiments run at low $H_2S_{(g)}$ (for example, experiments 29 and 30, table 1) are texturally and morphologically similar to spheres formed at high $H_2S_{(g)}$ concentrations. However, development of the rough sphere texture was slower and modal sphere diameters (MD) smaller. Experiment 30 was run at low $H_2S_{(g)}$ at an initial pH of 4.59 (table 1). The pyrite spheres at 126 hours (fig. 5A) have a smoother, less platy surface

than spheres formed in experiment 7 (compare with fig. 4E). Thus, for a similar amount of reaction time, the rough texture seen in experiment 7 had not yet developed.

Experiments 30 and 7 were similar except for the $H_2S_{(g)}$ concentration but produced spheres of different diameters. The modal diameter of the spheres from experiment 30 (1.8 μm , table 1) is smaller than in experiment 7 (4.4 μm , table 1) for comparable reaction times.

Spheres formed in experiments at low $H_2S_{(g)}$ acquire the rough texture later than in experiments at high $H_2S_{(g)}$. Figure 5B shows a sample taken at 188 hours from experiment 29, which was also run at low $H_2S_{(g)}$. The sample was treated with 6N HCl but not acetone leached, and XRD indicated that only sulfur and pyrite were present. SEM-EDS analysis detected only sulfur in the large dipyramid-shaped solid, and analysis of one sphere in the field of view is 44.1 weight percent Fe and 55.9 weight percent S, similar to the expected values for pyrite (46.5 weight percent Fe and 53.4 weight percent S). The spheres shown in figure 5B also exhibit the rough, nodular surface features that resemble the physical arrangement of crystallites in framboids. Internal nucleation of pyrite crystals has been invoked as a possible mechanism for the formation of pyrite framboids from spherical greigite precursors (Sweeney and Kaplan, 1973); however, the reactions and processes that lead to framboidal pyrite formation remain unknown.

Sphere Diameters

The modal sphere diameter of FeS_2 increases with time within individual experiments. Figure 6 shows the particle size distribution from a sample at 128 hours from experiment 6; the modal diameter is 4.7 μm , and the range of sizes is from 0.6 to 5.3 μm . The reasons for the range in sphere sizes are not known, but the range may represent a dependence of growth rate on the size of the initial precipitate nuclei or changing saturation state of the solution (Skoog and West, 1982). Spheres larger than approximately 5 μm may result from growth at the expense of the smaller, early formed spheres (Shaw, 1980; Stumm and Morgan, 1981). Spheres having diameters of 3–4 μm are larger than those that precipitated at the start of FeS_2 formation (0.5–1.7 μm at 20 hours).

Comparison of size distributions from similar experiments at 10 percent $H_2S_{(g)}$ shows that the modal sphere diameter increases with time of reaction. The modal sphere diameter in experiment 7 markedly increased after 68 hours, at which time the solution was no longer saturated with FeS. Spheres from experiment 6 at 128 hours (fig. 6) have a modal diameter of 4.7 μm . Spheres from experiment 7 at 139 hours have an modal sphere diameter of 4.4 μm (fig. 7, table 3), and the minimum diameter increased from 0.7 μm at 68 hours to 2.4 μm at 93 hours. The maximum

diameter increased only by small amounts after 93 hours; apparently, the maximum sphere diameter (approximately 5.0–5.5 μm) was attained shortly after FeS undersaturation was reached. The rate of size increase coincides with the increase in the rate of FeS₂ formation and perhaps reflects growth due to the more rapid formation of FeS₂.

The size of the pyrite spheres decreases in diameter with increasing ionic strength. Data presented in figure 7 and table 3 contrast the sphere sizes of experiment 7 ($I=0.1$ M) and experiment 12 ($I=2.0$ M).

The modal diameter of the spheres in experiment 7 ($I=0.1$) is 4.4 μm , (range 2.5–5.7 μm). In experiment 12 ($I=2.0$), the modal size is from 0.5 to 0.6 μm , (range 0.4–1.1 μm) (see table 3). The modal sizes in the other two experiments of intermediate ionic strength (10 and 11) are intermediate between these end members, 1.9–2.0 μm and 0.7–0.8 μm for experiments 10 ($I=0.3$) and 11 ($I=0.7$), respectively.

The contrasting size relationships for experiments 7, 10, 11, and 12 are also illustrated by the series of SEM micrographs in figure 8. Particle size analysis, based on visual measurements of almost 100 spheres from these four experiments, shows that the modal diameter is consistent within individual runs and decreases with increasing ionic strength (figs. 8, 9). Differing size ranges were obtained for samples taken at almost the same time during each experiment (~ 140 – 150 hours). The rate of FeS₂ formation was more rapid in experiment 7 but similar for experiments 10, 11, and 12.

Either nucleation or precipitate growth (but not both) is the dominant mechanism for controlling the sizes of solids. Generally, increases in the saturation state of a solution lead to increased nucleation rates, smaller particles, and slower precipitate growth (Skoog and West, 1982). More nucleation sites may develop as a result of higher ionic strength influences on FeS, S^o, or other possible nuclei. Alternatively, the same number of nuclei may form, but slower growth adds less pyrite to these nuclei (Adams, 1976). In addition, specific cations or anions (such as Cl⁻, NO₃⁻, K⁺) may selectively influence growth or nucleation processes and, thus, particle sizes (van Straten and others, 1985). It is unknown which of these processes is dominant in our experimental system.

High pH Results

At high pH (>7.0), iron was slowly incorporated into FeS and (Fe²⁺, Fe³⁺)-oxyhydroxide phases or remained as unreacted α -FeOOH. Solid reaction products are FeS, S^o, and ferrous-ferric solids known as green rust. FeS and S^o formed at all pH values, but in experiments at pH greater than 7.0 FeS formed in smaller amounts compared to low pH experiments and was only a minor component of the solids as the pH exceeded 9.0. Elemental sulfur formed slowly during all high pH runs and was most abundant and

becoming a dominant product (relative to iron monosulfide) only toward the end of most experiments. By contrast, at low pH, maximum sulfur values were reached about the same time (2–8 hours) as maximum FeS values (fig. 2). Thus, formation of sulfur by sulfide oxidation by Fe(III) occurred more slowly at high pH as compared to low pH. Goethite remained as a major constituent of the solids during most high pH experiments.

At the neutral pH values of experiments 16 (pH 7.1) and 19 (pH 7.0), a black solid slowly formed on the goethite surface and persisted for most of the experiment. X-ray diffraction of an unleached, late-stage (94 hours) sample from experiment 19 indicated that the black coating was FeS. This layer of FeS was removed by treatment with 6N HCl and orange-yellow goethite was beneath it. X-ray diffraction of the 6N HCl-leached solids from experiment 19 indicated that sulfur and goethite were the major solids from early in the experiment (3 hours) until 119 hours later. This is in marked contrast to the low pH experiments in which goethite completely dissolved and FeS formed within the first 2–8 hours. After 119 hours in experiment 19, goethite was not present in the 6N HCl-leached solids. Beyond 119 hours, S^o was the dominant solid product in addition to FeS. It should be pointed out that experiment 19 had the slowest rate of pyrite formation of any run in which pyrite formed. This slow rate is probably a reflection of the slow initial sulfide-Fe(III) reaction at high pH and low H₂S_(g). Solid green rust was not seen in experiments 16 and 19, but the light-green color of the raw sample filtrates until late in the reaction (>100 hours) indicates the presence of ferrous iron. The dominant form of aqueous iron is predicted to be Fe(OH)⁺ in the pH range 7.0–8.5 (Pyzik and Sommer, 1981).

At the highest pH values (pH ≥ 9.0) (experiments 18, 32, and 33, table 1), mixed (Fe²⁺, Fe³⁺)-oxyhydroxide solids known as green rust formed (Rickard, 1969a; Newman, 1987). Reduced iron (Fe²⁺) in these minerals imparted a green color to the solid, although Fe³⁺ was also present. The color of these solids and the reaction solution intensified from light green to a dark blue green with higher solution pH. Oxidation of the Fe²⁺ in these minerals to Fe³⁺ after a few hours of exposure to air is indicated by a change in color from green to brown. These solids were not well characterized due to their instability, variable composition, and poor crystallinity.

Small black particles coexisted with the green rust. These particles were likely FeS, but this could not be verified because XRD results were inconclusive. The solubility of the black coating in 6N HCl and the high pH of formation is consistent with FeS.

The green rust is a thin layer coating the α -FeOOH. X-ray diffraction of an untreated green rust sample from an early sample (24 hours) in experiment 33 detected only goethite and a few peaks characteristic of sulfur. The presence of sulfur was verified by ultraviolet analysis of the

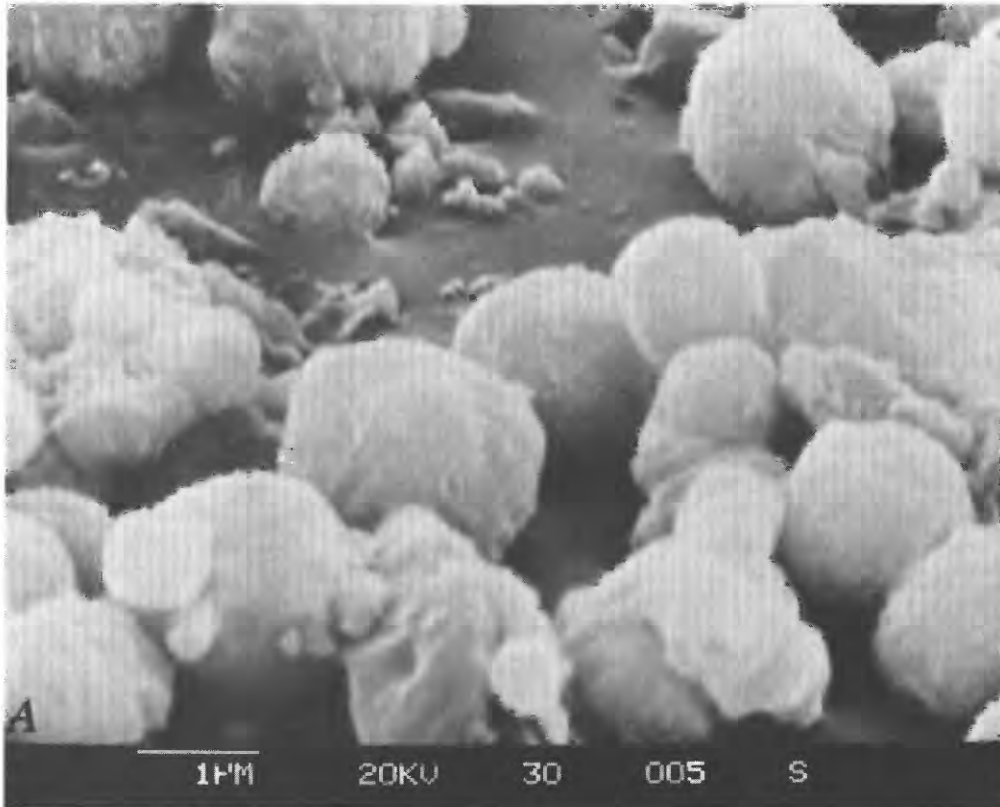


Figure 5 (above and facing page). Scanning electron microscope photomicrographs of pyrites formed in experiments 29 and 30. *A*, Pyrite spheres formed at low $H_2S_{(g)}$ concentration (0.1 percent), experiment 30. Spheres have smoother surfaces than spheres from experiment 7 (fig. 4E) for similar reaction times. Bar, 1 μm ; time, 126 hours. *B*, Pyrite spheres from an unleached sample at 188 hours from experiment 29 run at low $H_2S_{(g)}$ concentration (0.1 percent). With increasing reaction time, spheres formed at low $H_2S_{(g)}$ became similar to rough-textured spheres formed at high $H_2S_{(g)}$ concentration. Large dipyrramid in center is S° . Nodular surface of FeS_2 spheres is similar to framboidal texture of naturally formed sedimentary pyrite. Bar, 2 μm .

acetone-extracted solids. Treatment of this sample with 6N HCl resulted in immediate removal of the green rust and revealed orange-yellow goethite underneath. X-ray diffraction of the 6N HCl-treated sample again revealed only goethite and sulfur; the green rust apparently was present in amounts less than 5 volume percent in the raw sample. As reaction time increased, more of the goethite was converted to green rust, but goethite remained as a major component of the 6N HCl-leached solids. Elemental sulfur was also present; thus, Fe(III) was reacting with aqueous sulfide to produce S° but at a rate slower than similar experiments at low pH. The layer of green rust seemingly inhibited Fe^{3+} reduction and goethite dissolution.

Thus, over the pH range 7–10, the rate of $\alpha\text{-FeOOH}$ reduction-dissolution decreases, S° and FeS form more slowly, and FeS_2 formation is inhibited. Both the green rust and FeS inhibit goethite dissolution (and presumably subsequent pyrite formation) at high pH values. Pankow and Morgan (1979, 1980) noted that the rate of mackinawite dissolution is dependent on $[H^+]$ if the pH is less than 5.3. Adsorption of Fe^{2+} onto goethite at acidic pH values is

enhanced as the pH increases (LaKind and Stone, 1989) and may act as an additional barrier to goethite dissolution. Similarly, Tewari and Campbell (1976) have shown that the rate of anoxic dissolution of FeS (troilite) is slower as the pH increases to 6.5. This inhibition of reduction and dissolution of goethite is consistent with increased FeS saturation and therefore diminished tendency of FeS to dissolve at pH greater than 7.0. The slowness of pyrite formation as the solution becomes more alkaline may be due to changes in the solubility and rate of dissolution of both green rust and FeS.

RELATIONSHIPS TO IRON AND SULFUR DIAGENESIS

Various iron minerals react differently during sulfidization due to variations in crystallinity, solubility, or surface charge. For example, at neutral pH values crystalline $Fe(OH)_3$ is more readily sulfidized to FeS than is crystalline $\alpha\text{-FeOOH}$ (Pyzik, 1976). The reactivity of iron minerals depends upon several factors, some of which are

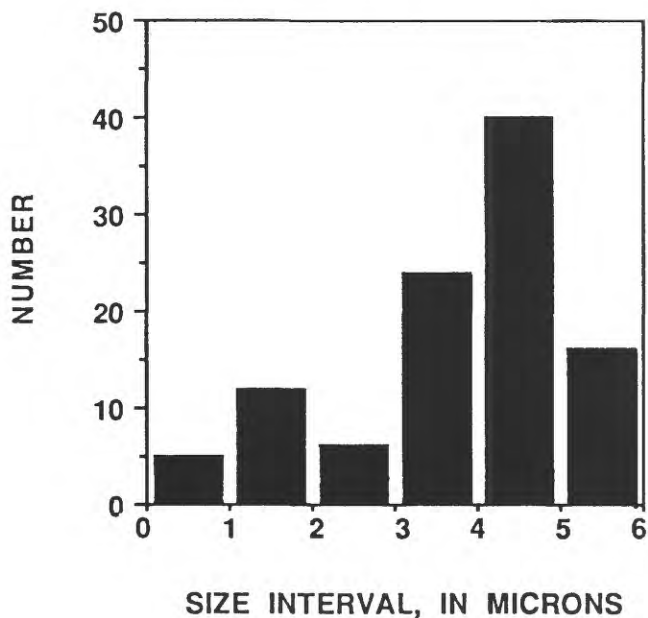
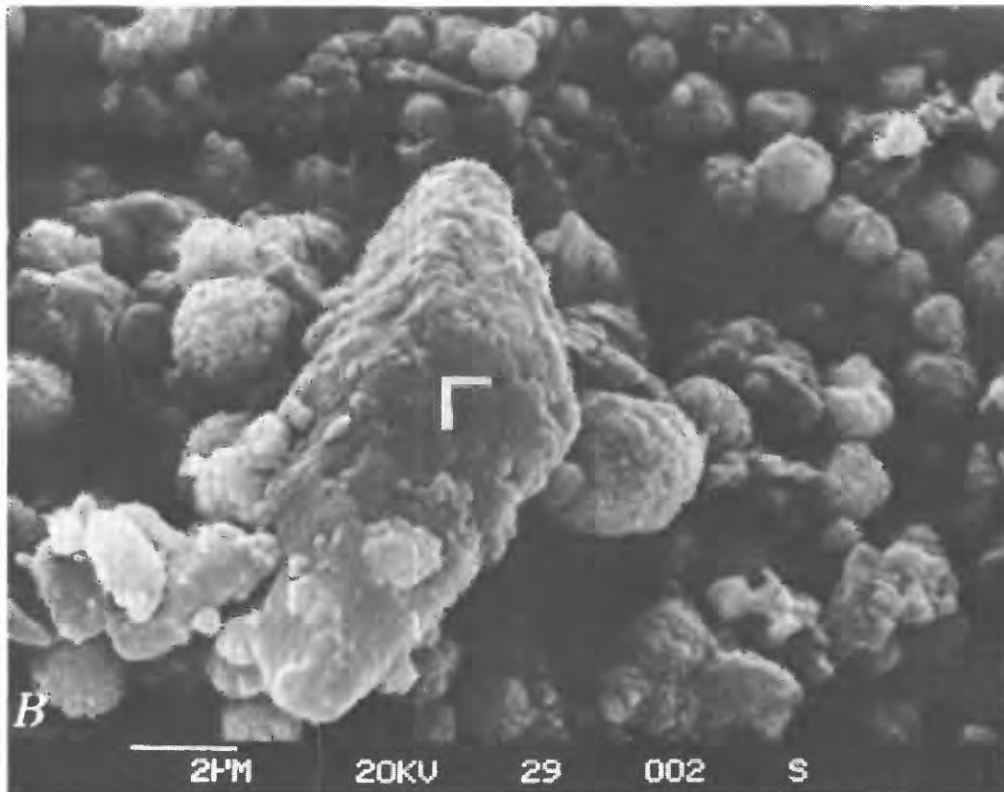


Figure 6. Histogram of modal sphere diameters from experiment 6 (128 hours). Modal sphere diameter is centered in the 4–5 μm interval. Increase in modal sphere diameters as compared to those of earlier samples from same experiment indicates an increase in sphere size with reaction time.

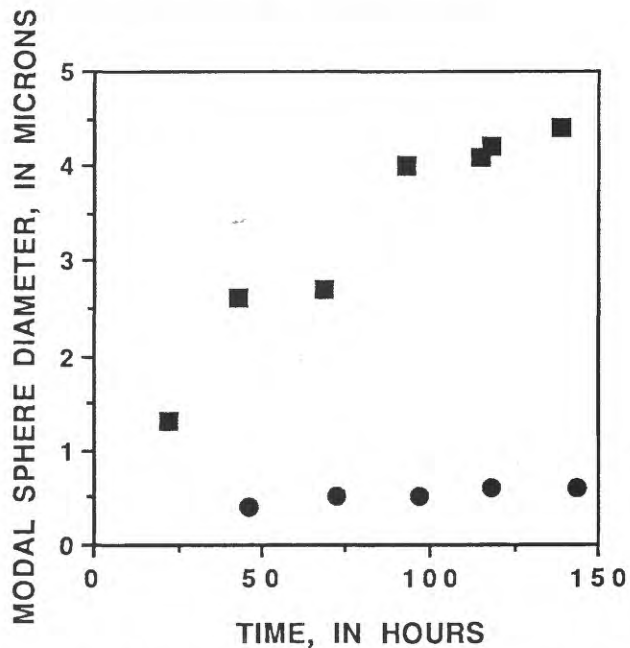


Figure 7. Modal sphere diameter versus reaction time at two ionic strengths : experiment: 7 ($I=0.1\text{ M}$) (squares) and experiment 12 ($I=2.0\text{ M}$) (circles). At $I=0.1\text{ M}$ sphere diameter increases with reaction time, whereas at $I=2.0\text{ M}$ sphere diameter remains constant with reaction time. Increasing ionic strength promotes formation of smaller sized spheres for otherwise similar experimental conditions.

Table 3. Modal sphere diameter and size range for pyrite spheres formed in experiments 7 and 12

[na, not applicable; nd, not determined. Ionic strength experiment 7, 0.1 M; experiment 12, 2.0 M]

Sample no.	Time (hours)	Modal diameter (μm)	Size range (μm)
Experiment 7			
1	2	na	na
2	22	1.3	0.6-1.4
3	43	2.6	0.7-3.5
4	68	2.7	0.7-3.4
5	93	4.0	2.4-5.2
6	115	nd	nd
7	118	4.2	2.2-5.1
8F	139	4.4	2.5-5.7
Experiment 12			
4	46	0.4	0.3-0.5
5	72	0.5	0.3-0.8
6	97	0.5	0.4-0.8
7	118	0.6	0.3-1.1
9	144	0.6	0.4-1.1

detailed by Canfield (1988, 1989). Iron oxyhydroxides such as goethite or lepidocrocite are common sources of iron available for sulfidization and are generally delivered to a depositional site as coatings on clay minerals (Carroll, 1958). The sum of adsorbed and detrital goethite may be as much as 50 percent of the total iron load carried by rivers (Gibbs, 1973). Our experimental results show that the reactive nature of goethite in a wide range of conditions results in formation of a variety of dissolved and solid reaction products. Goethite is completely converted to FeS and FeS₂ at low pH or partly converted to these sulfides as pH increases or H₂S decreases. As pH exceeds 7.0, goethite remains as an unreacted solid; at pH greater than 9.0, modeling indicates that goethite does not dissolve and may even form.

Rates of Pyrite Formation

FeS, FeS₂, and S⁰ concentrations in the upper layers of marsh sediments are subject to temporal variation as a result of seasonal oxidative recycling (such as FeS → Fe(OH)₃ → FeS), whereas the concentration of FeS₂ remains generally constant below approximately the top 10–15 cm of sediments (Luther and others, 1982; Cutter and Velinsky, 1988). Depending on the predominance of sulfide-mineral-forming reactions as seen in this study, rapidly formed FeS and S⁰ are either sinks or sources for iron and sulfur over short time periods (less than one year), and short-term shifts in the iron and sulfur budgets of these sediments may result. The results here reinforce the fact that pyrite formation from iron monosulfide and zerovalent sulfur is very slow at neutral to slightly alkaline pH and

possibly inhibited at pH of 9.0 or more. As diagenesis proceeds, however, there is more time for the slow conversion of FeS to pyrite at high pH (Berner, 1969). Pyrite formation and subsequent burial below the oxidizing zone would remove some of the available iron and sulfur from further diagenetic cycling because pyrite is the thermodynamically stable iron-sulfur mineral in reducing sediments (Berner, 1964a).

The buffering of porewaters maintains most natural environments within the pH range of approximately 6.9–8.3 (Ben-Yaakov, 1973). Thus, goethite sulfidization and pyritization should occur more slowly under natural conditions than in the very low pH (<5) experiments. The major effect of high pH is to slow down the initial Fe(III)-sulfide redox reaction, which is rapid at acidic pH. Acidic conditions can be generated, however, by bacterial processes in micro-environments or in organic-rich swamps and marshes (ZoBell, 1954; Birnbaum and Wireman, 1984). Thus, the very low pH of some experiments could be encountered in these natural environments, and the formation of FeS and FeS₂ may be rapid; however, in most terrestrial environments pyrite formation is limited by sulfate availability and not by iron or pH controls (Goldhaber and Kaplan, 1975).

The rates of iron monosulfide and pyrite formation in our study are more rapid than would occur in natural settings because diffusion of reactants in a heterogeneous sediment-water system is slow (Rickard, 1969a, b; Berner, 1970; Canfield, 1989). Because our system was well mixed, unlike natural sediments, diffusive control of the reactions was minimized.

Pyrite Texture

The morphology of the solids produced in our experiments implicates chemical dissolution of α -FeOOH, S⁰, and FeS in the sequence α -FeOOH + H₂S → FeS + S⁰ → FeS₂. The discrete blade morphology of the α -FeOOH was not retained by the FeS or S₈ that formed (as shown in fig. 4A). In addition, pseudomorphic replacement of FeS or S₈ by FeS₂ was not observed in the early stages of experiments. Instead, pyrite spheres were formed that did not resemble FeS or S₈ textures or sizes. The rapid formation of pyrite as the result of undersaturation of FeS indicates that dissolution of FeS is important in the growth of pyrite. Low-temperature FeS₂ formation likely involves dissolution of both FeS and S⁰, but as temperature increases the solid-solid reaction of FeS and S⁰ may become more important (Rickard, 1975). The spatial association of FeS₂ and S⁰ shown in figure 5B suggests that solid surfaces may be involved in pyrite formation, but our results do not allow for conclusive identification of the mechanisms involved in the conversion of FeS to FeS₂ under these conditions.

The only apparent difference in pyrite specifically attributable to the slow or fast FeS₂ precipitation sequences

is an increase in sphere size with time (figs. 6, 7). This increase suggests that iron and sulfur continue to be added to the early formed pyrite spheres. The spherical texture may represent the result of one of the major, early FeS₂-forming pathways in natural environments. Pyritic microspheres have been observed in different sedimentary environments, including near-shore sediments of Long Island Sound (Canfield and Berner, 1987) and the Gulf of California (Berner, 1964b, 1969) and organic-rich swamps (Postma, 1982). Our ionic strength results indicate that the size of a pyrite sphere may depend, in part, on salinity and thus reflect the environment of formation. Euhedral pyrite may result from pyrite precipitation without formation of an intermediate FeS solid (for example, Fe_(aq)²⁺ + S_{n(aq)}²⁻ → FeS₂ + S_{n-2(aq)}²⁻) (Howarth, 1978; Raiswell, 1982) rather than from conversion of monosulfides to pyrite (Goldhaber and Kaplan, 1974). The lack of euhedral pyrite under these experimental conditions—that is, in the presence of an FeS precursor—supports this observation.

Other Reaction Products

The inorganic formation of iron mono- and disulfides from iron oxyhydroxide produces and consumes elemental sulfur, a recognized mineral phase in marine sediments (Berner, 1964b). Pyzik (1976) reported that elemental sulfur comprises as much as 90 percent of the sulfide oxidation products of α-FeOOH sulfidization at pH 7.0–8.5; however, the quantitative significance of this inorganic sulfur formation mechanism in natural systems is not known because many reactions involving sulfur are biologically mediated. The distribution of sulfur among the pyrite, monosulfide, sulfate, and elemental sulfur phases represents the difference between zerovalent sulfur production and consumption, including oxidation and reduction of sulfur species by microorganisms (Troelsen and Jorgensen, 1982). Because elemental sulfur is not abundant in most marine sediments (2–4 weight percent), it may become limiting in the conversion of monosulfides to pyrite (Berner, 1964b).

Pyrite did not form in any low pH experiment until after elemental sulfur was produced. Berner and others (1979) noted that the conversion of mackinawite and greigite to FeS₂ in marine sediments requires excess H₂S. Thus, excess zerovalent sulfur or H₂S_(aq), or both, may be critical to the subsequent formation of pyrite under these conditions (Berner, 1970; Sweeney and Kaplan, 1973). In the absence of excess sulfide, mackinawite and greigite are metastable phases in marine sediments.

The reduction of iron(III) by sulfide species at low pH and high H₂S produces aqueous iron(II). Measured values of dissolved iron and H₂S in marsh sediments indicate that greigite solubility controls aqueous iron concentrations in the top 10–15 cm of sediment and FeS solubility controls

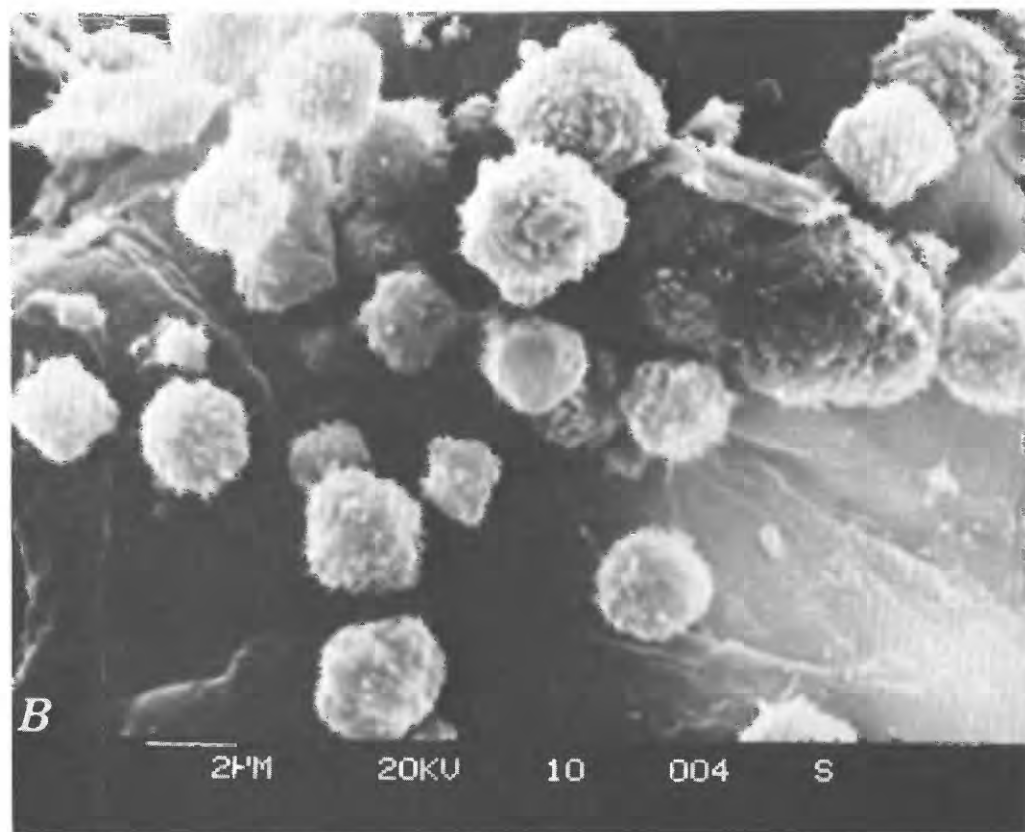
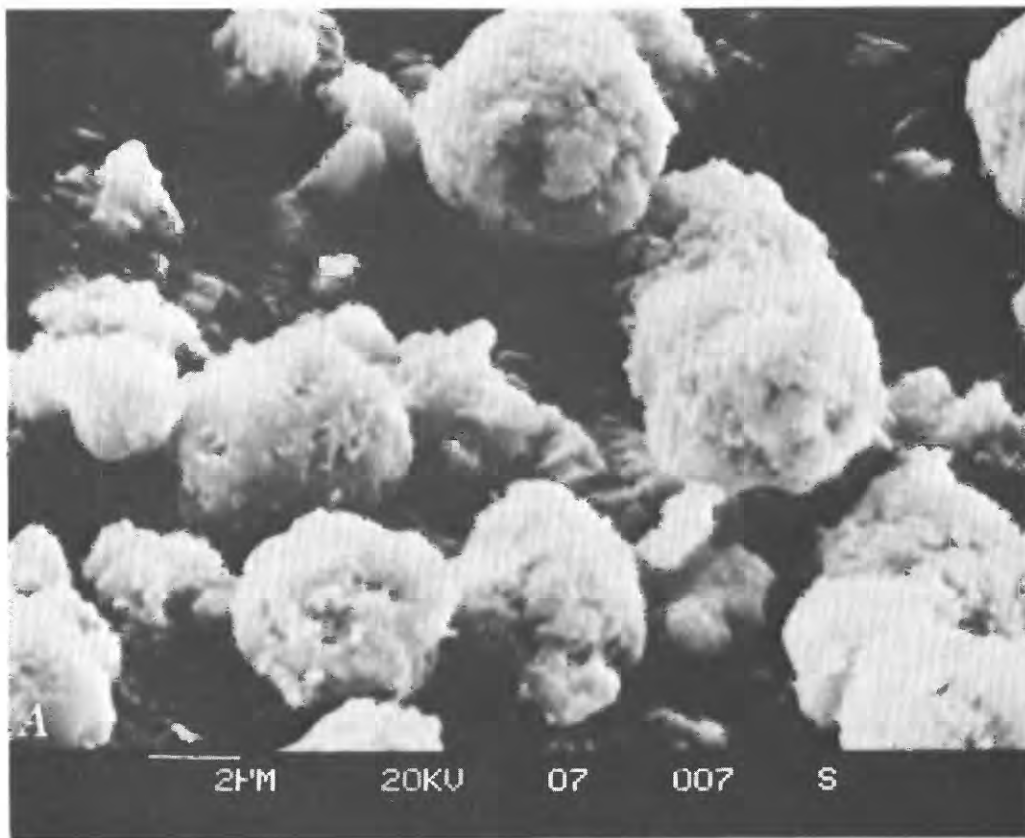
aqueous iron in the 50–55 cm interval (Boulegue and others, 1982). The concentration of aqueous iron(II) in our experiments (10⁻⁴–10⁻⁶ M) indicates that FeS, not FeS₂, is the controlling phase for dissolved iron in most sediments. Aqueous iron can react with different sulfide species in solution to form a variety of iron sulfides (Berner, 1964a; Rickard, 1969a, b). Once Fe³⁺ is reduced, the more mobile, soluble Fe²⁺_(aq) may form sulfides at sites removed from the point of dissolution of the iron source (goethite).

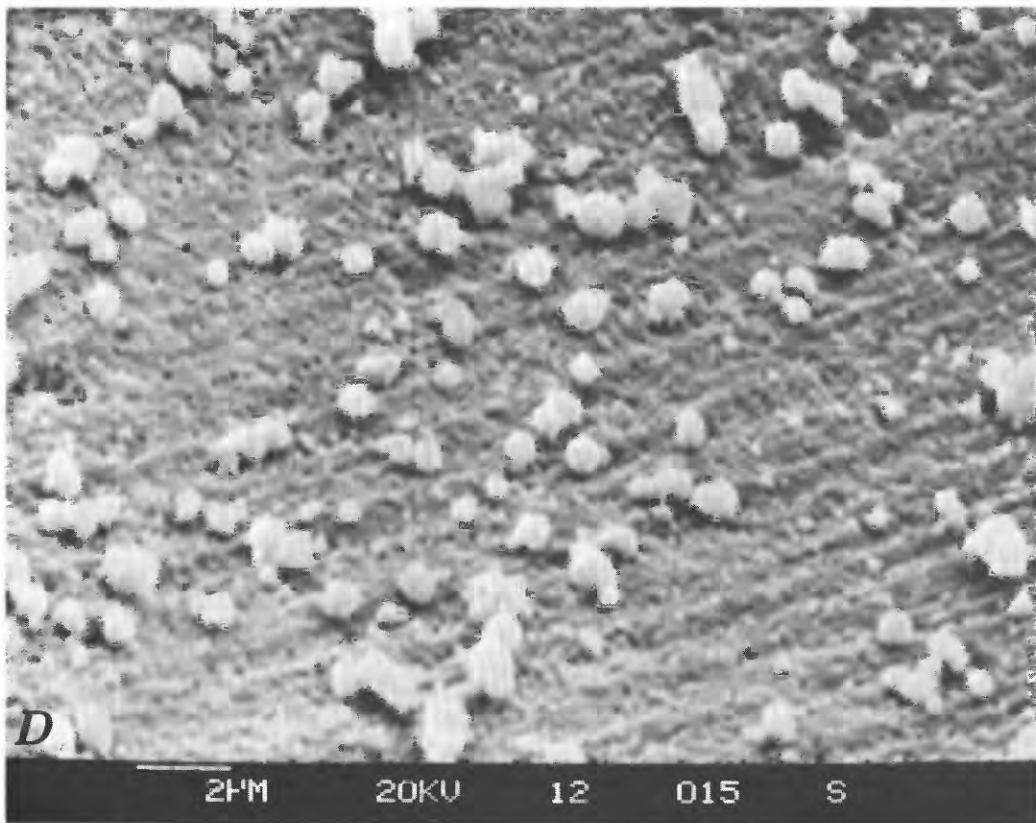
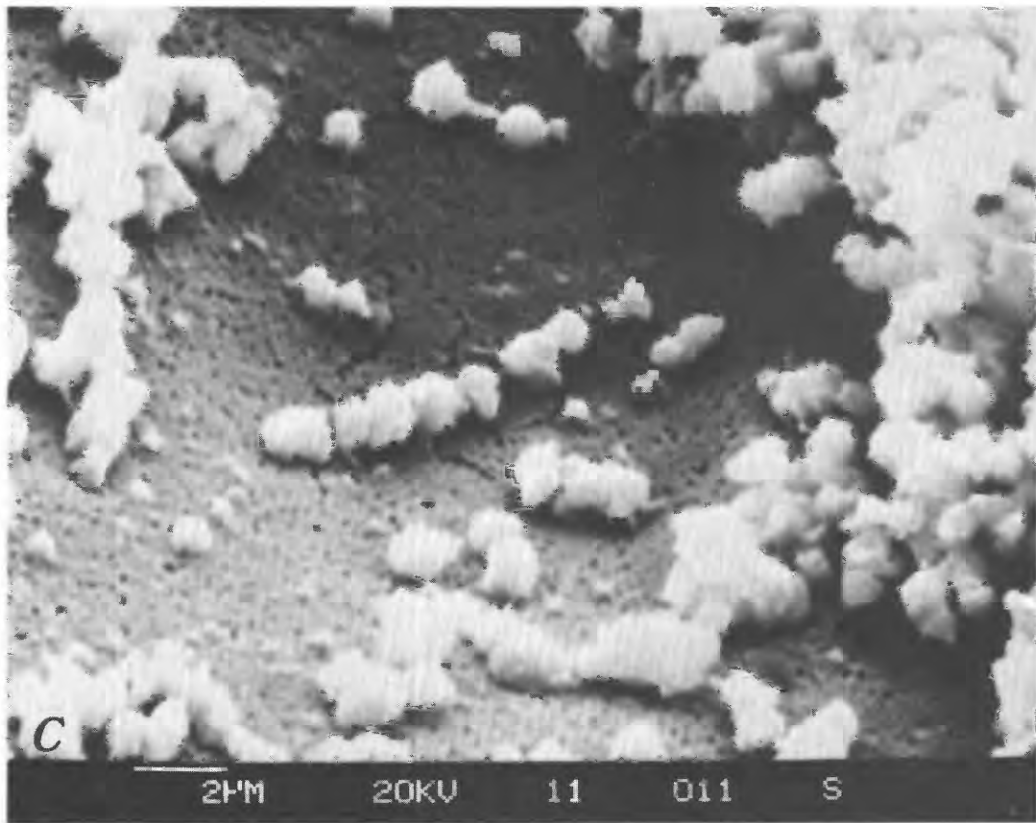
Green rust phases are formed primarily through reaction of Fe(II)-hydroxy and Fe(III)-hydroxy species (Newman, 1987) and commonly are intermediate-stage products resulting from the incomplete oxidation or reduction of iron-bearing substances. In natural environments, anaerobic conditions provide soluble iron(II)-hydroxy species necessary for formation of these minerals. The mottling of some gleyed soil horizons and the gray-green color in the uppermost layers of some lake and marine sediments have been attributed to the presence of mixed reduced and oxidized iron minerals, which may include green rust phases (Buurman, 1980; Newman, 1987). Soils and lake sediments containing available iron and having seasonal fluctuations of photosynthetic and respiratory processes and thus unstable redox conditions are likely environments in which green rusts may form. However, green rusts probably are transient phases that are unstable with respect to goethite and lepidocrocite (Newman, 1987). Our experimental results point to variations in pH and redox conditions as key factors in green rust formation.

Absence of Other Sulfide Reaction Products

Marcasite was not detected by X-ray diffraction or reflected-light petrography. Marcasite, which is commonly found in association with pyrite, requires a low pH to form (Goldhaber and Stanton, 1987), but it did not form in our experiments despite the low pH_(init) (4–5) in the free-drift runs. Evidently, under the conditions studied, marcasite formation is inhibited by some unknown mechanism if α-FeOOH is the iron source.

Figure 8 (following pages). Scanning electron microscope photomicrographs illustrating decrease in pyrite sphere size with increasing ionic strength. Micrographs are arranged in order from lowest to highest ionic strength and from highest to lowest modal sphere diameter. Bar scale on all micrographs is 2 μm. *A*, Pyrite spheres from experiment 7. Ionic strength, 0.1 M; modal diameter, 4.4 μm; time, 139 hours. *B*, Pyrite spheres from experiment 10. Ionic strength, 0.3 M; modal diameter, 2.7 μm; time, 143 hours. Small needles are probably melanterite, an oxidation product of pyrite. *C*, Pyrite spheres from experiment 11. Ionic strength, 0.7 M; modal diameter, 0.7 μm; time, 144 hours. *D*, Pyrite spheres from experiment 12. Ionic strength, 2.0 M; modal diameter, 0.6 mm; time, 144 hours.





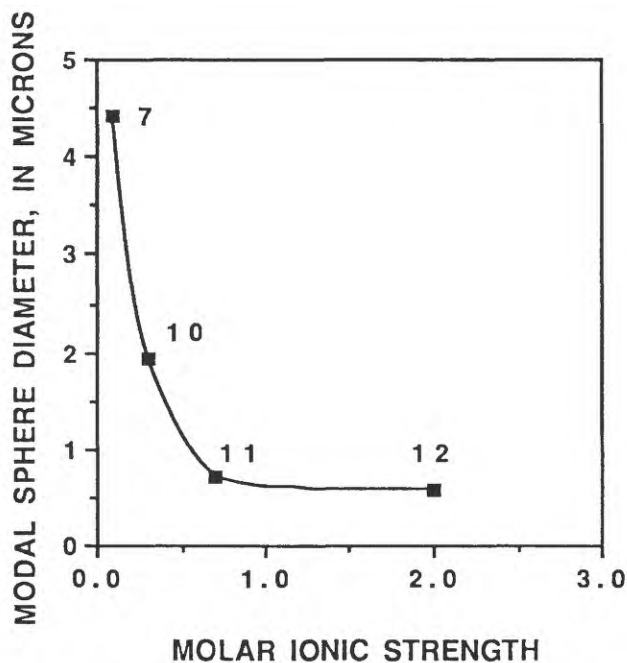


Figure 9. Modal sphere diameter (MD) versus ionic strength for experiments 7, 10, 11, and 12. Sphere diameters are from samples taken at approximately the same time from each experiment.

X-ray diffraction data suggest that greigite either did not form during the experiment, formed in low quantities (<5 volume percent), or formed and was converted rapidly to another phase. Rickard (1969b) noted that greigite forms in the pH range of 2.5–6.5, well within the range employed in this study. The formation of greigite may require, in a manner similar to marcasite, a different mechanism at low pH if goethite is the iron source. It has been postulated that greigite contains ferric iron and therefore requires small amounts of oxygen for formation (Goldhaber and Kaplan, 1974). The rigorous exclusion of air and the strongly reducing conditions employed at low pH and 10 percent $H_2S_{(g)}$ should rapidly reduce ferric iron.

The stable form of pyrrhotite ($Fe_{1-x}S$) under sedimentary conditions, hexagonal pyrrhotite (Arnold, 1969), has been synthesized at low temperatures, but there is little evidence for its rapid formation in modern sediments (Pyzik, 1976). In our study, pyrrhotite was not detected. Similar to greigite, it could not be determined if it was not formed or if it was rapidly produced and converted to some other sulfide phase. The ratio of iron to sulfur in pyrrhotite is approximately 0.9, based on the mineral formula $Fe_{1-x}S$, where x is less than 0.125 (Ward, 1970). Pyrrhotite contains less iron than mackinawite and iron:sulfur ratios of our experimental products indicate that the initial FeS phases were iron rich (Fe:S >1.0) rather than iron deficient (table 2).

CONCLUSIONS

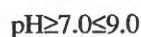
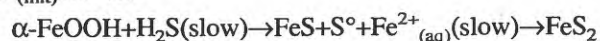
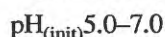
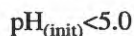
A variety of solid and aqueous iron-bearing products are initially formed from the reaction of goethite and aqueous hydrogen sulfide. The transformation of goethite to pyrite takes place slowly at the near-neutral pH of most natural sediments and perhaps not at all at the high pH (>9.0) of some alkaline lake systems. Thus, the early diagenesis of iron and sulfur may follow any of several pathways that are controlled primarily by pH; however, other factors operating in natural depositional settings (for example, rate of sulfate reduction) that were not taken into account in this inorganic system may influence these pathways.

It has been postulated that the Green River Formation was deposited in an alkaline environment that had a pH of more than 8.0 (Tuttle, 1988). High pH results of our study indicate that iron probably was not immediately or directly incorporated into pyrite. High pH may also explain the lack of pyrite in modern analogs of the Green River lacustrine system, such as Walker Lake and Soap Lake (Tuttle, 1988). A more complex, long-term sequence of diagenetic events must have produced the present-day suite of iron sulfide minerals in the Green River Formation. The absence of pyrrhotite, greigite, and marcasite indicates that these minerals may form only after extended time periods or under different conditions than examined in our study.

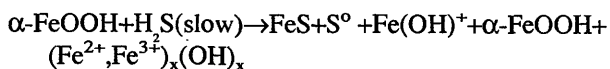
Pyrite produced during the experiments has a spherical morphology that superficially resembles early stages of framboidal development. Euhedral crystals were not formed in our study. Thus, formation of euhedral or framboidal forms of pyrite may also require extended reaction time or other mechanistic pathways. Increasing ionic strength produces smaller spheres for otherwise similar conditions. Pyrite formed under controlled conditions, however, may differ from that in natural unconsolidated sediments; other factors not considered here may significantly affect pyrite formation rates and textures (Goldhaber and Kaplan, 1974; Raiswell, 1982; Berner and Westrich, 1984; Canfield and Berner, 1987).

SUMMARY

The pathways of formation of iron monosulfide and pyrite from goethite, with qualitative indicators of the reaction rates, are summarized below.



pH \geq 9.0



Differing amounts of solid α -FeOOH were reacted with H_2S over a range of chemical conditions at 30 °C. Variations in the pH, ionic strength, and concentrations of iron and sulfur species led to a variety of reaction products that formed at differing rates. The solid products of the goethite–hydrogen sulfide reaction at acidic pH (4–7) were zerovalent sulfur, iron monosulfide, and, eventually, pyrite. Pyrite was not a product of experiments conducted at pH greater than 7.0. The overall rate of pyrite formation for varied total dissolved sulfide and iron concentrations was from 10^{-7} to 10^{-9} M/min for pH 4–7.

The major solids formed during experiments conducted at higher pH (>7–10) were iron monosulfide, zerovalent sulfur, and ferrous-ferric oxyhydroxides. Unreacted goethite was a common constituent of the solids over the time span of high pH experiments.

REFERENCES CITED

- Adamson, A.W., 1976, *Physical chemistry of surfaces* (3rd ed.): New York, John Wiley and Sons, 698 p.
- Arnold, R.G., 1969, Pyrrhotite phase relationships below 304 \pm 6 °C at <1 atm total pressure: *Economic Geology*, v. 64, p. 405–419.
- Atkinson, R.J., Posner, A.M., and Quirk, J.P., 1968, Crystal nucleation in Fe(III) solutions and hydroxide gels: *Journal of Inorganic and Nuclear Chemistry*, v. 30, p. 2371–2381.
- Bartlett, J.K., and Skoog, D.A., 1954, Colorimetric determination of elemental sulfur in hydrocarbons: *Analytical Chemistry*, v. 26, no. 6, p. 1008–1011.
- Ben-Yaakov, S., 1973, pH buffering of pore water of recent anoxic marine sediments: *Limnology and Oceanography*, v. 18, no. 1, p. 86–94.
- Berner, R.A., 1964a, Iron sulfides formed from aqueous solution at low temperatures and atmospheric pressures: *Journal of Geology*, v. 72, p. 293–306.
- _____, 1964b, Distribution and diagenesis of sulfur in some sediments from the Gulf of California: *Marine Geology*, v. 6, p. 117–140.
- _____, 1969, The synthesis of framboidal pyrite: *Economic Geology*, v. 64, p. 383–384.
- _____, 1970, Sedimentary pyrite formation: *American Journal of Science*, v. 268, p. 1–23.
- _____, 1972, Sulfate reduction, pyrite formation, and the oceanic sulfur budget, in Dyrssen, D., and Jagner, D., *The changing chemistry of the oceans—Nobel Symposium 20*: Stockholm, Almquist and Wiksell, p. 347–361.
- Berner, R.A., Baldwin, B., and Holdren, G.R., 1979, Authigenic iron sulfides as paleosalinity indicators: *Journal of Sedimentary Petrology*, v. 49, no. 4, p. 1345–1350.
- Berner, R.A., and Westrich, J.T., 1984, The role of sedimentary organic matter in bacterial sulfate reduction—The G model tested: *Limnology and Oceanography*, v. 29, no. 2, p. 236–249.
- Birnbaum, S.J., and Wireman, J.W., 1984, Bacterial sulfate reduction and pH—Implications for early diagenesis: *Chemical Geology*, v. 43, p. 143–149.
- Boulegue, J., Lord, J.L., III, and Church, T.M., 1982, Sulfur speciation and associated trace metals (Fe, Cu) in the pore waters of Great Marsh, Delaware: *Geochimica et Cosmochimica Acta*, v. 46, p. 453–464.
- Buurman, P., 1980, *Paleosols in the Reading Beds (Paleocene) of Alum Bay, Isle of Wight, U.K.*: *Sedimentology*, v. 27, p. 593–606.
- Canfield, D.E., 1988, *Sulfate reduction and the diagenesis of iron in anoxic marine sediments*: New Haven, Connecticut, Yale University, Ph.D. thesis, 248 p.
- _____, 1989, Reactive iron in marine sediments: *Geochimica et Cosmochimica Acta*, v. 53, p. 619–632.
- Canfield, D.E., and Berner, R.A., 1987, Dissolution and pyritization of magnetite in anoxic marine sediments: *Geochimica et Cosmochimica Acta*, v. 51, p. 645–659.
- Carroll, D., 1958, Role of clay minerals in the transportation of iron: *Geochimica et Cosmochimica Acta*, v. 14, p. 1–27.
- Cutter, G.A., and Velinsky, D.J., 1988, Temporal variations of sedimentary sulfur in a Delaware salt marsh: *Marine Chemistry*, v. 23, p. 311–327.
- Garrels, R.M., and Christ, C.L., 1965, *Solutions, minerals, and equilibria*: San Francisco, Freeman, Cooper, 450 p.
- Gibbs, R.J., 1973, Mechanism of trace metal transport in rivers: *Science*, v. 180, p. 71–73.
- Goldhaber, M.B., and Kaplan, I.R., 1974, The sedimentary sulfur cycle, in Goldberg, E.D., ed., *The sea*, v. 5: New York, John Wiley and Sons, p. 569–655.
- _____, 1975, Controls and consequences of sulfate reduction in recent marine sediments: *Soil Science*, v. 119, p. 42–55.
- Goldhaber, M.B., and Stanton, M.R., 1987, Experimental formation of marcasite at 150–200 °C—Implications for the origin of carbonate-hosted Pb/Zn deposits: *Geological Society of America, Abstracts with Programs*, v. 19, no. 7, p. 678.
- Goldstein, J.I., Newburg, D.E., Echlin, P., Joy, D.C., Fiori, C., and Lifshin, E., 1981, *Scanning electron microscopy and X-ray microanalysis*: New York, Plenum Press, 673 p.
- Hallberg, R.O., 1972, Iron and zinc sulfides formed in a continuous culture of sulfate-reducing bacteria: *Neues Jahrbuch für Mineralogie Monatshefte*, v. 11, p. 481–500.
- Howarth, R.W., 1978, Pyrite—Its rapid formation in a salt marsh and its importance in ecosystem metabolism: *Science*, v. 203, p. 49–51.
- Kester, D.R., Byrne, R.H., and Liang, Y., 1975, Redox reactions and solution complexes of iron in marine systems in Church, T.M., ed., *Marine chemistry of the coastal environment*: American Chemical Society, p. 56–79.
- Kribek, B., 1975, The origin of framboidal pyrite as a surface effect of sulphur grains: *Mineralium Deposita*, v. 10, p. 389–396.
- LaKind, J.S., and Stone, A.T., 1989, Reductive dissolution of goethite by phenolic reductants: *Geochimica et Cosmochimica Acta*, v. 53, p. 961–971.
- Love, L.G., and Amstutz, G.C., 1966, Review of microscopic pyrite: *Fortschritte der Mineralogie*, v. 43, p. 273–309.

- Luther, G.W., Giblin, A., Howarth, R.W., and Ryans, R.A., 1982, Pyrite and oxidized mineral phases formed from pyrite oxidation in salt marsh and estuarine sediments: *Geochimica et Cosmochimica Acta*, v. 46, p. 2665–2669.
- Morse, J.W., Millero, F.J., Cornwell, J.C., and Rickard, D., 1987, The chemistry of the hydrogen sulfide and iron sulfide systems in natural waters: *Earth Science Reviews*, v. 24, p. 1–42.
- Murowchick, J.B., and Barnes, H.L., 1987, Effects of temperature and degree of supersaturation on pyrite morphology: *American Mineralogist*, v. 72, p. 1241–1250.
- Newman, A.C.D., ed., 1987, Chemistry of clays and clay minerals, in *Mineralogical Society Monograph 6*: New York, John Wiley and Sons, 480 p.
- Pankow, J.F., and Morgan, J.J., 1979, Dissolution of tetragonal ferrous sulfide (mackinawite) in anoxic aqueous systems; 1, Dissolution rate as a function of pH, temperature, and ionic strength: *Environmental Science and Technology*, v. 13, no. 10, p. 1248–1255.
- _____, 1980, Dissolution of tetragonal ferrous sulfide (mackinawite) in anoxic aqueous systems; 2, Implications for the cycling of iron, sulfur, and trace metals: *Environmental Science and Technology*, v. 14, no. 2, p. 183–186.
- Parkhurst, D.L., Thorstenson, D.C., and Plummer, L.N., 1980, PHREEQE—A computer program for geochemical calculations: U.S. Geological Survey Water Resources Investigations 80–96, 216 p.
- Postma, D., 1982, Pyrite and siderite formation in brackish and freshwater swamp sediments: *American Journal of Science*, v. 282, p. 1151–1183.
- Pyzik, A.J., 1976, The kinetics and mechanism of sedimentary iron sulfide formation: Baltimore, University of Maryland, Ph.D. thesis, 143 p.
- Pyzik, A.J., and Sommer, S.E., 1981, Sedimentary iron monosulfides—Kinetics and mechanism of formation: *Geochimica et Cosmochimica Acta*, v. 45, p. 687–698.
- Raiswell, R.A., 1982, Pyrite texture, isotopic composition, and the availability of iron: *American Journal of Science*, v. 282, p. 1244–1263.
- Rickard, D.T., 1969a, The chemistry of iron sulfide formation at low temperatures: *Stockholm Contributions in Geology*, v. 20, p. 67–95.
- _____, 1969b, The microbiological formation of iron sulfides: *Stockholm Contributions in Geology*, v. 20, p. 49–66.
- _____, 1975, Kinetics and mechanism of pyrite formation at low temperatures: *American Journal of Science*, v. 275, p. 636–652.
- Roberts, W.M.B., Walker, A.L., and Buchanan, A.S., 1969, The chemistry of pyrite formation in aqueous solution and its relation to the depositional environment: *Mineralium Deposita*, v. 4, p. 18–29.
- Schoonen, M.A.A., and Barnes, H.L., 1988, Kinetics of hydrothermal pyrite and marcasite formation from solution: *Geological Society of America, Abstracts with Programs*, v. 20, no. 7, p. A43.
- Shaw, D. J., 1980, Introduction to colloid and surface chemistry (3rd ed.): London, Butterworths, 273 p.
- Skoog, D.A., and West, J.K., 1982, Fundamentals of analytical chemistry (4th ed.): Philadelphia, Saunders College Publishing, 859 p.
- Stumm, W., and Morgan, J.J., 1981, Aquatic chemistry (2nd ed.): New York, John Wiley and Sons, 780 p.
- Sweeney, R.E., and Kaplan, I.R., 1973, Pyrite framboid formation—Laboratory synthesis and marine sediments: *Economic Geology*, v. 68, p. 618–634.
- Tewari, P.H., and Campbell, A.B., 1976, Dissolution of iron sulfide (troilite) in aqueous sulfuric acid: *Journal of Physical Chemistry*, v. 80, no. 17, p. 1844–1848.
- Troelsen, H., and Jorgensen, B.B., 1982, Seasonal dynamics of elemental sulfur in two coastal sediments: *Estuarine, Coastal, and Shelf Science*, v. 15, p. 255–266.
- Tuttle, M.L., 1988, Geochemical evolution and depositional history of sediment in modern and ancient saline lakes—Evidence from sulfur geochemistry: Golden, Colorado School of Mines, Ph.D. thesis, 312 p.
- van Straten, H.A., Schoonen, M.A.A., Verheul, R.C.S., and deBruyn, P.L., 1985, Precipitation from supersaturated aluminate solutions; IV, Influence of citrate ions: *Journal of Colloid and Interface Science*, v. 106, p. 175–185.
- Ward, J.C., 1970, The properties of some iron sulphides: *Pure and Applied Chemistry*, v. 20, p. 175–206.
- ZoBell, C.E., 1954, Changes produced by microorganisms in sediments after deposition: *Journal of Sedimentary Petrology*, v. 24, no. 3, p. 127–136.

Chapter F

Effects of Source, Depositional Environment, and Diagenesis on Characteristics of Organic Matter in Oil Shale from the Green River Formation, Wyoming, Utah, and Colorado

By WALTER E. DEAN and DONALD E. ANDERS

U.S. GEOLOGICAL SURVEY BULLETIN 1973

GEOCHEMICAL, BIOGEOCHEMICAL, AND SEDIMENTOLOGICAL STUDIES OF THE
GREEN RIVER FORMATION, WYOMING, UTAH, AND COLORADO

CONTENTS

Abstract	F1
Introduction	F1
Analytical methods	F3
Results and discussion	F3
Pyrolysis and gas chromatography data	F3
Carbon isotope data	F11
Conclusions	F14
References cited	F15

FIGURES

1. Map showing Laramide basins and uplifts, southwestern Wyoming, northwestern Colorado, and northeastern Utah F2
2. Chart showing stratigraphy of cores of Green River Formation F3
- 3-6. Plots of:
 3. Depth versus total organic carbon, hydrogen index, oxygen index, and $\delta^{13}\text{C}$ F7
 4. Oxygen index versus hydrogen index F8
 5. Pyrolysis data F9
 6. Pyrolysis $S_1 + S_2$ yield for samples of oil shale of different geologic ages and from different geologic environments F9
- 7-9. Gas chromatograms of saturated-hydrocarbon fraction of:
 7. Samples from three depths in Blacks Fork core F10
 8. A sample from Mahogany zone in Coyote Wash core F11
 9. Samples from three depths in WOSCO EX-1 core F12
10. Chart showing range of $\delta^{13}\text{C}$ values in lake sediments, peat, lake plankton, plants, and samples of Green River Formation F12
11. Plots of hydrogen index versus $\delta^{13}\text{C}$ in samples of Green River Formation F13

TABLES

1. Fischer assay oil yield, total organic carbon content, Rock-Eval pyrolysis results, and values of $\delta^{13}\text{C}$ of organic carbon for samples of oil shale from the Coyote Wash, Blacks Fork, and 01A cores of the Green River Formation F4
2. Fischer assay oil yield, total organic carbon content, and Rock-Eval pyrolysis results for samples of oil shale from the WOSCO EX-1 core of the Green River Formation F6

Effects of Source, Depositional Environment, and Diagenesis on Characteristics of Organic Matter in Oil Shale from the Green River Formation, Wyoming, Utah, and Colorado

By Walter E. Dean and Donald E. Anders

Abstract

Results of Rock-Eval pyrolysis and stable-carbon isotope analysis were used to assess the richness, source, and degree of degradation of oil shale in the Green River Formation sampled in basin-center cores from the Green River basin of Wyoming, Piceance basin of Colorado, and Uinta basin of Utah. By far the richest oil-shale samples are from the Piceance basin, particularly from the Mahogany zone near the top of the Parachute Creek Member of the Green River Formation. Some samples of oil shale from the other two basins are as rich, but, in general, greater oxidation of organic matter and dilution of organic matter by terrigenous clastic material has taken place in these shallower lake basins.

Hydrogen-rich organic matter accumulated in deeper, less saline phases of Eocene Lake Gosiute, represented by the Tipton Shale and Laney Members of the Green River Formation in the Green River basin, but much of the organic matter that accumulated during deposition of the shallower, more saline intervening Wilkins Peak Member was from both algal and terrestrial sources. Extremely high algal productivity and rapid burial of ^{13}C -depleted organic carbon in Eocene Lake Uinta, culminating in the highly organic-carbon-rich strata of the Mahogany zone in the Piceance and Uinta basins, produced enrichment of ^{13}C in surface waters of the lake that eventually affected the isotopic composition of organic carbon fixed by phytoplankton.

INTRODUCTION

The Green River Formation (Eocene) of the Green River, Piceance, and Uinta basins of Wyoming, Colorado, and Utah, respectively, is one of the most remarkable accumulations of organic matter in the world. The "oil

shales" of this formation commonly contain more than 10 weight percent organic carbon in a suite of sedimentary rocks that is as varied as any imaginable, from dolomitic marlstone to mudstone, siltstone, sandstone, and volcanic ash and containing a multitude of exotic sulfide, evaporite, and authigenic silicate minerals (Desborough and Pitman, 1974). With all of this lithologic variability, it is surprising that few of the rocks in the Green River Formation called "oil shale" can be classified as shales. The dominant lithology of the richest oil shales in the Piceance and Uinta basins is dolomitic marlstone, but even that classification belies the complexity of the rock, which is a mixture of almost every possible combination of carbonate minerals in the system Ca-Mg-Fe-CO_3 (Desborough and Pitman, 1974; Desborough, 1978). The complex mineralogy and geochemistry of the Green River make it even more remarkable because these minerals, most of which are autochthonous or authigenic, act as dilutants to the organic matter; without these diluting minerals, the Green River Formation would consist almost entirely of solid kerogen. The purposes of this paper are to characterize kerogen in the Green River Formation using results of Rock-Eval pyrolysis, gas chromatography, and stable-carbon isotope analysis and to interpret these results in terms of source, depositional environment, and diagenesis of organic matter.

Splits of selected samples of the Green River Formation from the Blacks Fork core in the Green River basin, Wyoming, the 01A core in the Piceance basin, Colorado, and the Coyote Wash core in the Uinta basin, Utah (figs. 1, 2), collected for inorganic geochemical analysis (P.H. Briggs and M.L. Tuttle, written commun., 1985) were used. Descriptions of these samples are given in

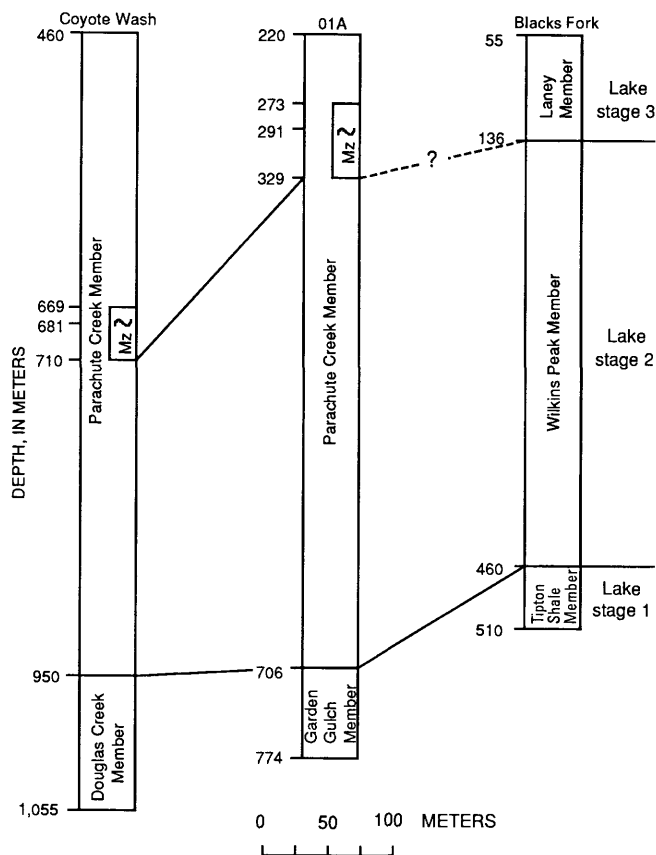


Figure 2. Stratigraphy of cores of Green River Formation analyzed in this study. Location of core holes shown in figure 1. Mz, Mahogany zone.

EX-1 core (fig. 1) (Anders and Gerrild, 1984), and from the Piceance basin we will use additional data from the entire Green River Formation in the Colorado no. 1 core (fig. 1) (Smith and others, 1968; Anders and Robinson, 1973; Robinson and Cook, 1975).

ANALYTICAL METHODS

The Rock-Eval pyrolysis method provides a rapid estimate of the type and hydrocarbon-generating potential of sedimentary organic matter (Espitalié and others, 1977). Programmed heating of a sample in a helium atmosphere results in the generation of hydrocarbons (HC) and carbon dioxide. Free or adsorbed HC yield is recorded as the area under the first peak on a program (S_1) (mg HC/g sample) during heating of the sample to 250 °C for 5 min. The second pyrolysis peak (S_2) represents hydrocarbons generated by thermal breakdown of kerogen during heating of the sample from 250 to 550 °C. CO_2 is also generated by kerogen degradation and is retained during the heating interval from 250 to 390 °C and analyzed as the integrated area under the third peak on the pyrogram (S_3) (mg CO_2 /g sample). The Rock-Eval II instrument used for these

analyses also measures total organic carbon (TOC) as the sum of carbon in the S_1 and S_2 hydrocarbons plus that determined by oxidizing the residual carbon at 600 °C. In addition to the S_1 , S_2 , and S_3 integrated peaks, the results are expressed in terms of a hydrogen index (HI), which is the S_2 peak normalized to the total organic carbon (TOC) content of the sample (mg HC/g TOC), and an oxygen index (OI), which is the S_3 peak normalized to TOC content of the sample (mg CO_2 /g TOC).

The soluble-organic-matter (SOM) fraction of whole-rock samples was obtained by Soxhlet extraction with chloroform for 24 hours. The extract was concentrated under nitrogen to remove the chloroform, then diluted with iso-octane. A concentrate of the SOM in iso-octane was fractionated by column chromatography on silica gel/alumina by eluting successively with iso-octane, benzene, and benzene-methanol to collect the saturated hydrocarbon, aromatic hydrocarbon, and resin fractions, respectively. The saturated hydrocarbon fractions were analyzed by capillary-column gas chromatography using a Hewlett-Packard 5880 instrument with a flame-ionization detector. Peaks on chromatograms were identified by co-elution using standards or by fragmentation patterns of gas chromatography/mass spectrometry (GC/MS) electron impact spectra. Relative abundances of hydrocarbons are indicated by the relative intensities of detector responses.

Stable-carbon isotope ratios of organic carbon were determined by standard techniques (for example, Pratt and Threlkeld, 1984). Powdered samples were oven dried at 40 °C and reacted with 0.5N HCl for 24 hours to dissolve carbonate minerals. If all of the carbonate was not removed by the first acid leach, the sample was reacted with acid for an additional 24-hour period. The residue was centrifuged, decanted, washed three times with deionized water, dried under a stream of flowing nitrogen at 50 °C, and combusted at 1,000 °C under oxygen pressure in a LECO induction furnace. The resulting CO_2 was dehydrated and purified in a high-vacuum gas-transfer system, and the isotope ratios determined using a Finnigan MAT 251 6 in., 90° sector, isotope-ratio mass spectrometer. Results are reported in the usual delta notation as the per mil difference relative to the Pee Dee belemnite marine-carbonate standard (PDB):

$$\delta^{13}C (\text{‰}) = [(R_{\text{sample}}/R_{\text{PDB}}) - 1] \times 10^3,$$

where R is the ratio $^{13}C : ^{12}C$.

RESULTS AND DISCUSSION

Pyrolysis and Gas Chromatography Data

Results of Rock-Eval pyrolysis of samples from the Coyote Wash, Blacks Fork, and 01A cores are given in table 1 along with TOC values determined by LECO (Tuttle and

Table 1. Fischer assay oil yield, total organic carbon content, Rock-Eval pyrolysis results, and values of $\delta^{13}\text{C}$ of organic carbon for samples of oil shale from the Coyote Wash, Black Forks, and 01A cores of the Green River Formation
 [TOC, total organic carbon; CW, Coyote Wash; BF, Blacks Fork; LECO indicates using a LECO induction furnace]

Sample number	Depth (meters)	Oil (gpt)	Oil (L/mt)	Percent TOC	
				LECO	Rock-Eval
CW-38	571	8	33	3.4	3.17
CW-31	661	16	67	5.6	5.08
CW-29	681	65	271	26.5	28.9
CW-28	697	16	66	2.5	2.59
CW-26	716	3	12	2.4	2.05
CW-20	789	18	75	7.6	7.25
CW-18	815	2	8	1.2	1.48
CW-13	880	13	54	5.8	6.41
CW-11	907	3	13	1.8	1.71
CW-01	1,043	14	58	3.3	4.31
BF-04	98	17	69	8.3	6.82
BF-06	125	12	52	4.1	3.64
BF-07	134	17	73	7.0	6.82
BF-08	144	2	9	1.5	2.18
BF-13	217	5	21	2.8	2.75
BF-19	299	5	19	4.1	4.65
BF-22	344	1	5	0.58	0.56
BF-23	353	23	98	8.3	8.69
BF-31	464	28	117	12.0	12.0
BF-34	500	3	10	10.6	12.0
01A-006	268	15	63	9.6	10.8
01A-014	290	70	292	33.7	37.5
01A-024	321	21	88	10.2	10.7
01A-036	358	15	63	23.0	27.3
01A-054	415	16	67	5.6	5.42
01A-062	437	17	71	17.9	20.10
01A-072	468	34	142	13.3	14.8
01A-084	504	4	17	7.4	7.51
01A-089	521	4	17	1.2	1.23
01A-102	559	30	125	15.0	18.0
01A-113	595	37	154	14.1	16.9
01A-132	651	17	71	8.5	9.06
01A-150	705	41	171	21.6	24.1
01A-154	717	23	96	11.8	12.5
01A-165	755	12	50	8.6	8.52
01A-172	773	12	50	3.7	3.67

Goldhaber, this volume). Results of Rock-Eval pyrolysis and TOC analyses of samples from the WOSCO EX-1 core are given in table 2. The results show that, in general, the agreement is good between TOC determined by the two methods. Values of TOC, HI, and OI are plotted versus depth for each of the three cores in figure 3. Values of HI and OI are plotted as cross plots for the three primary cores and the WOSCO core in figure 4. These cross plots are

equivalent to van Krevelen-type cross plots of H/C versus O/C and can be used to identify types of organic matter (types I, II, and III of Espitalié and others, 1977).

The richness of oil shale can be measured using our results by the organic-carbon content (TOC), the pyrolytic hydrocarbon yield ($S_1 + S_2$), or the hydrogen index (HI). The most commonly used measure of richness of Green River oil shale, however, is the amount of oil produced by

Table 1. Fischer assay oil yield, total organic carbon content, Rock-Eval pyrolysis results, and values of $\delta^{13}\text{C}$ of organic carbon for samples of oil shale from the Coyote Wash, Black Forks, and O1A cores of the Green River Formation—Continued

Sample number	S1 (mg/g)	S2 (mg/g)	S3 (mg/g)	H-index (mg/g)	O-index (mg/g)	$\delta^{13}\text{C}_{\text{org}}$ (per mil PDB)
CW-38	3.88	20.1	4.23	635	133	-29.6
CW-31	5.71	35.4	5.23	698	102	-29.8
CW-29	10.0	287	7.59	993	26	-28.5
CW-28	3.05	15.0	1.84	579	71	--
CW-26	3.63	12.2	1.29	595	63	-30.8
CW-20	1.21	61.6	2.02	849	27	-28.3
CW-18	0.51	5.0	0.68	339	45	-30.3
CW-13	0.78	42.8	2.69	667	41	-30.3
CW-11	0.78	10.3	0.91	603	53	-30.8
CW-01	1.80	24.6	1.68	570	38	-30.5
BF-04	1.27	55.3	5.10	810	74	-32.4
BF-06	1.07	33.5	2.28	921	62	-30.4
BF-07	1.66	51.8	5.38	816	84	-29.8
BF-08	0.35	7.3	1.96	333	89	-29.3
BF-13	0.94	14.9	3.77	541	137	-31.1
BF-19	0.87	26.0	3.50	559	75	-31.2
BF-22	0.29	2.7	9.95	480	1,800	-25.7
BF-23	1.63	60.3	6.88	694	79	-32.1
BF-31	0.92	97.0	6.11	809	50	-33.9
BF-34	1.95	113	3.15	938	26	-31.8
O1A-006	1.51	79.5	4.72	734	43	-29.9
O1A-014	5.63	365	16.3	973	43	-30.9
O1A-024	1.32	76.7	5.71	715	53	-29.8
O1A-036	5.20	246	7.10	901	25	-29.2
O1A-054	0.83	44.0	3.05	811	56	-30.1
O1A-062	4.36	169	71.3	839	354	-31.4
O1A-072	5.75	121	30.0	819	203	-30.6
O1A-084	2.96	60.7	33.3	808	443	-30.9
O1A-089	0.91	7.3	75.7	595	6,200	-30.1
O1A-102	6.82	146	27.7	815	153	-31.1
O1A-113	7.40	138.6	22.8	812	134	-31.0
O1A-132	3.55	77.3	73.2	852	808	-32.3
O1A-150	8.28	240	4.14	997	17	-32.9
O1A-154	5.31	119	2.55	955	20	-30.0
O1A-165	3.44	63.9	1.81	749	21	-30.9
O1A-172	1.58	27.6	1.39	751	37	-29.9

retorting by Fischer assay analysis, expressed as percent oil yield, gallons per ton (gpt), or liters per metric ton (L/mt) of rock. For comparison, Fischer assay results (tables 1 and 2), (S_1+S_2) yield, and HI for Green River oil shale are plotted in figure 5, all versus TOC. Results of Fischer assay analysis most closely approximate those of pyrolytic hydrocarbon yield (S_1+S_2) from Rock-Eval pyrolysis. Dyni and others (1990) presented Fischer assay and (S_1+S_2) hydrocarbon-yield data for 74 samples of oil shale from different ages

and geologic settings from around the world. These data are plotted in figure 6 along with a plot of data for Green River oil shale. Using the plots in figures 5 and 6 it should be possible to convert values of any one richness parameter to values of any other richness parameter.

By far the richest oil-shale samples in the three primary cores studied are from the O1A core from the Piceance basin. This is in line with resource estimates that show the richest oil shales of the Green River Formation are

Table 2. Fischer assay oil yield, total organic carbon content, and Rock-Eval pyrolysis results for samples of oil shale from the WOSCO EX-1 core, Utah, of the Green River Formation
 [TOC, total organic carbon; LECO indicates using a LECO induction furnace]

Depth. (feet)	Depth (meters)	Oil (gpt)	Oil (L/mt)	Percent TOC		S1 (mg/g)	S2 (mg/g)	S3 (mg/g)	H-index (mg/g)	O-index (mg/g)
				LECO	Rock-Eval					
2,181.5	664.92	9.1	37.95	4.3	3.7	1.73	26.34	3.65	717	99
2,200.4	670.68	9.6	40.03	4.4	4	3.99	30.53	1.95	772	49
2,240.5	682.90	11	45.87	5.2	4.4	3.25	34.05	3.39	766	75
2,270.5	692.05	34.2	142.61	14.3	11.5	1.4	105.96	10.52	921	91
2,280.5	695.10	22.6	94.24	9.9	8.3	2.15	78.62	5.17	946	62
2,290.5	698.14	9.4	39.20	3.8	3.7	0.63	32.57	2.89	873	77
2,300.6	701.22	37	154.29	15.8	12.8	1.91	118.29	14.04	924	109
2,320.5	707.29	15.8	65.89	6.9	5.7	2	48.38	5.52	851	97
2,341.0	713.54	30.3	126.35	13.6	11.2	1.33	99.3	10	885	89
2,359.5	719.18	5.7	23.77	2.9	2.8	1.14	18.97	2.05	677	73
2,377.2	724.57	--	--	3	2.6	0.27	18.88	2.51	723	96
2,408.5	734.11	1.4	5.84	0.8	0.7	1.79	2.3	1.48	353	227
2,422.6	738.41	0.9	3.75	0.9	0.9	2.09	3.67	1.77	412	198
2,444.5	745.08	5.9	24.60	3.1	2.7	0.54	15.76	4.24	594	163
2,459.5	749.66	8.4	35.03	3.7	4	1.97	20.61	7.53	516	188
2,480.5	756.06	20.8	86.74	9.3	7.6	1.37	66.5	9.25	877	122
2,500.5	762.15	27.2	113.42	12.1	10	2.94	85.12	8.71	851	87
2,521.5	768.55	15.2	63.38	7.7	5.8	1.08	47.52	5.84	826	101
2,536.5	773.13	8.5	35.45	4	2.9	0.3	21.63	3.46	748	119
2,560.5	780.44	2	8.34	1.3	1.9	0.06	4.9	1.34	526	144
2,573.5	784.40	2.6	10.84	1.4	1.3	0.17	7.9	1.84	589	137
2,607.5	794.77	6.6	27.52	3	2.2	0.24	12.83	3.08	580	139
2,618.5	798.12	5.5	22.94	2.2	1.8	0.34	9.91	2.52	538	136
2,640.5	804.82	14.8	61.72	5.9	4.1	0.23	32.32	4.88	786	118
2,660.5	810.92	5.3	22.10	2.6	2.2	1.08	13.41	4.08	615	187
2,680.5	817.02	6.7	27.94	3.7	3	0.76	18.11	3.76	607	126
2,706.5	824.94	6.7	27.94	3.2	3.4	0.73	20.05	3.34	597	99
2,723.5	830.12	10.9	45.45	5.3	4.7	0.57	34.57	4.57	741	98
2,746.5	837.13	19.1	79.65	8.5	6.5	0.63	55.69	6.07	863	94
2,760.5	841.40	19.1	79.65	8.4	6.6	2.62	50.5	9.67	761	145
2,780.5	847.50	6.9	28.77	2.9	2.4	0.27	15.23	3.33	634	138
2,800.5	853.59	8.5	35.45	3.8	2.8	0.2	20.4	3.2	725	113
2,820.5	859.69	5.3	22.10	2.3	2.2	0.43	15.75	2.99	574	134
2,844.5	867.00	--	--	0.4	0.4	0.03	0.72	0.93	167	216
2,860.5	871.88	--	--	0.2	0.2	0.03	0.09	1.13	50	627
2,880.5	877.98	--	--	0.4	0.4	0.08	0.4	1.13	108	305
2,901.5	884.38	--	--	2.5	1.3	0.09	5.46	1.21	426	94
2,923.5	891.08	--	--	5	4.2	0.85	35.72	3.63	773	85
2,940.5	896.26	--	--	8.7	7.4	0.39	65.62	5.46	883	73
2,962.5	902.97	--	--	7.2	6.7	1.03	18.29	4.21	740	170

in the Piceance basin (Donnell, 1980). The only rich sample in the Coyote Wash core from the Uinta basin is a sample from the Mahogany zone at the top of the Parachute Creek Member (fig. 3). Samples from other cores in the Uinta

basin, however, generally are more organic carbon rich; rocks from the Mahogany zone typically contain about 10 percent TOC (Anders and Gerrild, 1984). The richest samples from the Blacks Fork core are from the Tipton

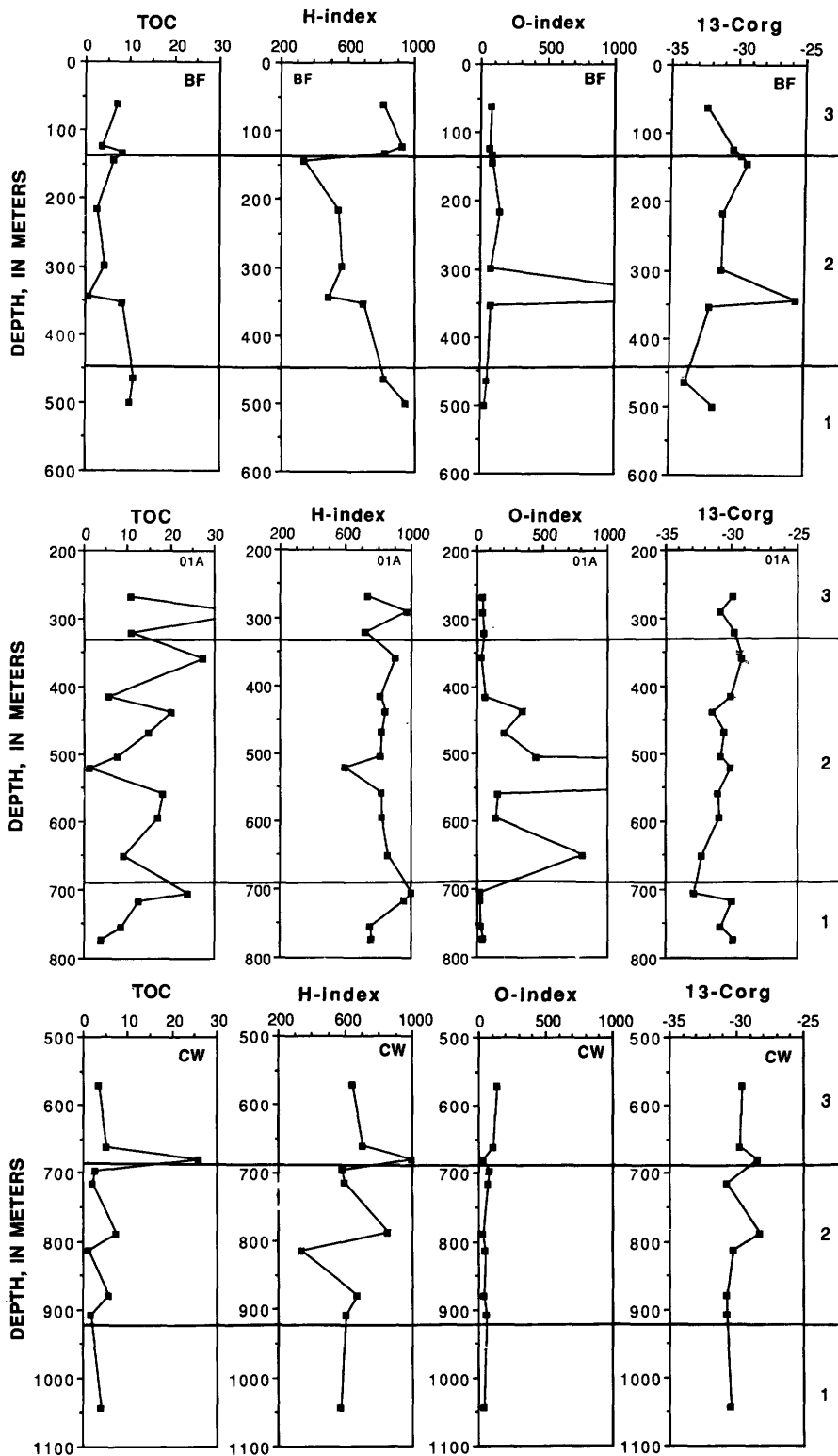


Figure 3. Plots of depth versus percent total organic carbon (TOC), hydrogen index (H-index, in milligrams of hydrocarbons per gram organic carbon), oxygen index (O-index, in milligrams of carbon dioxide per gram organic carbon), and $\delta^{13}\text{C}$ organic carbon (13-Corg, in per mil difference relative to PDB marine carbonate standard) in samples of Green River Formation from Blacks Fork core (BF), Green River basin, Wyoming; 01A core, Piceance basin, Colorado; and Coyote Wash core (CW), Uinta basin, Utah. Numbers (1, 2, and 3) to right of each panel refer to three lake stages of Tuttle (this volume).

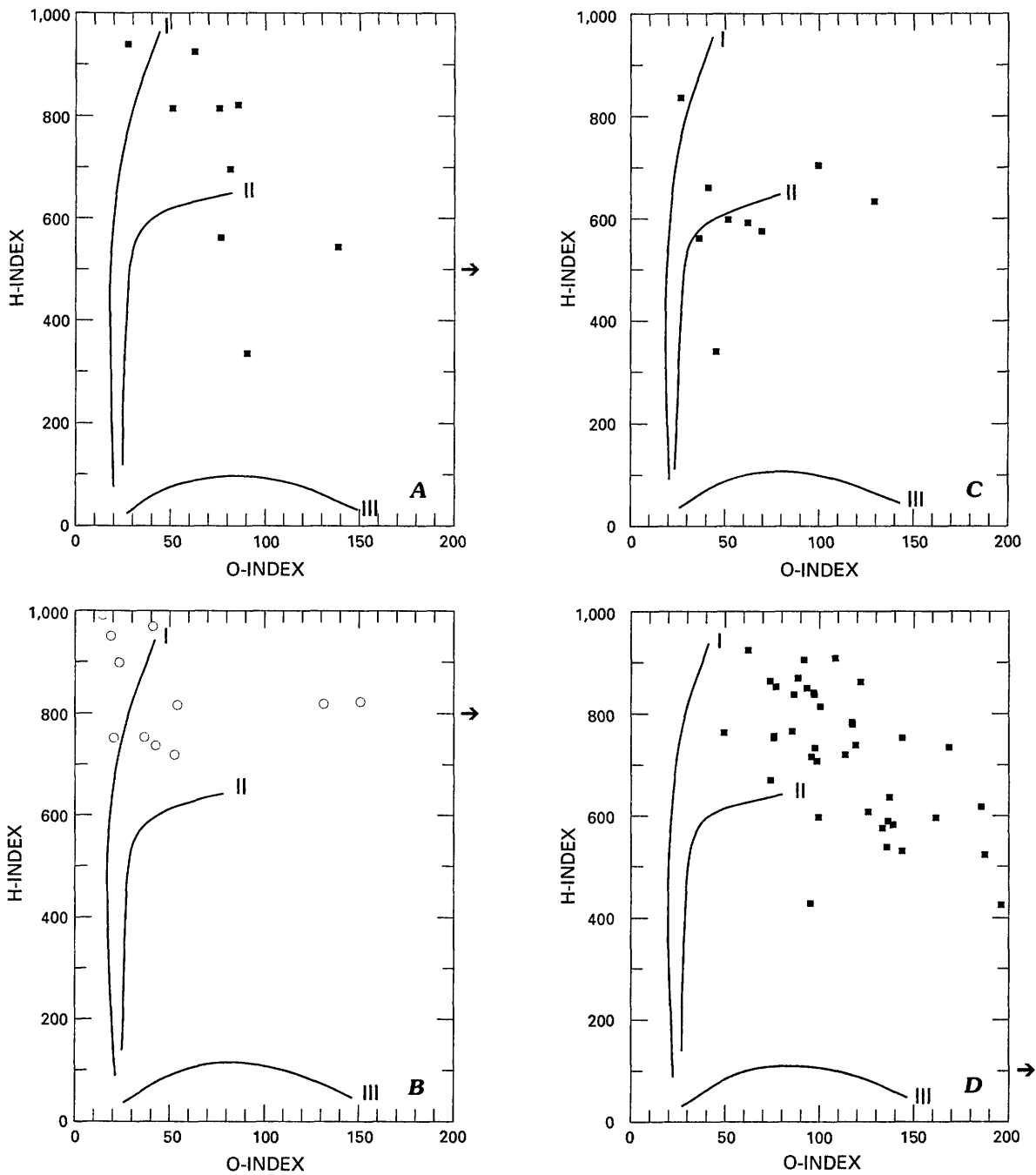


Figure 4. Plots of oxygen index (in milligrams of carbon dioxide per gram organic carbon) versus hydrogen index (in milligrams of hydrocarbons per gram organic carbon) in samples of Green River Formation. Curves marked I, II, and III represent thermal maturation pathways of type I, type II, and type III kerogen, respectively (Espitalié and others, 1977). A, Blacks Fork core. B, 01A core. C, Coyote Wash core. D, WOSCO core. Arrows to right of the plots for Blacks Fork, 01A, and WOSCO cores represent points having oxygen-index values of more than 200 (tables 1, 2).

Shale and Laney Members, both of which were deposited in fresher deeper waters than the intervening Wilkins Peak Member, which was deposited during a shallower, much more areally restricted phase of Eocene Lake Gosiute (Eugster and Hardie, 1975; see summary by Tuttle, this volume).

Values of percent TOC in the 01A core tend to increase above 400 m. Some of the lower TOC values between about 420 and 680 m are due to dilution of oil shale with nahcolite and halite. High values of HI throughout the saline zone (lake stage 2) indicate that the diluted organic matter is still hydrogen-rich, type II kerogen. The nahcolite

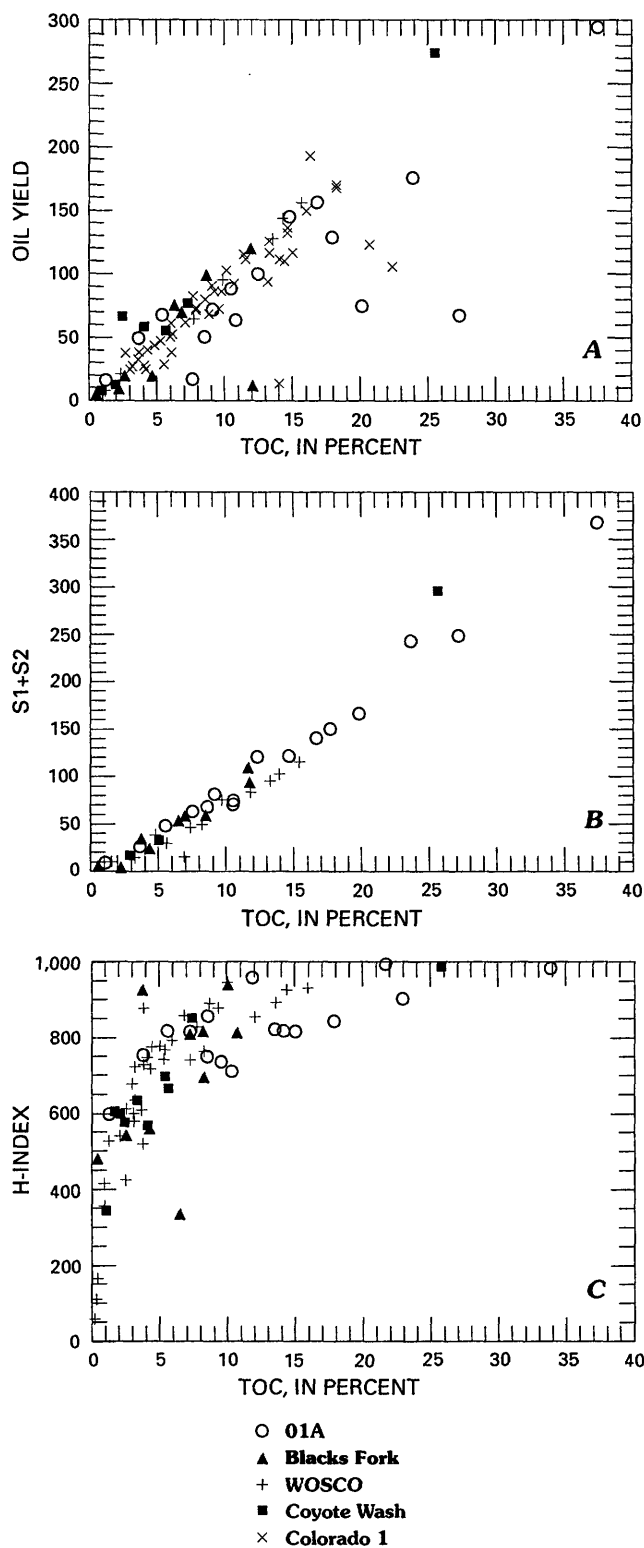


Figure 5. Plots of pyrolysis data for samples of Green River Formation. Data are from tables 1 and 2. *A*, Total organic carbon (TOC) versus Fischer assay oil yield. *B*, TOC versus (S_1+S_2) pyrolytic hydrocarbon yield from Rock-Eval pyrolysis (milligrams of hydrocarbons per gram of sample). *C*, TOC versus hydrogen index from Rock-Eval pyrolysis (milligrams of hydrocarbons per gram organic carbon).

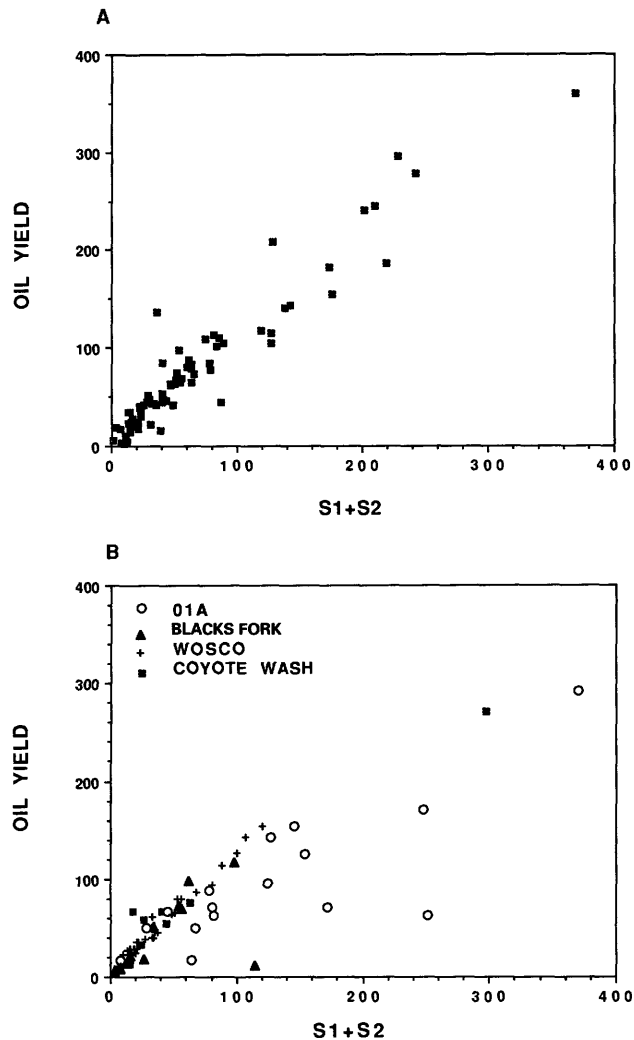


Figure 6. Plots of pyrolysis (S_1+S_2) yield (milligrams of hydrocarbons per gram of sample) versus Fischer assay oil yield (liters per metric ton). *A*, 69 samples of oil shale of different ages and from different geologic environments (modified from Dyni, 1988). *B*, Green River Formation (data from tables 1 and 2).

also has had a large effect on the oxygen index (figs. 3, 4*B*) because of the evolution of CO_2 from this sodium carbonate mineral during pyrolysis. Most carbonate minerals evolve CO_2 at temperatures much higher than that reached during Rock-Eval pyrolysis (550 °C). For example, the Green River Formation, particularly in the Piceance basin, contains abundant calcium, magnesium, and iron carbonate minerals (Desborough, 1978), but evolution of CO_2 from these minerals apparently does not affect the S_3 peak as judged by the low OI values outside the saline zone (fig. 3); however, nahcolite in samples from lake stage 2 in the O1A core must be contributing significant amounts of CO_2 in order to explain the unusually high OI values. One sample from the Blacks Fork core also has an unusually high OI value (1,800; table 1, fig. 3), which is probably due to evolution of CO_2 from sodium carbonate minerals (trona

and shortite) in this sample (Tuttle, this volume). Apparently no sodium carbonate or other saline minerals were deposited in the Uinta basin during lake stage 2 of Eocene Lake Uinta (Johnson, 1985). Very high hydrogen indices and very low oxygen indices for all samples from the 01A core outside lake stage 2 (figs. 3, 4B) indicate that the organic matter in these samples is very well preserved algal (type I) organic matter with little oxidation.

Some samples from the other two basins have hydrogen indices that are as high as those from the Piceance basin, but their much wider range of values of both HI and OI (fig. 4) suggests that they may contain varying mixtures of algal (type I) and terrestrial (type III) organic matter. Alternatively, oxidation of organic matter also can produce a pyrolysis response equivalent to organic matter of type III composition (Tissot and Welte, 1984).

Additional evidence for organic-matter type is provided by gas chromatograms of the soluble organic fraction (figs. 7–9). Gas chromatograms of saturated-hydrocarbon fractions of immature Green River oil shale typically are characterized by a strong odd-carbon-number predominance and a bimodal distribution, with n -C₁₇ dominating the n -alkanes made up of less than 20 carbon atoms, and higher molecular weight hydrocarbons (>20 carbon atoms) dominated by C₂₇, C₂₈, and C₂₉ steranes, C₃₀ hopane, and β -carotene (figs. 7A, 8). The chain isoprenoids in the intermediate-weight hydrocarbons generally contain more phytane than pristane (figs. 7A, 8), characteristic of a highly reducing environment. The predominance of n -C₁₇ in the n -alkanes is particularly characteristic of Green River oil shale (Tissot and others, 1978), and many aquatic algae produce hydrocarbons in which n -C₁₇ is the dominant hydrocarbon (see, for example, Clark and Blumer, 1967). Anders and Robinson (1973) concluded that most of the principal isoprenoid compounds (pristane, phytane, steranes, and pentacyclic triterpanes) and β -carotene in the Colorado no. 1 core do not come from thermal cracking of kerogen but are the chemical, catalytic, and microbial hydrolysis products of lipids generated during the beginning phase of diagenesis. Normal alkanes of high molecular weight (C₂₅–C₃₃ range) and with odd-carbon predominance that are characteristic of higher plant waxes of terrestrial origin (Simoneit, 1978; Tissot and Welte, 1984) have been identified in Green River oil shale (Robinson and others, 1965; Tissot and others, 1978), but their peaks would be masked by those of the steranes and pentacyclic triterpanes (mostly hopane derivatives) that are common in Green River oil shale (Anderson and others, 1965; Tissot and Welte, 1984).

The overwhelming predominance of C₁₇ normal alkanes shows that most organic matter in Green River oil shale is of algal origin (see review by Tissot and Welte, 1984). The lower HI values in samples from cores from the

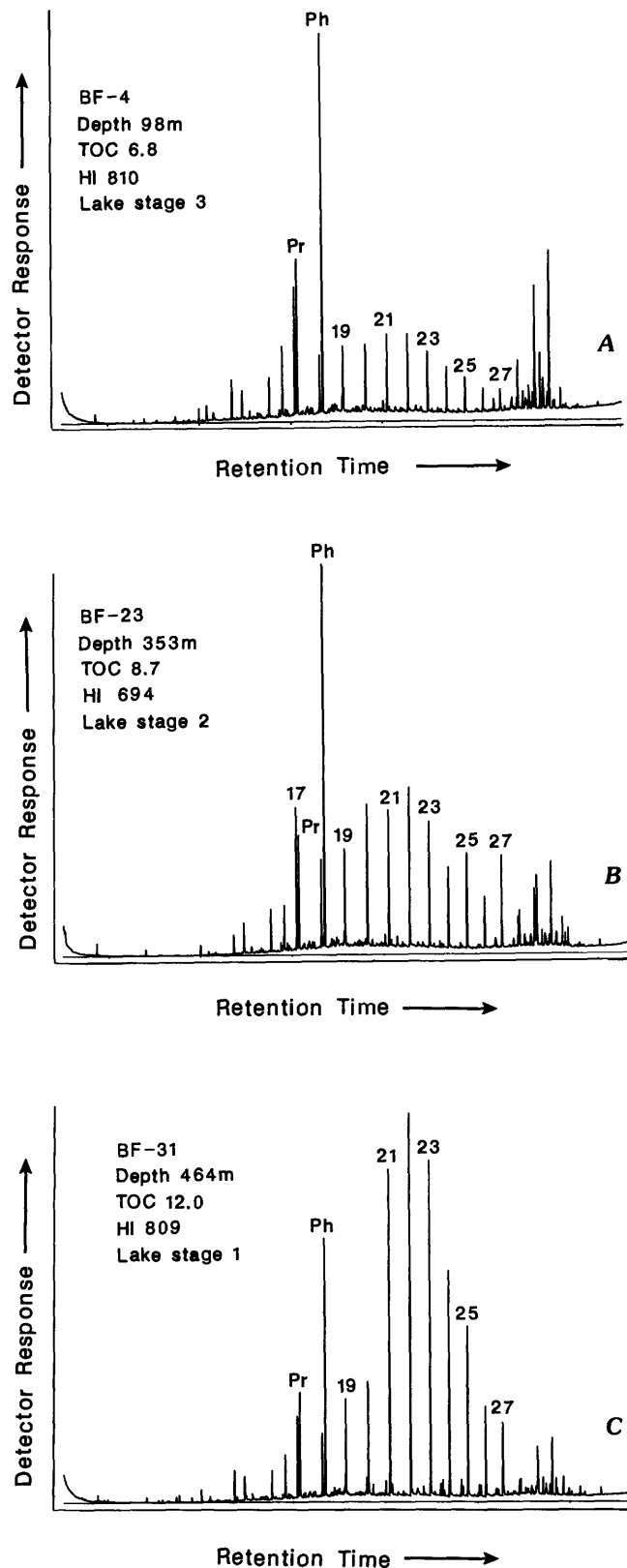


Figure 7. Gas chromatograms of saturated-hydrocarbon fraction of samples from three depths in Blacks Fork (BF) core. Location of core hole shown in figure 1. Selected peaks are labeled by carbon number. Ph, phytane; Pr, pristane.

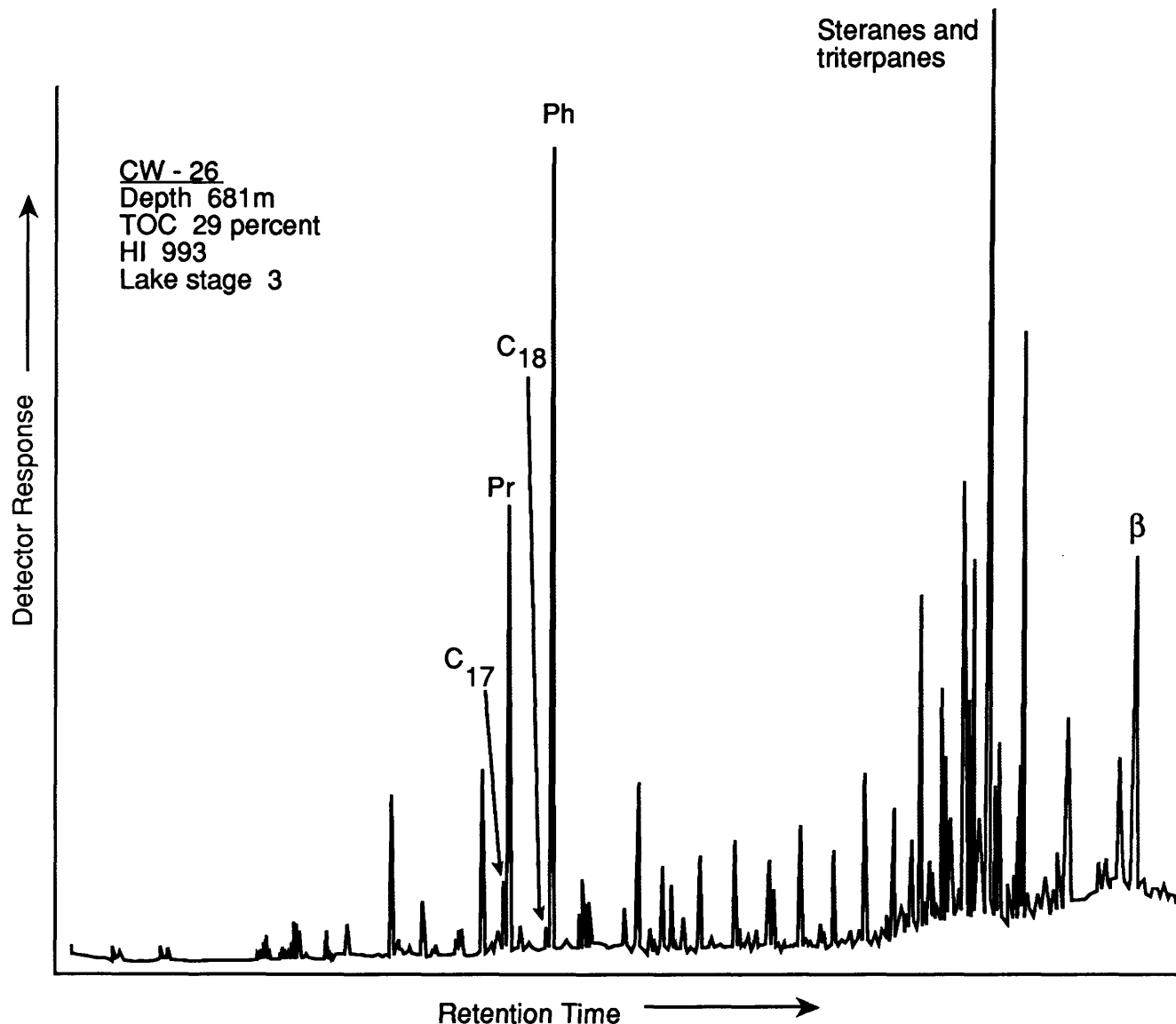


Figure 8. Gas chromatogram of saturated-hydrocarbon fraction of a sample from the Mahogany zone in Coyote Wash (CW) core. Location of core hole shown in figure 1. Selected peaks are labeled by carbon number. Ph, phytane; Pr, pristane; β , beta carotene.

Uinta and Green River basins thus probably are the result of greater oxidation of type I (algal) organic matter rather than dilution by type III (terrestrial) organic matter.

Another characteristic of gas chromatograms of Green River oil shale is the change with depth from a bimodal distribution of hydrocarbons having an odd-carbon predominance (fig. 7A) to a bell-shaped distribution centered on C_{21} - C_{23} and a loss of odd-carbon predominance (fig. 7C). Anders and Robinson (1973) concluded that development of this bell-shaped distribution of normal alkanes in the Colorado no. 1 core was due to increasing thermal maturity with depth; however, subsequent thermal maturity measurements in samples from this core (Rock-Eval, Tmax, and vitrinite reflectance) indicate that there is no significant difference in level of maturity between

shallow samples having a bimodal *n*-alkane distribution and deeper samples having a bell-shaped *n*-alkane distribution. Perhaps the change in *n*-alkane distribution is the result of increasing microbial degradation with increasing age, as suggested by Tissot and others (1978). In addition, there is always the possibility of contamination with core-box wax, which usually contains *n*-alkanes in the range of C_{20} - C_{24} ; however, contamination would not explain the progressive changes with depth.

Carbon Isotope Data

The sources of organic matter in lake sediments may include planktonic algal debris, rooted aquatic macrophytes,

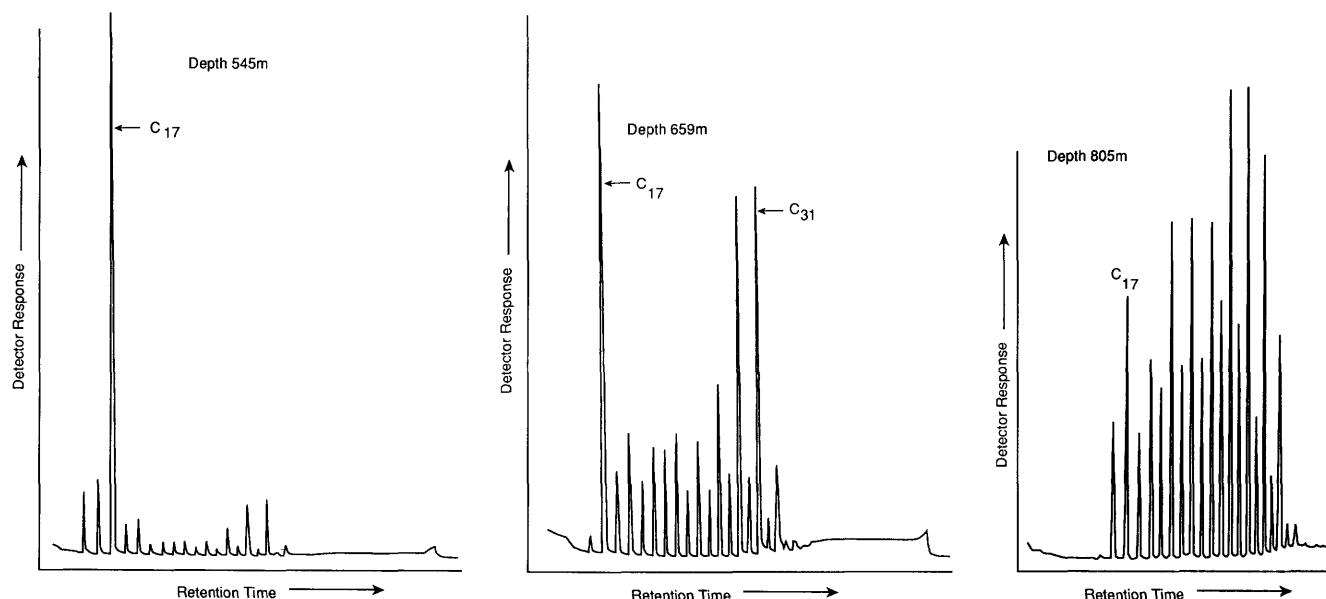


Figure 9. Gas chromatograms of saturated-hydrocarbon fraction of samples from three depths in WOSCO EX-1 core. Location of core hole shown in figure 1. Selected peaks are labeled by carbon number.

and terrestrial vegetation washed in from the drainage basin. Each of these sources has a carbon-isotope signature that is not necessarily unique (fig. 10). Probably the most unique isotopic signature of source organic matter is the highly ^{13}C -depleted character of lacustrine plankton, which has values of $\delta^{13}\text{C}$ generally in the low negative 30's (fig. 10). The sedimentary signature of ^{13}C -depleted algal debris is illustrated by the algal-rich end of the distribution of ^{13}C values in surface sediments of Minnesota lakes (fig. 10) Dean, unpublished data). Within this framework of $\delta^{13}\text{C}$ values (fig. 10) in modern organic matter, the carbon-isotope signature of organic matter in Green River oil shales clearly is dominated by algal debris (type I and II organic matter).

Changes in the carbon-isotope composition of sedimentary organic matter with time in a lake system (fig. 3) can be related to changes in source of the organic matter, changes in climate and associated environmental conditions in the lake, particularly temperature, and (or) changes in organic productivity. For example, the steady increase in values of $\delta^{13}\text{C}$ through the Parachute Creek Member in the 01A core and through the Wilkins Peak Member in the Blacks Fork core may be due to an influx of more ^{13}C -enriched terrestrial organic matter, higher temperature and a lower pCO_2 in the lake water, or an increase in productivity. Each of these possibilities needs to be explored.

A plot of $\delta^{13}\text{C}$ versus some other indicator of organic-matter source, such as HI, can provide a means of separating source and environmental effects in carbon-isotope data (for example, Dean and others, 1986). On a plot of $\delta^{13}\text{C}$ versus HI, organic matter that is a mixture of terrestrial and algal origin shows as a negative slope reflecting ^{13}C depletion

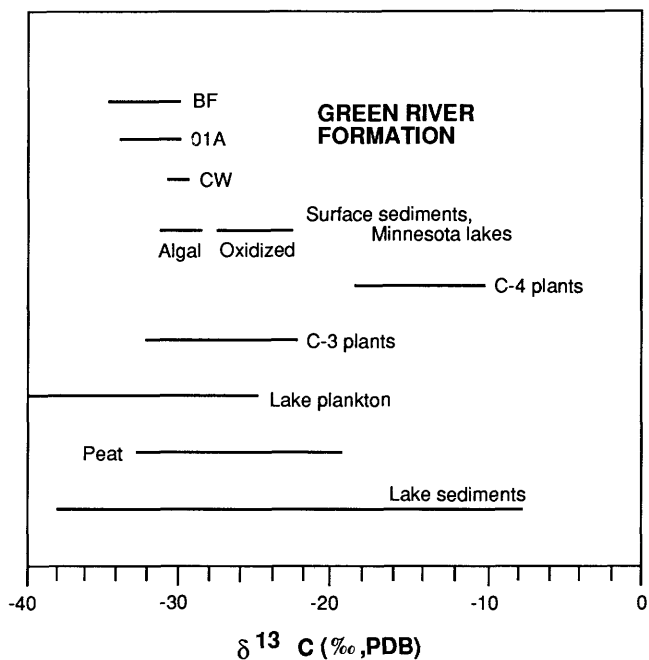


Figure 10. Range of $\delta^{13}\text{C}$ values in lake sediments, peat, lake plankton, C-3 plants, C-4 plants, Minnesota lake sediments, and samples of the Green River Formation. Data for lake sediments, peat, lake plankton, and C-3 and C-4 plants were compiled by Deines (1980); data for Minnesota sediments are from Dean (unpublished); data for Green River Formation are from table 1.

and hydrogen richness of algal organic matter and ^{13}C enrichment and low hydrogen content of terrestrial organic matter. If all of the organic matter is of algal origin but has undergone varying degrees of oxidation or decomposition,

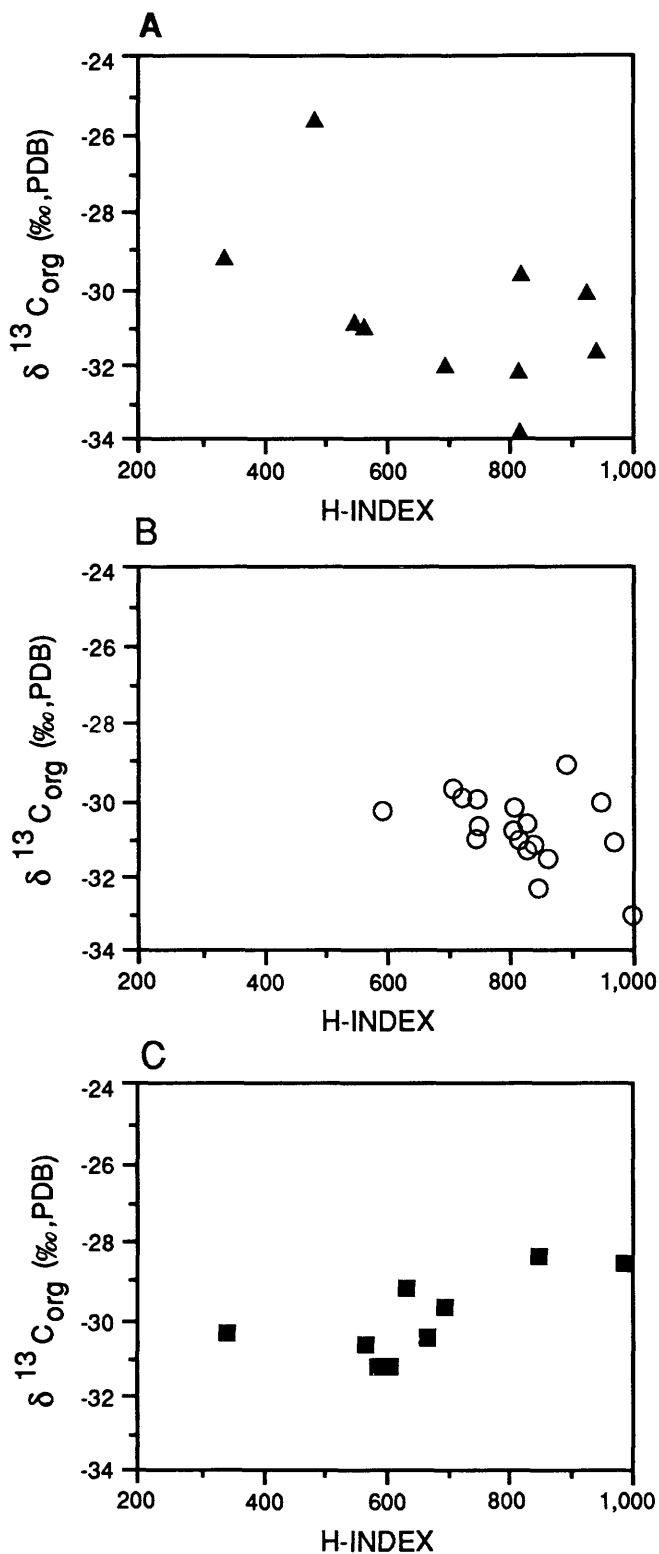


Figure 11. Plots of hydrogen index (in milligrams of hydrocarbons per gram organic carbon) versus $\delta^{13}\text{C}$ of organic matter in samples of Green River Formation. A, Blacks Fork core. B, 01A core. C, Coyote Wash core. Location of core holes shown in figure 1.

then an HI- $\delta^{13}\text{C}$ plot shows a large variation in values of HI and low and uniform values of $\delta^{13}\text{C}$. If all values of HI are high, and values of $\delta^{13}\text{C}$ vary somewhat, then all of the organic matter was algal, but some environmental changes probably have altered the isotopic composition of that organic matter. The isotopic fractionation between algal cells and dissolved CO_2 is highly dependent on pCO_2 in that less fractionation occurs at lower pCO_2 (Deuser and others, 1968; Calder and Parker, 1973). Variations in pCO_2 caused by changes in productivity or temperature could induce ^{13}C enrichment or depletion in organic carbon fixed by photosynthesis (Herczeg and Fairbanks, 1987).

The three data sets from this investigation show three distinct distributions on an HI- $\delta^{13}\text{C}$ plot (fig. 11). Data from the Blacks Fork core show the greatest variability in both $\delta^{13}\text{C}$ and HI (fig. 11A). Values of HI decrease and values of $\delta^{13}\text{C}$ increase throughout the shallow-water Wilkins Peak Member so that the most ^{13}C -enriched, hydrogen-poor organic matter is in the upper part of the Wilkins Peak (fig. 3). We interpret this distribution as representing dilution of algal organic matter with more terrestrial organic matter (negative slope on HI- $\delta^{13}\text{C}$ plot, fig. 11A). The $\delta^{13}\text{C}$ value of -25.7 (table 1, fig. 3) is for a sample containing shortite and trona and, therefore, may reflect extreme environmental conditions (such as high alkalinity or temperature), although such conditions probably have not affected the isotopic composition of organic matter in the saline zone in the Piceance basin (fig. 3). More likely this ^{13}C -enriched sample represents a pulse of influx of more terrestrial organic matter during a particularly low lake level. The Tipton Shale and Laney Members in the Blacks Fork core contain the highest values of HI and most ^{13}C -depleted values of $\delta^{13}\text{C}$, and the organic matter in these two members was mostly algal rich.

The plot of $\delta^{13}\text{C}$ versus HI for samples from the Colorado 01A core (fig. 11B) shows that most of the organic matter in this core is very hydrogen rich and very ^{13}C depleted. There is a slight trend toward less ^{13}C -depleted organic matter in the upper part of the Parachute Creek Member, similar to the trend observed for the Wilkins Peak Member in the Blacks Fork isotope data. The samples having lower HI values are scattered throughout the core (fig. 3), are not part of a systematic stratigraphic trend, and do not correspond to samples containing ^{13}C -enriched organic matter. These observations suggest that the lower values of HI are due to greater oxidation of organic matter, perhaps during lower lake levels. If we were to apply the interpretation of the data for Wilkins Peak Member in the Blacks Fork core to the data for the Parachute Creek Member in the 01A core (fig. 3), the stratigraphic trend toward increasing values of $\delta^{13}\text{C}$ should indicate a progressive increase in the amount of terrestrial organic matter during deposition of this unit. However, this interpretation goes against the organic-carbon and HI data, which suggest that production of hydrogen-rich algal

organic matter was high throughout the Parachute Creek Member and, if anything, increased through the unit to culminate in the accumulation of very rich algal organic matter in the Mahogany zone (fig. 3). If the enrichment of ^{13}C in the Parachute Creek were due to some environmental factor such as increased alkalinity or temperature, then we would expect the maximum values to be within the saline zone where presumably the alkalinity and temperature of the water were greatest.

Increase in the richness of oil shale upward within the Parachute Creek Member suggests that organic productivity in the lake increased, which, in turn, caused an increase in the rate of burial of ^{13}C -depleted organic carbon. This increase in burial rate culminated during deposition of the extremely rich Mahogany zone, which represents maximum expansion of Lake Uinta. Rapid photosynthetic removal of ^{13}C -depleted organic carbon during such a burial event would leave the surface-water carbon reservoir enriched in ^{13}C , as was demonstrated for increased organic carbon burial as a result of eutrophication of Lake Greifen, Switzerland (McKenzie, 1985). Such an event certainly would have affected the isotopic composition of any carbonate minerals precipitated from the lake water and may have affected the isotopic composition of organic carbon. Unfortunately because most of the carbonate minerals in the Green River Formation are diagenetic (Desborough, 1978), the carbon isotopic composition of carbonate minerals is dominated by a diagenetic signal (J.K. Pitman, U.S. Geological Survey, written commun., 1990). Values of $\delta^{13}\text{C}$ of carbonate minerals become heavier with depth in the 01A core rather than lighter, as do values of $\delta^{13}\text{C}$ of the organic matter (fig. 3), presumably due to a greater influence of methanogenesis and fermentation with increasing burial depth (J.K. Pitman, written commun., 1990).

Scholle and Arthur (1980) and Arthur and others (1985) showed that periods of accumulation of ^{13}C -depleted marine carbonate rocks throughout the Phanerozoic can be correlated with periods of rapid burial of marine organic matter (so-called oceanic anoxic events). During periods of extremely high burial rate of organic carbon, such as occurred at the Cretaceous Cenomanian/Turonian (C/T) boundary, the isotopic composition of organic carbon fixed by photosynthesis also can be enriched in ^{13}C by as much as 4–6‰ on a global scale (Pratt and Threlkeld, 1984; Arthur and others, 1988). If an organic-carbon burial event, such as the C/T boundary event, can alter the isotopic composition of the surface-water carbon reservoir of the world ocean, surely a burial event such as that recorded in the Mahogany zone of the Green River Formation would have altered the isotopic composition of the much smaller surface-water reservoir of a lake, even a lake as large as Lake Uinta. We conclude that the increase in $\delta^{13}\text{C}$ values at the top of the Parachute Creek Member in the 01A core, and perhaps

some of the increase in $\delta^{13}\text{C}$ values at the top of the Wilkins Peak Member in the Blacks Fork core, is due to extreme ^{13}C enrichment of the entire surface-water carbon reservoir.

Most of the data in the HI– $\delta^{13}\text{C}$ plot for the Coyote Wash core (fig. 11C) show little variation in values of $\delta^{13}\text{C}$ but considerable variation in values of HI. The small variation of $\delta^{13}\text{C}$ values suggests that there was little variation in the source of organic matter, and therefore the large variation in values of HI probably is due to different degrees of decomposition of algal organic matter; however, the two samples having the highest values of HI also are the most ^{13}C enriched. One of these samples is from the Mahogany zone and the other is from an organic-carbon-rich unit below the Mahogany zone (fig. 3). These two anomalously high $\delta^{13}\text{C}$ values, relative to other values in the core, suggest that organic carbon fixed by photosynthesis in the Uinta basin, as in the Piceance basin, was at times affected by extreme ^{13}C -enrichment of the surface-water reservoir in Lake Uinta.

CONCLUSIONS

The richest oil shale samples from the three cores of the Green River Formation studied are from the Piceance basin in Colorado. These samples are from a core in the depocenter of the saline facies in the Piceance basin and would be even richer if the kerogen was not diluted by evaporite minerals (nahcolite and halite). The organic matter in the Piceance basin is very well preserved and little oxidized. The organic matter in samples of oil shale that accumulated in shallower water in the Uinta and Green River basins is lower in amount and is more highly oxidized.

Variations in source of organic matter, degree of preservation of that organic matter, and environmental conditions during formation and accumulation of organic matter commonly can be detected by consideration of type (such as by using pyrolysis hydrogen index, HI) and carbon isotopic composition ($\delta^{13}\text{C}$) of the organic matter. On a plot of HI versus $\delta^{13}\text{C}$, a mixture of terrestrial and algal organic matter shows as a negative slope reflecting ^{13}C -depletion and hydrogen-richness of algal organic matter and ^{13}C -depletion and low hydrogen content of terrestrial organic matter. An example of such a mixture is the organic matter in the shallow-water Wilkins Peak Member of the Green River Formation in Wyoming.

If all of the organic matter is of algal origin but has undergone varying degrees of oxidation or decomposition, then an HI– $\delta^{13}\text{C}$ plot will show a large variation in HI but low and uniform values of $\delta^{13}\text{C}$. Such a distribution is exemplified by most samples of oil shale from the Coyote Wash core from the Uinta basin. Algal organic matter that is well preserved will be very hydrogen rich and very ^{13}C depleted. Much of the organic matter in the Piceance basin core has these characteristics; however, there is an unusual

enrichment in ^{13}C toward the top of the Parachute Creek Member of the Green River Formation in the Piceance basin, culminating in the extremely algal rich organic matter of the Mahogany zone. This ^{13}C enrichment is interpreted as due to rapid burial of ^{13}C -depleted organic matter to the point that the entire surface-water carbon reservoir became ^{13}C enriched.

REFERENCES CITED

- Anders, D.E., and Gerrild, P.M., 1984, Hydrocarbon generation in lacustrine rocks of Tertiary age, Uinta Basin, Utah—Organic carbon, pyrolysis yield, and light hydrocarbons, *in* Woodward, J., Meissner, F.F., and Clayton, J.L., eds., Hydrocarbon source rocks of the greater Rocky Mountain region: Rocky Mountain Association of Geologists, Denver, p. 513–529.
- Anders, D.E., and Robinson, W.E., 1973, Geochemical aspects of the saturated hydrocarbon constituents of Green River oil shale—Colorado No. 1 core: U.S. Bureau of Mines, Report of Investigations 7737, 23 p.
- Anderson, P.C., Gardner, P.M., Whitehead, E.V., Anders, D.E., and Robinson, W.E., 1969, The isolation of steranes from Green River oil shale: *Geochimica et Cosmochimica Acta*, v. 33, p. 1304–1307.
- Arthur, M.A., Dean, W.E., and Pratt, L.M., 1988, Geochemical and climatic effects of increased marine organic carbon burial at the Cenomanian/Turonian boundary: *Nature*, v. 335, p. 714–717.
- Arthur, M.A., Dean, W.E., and Schlanger, S.O., 1985, Variations in the global carbon cycle during the Cretaceous related to climate, volcanism, and changes in atmospheric CO_2 , *in* Sundquist, E.T., and Broecker, W.S., eds., The carbon cycle and atmospheric CO_2 —Natural variations Archean to Present: American Geophysical Union Monograph 32, p. 504–529.
- Calder, J.A., and Parker, P.L., 1973, Geochemical implications of induced changes in ^{13}C fractionation by blue-green algae: *Geochimica et Cosmochimica Acta*, v. 37, p. 133–140.
- Clark, R., and Blumer, M., 1967, Distribution of n-paraffins in marine organisms and sediment: *Limnology and Oceanography*, v. 12, p. 79–87.
- Dean, W.E., Arthur, M.A., and Claypool, G.E., 1986, Depletion of ^{13}C in Cretaceous marine organic matter—Source, diagenetic, or environmental signal?: *Marine Geology*, v. 70, p. 119–157.
- Deines, P., 1980, The isotopic composition of reduced carbon, *in* Fritz, P., and Fontes, J.C., eds., Handbook of environmental isotope geochemistry, v. 1, The terrestrial environment: Amsterdam, Elsevier, p. 329–406.
- Desborough, G.E., 1978, A biogenic-chemical stratified lake model for the origin of oil shale of the Green River Formation—An alternative to the playa-lake model: *Geological Society of America Bulletin*, v. 89, p. 961–971.
- Desborough, G.E., and Pitman, J.R., 1974, Significance of applied mineralogy to oil shale in the upper part of the Parachute Creek Member of the Green River Formation, Piceance Creek basin, Colorado, *in* Murray, D.K., ed., Energy resources of the Piceance Creek basin, Colorado: Rocky Mountain Association of Geologists, Field Conference, 25th, Denver, p. 81–89.
- Deuser, W.G., Degens, E.T., and Guillard, R.R.L., 1968, Carbon isotope relationships between plankton and sea water: *Geochimica et Cosmochimica Acta*, v. 32, p. 657–660.
- Donnell, J.R., 1980, Western United States oil-shale resources and geology, *in* Synthetic fuels from oil shale: Chicago, Institute for Gas Technology, p. 17–19.
- Dyni, J.R., 1988, Review of the geology and oil-shale resources of the tripolitic oil-shale deposits of Sicily, Italy: U.S. Geological Survey Open-File Report 88–270, 23 p.
- Dyni, J.R., Anders, D.E., Rex, R.C., Jr., 1990, Comparison of hydroretorting, Fischer assay, and Rock-Eval analyses of some World oil shales, *in* Proceedings of the 1989 Eastern Oil Shale Symposium: University of Kentucky, Institute for Mining and Minerals Research, p. 270–286.
- Espitalié, J., LaPorte, J.L., Madec, M., Marquis, F., Leplat, P., Paulet, J., and Boutefeu, A., 1977, Methode rapide de caracterisation des roches meres de leur potentiel petrolier et de leur degré d'évolution: *Revue Institut Francais du Petrole*, v. 32, p. 23–42.
- Eugster, H.P., and Hardie, L.A., 1975, Sedimentation in an ancient playa-lake complex—The Wilkins Peak Member of the Green River Formation of Wyoming: *Geological Society of America Bulletin*, v. 86, p. 319–334.
- Herczeg, A.L., and Fairbanks, R.G., 1987, Anomalous carbon isotope fractionation between atmospheric CO_2 and dissolved inorganic carbon induced by intense photosynthesis: *Geochimica et Cosmochimica Acta*, v. 51, p. 895–899.
- Johnson, R.C., 1985, Early Cenozoic history of the Uinta and Piceance Creek basins, Utah and Colorado, with special reference to the development of Eocene Lake Uinta, *in* Flores, R.M., and Kaplan, S.S., eds., Cenozoic paleogeography of the western United States: Denver, Society of Economic Paleontologists and Mineralogists, Rocky Mountain Symposium 3, p. 247–276.
- McKenzie, J.A., 1985, Carbon isotopes and productivity in the lacustrine and marine environments, *in* Stumm, W., ed., Chemical processes in lakes: New York, Wiley-Interscience, p. 99–118.
- Pratt, L.M., and Threlkeld, C.N., 1984, Stratigraphic significance of $^{13}\text{C}/^{12}\text{C}$ ratios in mid-Cretaceous rocks of the western interior, U.S.A., *in* Scott, D.F., and Glass, D.J., eds., The Mesozoic of middle North America: Canadian Society of Petroleum Geology Memoir 9, p. 305–312.
- Robinson, W.E., and Cook, G.L., 1975, Compositional variations of organic material from Green River oil shale—WOSCO EX-1 core (Utah): U.S. Bureau of Mines, Report of Investigations 8017, 40 p.
- Robinson, W.E., Cummins, J.J., and Dinneen, G.U., 1965, Changes in Green River oil-shale paraffins with depth: *Geochimica et Cosmochimica Acta*, v. 29, p. 249–258.
- Scholle, P.A., and Arthur, M.A., 1980, Carbon isotope fluctuations in Cretaceous pelagic limestones—Potential stratigraphic and petroleum exploration tool: *American Association of Petroleum Geologists Bulletin*, v. 64, p. 67–87.

- Simoneit, B.R.T., 1978, The organic chemistry of marine sediments, *in* Riley, J.P., and Chester, R., eds., *Chemical oceanography* (v. 7): New York, Academic Press, p. 233–311.
- Smith, J.W., Trudell, L.G., and Dana, G.F., 1968, Oil yields of Green River oil shale from Colorado corehole No. 1: U.S. Bureau of Mines, Report of Investigations 7071, 28 p.
- Tissot, B., Deroo, G., and Hood, A., 1978, Geochemical study of the Uinta Basin—Formation of petroleum from the Green River Formation: *Geochimica et Cosmochimica Acta*, v. 42, p. 1469–1485.
- Tissot, B.G., and Welte, D.H., 1984, *Petroleum formation and occurrence* (2nd ed.): New York, Springer-Verlag, 699 p.

Chapter G

Petrography of Iron Sulfide Minerals in the Green River Formation of Wyoming, Utah, and Colorado

By MICHELE L. TUTTLE

U.S. GEOLOGICAL SURVEY BULLETIN 1973

GEOCHEMICAL, BIOGEOCHEMICAL, AND SEDIMENTOLOGICAL STUDIES OF THE
GREEN RIVER FORMATION, WYOMING, UTAH, AND COLORADO

CONTENTS

Abstract	G1
Introduction	G1
Methods	G2
Results	G3
Blacks Fork core	G3
01A core	G3
Coyote Wash core	G4
Discussion	G5
Pyrite formation	G8
Pyrrhotite formation	G10
Marcasite formation	G11
Conclusions	G11
References cited	G12

FIGURES

1. Map showing Laramide uplifts and basins in parts of Wyoming, Utah, Colorado, and Idaho G2
2. Chart showing stratigraphy of cores used in study G3
- 3-5. Diagrams showing iron sulfide mineralogy and morphology for samples of Green River Formation from:
 3. Blacks Fork core G5
 4. 01A core G6
 5. Coyote Wash core G7
6. Photomicrographs showing typical sulfide-mineral morphology G8
7. Chart showing paragenetic sequence of sulfide mineral formation G10
8. Eh-pS²⁻ stability field diagrams for pyrite, pyrrhotite, siderite, and hematite G11

TABLE

1. Summary of lake stages represented by the samples in this study G4

Petrography of Iron Sulfide Minerals in the Green River Formation of Wyoming, Utah, and Colorado

By Michele L. Tuttle

Abstract

The Paleogene Green River Formation contains three iron sulfide minerals that are easily examined using reflected-light microscopy: pyrite, pyrrhotite, and marcasite. At least four generations of pyrite were identified. Framboidal pyrite formed in organic stringers by the sulfidization of iron oxide minerals that coat clay minerals and were very reactive to H₂S (episode 1). Euhedral and anhedral pyrite grains and pyrite infilling framboids formed when less reactive iron oxide minerals were dissolved, possibly during iron reduction by bacteria (episode 2).

Pyrrhotite then formed from unstable iron sulfide phases that were never converted to pyrite because of the extremely reducing conditions in the sediments (episode 3). Later, iron loss from pyrrhotite and partial oxidation of sulfur led to pseudomorphic replacement of pyrrhotite by marcasite (episode 4). Subsequent alteration of some marcasite to the more stable disulfide phase pyrite produced the unusual bladed pyrite.

INTRODUCTION

The Paleogene Green River Formation, deposited in ancient Lakes Uinta and Gosiute in Utah, Colorado, and Wyoming, contains iron sulfide minerals that have highly unusual mineralogy and morphology. Iron disulfide minerals are the most common sulfide minerals; of these, pyrite (cubic FeS₂) (described in Milton and Eugster, 1959; Pabst, 1970; Cole and others, 1978; Cole and Picard, 1981) is more abundant than marcasite (orthorhombic FeS₂) (Milton and Eugster, 1959; Cole and others, 1978; Cole and Picard, 1981). Some pyrite has an unusual bladed morphology (Cole, 1975; Boyer and Cole, 1983; Dyni,

1983). Pyrrhotite (monoclinic Fe_{1-x}S) is locally abundant (Milton and Eugster, 1959; Cole and others, 1978; Cole and Picard, 1981; Melchior and others, 1982), and wurtzite (hexagonal ZnS) is rare (Milton and Eugster, 1959).

The presence of marcasite in unmetamorphosed lacustrine rocks is unknown outside the Green River Formation. Marcasite commonly forms in sedimentary environments where the pH is less than 4 (Goldhaber and Kaplan, 1974; Murowchick and Barnes, 1986), environments much more acidic than those postulated for pore waters in Green River sediments (pH ~10; Bradley and Eugster, 1969). Authigenic pyrrhotite is rare in sedimentary environments and, similar to marcasite, has not been reported in unmetamorphosed lacustrine rocks other than those in the Green River Formation.

In this report, I discuss the petrography (mineralogy and morphology) of iron sulfide minerals in core material of the Green River Formation from the centers of the three depositional basins occupied by the Green River lakes (fig. 1). The petrographic characteristics indicate a complex paragenetic sequence of iron sulfide formation. Identification of four distinct episodes allows a separation, in time, of processes affecting sulfur in the Green River Formation. Determining the paragenetic sequence is crucial for guiding interpretation of sulfur chemistry and isotopy (Tuttle and Goldhaber, this volume), which in turn is used to reconstruct the depositional and diagenetic history of the Green River Formation, the primary goal of the studies presented in this volume.

Acknowledgments.—This report has benefited greatly from the thorough reviews of Richard Reynolds, Neil Fishman, and Robert Zielinski. The work on which this chapter is based was funded by the U.S. Geological Survey Evolution of Sedimentary Basins Program.

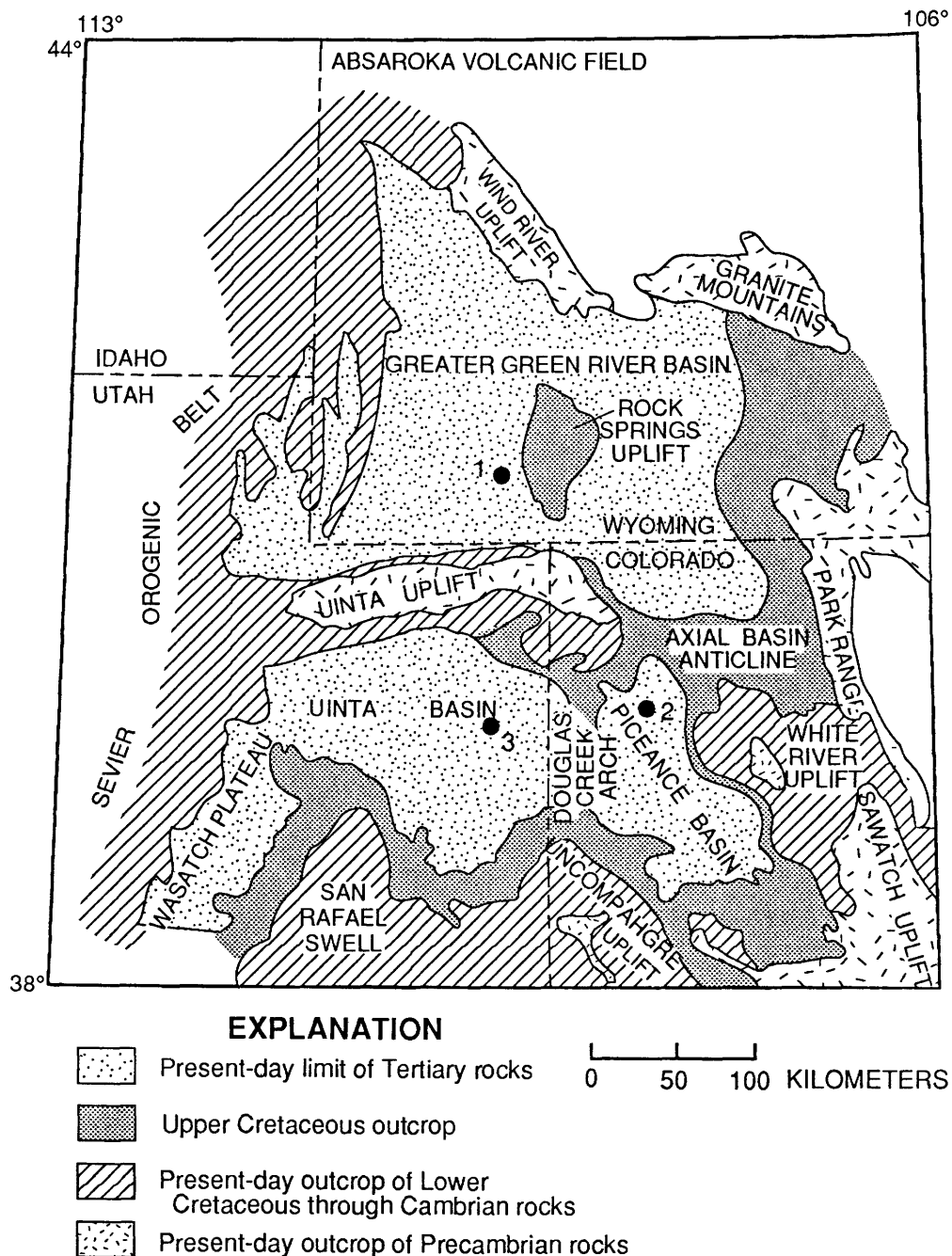


Figure 1. Map showing Laramide uplifts and basins in parts of Wyoming, Utah, Colorado, and Idaho. Core holes (solid circles): 1, Blacks Fork no.1 core, greater Green River basin, Wyoming; 2, 01A core, Piceance basin, Colorado; 3, Coyote Wash core, Uinta basin, Utah. Modified from Johnson (1985).

METHODS

A hierarchical, unbalanced analysis of variance sampling design was used to assure optimal coverage of cores given the limitations on the number of samples analyzed. Polished thin sections were prepared from plugs of 114 samples: 41 (39 petrographically examined) samples from Piceance basin, Colorado (01A core), 35 samples from

the greater Green River basin, Wyoming (Blacks Fork core), and 38 samples from the Uinta basin, Utah (Coyote Wash core). Each original sample was about 3 cm long and lithologically homogeneous. Locations of the three depositor cores are shown in figure 1. The stratigraphy of rocks in each core and the division of each core into the three major lake stages are shown in figure 2. The cores, samples, and lake stages are described in detail in Tuttle (this

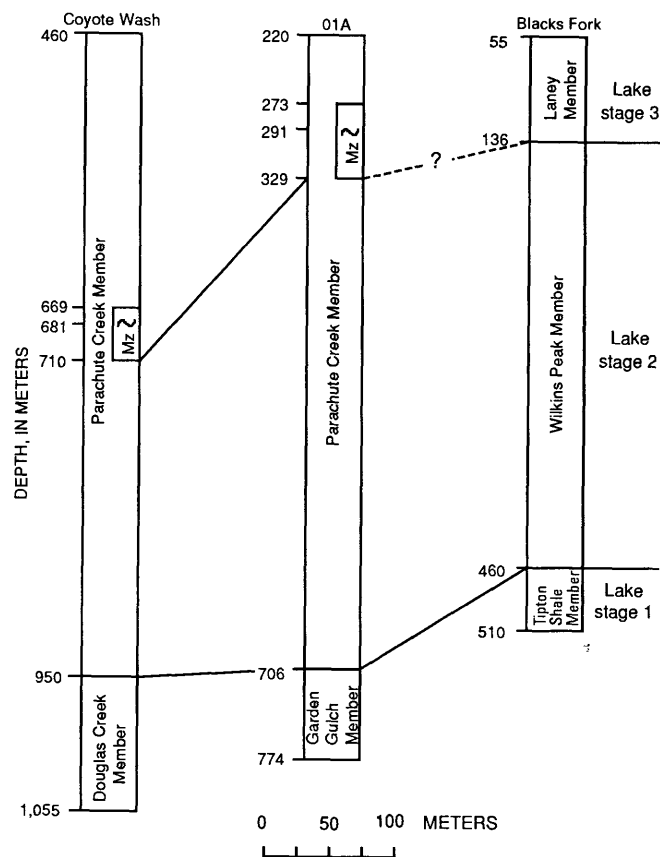


Figure 2. Stratigraphy of cores from depocenters of greater Green River (Blacks Fork), Piceance (01A), and Uinta (Coyote Wash) basins. Mz, Mahogany zone; ~Mahogany bed. Location of core holes shown in figure 1.

volume), and lake stages (and number of samples within each stage examined in this study) are summarized in table 1.

The polished thin sections were commercially prepared by cutting and grinding in oil because many samples contain water-soluble minerals. Pyrrhotite, marcasite, and pyrite were optically identified using color, bireflectance, and anisotropy under reflected light. The relative sulfide abundance was visually estimated under the microscope. In most samples, the carbonate and silicate minerals are too fine grained to be identified using transmitted-light techniques.

RESULTS

Depth profiles for sulfide-mineral abundances based on visual inspection of thin sections are similar to profiles based on measured sulfide chemical abundance data (figs. 3–5). In figures 3–5 an estimated abundance of one dot corresponds to less than 0.03 weight percent sulfur as sulfide minerals (dry-weight basis), and the highest estimated abundance (five dots) corresponds to greater than

1.6 weight percent. Representative examples of iron sulfide morphology in the three cores are shown in figure 6 and referred to in the discussion of each core. Wurtzite (ZnS) was not observed in any of the thin sections, consistent with its reported “microscopic” occurrence (Milton and Eugster, 1959).

Blacks Fork Core

Pyrite is the dominant sulfide mineral in sediments of lake stage 1 in the Blacks Fork core (fig. 3). All stage 1 samples contain either pyrite framboids (as much as 30 μm in diameter; as represented in fig. 6A) or anhedral pyrite grains. Fine-grained pyrite fills shell fragments in the deepest sample (509 m). One sample (464 m) also contains minor amounts of marcasite and pyrrhotite. The marcasite is within pyrrhotite blades as long as 400 μm .

Pyrite is the dominant sulfide in sediments of lake stage 2. It is commonly anhedral, although some samples contain euhedral pyrite cubes as much as 75 μm on edge (fig. 6B) and bladed pyrite as long as 500 μm . Bladed pyrrhotite was observed in six samples; the blades commonly are in splays (as long as 1 μm) that cut across bedding (fig. 6C). Pyrrhotite in one sample (144 m depth; fig. 6D) borders shortite ($\text{Na}_2\text{Ca}_2(\text{CO}_3)_3$) grains that, in turn, enclose pyrite cubes similar to that shown in figure 6B. Both anhedral and euhedral marcasite are associated with pyrite in three samples and with bladed pyrrhotite in two other samples (fig. 6E). No pyrite framboids were identified in samples of stage 2 sediments.

Sulfide minerals in lake stage 3 are predominantly anhedral pyrite; several samples contain euhedral and (or) framboidal pyrite. Euhedral marcasite was identified in three samples containing pyrite; one of these samples also contains sparse anhedral pyrrhotite. Several samples contain what probably is large (as much as 100 μm in diameter) iron-titanium-oxide aggregates or concretions that have been replaced by sulfide mineral(s) (fig. 6F); the sulfide mineral(s) in these samples is too fine grained to identify petrographically.

01A Core

Most iron sulfide minerals in lake stage 1 samples of the 01A core are framboids and euhedral or anhedral grains of pyrite (fig. 6). The framboids (fig. 6A) are as much as 30 μm in diameter; the euhedral and anhedral grains are commonly as much as 100 μm in diameter. Two samples contain euhedral and anhedral marcasite. Bladed textures were not observed.

Sediments from lake stage 2 contain framboidal, euhedral, and anhedral pyrite similar to that in stage 1 sediments; framboidal pyrite is rare in the upper 100 m of

Table 1. Summary of lake stages 1, 2 (2B in the Green River basin), and 3 represented by samples in this study [Samples are from the Blacks Fork core no. 1 (BF), greater Green River basin, Wyoming; 01A core (01A), Piceance basin, Colorado; Coyote Wash no. 1 core (CW), Uinta basin, Utah. Number of samples in parentheses is number of samples for which sulfur forms and their isotopic compositions were analyzed]

Lake stage	Green River basin	Greater Piceance basin	Uinta basin
1	Fresh water	Moderate salinity	Fresh water
	Transgression	Transgression	Transgression
	High productivity	Low productivity	Low productivity
	Organics preserved	Organics preserved	Lake-margin facies
	Open-water facies	Open-water facies	
Number of samples	5 (5)	7 (4)	8 (4)
2	High salinity	High salinity	High salinity
	Regression	Regression	Regression
	Low productivity	High productivity	Moderate productivity
	Organics mineralized	Organics preserved	Organics preserved
	Shallow-water facies	Open-water facies	Open-water facies
Number of samples	23 (23)	27 (11)	21 (15)
3	Fresh water	Moderate-high salinity	Low-moderate salinity
	Transgression	Transgression	Transgression
	High productivity	High productivity	High productivity
	Organics preserved	Organics preserved	Organics preserved
	Open-water facies	Open-water facies	Open-water facies
Number of samples	7 (7)	7 (5)	10 (6)

stage 2 (the leached zone¹). Fine-grained pyrite has replaced some unidentified grains similar to those in figure 6F. Euhedral or anhedral grains of marcasite, commonly within pyrrhotite blades (fig. 6E), are in the upper part of stage 2 beds. In the 01A core pyrrhotite is exclusive to stage 2 and is concentrated near the top of the sequence (leached zone). It is present as blades in four samples, two of which also contain anhedral or euhedral pyrrhotite. The pyrrhotite blades commonly are present together in splays that cut bedding and are as long as 1 μm (fig. 6C).

Lake stage 3 samples contain pyrite and marcasite. Pyrite framboids and anhedral pyrite or marcasite are common; fine-grained replacement sulfide minerals (fig. 6F) and pyrite blades were observed in samples from near the base of stage 3. The bladed texture is similar to that observed for pyrrhotite; pyrite and marcasite probably are pseudomorphs after pyrrhotite.

¹The leached zone is in the upper part of the saline stage of the Green River Formation in the Piceance basin of Colorado and represents a zone leached of its water-soluble salts as evidenced by vugs, crystal cavities, and marlstone solution breccias (Dyini, 1981). There is no evidence of sulfide-mineral leaching such as iron oxide staining.

Coyote Wash Core

Pyrite is the predominant sulfide mineral in lake stage 1 of the Coyote Wash core. It is present as anhedral and euhedral grains, framboids, and infilled framboids (fig. 6). Infilled framboids (Love and Amstutz, 1966) formed by the addition of pyrite to the interstices of the framboidal structure. Framboid infilling is illustrated in figure 6A. Minor amounts of marcasite are present as anhedral and euhedral grains.

Lake stage 2 samples contain pyrite, marcasite, and pyrrhotite. Two samples in the lower part of stage 2 contain only pyrite as anhedral and euhedral grains. Bladed pyrrhotite (fig. 6C) is the predominant sulfide mineral in two samples in the middle part of the stage; these samples also contain minor euhedral and anhedral marcasite and (or) pyrite. The other lake stage 2 samples contain marcasite and pyrite; bladed pyrrhotite may be present. Pyrite is present as anhedral or euhedral grains, framboids, or infilled framboids, and marcasite is present as either anhedral or euhedral grains. Pyrite and marcasite are typically present as replacement sulfide minerals within pyrrhotite blades (fig. 6G).

In stage 3 samples, anhedral pyrite is the dominant sulfide mineral; framboids were not observed. Marcasite is

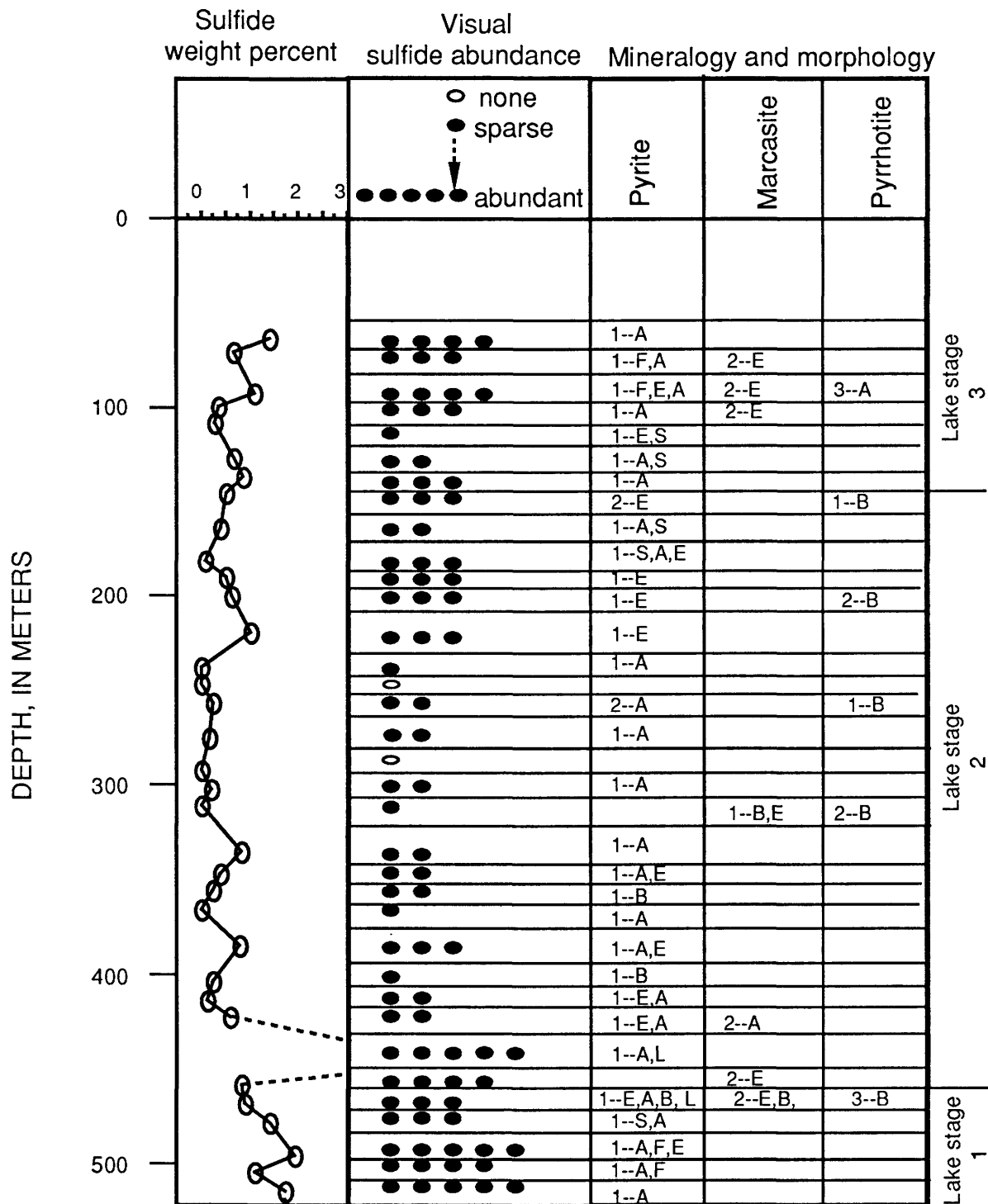


Figure 3. Iron sulfide mineralogy and morphology for samples of Green River Formation from Blacks Fork core, greater Green River basin, Wyoming. A, anhedral; B, blades; E, euhedral; F, framboids; L, lens; S, iron-sulfide minerals replacing (iron-titanium oxide?) grains. Numbers refer to relative abundance with 1 being most abundant. Location of core hole shown in figure 1.

common in lower beds but absent at depths shallower than about 620 m. The only stage 3 sample devoid of pyrite (642 m) contains euhedral and bladed marcasite and bladed pyrrhotite.

DISCUSSION

Iron sulfide minerals in the Green River Formation formed in response to changing diagenetic conditions and

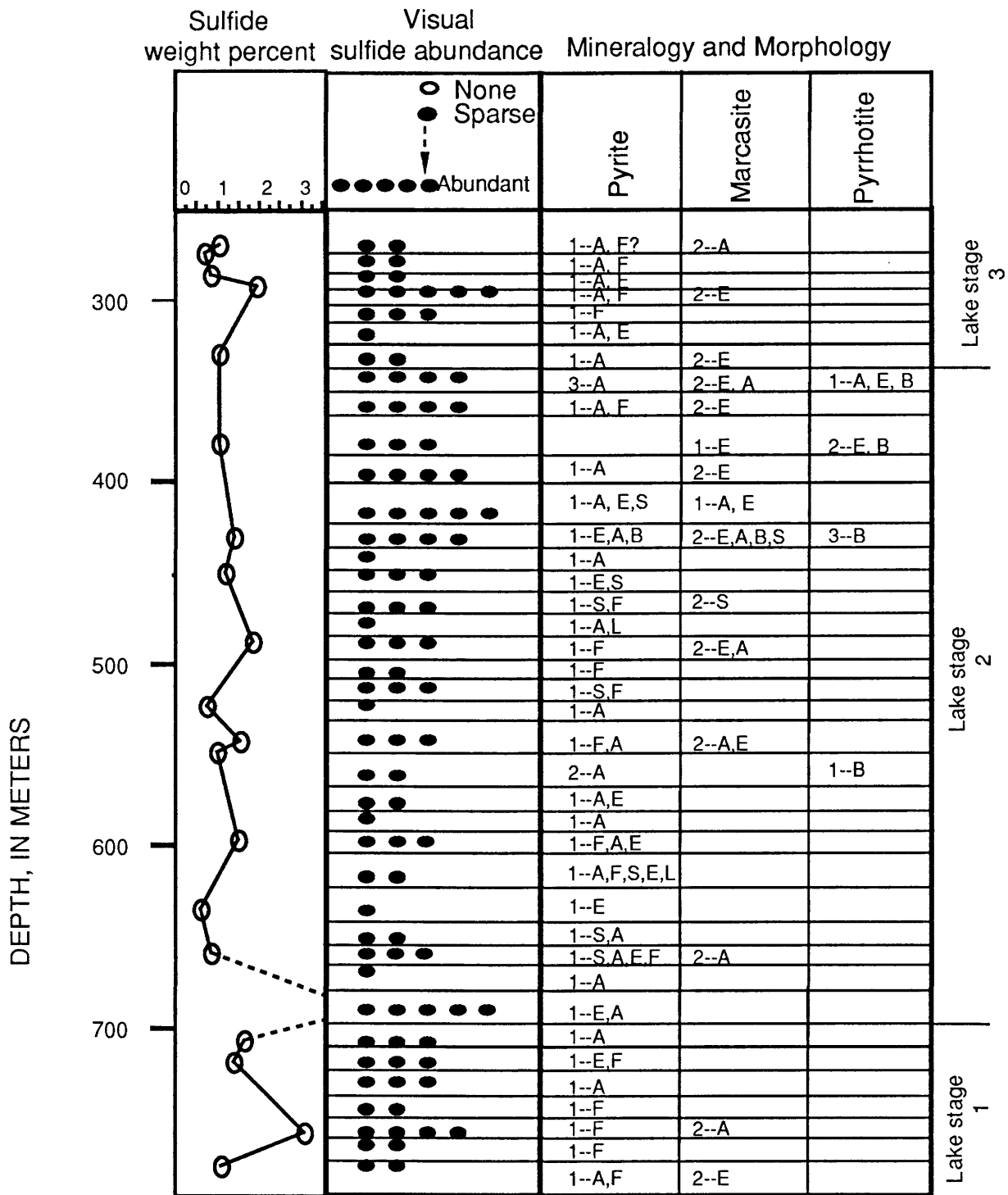


Figure 4. Iron sulfide mineralogy and morphology for samples of Green River Formation from 01A core, Piceance basin, Colorado. A, anhedral; B, blades; E, euhedral; F, framboids; L, lens; S, iron-sulfide minerals replacing (iron-titanium oxide?) grains. Numbers refer to relative abundances with 1 being most abundant. Location of core hole shown in figure 1.

thus have different mineralogies and morphologies. The history of iron sulfide formation in a typical lake bed of ancient Lakes Uinta and Gosiute was divided into four

episodes (fig. 7) that span the periods of sediment deposition (episode 1) through subsequent compaction and possibly deeper burial (episodes 3 and 4). The paragenetic

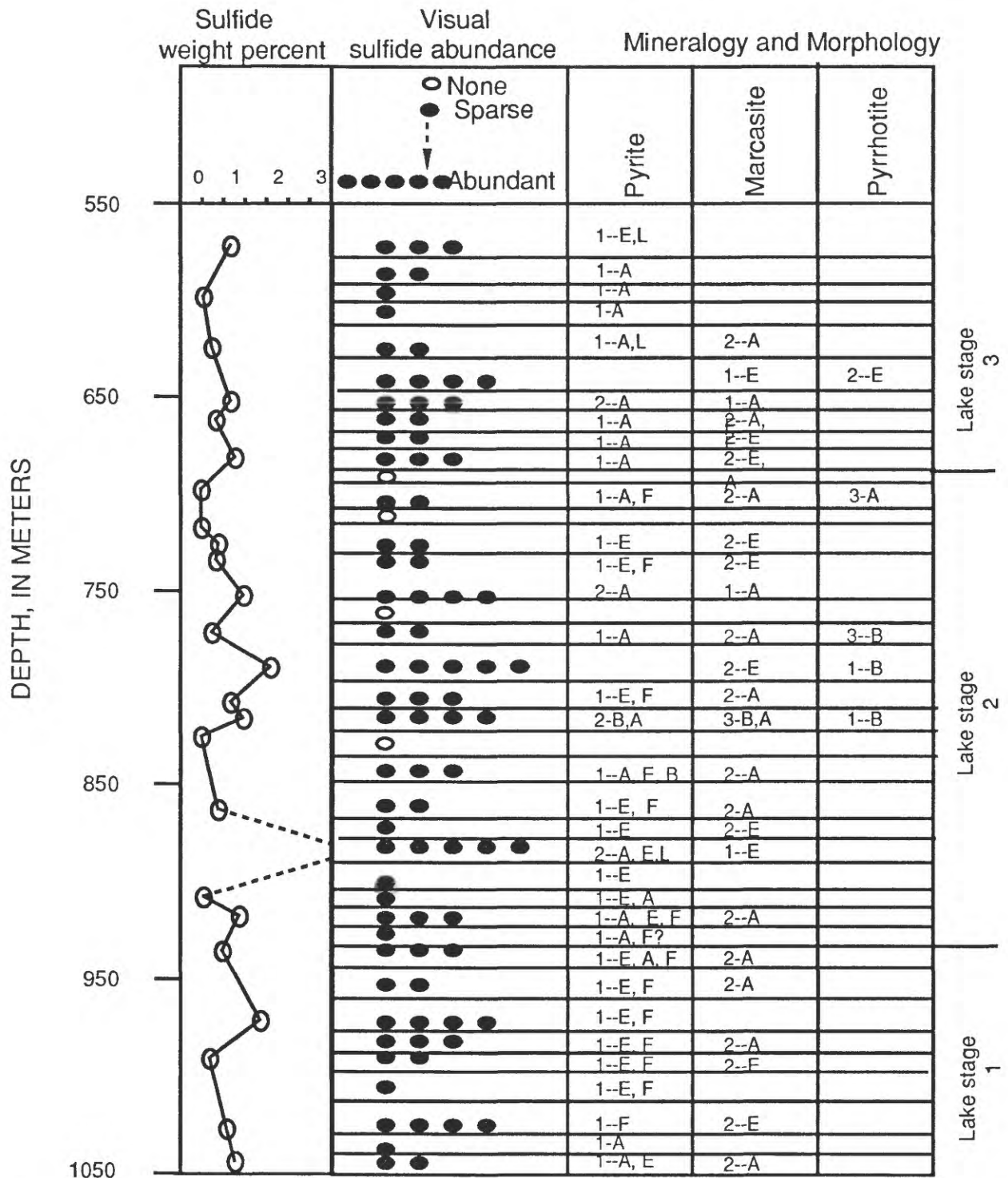


Figure 5. Iron sulfide mineralogy and morphology for samples of Green River Formation from Coyote Wash core, Uinta basin, Utah. A, anhedral; B, blades; E, euhedral; F, framboids; L, lens; S, iron-sulfide minerals replacing (iron-titanium oxide?) grains. Numbers refer to relative abundances with 1 being most abundant. Location of core hole shown in figure 1.

sequence was constructed using petrographic observations and inferences from sulfide-mineral genesis in modern marine sediments. The formation of iron sulfide minerals probably began with fine-grained, unstable iron monosul-

fides (FeS), which are thought to be the precursors of all sedimentary iron sulfide minerals (Roberts and others, 1969; Rickard, 1974; Pyzik and Sommer, 1981). Based on analogy with modern marine sediments, these ephemeral

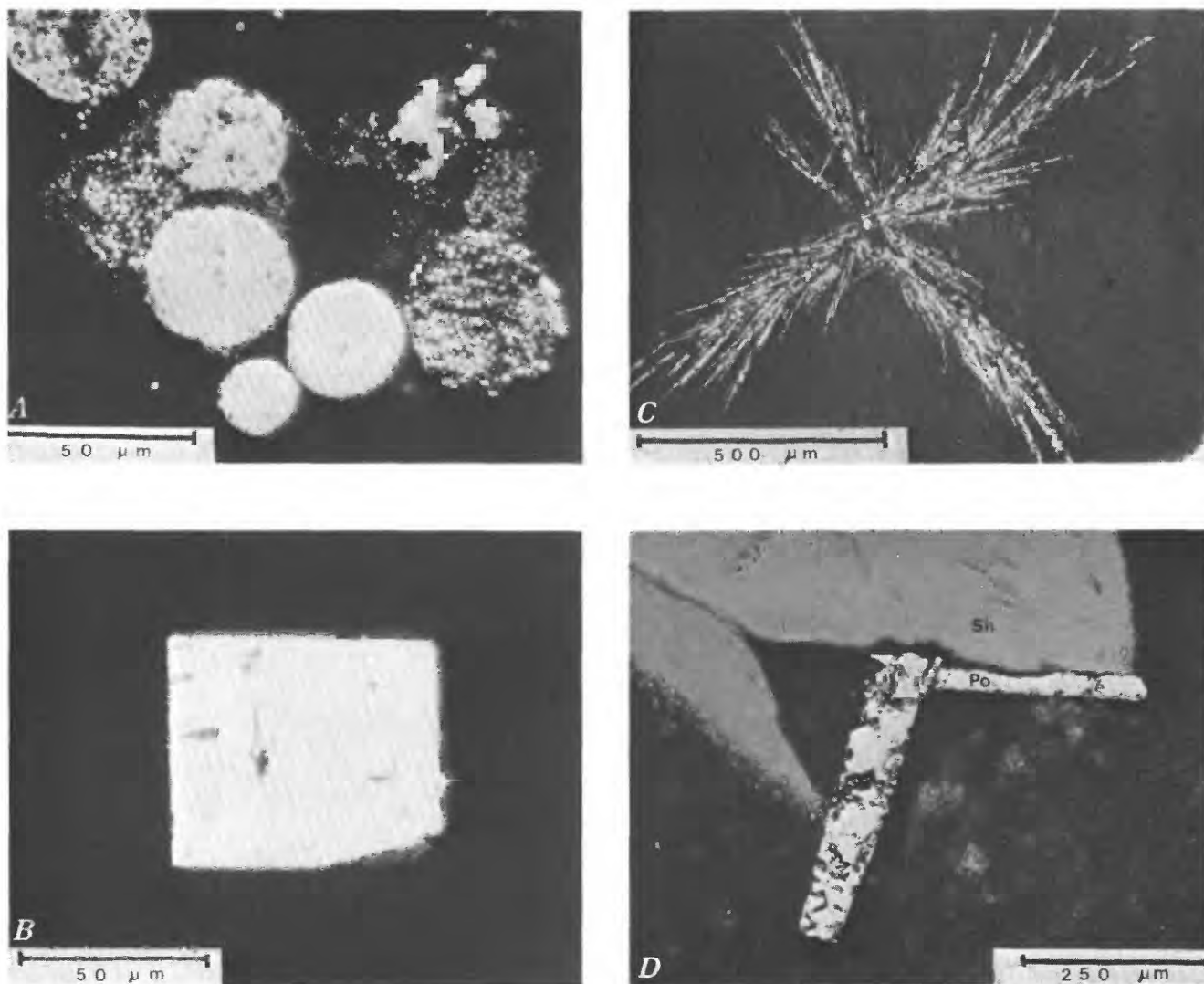


Figure 6 (above and facing page). Photomicrographs showing typical sulfide-mineral morphology in the Green River Formation. Location of core hole shown in figure 1. *A, B, E, F, G*, reflected-light photomicrographs under oil; *C, D*, under air. Py, pyrite; M, marcasite; Po, pyrrhotite; Sh, shortite. *A*, Pyrite framboids and framboids in which pyrite has filled spaces between crystals. Coyote Wash core, 971 m. *B*, Euhedral pyrite cube. Blacks Fork core, 144 m. *C*, Splays of pyrrhotite blades. Coyote Wash core, 815 m. *D*, Pyrrhotite blades rimming shortite grain. Blacks Fork core, 144 m. *E*, Euhedral marcasite that may have replaced pyrrhotite. Blacks Fork core, 464 m. *F*, Sulfidized (iron-titanium oxide?) mineral grains having pyrite centers surrounded by fine-grained sulfide minerals. 01A core, 437 m. *G*, Pyrrhotite blades partly replaced by pyrite; crossed nicols. Coyote Wash core, 815 m.

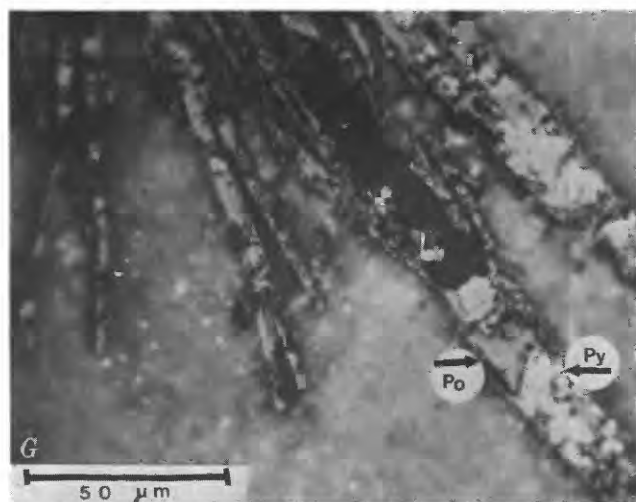
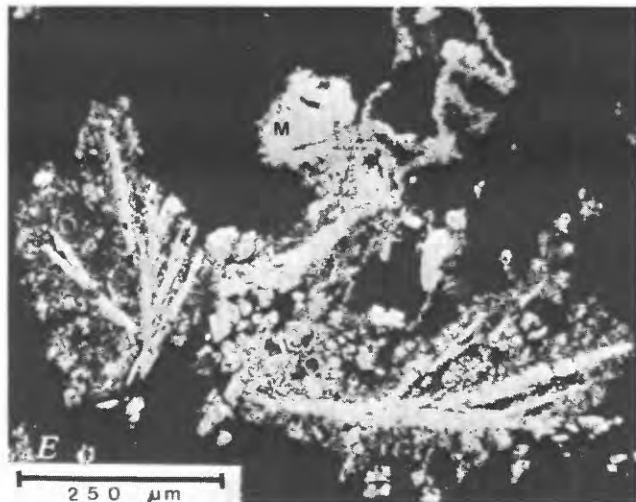
FeS phases probably formed very near the sediment-water interface. They are not present in any of our samples nor are they shown in figure 7.

Pyrite Formation

Pyrite is the predominant sulfide mineral in the Green River Formation. In order of decreasing abundance, it is present as euhedral and anhedral grains, framboids, infilled framboids, and lenses (accumulations of pyrite cement). The various forms of pyrite of the Green River Formation

probably formed in a sequence similar to that observed in marine sediments even though the overall geochemical controls on pyrite formation in the two environments may differ.

One of the earliest crystalline iron sulfides to form in marine sediments is microscopic pyrite (0.5–100 μm) (Love and Amstutz, 1966) that commonly aggregates to form framboids (Raiswell, 1982). Raiswell associated framboidal morphology with sulfidization of reactive “*in situ*” iron in the sediment. Likely sources of what Raiswell called *in situ* iron are iron oxyhydroxides that coat clay-sized minerals and very likely contain ferrihydrite (approximately $\text{Fe}(\text{OH})_3$) and lepidocrocite ($\gamma\text{-FeOOH}$)—the two iron



phases most reactive to reduction by H_2S (Pyzik and Sommer, 1981; Canfield, 1989). Framboidal pyrite almost always is found in organic stringers (filaments) in Green River Formation samples. The intimate association of framboids and organic stringers is not surprising because clay-size particles, and their iron oxyhydroxide coatings, and organic matter have similar slow settling rates through the water column (Anderson and others, 1985). No framboids were observed in organic-rich samples from stage 3 in the Uinta basin core (Coyote Wash). The relative rarity of clay minerals throughout this stage suggests that associated iron oxide minerals were insufficient to form framboids. In the model proposed here, framboids formed near the sediment-water interface by sulfidization of iron oxide coatings on clay particles associated with organic stringers. This period of sulfide mineral generation is referred to as episode 1.

The large size of euhedral and anhedral pyrite grains in most Green River Formation samples (fig. 6B) suggests slow growth. Raiswell (1982) hypothesized that euhedral pyrite in marine sediments grows after the most reactive local source of iron is exhausted and depends on diffusive input of additional iron. A similar process could have occurred in the Green River sediment. After the most reactive iron oxyhydroxide coatings were sulfidized to form framboids, other iron minerals in the sediments provided a reduced flux of dissolved iron for further sulfidization. Mineralogical sources of iron, listed in decreasing order of reactivity toward H_2S , include goethite ($\alpha\text{-FeOOH}$), hematite (Fe_2O_3), magnetite (Fe_3O_4), iron-bearing clays, and iron silicates. The relatively large size of the pyrite grains indicates that the sediment never became supersaturated with respect to pyrite, possibly because iron was very slowly released during diagenetic dissolution of the above mineral phases. I suggest that both anhedral and euhedral pyrite in the Green River Formation are probably cogenetic and formed from iron that was slowly released from minerals such as magnetite (episode 2). Bacterial reduction of ferric iron, as discussed by Canfield (1989), may have been the dominant dissolution mechanism because iron-reducing bacteria are known to exist in relatively saline sedimentary environments (11 per mil salinity) (Lovley and Phillips, 1986). Sediment matrix probably controlled the morphology of these grains. Where pyrite growth was unconstrained by competitive crystallization or pore-space volume, euhedral crystals formed; constrained growth, however, resulted in irregularly shaped crystals (Carstens, 1986).

Many organic stringers contain framboids that are variably infilled with pyrite (fig. 6A) (framboidal infilling is described in Love and Amstutz, 1966). Complete infilling of some framboids has produced spherical grains of pyrite. The controls on infilling processes are difficult to assess but may be linked to amalgamation of distinct pyrite crystals within the framboids by addition of new pyrite (Love and Amstutz, 1966). The process of pyrite infilling framboids

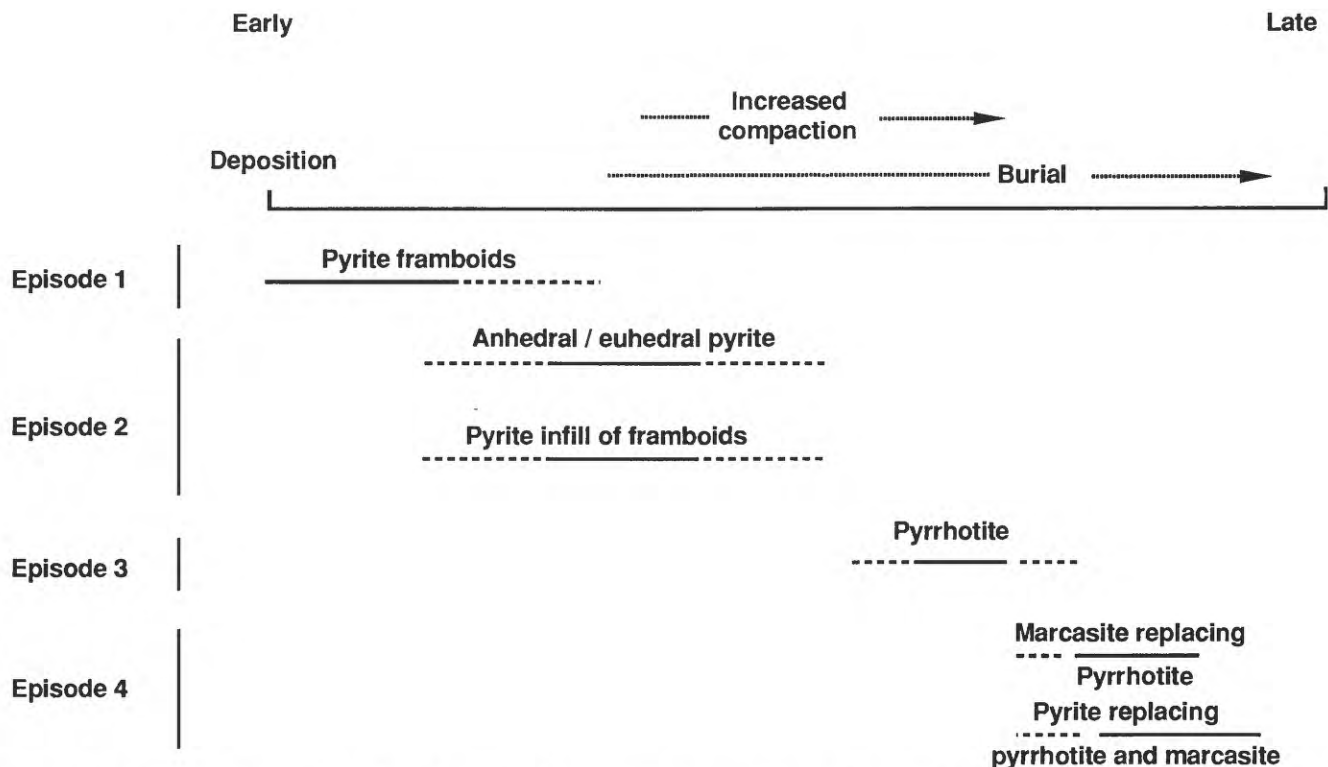


Figure 7. Paragenetic sequence of sulfide-mineral formation in Green River sediments deposited in ancient Lakes Uinta and Gosiute.

in Green River rocks is assigned to episode 2 because the iron source for the additional pyrite is probably the same as for the euhedral and anhedra pyrite; that is, the dissolution of relatively less reactive iron minerals.

The massive sulfide lenses in Green River samples probably are pyritic cement in concretionlike shapes. The fine-grained nature of these cements suggests that pyrite was supersaturated locally, possibly due to rapid release of iron. The time of lens formation is unconstrained by the data in this study and therefore is not shown on figure 7.

Pyrite that replaces marcasite and pyrrhotite represents the most recent generation of iron sulfide mineral, episode 4 (fig. 7). Such pyrite is generally anhedra or euhedral, and it is commonly bladed where it pseudomorphically has replaced bladed pyrrhotite.

Sulfide minerals that fill fractures in rocks of the Green River Formation probably formed during a late postlithification episode (Dyner, 1983). This episode of pyrite formation is not shown in the paragenetic sequence (fig. 7) because fracture fillings were not observed in the core intervals of this study.

Pyrrhotite Formation

Pyrrhotite has not been reported in unmetamorphosed lacustrine rocks outside the Green River Formation. Its local abundance in the Green River rocks indicates unusual

chemical conditions at the time of formation. Eh-pS²⁻ stability fields of pyrite, pyrrhotite, siderite, and hematite for two CO₂ partial pressures (P_{CO2}) are plotted in figure 8 (the equations used to construct these diagrams are in Berner, 1964). The pyrrhotite stability field is constrained by very reducing conditions (Eh < -0.5 volts) and by relatively high H₂S concentrations (pS²⁻ < 9) within the sediment (fig. 8). At an assumed upper limit of P_{CO2}=1 atm, the pyrite and siderite fields are large relative to that of pyrrhotite. At a value of P_{CO2}=10^{-2.5} atm, the estimated value for shallow-marine porewater (Berner, 1964), the pyrrhotite field expands relative to the siderite field, but the slope of the pyrite-pyrrhotite boundary remains unchanged.

Pyrrhotite is generally restricted to saline lake stage 2; thus, high salinity is added to the above requirements of very reducing conditions, low P_{CO2}, and relatively high H₂S concentrations. Commonly, these conditions are found in lakes containing euxinic hypolimnions (H₂S-bearing bottom waters) in which the oxidative conversion of precursor FeS phases (S²⁻) to disulfides (S₂²⁻) is inhibited (see discussion on Soap Lake in Tuttle, 1988). Failing to undergo any sulfur-oxidation reaction, unstable FeS phases will eventually recrystallize to pyrrhotite, the most thermodynamically stable FeS phase. Figure 8 indicates that pyrrhotite becomes more stable than siderite at low P_{CO2}—a condition expected in sediments subsequent to decomposition of most organic matter and to formation of

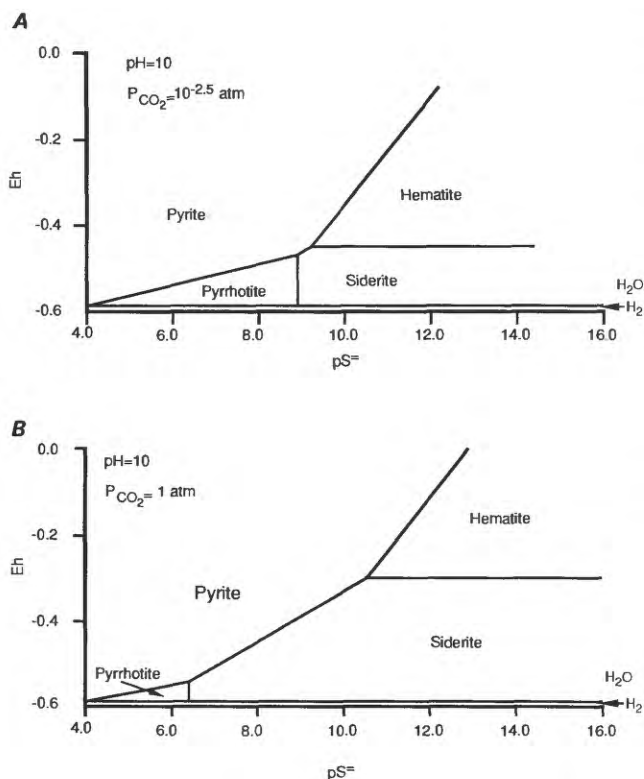


Figure 8. Eh-pS² stability field diagrams for pyrite, pyrrhotite, siderite, and hematite at pH 10. A, P_{CO₂} of 1 atm. B, P_{CO₂} of 10^{-2.5} atm. Equations used in calculations are from Berner (1964).

carbonate minerals. Some pyrrhotite in the greater Green River basin surrounds shortite (Na₂Ca₂(CO₃)₃) (fig. 6D). Based on examination of sediment flow lines around shortite crystals, Fahey (1962) proposed that shortite formed in "partially compressed" Lake Gosiute mud. Bradley and Eugster (1969) used experimental data to argue that the shortite formed at temperatures of about 90 °C (corresponding burial depth of 1,525 m). The Green River Formation, however, never reached temperatures as high as 90 °C according to vitrinite reflectance data (B. E. Law, U.S. Geological Survey, written commun., 1990). The timing of pyrrhotite formation, therefore, is not well constrained by its relation with shortite, but pyrrhotite likely formed in very reducing sediment during or after compaction (episode 3). Episode 3 could overlap with episode 2 (euhedral and anhedral pyrite formation) if the pyrrhotite and pyrite were forming in different microenvironments. These episodes are not shown as overlapping in figure 7 because the spatial distribution of the two minerals does not suggest that such microenvironments existed.

Marcasite Formation

Marcasite is present in about 40 percent of the Green River Formation samples (figs. 3–5). The occurrence of

marcasite in lacustrine rocks (or lake sediments) is unprecedented. Marcasite generally forms under acid conditions (Goldhaber and Kaplan, 1974; Murowchick and Barnes, 1986). Its formation in sediments deposited under high pH conditions such as those inferred for Lakes Uinta and Gosiute (pH estimated to be about 10) is inconsistent with experimental data, and its formation suggests that it did not form as a primary mineral during disulfide formation in episodes 1 or 2. Marcasite replacement of pyrrhotite has been reported to occur by the loss of iron from pyrrhotite and oxidation of the sulfide to disulfide (Kelley and Turneure, 1970; Fleet, 1978; De Waal, 1984).

Euhedral and anhedral marcasite is present in two types of samples—those containing pyrite and large amounts of organic matter and those containing pyrrhotite. The latter occurrence suggests that marcasite is a late alteration product of the pyrrhotite that formed during episode 3. The pyrrhotite is optically continuous along the blades, and the textures depicted in figure 6G suggest that marcasite and pyrite preferentially are in etched pits within the pyrrhotite blades. Oxidants made available during pyrrhotite alteration but not during its earlier formation include oxidants released during later stages of organic-matter mineralization or oxidants introduced by groundwater. Whatever the source, the amount was insufficient in most cases to completely oxidize the pyrrhotite. Possible exceptions are samples high in organic matter that contain only marcasite and do not exhibit relict pyrrhotite or pyrrhotite morphology. If pyrrhotite was originally present in these samples, either the replacement was not pseudomorphic or the original pyrrhotite did not occur as blades. Perhaps high concentrations of organic matter promote formation of pyrrhotite having a different morphology that readily alters to marcasite, but this hypothesis remains to be investigated.

CONCLUSIONS

Petrographic characteristics of samples from three cores of the Green River Formation indicate that iron geochemistry and redox conditions in the sediment controlled the mineralogy and morphology of the iron sulfide minerals. Four episodes of sulfide-mineral formation can be defined. Although the exact timing of these episodes is impossible to determine, the relative timing has been inferred by combining petrographic observations and observations of sulfide-mineral formation in marine sediments. Near the sediment-water interface, iron oxide coatings on clays were sulfidized and produced framboidal pyrite (episode 1). Euhedral and anhedral pyrite grains and pyrite infilling of framboids then formed when less reactive iron-mineral phases were dissolved, possibly by iron-reducing bacteria (episode 2). Pyrrhotite likely formed late in the sequence (episode 3) from unstable FeS phases that were not converted to disulfide because of extremely

reducing conditions in the sediments. Pyrrhotite was eventually and variably replaced by marcasite and (or) pyrite (episode 4).

REFERENCES CITED

- Anderson, R.Y., Dean, W.E., Bradbury, J.P., and Love, D., 1985, Meromictic lakes and varved lake sediments in North America: U.S. Geological Survey Bulletin 1607, 19 p.
- Berner, R.A., 1964, Stability fields of iron minerals in anaerobic marine sediments: *Journal of Geology*, v. 72, no. 6, p. 826-834.
- Boyer, D.L., and Cole, R.D., 1983, Variations in sulfur mineralization in the Parachute Creek Member of the Green River Formation, Colorado and Utah, in *Sixteenth Oil Shale Symposium proceedings: Golden, Colorado School of Mines*, p. 160-175.
- Bradley, W.H., and Eugster, H.P., 1969, Geochemistry and paleolimnology of the trona deposits and associated authigenic minerals of the Green River Formation of Wyoming: U.S. Geological Survey Professional Paper 496-B, 71 p.
- Canfield, D.E., 1989, Reactive iron in marine sediments: *Geochimica et Cosmochimica Acta*, v. 53, p. 619-632.
- Carstens, H., 1986, Displacive growth of authigenic pyrite: *Journal of Sedimentary Petrology*, v. 56, p. 252-257.
- Cole, R.D., 1975, Sedimentology and sulfur isotope geochemistry of the Green River Formation (Eocene), Uinta basin, Utah, Piceance Creek basin, Colorado: Salt Lake City, University of Utah, Ph.D. thesis, 274 p.
- Cole, R.D., Liu, J.H., Smith, G.V., Hinckley, C.C., and Saporschenko, M., 1978, Iron partitioning in oil shale of the Green River Formation, Colorado—A preliminary Mössbauer study: *Fuel*, v. 57, p. 514-520.
- Cole, R.D., and Picard, M.D., 1981, Sulfur-isotope variations in marginal-lacustrine rocks of the Green River Formation, Colorado and Utah: *Society of Economic Paleontologists and Mineralogists Special Publication 31*, p. 261-275.
- De Waal, S.A., 1984, Experimental simulation of the supergene reaction, pyrrhotite to marcasite+Fe²⁺+electrons: *Transactions of the Geological Society of South Africa*, v. 87, p. 273-279.
- Dyni, J.R., 1981, Geology of the nahcolite deposits and associated oil shales of the Green River Formation in the Piceance Creek Basin, Colorado: Boulder, University of Colorado, Ph.D. thesis, 144 p.
- , 1983, Distribution and origin of sulfur in Colorado oil shale, in *Sixteenth Oil Shale Symposium proceedings: Golden, Colorado School of Mines*, p. 144-159.
- Fleet, M.E., 1978, The pyrrhotite-marcasite transformation: *Canadian Mineralogist*, v. 16, p. 31-35.
- Goldhaber, M.B., and Kaplan, J.R., 1974, The sulfur cycle, in *Goldberg, E.D., ed., The sea*, v. 5: New York, John Wiley and Sons, p. 569-655.
- Kelly, W.C., and Turneure, F.S., 1970, Mineralogy, paragenesis and geothermometry of tin and tungsten deposits of Eastern Andes, Bolivia: *Economic Geology*, v. 65, p. 609-680.
- Love, L.G., and Amstutz, G.C., 1966, Review of microscopic pyrite: *Fortschritte der Mineralogie*, v. 43, p. 273-309.
- Lovley, D.R., and Phillips, E.J.P., 1986, Organic matter mineralization with reduction of ferric iron in anaerobic sediments: *Applied and Environmental Microbiology*, v. 51, p. 683-689.
- Melchior, D.C., Wildeman, T.R., and Williamson, D.L., 1982, Mössbauer investigation of the transformations of the iron minerals in oil shale during retorting: *Fuel*, v. 61, p. 516-522.
- Milton, C., and Eugster, H.P., 1959, Mineral assemblages of the Green River Formation, in *Abelson, P.H., ed., Researches in geochemistry: New York, John Wiley and Sons*, p. 118-150.
- Murowchick, J.B., and Barnes, H.L., 1986, Marcasite precipitation from hydrothermal solutions: *Geochimica et Cosmochimica Acta*, v. 50, p. 2615-2629.
- Pabst, A., 1970, Pyrite of unusual habit simulating twinning from the Green River Formation of Wyoming: *The American Mineralogist*, v. 56, p. 133-145.
- Pyzik, A.J., and Sommer, S.E., 1981, Sedimentary iron monosulfides—Kinetics and mechanism of formation: *Geochimica et Cosmochimica Acta*, v. 45, p. 687-698.
- Raiswell, R., 1982, Pyrite texture, isotopic composition and the availability of iron: *American Journal of Science*, v. 282, p. 1244-1263.
- Rickard, D.T., 1974, Kinetics and mechanism of sulfidization of goethite: *American Journal of Science*, v. 274, p. 941-952.
- Roberts, W.M.B., Walker, A.L., and Buchanan, A.S., 1969, The chemistry of pyrite formation in aqueous solution and its relation to the depositional environment: *Mineralium Deposita*, v. 4, p. 18-29.

SELECTED SERIES OF U.S. GEOLOGICAL SURVEY PUBLICATIONS

Periodicals

- Earthquakes & Volcanoes (issued bimonthly).
- Preliminary Determination of Epicenters (issued monthly).

Technical Books and Reports

Professional Papers are mainly comprehensive scientific reports of wide and lasting interest and importance to professional scientists and engineers. Included are reports on the results of resource studies and of topographic, hydrologic, and geologic investigations. They also include collections of related papers addressing different aspects of a single scientific topic.

Bulletins contain significant data and interpretations that are of lasting scientific interest but are generally more limited in scope or geographic coverage than Professional Papers. They include the results of resource studies and of geologic and topographic investigations; as well as collections of short papers related to a specific topic.

Water-Supply Papers are comprehensive reports that present significant interpretive results of hydrologic investigations of wide interest to professional geologists, hydrologists, and engineers. The series covers investigations in all phases of hydrology, including hydrology, availability of water, quality of water, and use of water.

Circulars present administrative information or important scientific information of wide popular interest in a format designed for distribution at no cost to the public. Information is usually of short-term interest.

Water-Resources Investigations Reports are papers of an interpretive nature made available to the public outside the formal USGS publications series. Copies are reproduced on request unlike formal USGS publications, and they are also available for public inspection at depositories indicated in USGS catalogs.

Open-File Reports include unpublished manuscript reports, maps, and other material that are made available for public consultation at depositories. They are a nonpermanent form of publication that maybe cited in other publications as sources of information.

Maps

Geologic Quadrangle Maps are multicolor geologic maps on topographic bases in 7 1/2- or 15-minute quadrangle formats (scales mainly 1:24,000 or 1:62,500) showing bedrock, surficial, or engineering geology. Maps generally include brief texts; some maps include structure and columnar sections only.

Geophysical Investigations Maps are on topographic or planimetric bases at various scales, they show results of surveys using geophysical techniques, such as gravity, magnetic, seismic, or radioactivity, which reflect subsurface structures that are of economic or geologic significance. Many maps include correlations with the geology.

Miscellaneous Investigations Series Maps are on planimetric or topographic bases of regular and irregular areas at various scales; they present a wide variety of format and subject matter. The series also includes 7 1/2-minute quadrangle photogeologic maps on planimetric bases which show geology as interpreted from aerial photographs. The series also includes maps of Mars and the Moon.

Coal Investigations Maps are geologic maps on topographic or planimetric bases at various scales showing bedrock or surficial geology, stratigraphy, and structural relations in certain coal-resource areas.

Oil and Gas Investigations Charts show stratigraphic information for certain oil and gas fields and other areas having petroleum potential.

Miscellaneous Field Studies Maps are multicolor or black-and-white maps on topographic or planimetric bases on quadrangle or irregular areas at various scales. Pre-1971 maps show bedrock geology in relation to specific mining or mineral-deposit problems; post-1971 maps are primarily black-and-white maps on various subjects such as environmental studies or wilderness mineral investigations.

Hydrologic Investigations Atlases are multicolored or black-and-white maps on topographic or planimetric bases presenting a wide range of geohydrologic data of both regular and irregular areas; the principal scale is 1:24,000, and regional studies are at 1:250,000 scale or smaller.

Catalogs

Permanent catalogs, as well as some others, giving comprehensive listings of U.S. Geological Survey publications are available under the conditions indicated below from the U.S. Geological Survey, Books and Open-File Reports Sales, Box 25425, Denver, CO 80225. (See latest Price and Availability List.)

"Publications of the Geological Survey, 1879-1961" may be purchased by mail and over the counter in paperback book form and as a set microfiche.

"Publications of the Geological Survey, 1962-1970" may be purchased by mail and over the counter in paperback book form and as a set of microfiche.

"Publications of the U.S. Geological Survey, 1971-1981" may be purchased by mail and over the counter in paperback book form (two volumes, publications listing and index) and as a set of microfiche.

Supplements for 1982, 1983, 1984, 1985, 1986, and for subsequent years since the last permanent catalog may be purchased by mail and over the counter in paperback book form.

State catalogs, "List of U.S. Geological Survey Geologic and Water-Supply Reports and Maps For (State)," may be purchased by mail and over the counter in paperback booklet form only.

"Price and Availability List of U.S. Geological Survey Publications," issued annually, is available free of charge in paperback booklet form only.

Selected copies of a monthly catalog "New Publications of the U.S. Geological Survey" is available free of charge by mail or may be obtained over the counter in paperback booklet form only. Those wishing a free subscription to the monthly catalog "New Publications of the U.S. Geological Survey" should write to the U.S. Geological Survey, 582 National Center, Reston, VA 22092.

Note.—Prices of Government publications listed in older catalogs, announcements, and publications may be incorrect. Therefore, the prices charged may differ from the prices in catalogs, announcements, and publications.

